FLUX-SPLIT ALGORITHMS FOR FLOWS WITH NON-EQUILIBRIUM CHEMISTRY AND THERMODYNAMICS

by

Pasquale Cinnella

Dissertation submitted to the Faculty of the
Virginia Polytechnic Institute and State University
in partial fulfillment of the requirements for the degree of

DOCTOR OF PHILOSOPHY

in

Aerospace Engineering

APPROVED:

B. Grossman, Chairman

R. W. Walters

J. A. Schetz

A. K. Jakubowski

J. P. Drummond

December, 1989

Blacksburg, Virginia

FLUX-SPLIT ALGORITHMS FOR FLOWS WITH NON-EQUILIBRIUM CHEMISTRY AND THERMODYNAMICS

by

Pasquale Cinnella

Committee Chairman: Bernard Grossman

Aerospace Engineering

(ABSTRACT)

New flux-split algorithms are developed for high velocity, high temperature flow situations, when finite-rate chemistry and non-equilibrium themodynamics greatly affect the physics of the problem. Two flux-vector-split algorithms, of the Steger-Warming and of the Van Leer type, and one flux-difference-split algorithm of the Roe type are established and utilized for the accurate numerical simulation of flows with dissociation, ionization and combustion phenomena. Several thermodynamic models are used, including a simplified vibrational non-equilibrium model and an equilibrium model based upon refined statistical mechanics properties. The framework provided is flexible enough to accomodate virtually any chemical model and a wide range of non-equilibrium, multi-temperature thermodynamic models.

A theoretical study of the main features of flows with free electrons, for conditions that require the use of two translational temperatures in the thermal model, is developed. Interesting and unexpected results are obtained, because acoustic wave speeds of the symmetric form $u \pm a$ no longer appear. A simple but powerful asymptotic analysis is developed which allows the establishment of the fundamental gasdynamic properties of flows with multiple translational temperatures.

The new algorithms developed demonstrate their accuracy and robustness for challenging flow problems. The influence of several assumptions on the chemical and thermal behaviour of the flows is investigated, and a comparison with results

obtained using different numerical approaches, in particular spectral methods, is provided, and proves to be favorable to the present techniques.

Other calculations in one and two space dimensions indicate large sensitivities with respect to chemical and thermodynamic modeling. The algorithms developed are of sufficient generality to begin to examine these effects in detail. Preliminary numerical simulations are performed using elementary modeling of transport phenomena.

ACKNOWLEDGEMENTS

My Committee Chairman and Research Advisor, Prof. B. Grossman, has provided me with constant and effective support for the duration of my studies at VPI. Working for him and with him has been a very pleasant experience.

I am very grateful to Prof. R. Walters for his help during the preparation of the three-dimensional flow solver. I learned very valuable lessons and profited by his experience.

Many thanks are due to the Head of the Aerospace Department, Prof. A. Schetz, for admitting me to the program and having words of support and appreciation for my job.

My undergraduate thesis Advisor, Prof. M. Napolitano, introduced me to the field of Computational Fluid Dynamics and strongly encouraged my decision to continue my education. I am indebted to him for this, and hope that nobody will hold him responsible for my future misfeats.

I thank Prof. A. Jakubowski and Dr. P. Drummond for accepting to serve on my Committee. Also, I would like to mention all of my friends and colleagues for their daily help and underline the usefulness of many challenging discussions that I have had with them in the last few years.

This work was made possible by grants from the NASA Langley Research Center, NAG-1-776, and the National Science Foundation, whose support is gratefully acknowledged.

TABLE OF CONTENTS

LIST OF SYMBOLS

A	cross-sectional area
$\mathbf{A}$, $\mathbf{B}$, $\mathbf{C}$	Jacobian matrices in Cartesian coordinates
$\tilde{\mathbf{A}}$, $\tilde{\mathbf{B}}$, $\tilde{\mathbf{C}}$	Jacobian matrices in generalized coordinates
a	speed of sound
$\mathbf{C}_v$	matrix of specific heats at constant volume
c'_s, c''_s	thermal velocities
$\tilde{c}_p$	portion of specific heat at constant pressure in equilibrium at T
$\tilde{c}_v$	portion of specific heat at constant volume in equilibrium at T
c_{v_e}	portion of specific heat at constant volume in equilibrium at T_e
$\tilde{c}_{v_e}$	heavy-particle averaged c_{v_e}
$\tilde{c}_{v_{tr}}$	translational contribution to specific heat at constant volume
D	diffusion coefficient
E	right eigenvector; *also*,
	electric field
e, e'	averaged and particle internal energy (per unit mass)
$\tilde{e}$, $\tilde{e}'$	averaged and particle portion of internal energy in equilibrium at T
e_e, e'_e	averaged and particle portion of internal energy in equilibrium at T_e
e_n, e'_n	averaged and particle portion of internal energy in non-equilibrium
e_0	total internal energy
F, G, H	inviscid flux vectors in Cartesian coordinates
$\tilde{F}$, $\tilde{G}$, $\tilde{H}$	inviscid flux vectors in generalized coordinates
$(F_s)_E$, $(F_s)_I$	elastic and inelastic force
F_v, G_v, H_v	viscous flux vectors in Cartesian coordinates
$\tilde{F}_v$, $\tilde{G}_v$, $\tilde{H}_v$	viscous flux vectors in generalized coordinates
f_e, f_m	energy and mass flux splitting
f_l, f_r	left and right fluxes
g	Gibb's free energy

$\boldsymbol{g}$	body force per unit mass
h	enthalpy per unit mass
h_f	heat of formation
h_0	total enthalpy per unit mass
$\boldsymbol{i}, \boldsymbol{j}, \boldsymbol{k}$	unit vectors for Cartesian coordinates
$\mathbf{I}$	identity matrix
J	number of chemical reactions; *also*, Jacobian of coordinate transformation
K_e	chemical equilibrium constant
k	thermal conductivity related to T
k_e	thermal conductivity related to T_e
k_f, k_b	forward and backward reaction rates
k_n	thermal conductivity related to T_n
Le	Lewis number
$\boldsymbol{l}, \boldsymbol{m}$	unit vectors in a plane perpendicular to $\boldsymbol{i}$ (or $\nabla\xi$)
M	number of nonequilibrium energy contributions
$\mathcal{M}$	molecular mass
$\tilde{M}$	contravariant Mach number
m	particle mass
n	number density
$\boldsymbol{n}$	unit vector normal to a surface $\partial\Omega$
N	number of species when $T_e \neq T$
N^*	number of species when $T_e \equiv T$, $\quad N^* = N-1$
N_A	Avogadro's number
Pr	Prandtl number
p	pressure
Q	vector of conserved variables
$(\dot{Q}_s)_E, (\dot{Q}_s)_I$	elastic and inelastic power (per unit volume)
$\boldsymbol{q}$	heat flux vector

q_n	non-equilibrium heat flux vector
R	gas constant
$\hat{R}$	universal gas constant
$\tilde{R}$	mixture gas constant
$\tilde{\mathbf{S}}$	matrix of right eigenvectors for the inviscid Jacobian
s	entropy per unit mass
$\tilde{s}$	portion of entropy corresponding to T
s_e	portion of entropy corresponding to T_e
s_n	portion of entropy corresponding to T_n
T	heavy-particle translational temperature
T_e	free electrons translational temperature
T_n	thermal non-equilibrium temperature
t	time
$\mathbf{T}$	shear stress tensor
u_s, u'_s	averaged and particle velocity
u_0	mass-averaged mixture velocity
$u_{0_1}, u_{0_2}, u_{0_3}$	components of velocity in Cartesian coordinates
$\tilde{u}_{0_1}, \tilde{u}_{0_2}, \tilde{u}_{0_3}$	components of velocity in generalized coordinates
V_s	diffusion velocity
W	vector of chemical and thermal source terms
W_A	vector of area variation contributions
w	chemical production rate
X	chemical species; *also*, mole fraction
x_1, x_2, x_3	Cartesian coordinates
x	position vector
z	charge number
α	wave strength

$\tilde{\gamma}$	ratio of equilibrium portions of specific heats
γ_e	ratio of specific heats for electrons
ϵ	electron charge
ϵ'_{int}	particle contribution to internal energy from internal structure
Θ_v	characteristic vibrational temperature
$\tilde{\mathbf{\Lambda}}$	matrix of inviscid Jacobian eigenvalues
μ	dynamic viscosity
ν', ν''	stoichiometric coefficients
ξ, η, ζ	generalized coordinates
ρ	density
σ	collision cross-section
τ	vibrational relaxation time
τ_{CH}, τ_{FD}	characteristic chemical and fluid dynamic times
Ω, $\partial\Omega$	arbitrary control volume and its boundary
Δt	time step
$\nabla\tilde{\xi}$, $\nabla\tilde{\eta}$, $\nabla\tilde{\zeta}$	unit vectors for generalized coordinates

1. INTRODUCTION

In recent years, a renewed interest in the field of hypersonic aerodynamics has been registered among the scientific community. Many successful attempts to broaden the understanding of high-speed-related effects have been completed, thus improving the state of the art in what is a critical sector in our technological future. Vehicles like the Space Shuttle or the European Hermes are fully operational or in an advanced design stage, respectively. Their conception would not have been possible without some knowledge of chemical and thermal non-equilibrium phenomena and how they affect the performance of engines, lifting surfaces and materials, to name a few examples.

Accurate prediction of the presence and level of ionization is essential for maintaining communication capabilities with earth, and, consequently, for the actual feasibility of manned flight at high Mach numbers in the presence of an atmosphere. The Aeroassisted Orbital Transfer Vehicle (AOTV), conceived as an essential tool for possible exploratory missions on Mars and for efficient satellite management in high earth-centered orbits [1], is anticipated to make use of aerobraking in conditions that are not reproducible on earth in existing experimental facilities, nor will be in the near future. Other aircraft, like the National Aero-Space Plane (NASP) or the European Hypersonic Transport Vehicle, are becoming national priorities and subjects for commercial competition. Newly designed engines for their flight régimes require a thorough understanding of supersonic combustion, diffusion phenomena, and turbulence in presence of chemically and thermally active surroundings.

At the present day, it is apparent that the new horizons of technological advancement, open to humankind by a productive effort in the sector of high-speed flight, are becoming less of a dream and more of a reality. However, many needs must be accomodated before a sufficient confidence is achieved in the newly and future developed theoretical and practical results.

In the first place, the physical understanding of many speed-related phenomena must be enhanced. The presence of chemical reactions, ionization and thermal

non-equilibrium requires an analysis based upon quantum mechanics and statistical thermodynamics as an essential complement to Newtonian mechanics and classical thermodynamics [2]. Therefore, the newest physical gasdynamics findings are necessary and will be used more and more in the future, to provide the scientific community with more reliable tools.

Strictly related to the physical investigation, a more complete mathematical insight of the peculiar characters of this discipline has to be obtained. Many approximations could be removed from the theoretical framework that has been used so far, provided new or improved mathematical tools are extensively employed. As an example, the governing differential equations are usually derived under the assumption of *small perturbations* from some equilibrium condition [3], and further restrictions apply to the derivation of theoretical formulas for transport properties. In actual practice, even more approximations are frequently made, some of which are no longer justified or necessary in the era of supercomputing. A *nonlinear* analysis of at least some aspects of the physics could be within reach of scientists in the near future, and bring about substantial improvements in the accurate prediction of hypersonic effects [4].

Finally, the great complication generated by the onset of chemical and thermal non-equilibrium poses a problem of efficiency for any numerical computation. Even with supercomputers available, the amount of work requested for realistic simulations of engineering-scale problems is overwhelming. Extensive use of vector and parallel capabilities is necessary, but not sufficient. It is still important to select key simplifications which render the analysis feasible without impairing its usefulness. Comparative studies of the relative importance of chemical reactions and reaction paths are a good example of such simplifications for flows of engineering interest [5].

Although a dramatic improvement in the knowledge of hypersonic phenomena has been achieved, there are many open questions and problems to be solved by the scientist and the engineer, before a satisfactory level of information is available and fully exploited. First, turbulence effects in very high-speed, high-temperature

flows are poorly understood [7]. Second, the definition of a translational temperature can become questionable. Third, simple asymptotic expansions for transport properties could seriously jeopardize the validity of flow simulations. Fourth, the *continuum* hypothesis, which will be maintained throughout the present work, is no longer sufficient to cover the entire range of applicability of hypersonic theory [8]. Fifth, wall catalysis must be better understood and should not be either ignored or considered to be unconditionally effective [9]. Lastly, shock tube, ballistic range and flight tests must be appropriately used to validate the numerical simulations, whenever possible.

The long term goal of this effort is to achieve an accurate numerical simulation of hypersonic flow fields. To this end, a few important steps have been completed, and will be fully detailed in the following sections. Very general, accurate and robust algorithms have been developed and published [6] as an essential basis for theoretical and numerical studies. Also, extensive physical investigations, mathematical analyses and efficiently-coded numerical computations of high velocity, high temperature fluid flows have been performed, using an approach that is flexible enough to be amended as soon as better results are available, yet is thorough enough to be used with some confidence. Alternative treatments, when existing, will be discussed, and justifications will be provided for all of the critical choices made. Many references will be made to recent work by scientists active in the area, and a critical analysis of their findings will be performed when relevant and necessary.

The essential core of this work is the extension and generalization of some classes of *flux-split* algorithms to flows beyond the chemical and thermal equilibrium régimes. These methods were originally developed for perfect gases (e.g., see the survey papers of Harten, Lax and Van Leer [10] and Roe [11]). They have produced accurate solutions of shock-wave dominated flows and have been successfully extended to flows in chemical equilibrium by many authors [12–22]. Their essential feature is the treatment of the convective terms in the Navier-Stokes equations using a characteristic-based differencing. In particular, only three types of approaches

will be discussed, namely the flux-vector splittings of Steger and Warming [23] and Van Leer [24], and the flux-difference splitting of Roe [25]. Extensions of these algorithms to chemically reacting flows have appeared in the literature [26–35], and some of them include thermodynamic non-equilibrium effects. The techniques developed as the main part of the present effort apply in a very broad range of physical conditions, including several different types of thermal non-equilibrium and virtually any type of finite-rate chemistry problems.

In some instances, one is confronted with the problem of flows where more than one translational temperature can be defined. This is the case of ionized plasmas, where the energy exchange between heavy particles and free electrons is not efficient enough, due to the disparity in molecular weight. Then, it is customary to assume that the mean-square thermal velocity for heavy particles gives rise to one translational temperature, whereas the mean-square thermal velocity for electrons will yield a second temperature [36]. At this stage, a translational temperature for the mixture cannot be rigorously defined, and the identification of translational temperature with thermodynamic temperature (a common procedure when linking microscopic and macroscopic approaches) is not possible. Some approximate approaches have been devised for this kind of flows [37–40], but in general they do not consider the implications of having a translational temperature that is ill-defined. In the present study, it will be shown that even an approximate analysis can yield some unusual results when dealing with this class of problems.

In the following, the mathematical foundations necessary for the study of flows out of chemical and thermal equilibrium will be presented, and general governing partial differential equations will be written, which model physical phenomena such as momentum, mass and energy transport. This general derivation has been carried out for completeness, so that the numerical algorithms developed can begin to be applied to meaningful physical situations and comparisons with experiments performed. However, the rigorous treatment of viscous fluxes and the modeling of mass, momentum and energy transport are still beyond the scope of the present

work. Some provisional results will be presented, for the most part equivalent to what is found in the most recent literature [9],[41], but the author must beg for forgiveness for the unavoidable unbalance between detailed derivations of results for the inviscid aspects of the flows and crude statements of approximate results and semi-empirical rules for the viscous features. It should be noticed here that even the linearized Chapman-Enskog theory for mixtures of gases with internal degrees of freedom has not been fully utilized at the present stage. The problem of viscosity in the presence of non-equilibrium thermodynamics is another open field with relatively few attempts of solution [26],[27]. It is not clear whether semi-empirical treatments will be accurate enough for these physical conditions. Further studies will be necessary to shed some light in this matter.

Another important aspect of the simulation presented here is the modeling of source terms due to finite-rate chemistry and thermal non-equilibrium. Only homogeneous chemical reactions will be presented, and hardly anything will be said about catalytic or photochemical reactions. A simple Landau-Teller-type vibrational relaxation of molecules [2] will be employed to model thermal non-equilibrium. Many improvements have been proposed in the past [42],[43], and recently [44–46], and a few of them try to incorporate some of the physics of internal degree-of-freedom energy exchanges, while accepting empirical corrections. Once again, nothing final has been said in this subject, and the model presented here is just an attempt to capture some of the physics involved, while remaining at a very simple and straightforward level.

The subject matter of this work will be organized in the following way. In Chapter 2, the influence of high-temperature, high-velocity effects on the thermodynamic behaviour of mixtures of chemical species will be examined, and significant departures from the predictions of simplified models such as the perfect gas assumption will be accounted for with more sophisticated approaches, including non-equilibrium, multiple-temperature predictions. In Chapter 3, the governing partial differential equations for viscous, heat-conducting flows which are out of

chemical and thermal equilibrium will be derived assuming weakly interacting particles in a continuous medium. Alternative formulations and simplified results will be given, including an integral form and a quasi-one-dimensional approximation, respectively. In Chapter 4, the treatment of chemical kinetics in homogeneous media and the modeling of thermal non-equilibrium will be discussed, with specific examples selected from the available literature for dissociating and ionizing air, hydrogen reacting in air and a simple Argon-based plasma. In Chapter 5, some introductory considerations on the treatment of viscous fluxes and transport properties will be presented. In Chapter 6, the mathematical and physical complications that arise when free electrons are assumed to have a different translational temperature than the heavy particles will be presented, and a consistent simplified approach is developed. The analysis yields new results for the characteristic velocities of propagation of sonic disturbances, and the essential gasdynamic properties of flows with multiple translational temperatures will be established. In Chapter 7, a finite-volume discretization of the governing equations in integral form will be discussed. New flux-split algorithms for the treatment of chemically and thermally active flows will be derived, which yield very accurate and efficient results when used for the numerical prediction of these physically complicated flows. Efficient techniques for time-accurate or steady-state calculations will be utilized in a fully-coupled, implicit integration. In Chapter 8, an extensive set of numerical simulations, performed in one and two space dimensions, will be analyzed. The effects of different chemical and thermal assumptions on the behaviour of several mixtures of gases will be investigated, resulting in a strong dependence of the flow properties upon the level of sophistication of the physical models selected. Finally, Chapter 9 will provide the reader with a summary of the material discussed and a set of conclusions, some of which will necessarily be provisional in nature at this time.

2. THERMODYNAMIC MODELS

2.1 Introduction

In the hypersonic régime, very high temperatures can be reached when the flow is decelerated, namely through shock waves and in shear layers. In these conditions, departures from the perfect gas assumption occur, originated by the onset of chemical reactions which lead to dissociation of molecules and ionization of neutral species. Also, the molecular vibrational states, which are neglected in perfect gases, can become excited. Their de-excitation typically requires a few hundred particle collisions and a time that is comparable to the flow time. Consequently, a finite-rate process has to be considered instead of an instantaneous return to equilibrium. In the boundary layer near solid walls or in a shock wave, the gradient of physical properties becomes drastic enough as to create translational and rotational non-equilibrium phenomena, such as viscous stresses, heat conduction and mass diffusion [3].

It is customary, when dealing with these phenomena, to assume that state variables can be defined, their mutual relationships being described by equations that are identical in form to the corresponding equations for equilibrium [2]. This assumption has been confirmed by experience when only chemical non-equilibrium is present, but it could be invalid if more complex physical situations are considered. Also, it is commonly assumed that the rate equations derived by theoretical or experimental consideration of non-equilibrium in a gas *at rest* apply to the moving fluid whenever the instantaneous state is the same. Other *quasi-equilibrium* hypothesis are common in related sectors of this field, such as the study of radiative transfer [47]. Their validity could be questionable for extreme cases, but the complications of more general approaches often leave the scientist with little choice.

In the following, an equation defining the internal energy for a species in a mixture of reacting gases will be presented, and the equation of state, relating pressure to internal energy of the mixture through one or more temperatures, will

follow. The frozen speed of sound for a gas in chemical and thermal non-equilibrium will be derived, and some of the complications which arise when the translational temperature is not defined will be examined. Finally, the specific thermodynamic models which will be used in our numerical simulations will be discussed.

2.2 Internal Energy

A general description for the internal energy per unit mass of a gaseous species in a mixture of other species chemically reacting and out of thermal equilibrium can be given by the following [31],[32]

$$e_i = \tilde{e}_i(T) + e_{e_i}(T_e) + e_{n_i}(\mathbf{x}, t), \tag{2.1}$$

where $\tilde{e}_i$ is the known portion of the internal energy in equilibrium at the translational temperature of heavy particles T, e_{e_i} is the known portion in equilibrium at the electron temperature T_e, and e_{n_i} is a portion out of thermal equilibrium, that has to be evaluated as a function of position and time. Appropriate rate equations will describe the energy interchange between these portions, in particular the tendency of e_{e_i} and e_{n_i} to reach equilibrium at the translational temperature T and their mutual interaction. The portion e_{n_i} generally represents the vibrational contribution to the internal energy of molecules, but the present analysis is valid for any fraction out of equilibrium. The term e_{e_i} generally represents the electronic contribution to the internal energy of heavy particles, as well as the *translational* energy of free electrons. No obstacles are assumed to exist for the interaction of bound and free electrons. In particular, the internal energy of free electrons will read

$$e_e = e_{e_e}(T_e) = \frac{3}{2} R_e T_e, \qquad \tilde{e}_e = e_{n_e} \equiv 0, \tag{2.2a,b}$$

where the gas constant R_e for the free electrons has been introduced. In general, the gas constant for any species may be written as

$$R_i = \frac{\hat{R}}{M_i}, \tag{2.3}$$

with $\hat{R}$ being the universal gas constant and $\mathcal{M}_i$ the species molecular mass.

It should be noticed that the additivity of the different contributions to the internal energy is a simplification of the more general statistical mechanics result that translational and internal structure contribution can be added. The breaking of the internal structure in summable portions is not always justifiable [48],[49]. However, this assumption allows a fairly simple treatment of thermal non-equilibrium processes.

There is always a certain degree of arbitrariness in the assumption that a specific contribution to the internal energy is in equilibrium at a certain temperature or in non-equilibrium. Specifically, the idea of a common electronic temperature for free and bound electrons does not seem to be entirely satisfactory. However, for most practical purposes, the contribution of bound electrons to the internal energy is very small, and has been neglected in the non-equilibrium model discussed in §2.5.

A more subtle problem arises when translational non-equilibrium is present. In this case, the translational temperature of a species is defined using the mean-square thermal or *peculiar* velocity and it is assumed that all of the heavy particles are at the same temperature. When no free electrons are present, or when they are treated as a generic monatomic species at the same translational temperature, then microscopic and macroscopic quantities can be linked together in a direct way and the thermodynamic temperature is identified with this translational temperature. However, for the general case, the thermodynamic temperature is ill-defined and extreme care must be taken in the definition of physical properties.

The presence of rotational non-equilibrium is found to be the reason for the appearance of *bulk* viscosity, whereby Stoke's hypothesis is no longer valid [2]. This effect is usually neglected, and so will it be in the following.

It is convenient to express $\tilde{e}_i$ in terms of a specific heat as

$$\tilde{e}_i = \int_{T_{ref}}^{T} \tilde{c}_{v_i}(\tau)\, d\tau + h_{f_i}\,, \tag{2.4}$$

where $\tilde{c}_{v_i} = d\tilde{e}_i/dT$ is the specific heat at constant volume, and h_{f_i} is the heat of formation of species i at $T = T_{ref}$. Similarly, e_{e_i} can be written in terms of specific heats as

$$e_{e_i} = \int_0^{T_e} c_{v_{e,i}}(\tau)\, d\tau. \tag{2.5}$$

Now, a gas mixture composed of N species, with the first M species assumed to contain a non-equilibrium portion of their internal energy, will be considered. The N-th species is the free electrons. The internal energy per unit mass of the mixture may then be written as

$$e = \sum_{i=1}^{N} \frac{\rho_i}{\rho} e_i = \tilde{e} + \sum_{i=1}^{N} \frac{\rho_i}{\rho} e_{e_i} + \sum_{i=1}^{M} \frac{\rho_i}{\rho} e_{n_i}\,, \tag{2.6}$$

where the definition of reduced specific internal energy has been introduced

$$\tilde{e} \equiv \sum_{i=1}^{N} \frac{\rho_i}{\rho} \tilde{e}_i = \sum_{i=1}^{N-1} \frac{\rho_i}{\rho} \tilde{e}_i\,. \tag{2.7}$$

In the above, ρ_i is the species density, and ρ the mixture density, defined as

$$\rho = \sum_{i=1}^{N} \rho_i. \tag{2.8}$$

It is convenient to define the reduced specific heats of the mixture as

$$\tilde{c}_v \equiv \sum_{i=1}^{N} \frac{\rho_i}{\rho} \tilde{c}_{v_i} = \sum_{i=1}^{N-1} \frac{\rho_i}{\rho} \tilde{c}_{v_i}, \qquad \tilde{c}_p \equiv \sum_{i=1}^{N} \frac{\rho_i}{\rho} \tilde{c}_{p_i} = \sum_{i=1}^{N-1} \frac{\rho_i}{\rho} \tilde{c}_{p_i}\,. \tag{2.9a,b}$$

Also, it is possible to define a heavy-particle gas constant as

$$\tilde{R} \equiv \sum_{i=1}^{N-1} \frac{\rho_i}{\rho} R_i = \tilde{c}_p - \tilde{c}_v\,, \tag{2.10}$$

and a heavy-particle electronic specific heat at constant volume

$$\tilde{c}_{v_e} \equiv \sum_{i=1}^{N-1} \frac{\rho_i}{\rho} c_{v_{e,i}}\,. \tag{2.11}$$

Finally, a quantity that will play an important role in our model is the ratio of the mixture specific heats,

$$\tilde{\gamma} \equiv \frac{\tilde{c}_p}{\tilde{c}_v}. \tag{2.12}$$

The definition of internal energy presented so far includes, as special cases, simpler models that can be useful in some instances. When electronic excitation and free electrons are considered to be in equilibrium at the heavy species temperature, the e_{e_i} terms drop from eqs.(2.1) and (2.6). At this stage, the gas mixture can be thought of as composed of $N^* = N - 1$ species, and all of the results that will be presented for the general case will be applicable to this model upon neglecting the N-th species equations. Free electrons, if present, will be considered as one of the species, and no particular treatment will be required. The electronic contribution to the internal energy will be included in the general expression for $\tilde{c}_{v_i}$.

Other models have been proposed [45], where only a global vibrational-electronic contribution to the mixture internal energy is considered. Results obtained in the present work can be easily specialized to those models.

A further simplification is possible by dropping the non-equilibrium contributions e_{n_i}. Then, a general mixture in thermal equilibrium can be considered, with any possible contributions to the internal energy being included in the $\tilde{c}_{v_i}$ terms. Very sophisticated models could be used in this instance [50], taking into account the interactions between internal states of a molecule and non-harmonic effects [51]. An even simpler model will ensue when only translational and rotational contributions are included in the species $\tilde{e}_i$, the perfect gas model resulting when only a mixture of diatomic molecules is examined.

2.3 Equation of State

A very important assumption that has been made in the preceding section is the consideration of *weakly interacting* particles, where the interaction potential is decaying very rapidly in space and is negligible after a typical distance of the order of the particle radius. The simplest model for such a potential is the *rigid sphere*

model, where only elastic collisions are considered. More refined models, such as that due to Lennard-Jones [52], yield different results as far as transport properties are concerned, but are still characterized by rapidly decaying potentials.

The most noticeable effect of this assumption is that the mixture components will behave as *thermally perfect* gases, where the internal energy is only function of temperature. Strictly related to this result is the validity of Dalton's Law, whereby the mixture pressure is the summation of partial pressures. The applicability of the weak-interaction assumption is restricted to conditions of low density and moderate to high temperature. However, most hypersonic flows meet these requirements. Therefore, no attempt will be made of considering more sophisticated interaction models, nor any *virial coefficient* correction will be introduced [53].

Consequently, the relationship between pressure and temperature will read

$$p = \sum_{i=1}^{N} p_i = \sum_{i=1}^{N-1} \rho_i R_i T + \rho_e R_e T_e = \rho \tilde{R} T + \rho_e R_e T_e. \tag{2.13}$$

In the following, a relationship between pressure and internal energy will be needed. It can be obtained implicitly through the temperatures, where use is made of the definition of internal energy, eq.(2.6), in terms of its components, eqs.(2.4), (2.5)

$$\rho e = \sum_{i=1}^{N^*} \rho_i \Big(\int_{T_{ref}}^{T} \tilde{c}_{v_i}(\tau)\, d\tau + h_{f_i} \Big) + \sum_{i=1}^{M} \rho_i e_{n_i} + \rho_e e_{e_e} + \sum_{i=1}^{N^*} \rho_i \int_{0}^{T_e} \tilde{c}_{v_{e,i}}(\tau)\, d\tau. \tag{2.14}$$

In the general case, iterative techniques are required to recover the value of T from known e, e_{e_e}, ρ_i, e_{n_i}, with the pressure determined from eq.(2.13). No iterations are necessary for T_e, because of the linearity of the relationship between e_{e_e} and T_e, found in eq.(2.2a). Newton's method has been used in the calculations, and was proven to be very efficient, with two to four iterations necessary for an accuracy of seven significant figures. However, specific models where the nonlinearity in T has been removed, and consequently no iterations are necessary, could be considered attractive for many practical situations. Physically, this will amount to considering only translational and rotational contributions in $\tilde{c}_i$, with vibrational and coupling effects neglected or included in the non-equilibrium portion [6].

2.4 Speed of Sound

The speed of sound plays a major role in the flux-split algorithms that will be discussed later. However, in the case of multiple translational temperatures, thermodynamic considerations that lead to the definition of a speed of sound are no longer applicable. In the following, the results for models with only one temperature will be discussed, and some problems that arise when the more general model is utilized will be examined. The appropriate speed of sound for the single translational temperature model is the frozen speed of sound, defined as

$$a^2 \equiv \left(\frac{\partial p}{\partial \rho}\right)_{s,\, \rho_i/\rho,\, e_{n_i}}, \tag{2.15}$$

where s is the entropy per unit mass. From the definitions of pressure, eq.(2.13), and internal energy, eq.(2.6), with the second terms dropped in their right hand sides, we see that $p = p(\rho, \rho_i/\rho, T)$, and that $e = e(\rho_i/\rho, e_{n_i}, T)$, the latter relationship providing an implicit definition for T. Then we can express

$$a^2 = \left(\frac{\partial p}{\partial \rho}\right)_{e,\, \rho_i/\rho,\, e_{n_i}} + \left(\frac{\partial p}{\partial e}\right)_{\rho,\, \rho_i/\rho,\, e_{n_i}} \left(\frac{\partial e}{\partial \rho}\right)_{s,\, \rho_i/\rho,\, e_{n_i}}, \tag{2.16}$$

the last of these derivatives being obtained utilizing the First Law of Thermodynamics, whereby

$$\left(\frac{\partial e}{\partial \rho}\right)_{s,\, \rho_i/\rho,\, e_{n_i}} = \frac{p}{\rho^2}. \tag{2.17}$$

The two remaining pressure derivatives in eq.(2.16) may be evaluated as

$$\left(\frac{\partial p}{\partial \rho}\right)_{e,\, \rho_i/\rho,\, e_{n_i}} = \tilde{R}T, \tag{2.18a}$$

and

$$\left(\frac{\partial p}{\partial e}\right)_{\rho,\, \rho_i/\rho,\, e_{n_i}} = \rho\tilde{R}\left(\frac{\partial T}{\partial e}\right)_{\rho_i/\rho,\, e_{n_i}}, \tag{2.18b}$$

where the temperature derivative may be found from a simplified form of the equation of state, eq.(2.14), and reads

$$\left(\frac{\partial T}{\partial e}\right)_{\rho_i/\rho,\, e_{n_i}} = \frac{1}{\tilde{c}_v}. \tag{2.19}$$

Upon substitution, we find the interesting result

$$a^2 = \tilde{\gamma}\tilde{R}T = \tilde{\gamma}\left(\frac{p}{\rho}\right), \tag{2.20}$$

which is not approximate, but corresponds to the frozen speed of sound for this chemically reacting, non-equilibrium flow. Note that the $\tilde{\gamma}$ appearing here is the ratio of specific heats corresponding to the equilibrium portion of the internal energy, defined in eq.(2.12). Also, an equivalent expression is given in Clarke and McChesney [54].

For the general model with two translational temperatures, it is possible to define both a frozen speed of sound with the electron temperature kept frozen, and a frozen speed of sound with the heavy-particle temperature kept frozen. Both definitions are based upon a generalized formula for the combined First and Second Law of Thermodynamics. The species differential entropy ds_i is written as

$$ds_i = d\tilde{s}_i + ds_{e_i} + ds_{n_i}, \tag{2.21a}$$

where the different contributions to the internal energy can be easily recognized, and are

$$T d\tilde{s}_i = d\tilde{e}_i + p_i d\left(\frac{1}{\rho_i}\right), \tag{2.21b}$$

$$T_e ds_{e_i} = de_{e_i}, \qquad i \neq N, \tag{2.21c}$$

$$T_e ds_{e_e} = de_e + p_e d\left(\frac{1}{\rho_e}\right), \tag{2.21d}$$

$$T_{n_i} ds_{n_i} = de_{n_i}, \tag{2.21e}$$

where T_{n_i} is the non-equilibrium species temperature. The total differential entropy ds will be defined as

$$ds \equiv \sum_{i=1}^{N} \frac{\rho_i}{\rho} ds_i. \tag{2.22}$$

Upon substitution of eqs.(2.21) into eq.(2.22) and some manipulations, the final result is obtained

$$Tds = de + \left[p + (\frac{T}{T_e} - 1)p_e\right]d(\frac{1}{\rho}) + (\frac{T}{T_e} - 1)(\tilde{c}_{v_e} + \frac{\rho_e c_{v_{e,e}}}{\rho})dT_e + \\ + \sum_{i=1}^{M}(\frac{T}{T_{n_i}} - 1)\frac{\rho_i}{\rho}de_{n_i} - \sum_{i=1}^{N} g_i d(\frac{\rho_i}{\rho}) - (\frac{T}{T_e} - 1)\frac{p_e}{\rho_e}d(\frac{\rho_e}{\rho}), \qquad (2.23)$$

where g_i is the species chemical potential (Gibb's free energy). Neglecting the electronic contributions yields the usual formula for the combined First and Second Law, and that was the basis for the derivation of the frozen speed of sound for a single translational temperature, eq.(2.20).

A speed of sound based upon freezing the electron translational temperature can now be evaluated as follows

$$a^2 = (\frac{\partial p}{\partial \rho})_{e,\rho_i/\rho,e_{n_i},T_e} + (\frac{\partial p}{\partial e})_{\rho,\rho_i/\rho,e_{n_i},T_e}(\frac{\partial e}{\partial \rho})_{s,\rho_i/\rho,e_{n_i},T_e} \qquad (2.24)$$

with

$$(\frac{\partial e}{\partial \rho})_{s,\rho_i/\rho,e_{n_i},T_e} = \frac{p}{\rho^2} + (\frac{T}{T_e} - 1)\frac{p_e}{\rho^2}. \qquad (2.25)$$

The final result is

$$a^2 = \tilde{\gamma}(\frac{p}{\rho}) + (\tilde{\gamma} - 1)(\frac{T}{T_e} - 1)\frac{p_e}{\rho}, \qquad (2.26)$$

which can also be written as follows

$$a^2 = \tilde{\gamma}(\frac{p - p_e}{\rho}) + \left[1 + \frac{T}{T_e}(\tilde{\gamma} - 1)\right]\frac{p_e}{\rho}. \qquad (2.27)$$

These formulas reduce to eq.(2.20) when the electronic contributions are neglected or if $T \equiv T_e$, with $\tilde{\gamma}$ including only contributions at the temperature T.

A similar expression can be obtained for the speed of sound with the heavy-particle temperature kept frozen. Defining a ratio of specific heats in equilibrium at the electron temperature T_e

$$\gamma_e = 1 + \frac{\rho_e R_e}{\rho\tilde{c}_{v_e} + \rho_e c_{v_{e,e}}}, \qquad (2.28)$$

the final result is obtained

$$a^2 = \tilde{\gamma}_e\left(\frac{p_e}{\rho}\right) + \left[1 + \frac{T_e}{T}(\tilde{\gamma}_e - 1)\right]\frac{p - p_e}{\rho}. \tag{2.29}$$

In this instance, when $T \equiv T_e$, the reduced form reads

$$a^2 = \tilde{\gamma}_e \frac{p}{\rho}. \tag{2.30}$$

It will be shown in the following that neither one of these speeds of sound is sufficient for a description of the mathematical behaviour of the governing partial differential equations. However, when an asymptotic analysis is attempted in §6, the relevant quantity to be considered will turn out to be a first-order approximation of the speed of sound based upon freezing the electronic temperature. The reason is that the approximate analysis will be based upon neglecting some of the effects of the electronic temperature, whereby the heavy-species translational temperature will become once again the essential translational temperature.

2.5 Practical Models

Three different thermodynamic models will be included in the numerical simulations. The first one groups translational and rotational contributions in $\tilde{e}_i$, thus considering them in equilibrium at the heavy-particle temperature T

$$\tilde{e}_i = n_i R_i T + h_{f_i}, \qquad i = 1, \ldots, N-1\,(N^*). \tag{2.31}$$

In eq.(2.31), the constants n_i are given by

$$n_i = \begin{cases} \frac{3}{2} & \text{for atoms,} \\ \frac{5}{2} & \text{for diatomic and linear polyatomic molecules,} \\ \frac{6}{2} & \text{for nonlinear polyatomic molecules.} \end{cases} \tag{2.32}$$

Vibrational contributions are supposed to be in non-equilibrium, $e_{n_i} = e_{vib_i}$, and free electrons are either considered in equilibrium at the temperature T_e or lumped together with the heavy particles when only one translational temperature is used.

Electronic excitation of atoms and molecules is neglected. In the following, this model will be referred to as Simplified Vibrational Non-Equilibrium Model.

It should be pointed out again that the previous non-equilibrium model is a specific simple application, and more refined models can be easily supported within the framework of the present approach.

The second model utilized in the simulation is a thermal equilibrium model, whereby $e_{n_i} \equiv 0$ and vibrational contributions are included in $\tilde{e}_i$ by means of a simple harmonic oscillator formula [55]

$$\tilde{e}_i = n_i R_i T + \frac{R_i \Theta_{v,i}}{e^{\Theta_{v,i}/T} - 1} + h_{f_i}, \qquad i = 1, \ldots, N^*, \tag{2.33}$$

where $\Theta_{v,i}$ are characteristic vibrational temperatures. More than one of such temperatures are found in polyatomic molecules (e.g., Strehlow [56] presents a model for water where three temperatures are sufficient for a good representation of its thermodynamic behaviour). Free electrons, if present, are considered to be in equilibrium at the only translational temperature T defined. In the following, this model will be referred to as Vibrational Equilibrium Model.

The third model is again a thermal equilibrium model ($e_{n_i} \equiv 0$), but fourth-order polynomials [57] are used to curve fit $\tilde{c}_{v_i}$

$$\tilde{e}_i = a_0 + \int_0^T \tilde{c}_{v_i}(\tau) d\tau, \qquad \tilde{c}_{v_i} = a_1 + a_2 T + a_3 T^2 + a_4 T^3 + a_5 T^4, \qquad i = 1, \ldots, N^*. \tag{2.34}$$

Many coupling and non-harmonic effects have been introduced in the previous curve fits, but the coefficients are valid in a range of temperatures, usually up to $5,000\ K$, and this turns out to be a serious limitation to their practical use. However, the methodology is not affected by these practical considerations, and as soon as improved curve fits become available, they could be implemented in a straightforward manner. In the following, this model will be referred to as Curve Fit Model.

Finally, more specialized models such as gases with no vibrational contributions and perfect gases are included in any of the thermal equilibrium models as particular cases.

3. GOVERNING EQUATIONS

3.1 Introduction

The governing partial differential equations for a mixture of gases out of chemical and thermal equilibrium can be derived by means of non-equilibrium kinetic theory [1],[3]. The basic assumptions for such a derivation are :

i) the particles are weakly interacting and the intermolecular forces can be neglected after a characteristic distance of the order of the particle radius. Consequently, every component of the mixture will behave as a *thermally perfect* gas;

ii) the particle radius is small compared with the mean-free path, therefore the density is low enough that only two-body (binary) collisions need to be taken into account;

iii) there is no correlation of the velocities of two particles in a binary collision (molecular chaos);

iv) the distribution function does not vary appreciably over a distance of the order of the range of intermolecular forces or a time comparable to the duration of a collision. Therefore, the Boltzmann equation for the rate of change of the species distribution function is *valid* [2].

Every species will have a distribution function f_s that for this general case will be a function of molecular velocity $\mathbf{c}'_s$, position $\mathbf{x}$, and time, or $f_s = f_s(\mathbf{c}'_s, \mathbf{x}, t)$. The mean value of a generic quantity ψ in the velocity space is usually referred to as a moment of the distribution function, and will play an important role in the derivation. It is given by

$$<\psi(\mathbf{x}, t)> = \int_{-\infty}^{+\infty}\int_{-\infty}^{+\infty}\int_{-\infty}^{+\infty} \psi(\mathbf{c}'_s, \mathbf{x}, t) f_s(\mathbf{c}'_s, \mathbf{x}, t) dc_1 dc_2 dc_3 . \qquad (3.1)$$

Other key quantities to be defined are the species mean velocities and the mass-averaged mixture velocity. They will be written as

$$\mathbf{u}_s = <\mathbf{u}'_s>, \qquad \rho \mathbf{u}_0 = \sum_{s=1}^{N} \rho_s \mathbf{u}_s, \qquad (3.2a, b)$$

where u'_s is the particle velocity. It is useful to rewrite u_s and u'_s as follows

$$u_s = u_0 + V_s, \qquad u'_s = u_0 + c'_s, \tag{3.3a,b}$$

where V_s is the *diffusion* velocity and c'_s is the *thermal* velocity. From the definitions above, the important relationships can be obtained

$$V_s = <c'_s>, \qquad \sum_{s=1}^{N} \rho_s V_s \equiv 0. \tag{3.4a,b}$$

It is noteworthy that the mean value of the thermal velocity is *not* identically zero, but is equal to the diffusion velocity. The reason for this is that the mass-averaged velocity has been utilized as a reference velocity. A different thermal velocity could have been defined by writing

$$u'_s = u_s + c''_s, \qquad <c''_s> \equiv 0, \tag{3.5a,b}$$

as done by Candler and MacCormack [26],[27] and partly by Lee [1]. The link between the two different definitions of thermal velocity is given by using eqs.(3.3b), (3.5a) and (3.3a)

$$c'_s = V_s + c''_s . \tag{3.6}$$

It can be noticed that the distinction between species mean velocity and mass-averaged mean velocity is brought about by translational non-equilibrium. Whenever viscosity, thermal conductivity and *diffusion* phenomena are neglected, the diffusion velocities will be identically zero and all of the species will have an identical $u_s \equiv u_0$.

Integration of Boltzmann's equation over the velocity space and some algebra yield a general equation of transfer for a species

$$\frac{\partial(n_s <\psi_s>)}{\partial t} + \nabla \cdot (n_s <u'_s \psi_s>) = I(<\psi_s>), \tag{3.7}$$

where n_s is the species number density and the *source* term $I(<\psi_s>)$ represents the contribution of external forces, interactions among different species and within the species, and production of the quantity ψ_s.

This equation will be the base for the derivation of the governing partial differential equations, as shown in the next section. These equations will be the extension of Navier-Stokes equations, usually derived for a perfect gas, to a mixture of gases out of chemical and thermal equilibrium. After presenting some considerations on the basic modeling of viscous terms, reduction of these equations to more specific and simpler cases will be discussed, including Thin-Layer Navier-Stokes and Euler equations for situations where some or all of the non-equilibrium effects can be neglected. An analysis of the transformation of the same equations to generalized, nonorthogonal, *structured* coordinate systems will precede a formulation in integral form, more useful when a finite-volume discretization is sought and rigorously valid in presence of shock waves. Finally, Appendix 2 will provide the reader with the inviscid flux Jacobians, and Appendix 3 will deal with the problem of finding eigenvalues and eigenvectors for those Jacobians. Approximate compatibility relationships that hold along characteristic lines will be given in Appendix 4.

3.2 Navier-Stokes Equations

The general equation of transfer for a species, eq.(3.7), can be specialized to yield continuity, momentum and energy equations, when specific values are assigned to the quantity ψ_s. Global conservation equations for the mixture can be obtained by direct summation over all of the components, and many simplifications will occur because of the disappearance of interaction terms. For a similar treatment of governing equations, the reader is referred to Lee [1] and Appleton and Bray [36]. An exhaustive analysis of non-equilibrium kinetic theory is found in Hirschfelder, Curtiss and Bird [3].

The species continuity equation can be written when $\psi_s = m_s$, the mass of a particle of species s. Then

$$n_s <m_s>= \rho_s, \qquad n_s <m_s u'_s>= \rho_s u_s, \qquad I(<m_s>) = w_s, \qquad (3.8a,b,c)$$

where ρ_s is the species density and w_s is the source contribution due to chemical reactions, that will be discussed in §4.1. Using the relationship between species, mass-averaged and diffusion velocities, eq.(3.3a), the final result is

$$\frac{\partial \rho_s}{\partial t} + \nabla \cdot (\rho_s \boldsymbol{u}_0) + \nabla \cdot (\rho_s \boldsymbol{V}_s) = w_s \,. \tag{3.9}$$

The same equation would have been derived using the second definition of thermal velocity, as discussed in §3.1.

It is possible to write the mixture continuity equation by simply adding the species contributions. Using the definition of density, eq.(2.8), the fact that the mass-averaged sum of diffusion velocity is zero, eq.(3.4b), and the useful result that the chemical interaction terms among species must cancel with each other, that is

$$\sum_{s=1}^{N} w_s \equiv 0, \tag{3.10}$$

the simple form is obtained

$$\frac{\partial \rho}{\partial t} + \nabla \cdot (\rho \boldsymbol{u}_0) = 0. \tag{3.11}$$

A similar procedure will be used for the derivation of the species momentum equation. In this case $\psi_s = m_s u'_s$ and

$$n_s <m_s u'_s>= \rho_s u_s, \qquad I(<m_s u'_s>) = \rho_s \mathbf{g}_s + (\boldsymbol{F}_s)_E + (\boldsymbol{F}_s)_I \,, \tag{3.12a,b}$$

where $\mathbf{g}_s$ is the body force, $(\boldsymbol{F}_s)_E$ the elastic interaction force, and $(\boldsymbol{F}_s)_I$ the inelastic interaction force, all acting on species s. The divergence term can be written as

$$n_s <m_s u'_s u'_s>= \rho_s <u'_s u'_s>= \boldsymbol{u}_0 \boldsymbol{u}_0 + \boldsymbol{u}_0 \boldsymbol{V}_s + \boldsymbol{V}_s \boldsymbol{u}_0 + <c'_s c'_s>, \tag{3.13}$$

where the *thermal* tensor $<c'_s c'_s>$ is usually identified with the *stress* tensor. The latter is written as the negative of a *shear stress* tensor plus the pressure contribution

$$\rho_s <c'_s c'_s>= -\mathbf{T}_s + p_s \mathbf{I}, \qquad p_s = \frac{\rho_s(<c'^2_{s_1}> + <c'^2_{s_2}> + <c'^2_{s_3}>)}{3}, \tag{3.14a,b}$$

where a *kinetic* definition of species temperature can be recovered if eq.(3.14b) is written

$$p_s = \rho_s R_s T_s, \tag{3.15a}$$

which yields

$$T_s = \frac{M_s \langle c_s''^2 \rangle}{3\hat{R}}. \tag{3.15b}$$

The final result reads

$$\frac{\partial \rho_s u_s}{\partial t} + \nabla\cdot(\rho_s u_0 u_0 + p_s \mathbf{I}) + \nabla\cdot(\rho_s V_s u_0) + \nabla\cdot(\rho_s u_0 V_s) - \nabla\cdot\mathbf{T}_s = \rho_s \mathbf{g}_s + (\boldsymbol{F}_s)_E + (\boldsymbol{F}_s)_I . \tag{3.16}$$

It should be noted that the second definition of thermal velocity, eq.(3.5a), allows the thermal tensor to be written in a different way

$$\langle c_s' c_s' \rangle = V_s V_s + \langle c_s'' c_s'' \rangle, \tag{3.17}$$

where use has been made of the relationship between the two definitions, eq.(3.6). Some authors [26],[27] identify $\langle c_s'' c_s'' \rangle$, not the full thermal tensor, with the stress tensor. Although this could seem to be a more meaningful approach, because only contributions whose statistical average is zero enter the definition of partial pressure and temperature, it is *not* the original formulation of the theory as reported in Vincenti and Kruger [2] or Hirschfelder, Curtiss and Bird [3]. The real problem, however, is that in *both* approaches the shear stress tensor is modeled using the *same* coefficient of viscosity and the assumption of Newtonian fluids. Since the theoretical derivation of expressions for viscosity and thermal conductivity in terms of asymptotic expansions is based on the original theory, the formulation that stems from eq.(3.14a) will be consistently followed in the present work.

The mixture momentum equation can then be derived by summing the species contributions. Elastic and inelastic interaction forces add up to zero, diffusion

velocities disappear again, partial pressures and strains add up to the mixture values (Dalton's Law for partial pressures)

$$\sum_{s=1}^{N} (\boldsymbol{F}_s)_E = \sum_{s=1}^{N} (\boldsymbol{F}_s)_I \equiv 0, \qquad \sum_{s=1}^{N} p_s = p, \qquad \sum_{s=1}^{N} \mathbf{T}_s = \mathbf{T}, \qquad (3.18a,b,c)$$

and using the definitions of mixture density, eq.(2.8), and mass-averaged velocity, eq.(3.2b), yields

$$\frac{\partial \rho \boldsymbol{u}_0}{\partial t} + \nabla \cdot (\rho \boldsymbol{u}_0 \boldsymbol{u}_0 + p\mathbf{I}) - \nabla \cdot \mathbf{T} = \sum_{s=1}^{N} \rho_s \mathbf{g}_s \,. \qquad (3.19)$$

The species energy equation can be recovered by letting ψ_s to be

$$\psi_s = m_s\left(\frac{u''^2}{2} + \epsilon'_{int_s}\right), \qquad \epsilon'_{int_s} = \tilde{\epsilon}'_s(T) + e'_{e_s}(T_e) + e'_{n_s}, \qquad (3.20a,b)$$

where ϵ'_{int} is the contribution to the energy from the *internal* structure of the particle, written in agreement with the thermodynamic model discussed in §2.2. Therefore, the translational energy is not included in $\tilde{\epsilon}'_s$ (or in e'_{e_s} for free electrons). Using the relationship between particle, mass-averaged and thermal velocities, eq.(3.3b), it is possible to rewrite eq.(3.20a) as follows

$$\psi_s = m_s\left(\frac{u_0^2}{2} + \boldsymbol{u}_0 \cdot \boldsymbol{c}'_s + e'_s\right), \qquad e'_s = \frac{c''^2_s}{2} + \tilde{\epsilon}'_s(T) + e'_{e_s}(T_e) + e'_{n_s}, \qquad (3.21a,b)$$

where e'_s is now the internal energy of the particle of species s. Averaging yields

$$n_s <\psi_s> = \rho_s\left(\frac{u_0^2}{2} + \boldsymbol{u}_0 \cdot \boldsymbol{V}_s + e_s\right) = \rho_s(e_{0_s} + \boldsymbol{u}_0 \cdot \boldsymbol{V}_s), \qquad e_{0_s} = e_s + \frac{u_0^2}{2}. \quad (3.22a,b)$$

The flux term can be written as

$$n_s <\psi_s \boldsymbol{u}'_s> = \rho_s(e_{0_s} + \boldsymbol{u}_0 \cdot \boldsymbol{V}_s)\boldsymbol{u}_0 + \frac{u_0^2}{2}\boldsymbol{V}_s + \rho_s <e'_s \boldsymbol{c}'_s> + \rho_s <(\boldsymbol{u}_0 \cdot \boldsymbol{c}'_s)\boldsymbol{c}'_s>, \quad (3.23)$$

where $\rho_s <(\boldsymbol{u}_0 \cdot \boldsymbol{c}'_s)\boldsymbol{c}'_s>$ can be written as

$$\rho_s <(\boldsymbol{u}_0 \cdot \boldsymbol{c}'_s)\boldsymbol{c}'_s> = -\boldsymbol{u}_0 \cdot \mathbf{T}_s + \boldsymbol{u}_0 \cdot p_s\mathbf{I}, \qquad (3.24)$$

and $\rho_s <e'_s c'_s>$ is defined to be the *heat flux* vector q_s. The source term becomes

$$I(<\psi_s>) = \rho_s <\mathbf{g}'_s \cdot \boldsymbol{u}'_s> + (\dot{Q}_s)_E + (\dot{Q}_s)_I = \rho_s \mathbf{g}_s \cdot \boldsymbol{u}_s + (\dot{Q}_s)_E + (\dot{Q}_s)_I , \quad (3.25)$$

where $(\dot{Q}_s)_E$, $(\dot{Q}_s)_I$ are the power generated per unit volume by elastic and inelastic interaction forces, respectively, and the body forces have been assumed to be independent of molecular velocity.

Putting everything together, the final result reads

$$\frac{\partial \rho_s e_{0_s}}{\partial t} + \frac{\partial \rho_s \boldsymbol{u}_0 \cdot \boldsymbol{V}_s}{\partial t} + \nabla \cdot (\rho_s e_{0_s} \boldsymbol{u}_0 + \boldsymbol{u}_0 \cdot p_s \mathbf{I}) + \nabla \cdot \left[\rho_s \left(\frac{u_0^2}{2} \boldsymbol{V}_s + (\boldsymbol{u}_0 \cdot \boldsymbol{V}_s)\boldsymbol{u}_0\right)\right] -$$
$$- \nabla \cdot (\boldsymbol{u}_0 \cdot \mathbf{T}_s) + \nabla \cdot \boldsymbol{q}_s = \rho_s \mathbf{g}_s \cdot \boldsymbol{u}_s + (\dot{Q}_s)_E + (\dot{Q}_s)_I . \quad (3.26)$$

Again,the global energy equation is obtained by summation over the species contributions, where

$$\sum_{s=1}^{N} (\dot{Q}_s)_E \equiv 0, \qquad \sum_{s=1}^{N} (\dot{Q}_s)_I \equiv 0, \qquad \sum_{s=1}^{N} \boldsymbol{q}_s = \boldsymbol{q} . \quad (3.27a,b,c)$$

After some algebra, a simple expression is recovered

$$\frac{\partial \rho e_0}{\partial t} + \nabla \cdot (\rho e_0 \boldsymbol{u}_0 + \boldsymbol{u}_0 \cdot p\mathbf{I}) - \nabla \cdot (\boldsymbol{u}_0 \cdot \mathbf{T}) + \nabla \cdot \boldsymbol{q} = \sum_{s=1}^{N} \rho_s \mathbf{g}_s \cdot \boldsymbol{u}_s . \quad (3.28)$$

In order for the mathematical formulation to be complete, M rate equations for the non-equilibrium contributions to the species internal energy must be written, where M is the number of species that have these contributions, $0 \leq M \leq N-1$. To accomplish that, it is possible to use the same approach followed so far, taking $\psi_s = m_s e'_{n_s}$. Now the source terms will also include interactions *within* species s, namely energy exchanges between degrees of freedom in equilibrium at different temperatures. Averaged values for ψ and its flux are

$$n_s <m_s e'_{n_s}> = \rho_s e_{n_s}, \quad n_s <m_s e'_{n_s} \boldsymbol{u}'_s> = \rho_s (e_{n_s} \boldsymbol{u}_0 + <e'_{n_s} c'_s>) = \rho_s (e_{n_s} \boldsymbol{u}_0 + \boldsymbol{q}_{n_s}) , \quad (3.29a,b)$$

where q_n is a non-equilibrium heat flux vector. The final result will read

$$\frac{\partial \rho_s e_{n_s}}{\partial t} + \nabla \cdot (\rho_s e_{n_s} u_0) + \nabla \cdot q_{n_s} = (\dot{Q}_s)_{n,E} + (\dot{Q}_s)_{n,I} . \tag{3.30}$$

The previous equations form a complete set for the solution of high-speed problems with chemical and thermal non-equilibrium, once some of the terms that appear are *modeled*, that is related to the *primitive* unknowns. The latter ones can be chosen to be : species density ρ_s, mass-averaged velocity u_0, non-equilibrium energy contributions e_{n_s}, pressure p and partial pressure of free electrons p_e. It is a total of $N+M+5$ scalar unknowns that will require the same number of equations, namely species continuity (eq.(3.9), $s = 1,\dots N$), global momentum, eq.(3.19), species non-equilibrium energy (eq.(3.30), $s = 1,\dots M$), electron energy (eq.(3.26), $s = N$), and global energy, eq.(3.28). The equations of state, eqs.(2.13), (2.14), will relate pressures to densities and internal energy, through the temperatures. Diffusion velocity, shear stress, heat transfer, source terms will require particular attention in the modeling process, as discussed in §3.3.

The electron energy equation will be somewhat simplified in the following. The unsteady contribution of diffusion $\partial(\rho_e u_0 \cdot V_e)/\partial t$ and the stress tensor $u_0 \cdot \mathbf{T}_e$ will be neglected, so that the equation will read

$$\frac{\partial \rho_e e_{0_e}}{\partial t} + \nabla \cdot (\rho_e e_{0_e} u_0 + u_0 \cdot p_e \mathbf{I}) + \nabla \cdot \left[\rho_e \left(\frac{u_0^2}{2} V_e + (u_0 \cdot V_e) u_0\right)\right] + \nabla \cdot q_e = \\ = \rho_e g_e \cdot (u_0 + V_e) + (\dot{Q}_e)_E + (\dot{Q}_e)_I . \tag{3.31}$$

In summary, the extended Navier-Stokes equations for a general flow out of chemical and thermal equilibrium will be written in conservative form, using an orthogonal Cartesian frame of reference (x_1, x_2, x_3) for simplicity, as follows

$$\frac{\partial Q}{\partial t} + \frac{\partial (F - F_v)}{\partial x_1} + \frac{\partial (G - G_v)}{\partial x_2} + \frac{\partial (H - H_v)}{\partial x_3} = W, \tag{3.32}$$

where Q is the vector of conserved variables, F, G, H are the inviscid flux vectors, F_v, G_v, H_v are the viscous flux vectors, and W is the vector of source terms. These vectors are given in detail in Appendix 1, along with a summary of the state relationships that link conserved variables to primitive unknowns.

3.3 Basic Modeling of Viscous Fluxes

In order to close the system of equations to be solved, some additional quantities that appear in the formulation must be related either to the primitive or to the conserved variables. In particular, the stress tensor, the heat flux vectors, and the diffusion velocities have to be modeled.

In the following, some of the basic results will be examined. For details on their derivation, the reader is referred to Bird, Stewart and Lightfoot [58]. Additional expressions will appear in §5.

The most common assumptions that are made when dealing with transport properties concern the treatment of the viscous stress tensor. Generally only *Newtonian* fluids are considered, where there is a linear relationship between stress and rate of deformation. Moreover, *bulk* viscosity effects, which should be accounted for when rotational non-equilibrium is present [2], are neglected.

Under these assumptions, the stress tensor components are expressed as

$$\tau_{ij} = \mu\left(\frac{\partial u_{0_i}}{\partial x_j} + \frac{\partial u_{0_j}}{\partial x_i}\right) - \frac{2}{3}\mu\left(\frac{\partial u_{0_1}}{\partial x_1} + \frac{\partial u_{0_2}}{\partial x_2} + \frac{\partial u_{0_3}}{\partial x_3}\right)\delta_{ij}, \qquad i,j = 1,2,3, \quad (3.33)$$

where μ is the viscosity coefficient and the symbol δ_{ij} stands for the Kroneker delta.

For mixture of gases in thermal equilibrium, the heat flux vector q is modeled by means of the product of a thermal conductivity coefficient k times the temperature gradient (Fourier's Law). The extension of this approach to flows in thermal non-equilibrium is usually done by considering similar contributions from the non-equilibrium temperatures [1],[26],[59], and accounting for the thermal effect due to the presence of diffusion velocities. The resulting expressions read

$$q_{n_s} = -k_{n_s}\nabla T_{n_s} + \rho_s e_{n_s} V_s, \qquad s = 1,\ldots,M,$$

$$q_e = -k_{e_s}\nabla T_e + \rho_e h_e V_e,$$

$$q = -k\nabla T - k_e \nabla T_e - \sum_{s=1}^{M} k_{n_s}\nabla T_{n_s} + \sum_{s=1}^{N} \rho_s h_s V_s, \qquad k_e = \sum_{s=1}^{N} k_{e_s}. \quad (3.34a,b,c,d)$$

This model neglects some supposedly secondary factors like temperature and pressure diffusion, which would greatly complicate the analysis. In addition, the validity of Fourier's Law for non-equilibrium conditions has not been fully assessed to date.

More details on the modeling of viscous terms, and in particular on the treatment of diffusion velocities, will be discussed in §5.

3.4 Simplified Governing Equations

For many practical computational applications, one can avoid some of the generality with which the governing partial differential equations were derived in §3.2 and obtain a reduced set of equation that can be handled more efficiently.

A fairly usual approximation consists in neglecting viscous contributions except in one space direction, normal to a solid surface [60]. The resulting equations are known as Thin-Layer Navier-Stokes equations [61]. The governing equations, eq.(3.32), reduce to

$$\frac{\partial \boldsymbol{Q}}{\partial t} + \frac{\partial \boldsymbol{F}}{\partial x_1} + \frac{\partial \boldsymbol{G}}{\partial x_2} + \frac{\partial \boldsymbol{H}}{\partial x_3} - \frac{\partial \boldsymbol{S_v}}{\partial x_1} = \boldsymbol{W}, \tag{3.35}$$

where $\boldsymbol{Q}$, $\boldsymbol{W}$ and the inviscid fluxes are unchanged from eqs.(A1.2), (A1.3), and $\boldsymbol{S_v}$ is a reduced form of $\boldsymbol{F_v}$. The other space directions can be treated in a similar way. The vector $\boldsymbol{S_v}$ reads

$$\boldsymbol{S_v} = \begin{pmatrix} -\rho_1 V_{1_1} \\ -\rho_2 V_{2_1} \\ \vdots \\ \vdots \\ -\rho_N V_{N_1} \\ 4\mu/3 \; \partial u_{0_1}/\partial x_1 \\ \mu \; \partial u_{0_2}/\partial x_1 \\ \mu \; \partial u_{0_3}/\partial x_1 \\ k_{n_1} \partial T_{n_1}/\partial x_1 - \rho_1 e_{n_1} V_{1_1} \\ \vdots \\ k_{n_M} \partial T_{n_M}/\partial x_1 - \rho_M e_{n_M} V_{M_1} \\ k_{e_e} \partial T_e/\partial x_1 - \rho_e (h_e + u_0^2/2) V_{e_1} - \rho_e (u_0 \cdot V_e) u_{0_1} \\ \Theta \end{pmatrix}, \tag{3.36}$$

where all the cross-derivative terms have been neglected and Θ is given by

$$\Theta = k\frac{\partial T}{\partial x_1} + k_e\frac{\partial T_e}{\partial x_1} + \sum_{s=1}^{M} k_{n_s}\frac{\partial T_{n_s}}{\partial x_1} - \sum_{s=1}^{N}\rho_s h_s V_{s_1} + \frac{\mu}{2}\frac{\partial u_0^2}{\partial x_1} + \frac{\mu}{3}u_{0_1}\frac{\partial u_{0_1}}{\partial x_1}. \quad (3.37)$$

When viscosity, thermal conductivity and diffusion effects are discarded, the *Euler* equations are recovered. For flows of sufficiently high density, the physical behaviour outside the boundary layer with a solid surface can be reasonably predicted by this simpler set of equations. Formally, Euler's equations can be obtained from eq.(3.32), by simply dropping the viscous fluxes $\boldsymbol{F}_v$, $\boldsymbol{G}_v$ and $\boldsymbol{H}_v$.

Another line of simplification can be undertaken when considering the thermodynamic model. For the full Navier-Stokes equations of eq.(3.32), considering only one translational temperature amounts to dropping the electron continuity and energy equations and dropping the electron-temperature-related heat transfer in the definition of the global heat flux vector $\boldsymbol{q}$. The source vector $\boldsymbol{W}$ is also simplified in a consistent way for this model of $N^* = N-1$ species. The Thin-Layer Navier-Stokes and Euler equations for the reduced thermodynamic model may be similarly derived. Dropping the non-equilibrium energy equations will yield a one-temperature model with finite-rate chemistry. Again, heat-transfer vector and source terms need to be consistently simplified.

For cases when chemical equilibrium can be assumed, the governing equations will have the same structure, but only global continuity needs to be considered. The governing equations can be recovered by simply setting $\rho_1 = \rho$ and $\rho_2 = \ldots = \rho_{N^*} \equiv 0$, which is tantamount to setting $N^* = 1$. Mass diffusion can still be retained in the model, if information on the diffusion velocities is available. This is not always the case, because for practical calculations global curve fits could be used [51]. These do not provide information on the internal composition of the mixture, which is essential for the modeling of diffusion.

Finally, once diffusion effects are discarded, the perfect gas viscous equations are easily obtained in the limit of no chemical reactions.

3.5 Transformation to Generalized Coordinates

In the previous sections, an orthogonal Cartesian reference system was utilized for simplicity. However, complex geometries cannot be handled by Cartesian grids, and a generalized nonorthogonal reference system is usually needed. Mathematically, the transformation between the two systems can be accomplished by writing the relations

$$\begin{aligned} \xi &= \xi(x_1, x_2, x_3), \\ \eta &= \eta(x_1, x_2, x_3), \\ \varsigma &= \varsigma(x_1, x_2, x_3), \end{aligned} \tag{3.38}$$

where ξ, η, ς represent a general *structured* coordinate system [62],[63].

Similar relationships involving time-dependent frames, and such that a strong conservation form of the equations is still maintained, can also be written [64],[65], but are not considered here. Applying the chain rule for partial derivatives, after some algebra eq.(3.32) can be written in generalized coordinates and in conservation form as follows

$$\frac{\partial \tilde{Q}}{\partial t} + \frac{\partial(\tilde{F} - \tilde{F}_v)}{\partial \xi} + \frac{\partial(\tilde{G} - \tilde{G}_v)}{\partial \eta} + \frac{\partial(\tilde{H} - \tilde{H}_v)}{\partial \varsigma} = \tilde{W}, \tag{3.39}$$

where

$$\tilde{Q} = \frac{Q}{J}, \qquad \tilde{W} = \frac{W}{J}, \tag{3.40a,b}$$

and

$$\begin{aligned} \tilde{F} - \tilde{F}_v &= \frac{|\nabla \xi|}{J}\left[\tilde{\xi}_{x_1}(F - F_v) + \tilde{\xi}_{x_2}(G - G_v) + \tilde{\xi}_{x_3}(H - H_v)\right], \\ \tilde{G} - \tilde{G}_v &= \frac{|\nabla \eta|}{J}\left[\tilde{\eta}_{x_1}(F - F_v) + \tilde{\eta}_{x_2}(G - G_v) + \tilde{\eta}_{x_3}(H - H_v)\right], \\ \tilde{H} - \tilde{H}_v &= \frac{|\nabla \varsigma|}{J}\left[\tilde{\varsigma}_{x_1}(F - F_v) + \tilde{\varsigma}_{x_2}(G - G_v) + \tilde{\varsigma}_{x_3}(H - H_v)\right]. \end{aligned} \tag{3.41a,b,c}$$

In the equations above, J is the Jacobian of the coordinate transformation

$$J = \frac{\partial(\xi, \eta, \varsigma)}{\partial(x_1, x_2, x_3)} = det \begin{pmatrix} \xi_{x_1} & \xi_{x_2} & \xi_{x_3} \\ \eta_{x_1} & \eta_{x_2} & \eta_{x_3} \\ \varsigma_{x_1} & \varsigma_{x_2} & \varsigma_{x_3} \end{pmatrix}, \tag{3.42}$$

and $\nabla\tilde{\xi}$, $\nabla\tilde{\eta}$, $\nabla\tilde{\zeta}$ are the unit vectors in the directions normal to the coordinate surfaces

$$\nabla\tilde{\xi} = \frac{\nabla\xi}{|\nabla\xi|} = \frac{\nabla\xi}{(\xi_{x_1}^2 + \xi_{x_2}^2 + \xi_{x_3}^2)^{1/2}},$$
$$\nabla\tilde{\eta} = \frac{\nabla\eta}{|\nabla\eta|} = \frac{\nabla\eta}{(\eta_{x_1}^2 + \eta_{x_2}^2 + \eta_{x_3}^2)^{1/2}}, \qquad (3.43a,b,c)$$
$$\nabla\tilde{\zeta} = \frac{\nabla\zeta}{|\nabla\zeta|} = \frac{\nabla\zeta}{(\zeta_{x_1}^2 + \zeta_{x_2}^2 + \zeta_{x_3}^2)^{1/2}}.$$

Denoting the components of the velocity in generalized coordinates, also known as the *contravariant* components, as follows

$$\begin{pmatrix} \tilde{u}_{0_1} \\ \tilde{u}_{0_2} \\ \tilde{u}_{0_3} \end{pmatrix} = \begin{pmatrix} \tilde{\xi}_{x_1} & \tilde{\xi}_{x_2} & \tilde{\xi}_{x_3} \\ \tilde{\eta}_{x_1} & \tilde{\eta}_{x_2} & \tilde{\eta}_{x_3} \\ \tilde{\zeta}_{x_1} & \tilde{\zeta}_{x_2} & \tilde{\zeta}_{x_3} \end{pmatrix} \begin{pmatrix} u_{0_1} \\ u_{0_2} \\ u_{0_3} \end{pmatrix}, \qquad (3.44)$$

the inviscid flux vectors can be written

$$\tilde{F} = \frac{|\nabla\xi|}{J}\begin{pmatrix} \rho_1\tilde{u}_{0_1} \\ \rho_2\tilde{u}_{0_1} \\ \vdots \\ \rho_N\tilde{u}_{0_1} \\ \rho\tilde{u}_{0_1}u_{0_1}+\tilde{\xi}_{x_1}p \\ \rho\tilde{u}_{0_1}u_{0_2}+\tilde{\xi}_{x_2}p \\ \rho\tilde{u}_{0_1}u_{0_3}+\tilde{\xi}_{x_3}p \\ \rho_1 e_{n_1}\tilde{u}_{0_1} \\ \vdots \\ \rho_M e_{n_M}\tilde{u}_{0_1} \\ \rho_e h_{0_e}\tilde{u}_{0_1} \\ \rho h_0\tilde{u}_{0_1} \end{pmatrix}, \quad \tilde{G} = \frac{|\nabla\eta|}{J}\begin{pmatrix} \rho_1\tilde{u}_{0_2} \\ \rho_2\tilde{u}_{0_2} \\ \vdots \\ \rho_N\tilde{u}_{0_2} \\ \rho\tilde{u}_{0_2}u_{0_1}+\tilde{\eta}_{x_1}p \\ \rho\tilde{u}_{0_2}u_{0_2}+\tilde{\eta}_{x_2}p \\ \rho\tilde{u}_{0_2}u_{0_3}+\tilde{\eta}_{x_3}p \\ \rho_1 e_{n_1}\tilde{u}_{0_2} \\ \vdots \\ \rho_M e_{n_M}\tilde{u}_{0_2} \\ \rho_e h_{0_e}\tilde{u}_{0_2} \\ \rho h_0\tilde{u}_{0_2} \end{pmatrix}, \quad \tilde{H} = \frac{|\nabla\zeta|}{J}\begin{pmatrix} \rho_1\tilde{u}_{0_3} \\ \rho_2\tilde{u}_{0_3} \\ \vdots \\ \rho_N\tilde{u}_{0_3} \\ \rho\tilde{u}_{0_3}u_{0_1}+\tilde{\zeta}_{x_1}p \\ \rho\tilde{u}_{0_3}u_{0_2}+\tilde{\zeta}_{x_2}p \\ \rho\tilde{u}_{0_3}u_{0_3}+\tilde{\zeta}_{x_3}p \\ \rho_1 e_{n_1}\tilde{u}_{0_3} \\ \vdots \\ \rho_M e_{n_M}\tilde{u}_{0_3} \\ \rho_e h_{0_e}\tilde{u}_{0_3} \\ \rho h_0\tilde{u}_{0_3} \end{pmatrix}. \qquad (3.45a,b,c)$$

The viscous flux vectors $\tilde{F}_v$, $\tilde{G}_v$, $\tilde{H}_v$ can be similarly expressed in terms of quantities related to the generalized coordinates. Taking $\tilde{F}_v$ as an example, the

result is

$$\tilde{F}_v = \frac{|\nabla\xi|}{J}\begin{pmatrix} -\rho_1\tilde{V}_{1_1} \\ -\rho_2\tilde{V}_{2_1} \\ \vdots \\ \vdots \\ -\rho_N\tilde{V}_{N_1} \\ \tilde{\xi}_{x_1}\tau_{11}+\tilde{\xi}_{x_2}\tau_{12}+\tilde{\xi}_{x_3}\tau_{13} \\ \tilde{\xi}_{x_1}\tau_{21}+\tilde{\xi}_{x_2}\tau_{22}+\tilde{\xi}_{x_3}\tau_{23} \\ \tilde{\xi}_{x_1}\tau_{31}+\tilde{\xi}_{x_2}\tau_{32}+\tilde{\xi}_{x_3}\tau_{33} \\ k_{n_1}(\nabla\xi\cdot\nabla T_{n_1})-\rho_1 e_{n_1}\tilde{V}_{1_1} \\ \vdots \\ k_{n_M}(\nabla\xi\cdot\nabla T_{n_M})-\rho_M e_{n_M}\tilde{V}_{M_1} \\ k_{e_e}(\nabla\xi\cdot\nabla T_e)-\rho_e h_{0_e}\tilde{V}_{e_1}-\rho_e(u_0\cdot V_e)\tilde{u}_{0_1} \\ \tilde{\Theta} \end{pmatrix}, \tag{3.46}$$

where

$$\begin{aligned}\tilde{\Theta} =& k(\nabla\xi\cdot\nabla T)+k_e(\nabla\xi\cdot\nabla T_e)+\sum_{s=1}^{M}k_{n_s}(\nabla\xi\cdot\nabla T_{n_s})- \\ &-\sum_{s=1}^{N}\rho_s h_s\tilde{V}_{s_1}+(u_{0_1}\tilde{F}_{v_{N+1}}+u_{0_2}\tilde{F}_{v_{N+2}}+u_{0_3}\tilde{F}_{v_{N+3}})\frac{J}{|\nabla\xi|}.\end{aligned} \tag{3.47}$$

In the above formulas, $\tilde{V}_s$ stands for the species diffusion velocity written in generalized coordinates, whose components are obtained by a formula similar to eq.(3.44). Similar results apply for the other space directions, when $\tilde{\xi}$ is replaced by $\tilde{\eta}$, $\tilde{\zeta}$ respectively, and the proper components of $\tilde{V}_s$ and $\tilde{u}_0$ are selected.

The space derivatives $\partial(\cdot)/\partial x_i$, for $i = 1,2,3$, need to be expanded according to the chain rule

$$\begin{aligned}\frac{\partial(\cdot)}{\partial x_1} =& |\nabla\xi|\tilde{\xi}_{x_1}\frac{\partial(\cdot)}{\partial\xi}+|\nabla\eta|\tilde{\eta}_{x_1}\frac{\partial(\cdot)}{\partial\eta}+|\nabla\zeta|\tilde{\zeta}_{x_1}\frac{\partial(\cdot)}{\partial\zeta}, \\ \frac{\partial(\cdot)}{\partial x_2} =& |\nabla\xi|\tilde{\xi}_{x_2}\frac{\partial(\cdot)}{\partial\xi}+|\nabla\eta|\tilde{\eta}_{x_2}\frac{\partial(\cdot)}{\partial\eta}+|\nabla\zeta|\tilde{\zeta}_{x_2}\frac{\partial(\cdot)}{\partial\zeta}, \\ \frac{\partial(\cdot)}{\partial x_3} =& |\nabla\xi|\tilde{\xi}_{x_3}\frac{\partial(\cdot)}{\partial\xi}+|\nabla\eta|\tilde{\eta}_{x_3}\frac{\partial(\cdot)}{\partial\eta}+|\nabla\zeta|\tilde{\zeta}_{x_3}\frac{\partial(\cdot)}{\partial\zeta}.\end{aligned} \tag{3.48a,b,c}$$

When the Thin-Layer approximation to the complete Navier-Stokes equations is used for the ξ direction, eqs.(3.48) reduce to

$$\frac{\partial(\cdot)}{\partial x_1} = |\nabla\xi|\tilde{\xi}_{x_1}\frac{\partial(\cdot)}{\partial\xi}, \qquad \frac{\partial(\cdot)}{\partial x_2} = |\nabla\xi|\tilde{\xi}_{x_2}\frac{\partial(\cdot)}{\partial\xi}, \qquad \frac{\partial(\cdot)}{\partial x_3} = |\nabla\xi|\tilde{\xi}_{x_3}\frac{\partial(\cdot)}{\partial\xi}, \tag{3.49a,b,c}$$

and the viscous flux terms in the ξ direction can be grouped to read

$$\tilde{S}_v = \frac{|\nabla\xi|^2}{J}\begin{pmatrix} -\rho_1\tilde{V}_{1_1}/|\nabla\xi| \\ -\rho_2\tilde{V}_{2_1}/|\nabla\xi| \\ \vdots \\ \vdots \\ -\rho_N\tilde{V}_{N_1}/|\nabla\xi| \\ \mu\partial u_{0_1}/\partial\xi + \mu\tilde{\xi}_{x_1}(\tilde{\xi}_{x_1}\partial u_{0_1}/\partial\xi + \tilde{\xi}_{x_2}\partial u_{0_2}/\partial\xi + \tilde{\xi}_{x_3}\partial u_{0_3}/\partial\xi)/3 \\ \mu\partial u_{0_2}/\partial\xi + \mu\tilde{\xi}_{x_2}(\tilde{\xi}_{x_1}\partial u_{0_1}/\partial\xi + \tilde{\xi}_{x_2}\partial u_{0_2}/\partial\xi + \tilde{\xi}_{x_3}\partial u_{0_3}/\partial\xi)/3 \\ \mu\partial u_{0_3}/\partial\xi + \mu\tilde{\xi}_{x_3}(\tilde{\xi}_{x_1}\partial u_{0_1}/\partial\xi + \tilde{\xi}_{x_2}\partial u_{0_2}/\partial\xi + \tilde{\xi}_{x_3}\partial u_{0_3}/\partial\xi)/3 \\ k_{n_1}\partial T_{n_1}/\partial\xi - \rho_1 e_{n_1}\tilde{V}_{1_1}/|\nabla\xi| \\ \vdots \\ k_{n_M}\partial T_{n_M}/\partial\xi - \rho_M e_{n_M}\tilde{V}_{M_1}/|\nabla\xi| \\ k_{e_e}\partial T_e/\partial\xi - \rho_e\left[h_{0_e}\tilde{V}_{e_1} + (u_0\cdot V_e)\tilde{u}_{0_1}\right]/|\nabla\xi| \\ \tilde{\Theta} \end{pmatrix}, \tag{3.50}$$

where

$$\begin{aligned}\tilde{\Theta} =& k\frac{\partial T}{\partial\xi} + k_e\frac{\partial T_e}{\partial\xi} + \sum_{s=1}^{M} k_{n_s}\frac{\partial T_{n_s}}{\partial\xi} - \sum_{s=1}^{N}\rho_s h_s\frac{\tilde{V}_{s_1}}{|\nabla\xi|} + \\ &+ \mu\frac{\partial u_0^2/2}{\partial\xi} + \mu\frac{\tilde{u}_{0_1}}{3}(\tilde{\xi}_{x_1}\frac{\partial u_{0_1}}{\partial\xi} + \tilde{\xi}_{x_2}\frac{\partial u_{0_2}}{\partial\xi} + \tilde{\xi}_{x_3}\frac{\partial u_{0_3}}{\partial\xi}).\end{aligned} \tag{3.51}$$

3.6 Integral Form

The derivation of the governing equations has been carried out in differential form. A problem associated with this formulation is that when in the presence of discontinuities such as shock waves, the differential equations are no longer valid because derivatives become ill-defined. In an integral approach, however, the conservation of species and mixture properties is written for a generic volume of arbitrary shape and size, fixed in space [2]. The resulting governing equations, written in

terms of volume and surface integrals, are equivalent to the differential ones in regions of smooth flows and are valid also across discontinuities [66], where they can be shown to reduce to the Rankine-Hugoniot jump relationships. An extensive investigation of the existence and properties of *weak* solutions to hyperbolic equations written in integral form can be found in Lax [67].

For an arbitrary volume Ω, closed by a boundary $\partial\Omega$, the governing equations in integral form read

$$\iiint_{\Omega} \frac{\partial Q}{\partial t} d\Omega + \oint_{\partial\Omega} (S - S_v) \cdot n d\partial\Omega = \iiint_{\Omega} W d\Omega, \tag{3.52}$$

where S and S_v are the inviscid and viscous flux vectors, respectively. When appropriate conditions on the smoothness of $\partial\Omega$ are fulfilled, eq.(3.52) is mathematically equivalent to the differential equations written in Cartesian or generalized coordinates, eq.(3.32) and eq.(3.39), respectively.

The integral form of the governing equations is especially useful when dealing with finite-volume discretization techniques, as will be discussed in §7.

3.7 Quasi-One-Dimensional Approximation

In many instances, order-of-magnitude analyses of complex flows can be performed by neglecting two and three-dimensional effects. One way of accomplishing this is to integrate the governing equations over two space dimensions, thus leaving only one-dimensional effects to be resolved [66]. Appropriate *area-averaged* values become the unknowns, and the resulting equations are still rigorously exact when written for a streamtube whose area varies in time and space, $A = A(x_1, t)$.

The most common application of this procedure is the prediction of performances of nozzles, where the area is only a function of space. Neglecting viscous, thermal, and diffusive effects, whose influence cannot be easily evaluated in a quasi-one-dimensional approach, the governing equations can be written, when $A = A(x_1)$ only, as follows

$$\frac{\partial Q}{\partial t} + \frac{\partial F}{\partial x_1} = W + W_A, \tag{3.53}$$

where W_A is a vector that includes the effect of area variation

$$W_A = -\frac{u}{A}\frac{dA}{dx_1}\begin{pmatrix} \rho_1 \\ \vdots \\ \vdots \\ \rho_N \\ \rho u \\ \rho_1 e_{n_1} \\ \vdots \\ \rho_M e_{n_M} \\ \rho_e h_{0_e} \\ \rho h_0 \end{pmatrix}, \tag{3.54}$$

and $u_{0_1} = u$, $V_\theta \equiv 0$ for this one-dimensional, inviscid approach.

In §8, results will be presented for simple simulations that solve discretized versions of eq.(3.53).

4. MODELING OF SOURCE TERMS

4.1 Finite-Rate Chemistry

In hypersonic flow conditions, behind a strong bow shock or in a combustion chamber, chemical reactions will occur. In general, these reactions will not have time to proceed to their equilibrium value, given by thermodynamic considerations, but will evolve according to their *kinetics* [68].

A classification of chemical phenomena according to the time available for the completion of reactions is usually employed for order-of-magnitude estimates. A typical fluid-dynamic time τ_{FD}, of the order of some relevant length divided by an average flow speed, can be defined for the flow under consideration. Then a typical reaction time $\tau_{CH,j}$ can be estimated, generally the time necessary for halving or doubling the quantity of a certain species for a given temperature and initial composition, when only reaction j is active. Three cases can occur

$$\tau_{FD} \begin{cases} \ll \tau_{CH,j}\,, \\ \approx \tau_{CH,j}\,, \\ \gg \tau_{CH,j}\,. \end{cases} \tag{4.1}$$

In the first case, reaction j has no time to occur, and a *frozen* flow can be assumed with respect to that specific reaction. The second case is the general case of finite-rate chemistry whereby the actual kinetics of the reaction must be taken into consideration. In the third case, reaction j has a virtually infinite time to evolve, and consequently it will reach its equilibrium value given by the Law of Mass Action.

In practice, calculations are performed where *all* of the chemical reactions are supposed to be either in equilibrium, as discussed in numerous papers [12–22],[69], or frozen (perfect gas results are a particular class of frozen chemistry simulations). These results are important *limiting cases*, but an accurate prediction of species concentrations and heat release requires simulating the actual kinetic behaviour of the chemical system.

There are many problems that render a realistic computation into a non-trivial task. The most important one is the uncertainty in the reaction paths and in the reaction rates [70]. Although the composition of a given mixture as a function of thermodynamic variables can be determined quite accurately by theoretical and experimental means, there is very scarce knowledge of the actual mechanism with which a given reaction occurs. Many paths, leading to intermediate products or highly unstable excited states, are available for virtually every reaction. It is a delicate theoretical work to rule out some of the possibilities with respect to others, and it is an impressive experimental work to confirm these results and to obtain kinetic rate data for specific reaction paths. However, some results have been obtained for air dissociative processes and for hydrogen combustion, as will be discussed in the next section.

A fairly general simulation of chemical effects can be included in the governing equations, eq.(3.32), for a system containing N species where J reactions take place

$$\nu'_{1,j}X_1 + \nu'_{2,j}X_2 + \cdots + \nu'_{N,j}X_N \rightleftharpoons \nu''_{1,j}X_1 + \nu''_{2,j}X_2 + \cdots + \nu''_{N,j}X_N \qquad j = 1, 2, \ldots, J, \quad (4.2)$$

where the $\nu'_{i,j}$ and the $\nu''_{i,j}$ are the stoichiometric coefficients of the reactants and products of species X_i in the jth reaction, respectively. Then, in the source vector W of eq.(3.32), the rate of production of species i may be written as [71]

$$w_i \equiv \frac{d\rho_i}{dt} = \mathcal{M}_i \sum_{j=1}^{J} (\nu''_{i,j} - \nu'_{i,j}) \left[k_{f,j} \prod_{l=1}^{N} \left(\frac{\rho_l}{\mathcal{M}_l} \right)^{\nu'_{l,j}} - k_{b,j} \prod_{l=1}^{N} \left(\frac{\rho_l}{\mathcal{M}_l} \right)^{\nu''_{l,j}} \right], \qquad i = 1, 2, \ldots, N, \quad (4.3)$$

where for reaction j the forward and backward reaction rates, $k_{f,j}$ and $k_{b,j}$, are assumed to be known functions of temperature, and are related by thermodynamics

$$k_{b,j} = \frac{k_{f,j}}{K_{e,j}}, \quad (4.4)$$

where $K_{e,j}$ is the equilibrium constant, which is a known function of the thermodynamic state. Using eq.(4.4), eq.(4.3) can be rewritten as follows

$$w_i \equiv \frac{d\rho_i}{dt} = \mathcal{M}_i \sum_{j=1}^{J} (\nu''_{i,j} - \nu'_{i,j}) k_{f,j} \left[\prod_{l=1}^{N} \left(\frac{\rho_l}{\mathcal{M}_l} \right)^{\nu'_{l,j}} - \frac{1}{K_{e,j}} \prod_{l=1}^{N} \left(\frac{\rho_l}{\mathcal{M}_l} \right)^{\nu''_{l,j}} \right], \quad i = 1, 2, \ldots, N, \tag{4.5}$$

where the term in the brackets goes to zero when equilibrium compositions are reached for ρ_i, because it reduces to a formulation of the Law of Mass Action

$$K_{e,j} = \frac{\prod_{l=1}^{N} (\rho_l / \mathcal{M}_l)^{\nu''_{l,j}}}{\prod_{l=1}^{N} (\rho_l / \mathcal{M}_l)^{\nu'_{l,j}}}, \qquad j = 1, \ldots, J, \tag{4.6}$$

valid for equilibrium concentrations.

From eq.(4.5), it is easy to recognize the limiting cases of frozen and equilibrium flows. When the forward rate $k_{f,j} \to 0$ for any j, then the source term associated with chemical reactions drops out of the governing equations, and it can be shown that the species mass fractions are unchanged if no diffusion occurs. On the other hand, when the forward rate $k_{f,j} \to \infty$ for any j, then the terms in brackets will tend to zero, because the equilibrium composition is maintained, and the source term will reach a limit value that will balance convection, diffusion and unsteady terms in the species continuity equation.

The results that have been presented in this section rest upon one basic assumption, that "the internal rate processes in a moving fluid at a given instantaneous rate are the same as those that occur at the same state in a closed system of fixed volume and temperature" [2]. Using this assumption, laboratory determinations of reaction rates have been transferred to hypersonic flow conditions. The validity of such an approach could be questioned, but no definite answer has been formulated at the present time.

The model presented so far includes homogeneous reactions only. Two-phase and photochemical reactions are neglected, and catalytic effects are discarded. Some

of these effects could be easily included, especially when approximate treatments of catalytic walls are considered [9].

The computational time for a complete simulation of complex mixtures can be overwhelming. In many cases, only some of the reactions are important, and secondary processes can be neglected without too great a loss of accuracy. Approximate methods for the determination of the key processes have been proposed [5], and constitute a promising tool for obtaining simplified approaches that still account for the salient physics of the flow.

4.2 Specific Chemical Models

Five simple chemical models have been used in the numerical simulations performed in this work, the first two for air, the third one for hydrogen combustion in air, and the last two for a simple argon-based plasma. These chemical systems have been extensively studied, and rate constants as well as equilibrium properties are available.

The first air model utilizes five species, N_2, O_2, NO, N, and O, and five basic reactions, three dissociation–recombination and two rearrangement (shuffle) reactions:

$$\begin{aligned} N_2 + M &\rightleftharpoons 2N + M, \\ O_2 + M &\rightleftharpoons 2O + M, \\ NO + M &\rightleftharpoons N + O + M, \\ N_2 + O &\rightleftharpoons NO + N, \\ NO + O &\rightleftharpoons O_2 + N, \end{aligned} \tag{4.7}$$

where M is a catalytic particle (any of the species present). Reaction rates are given in Kang and Dunn [72], and equilibrium constants in Vincenti and Kruger [2]. In the following, this model will be referred to as Air Model 1.

The second air model utilizes eleven species, the five above plus the corresponding five ions and electrons, N_2, O_2, NO, N, O, N_2^+, O_2^+, NO^+, N^+, O^+, and

e^-. In addition to the previous reactions, 7 more shuffle reactions involving ions, 3 associative ionization and 2 electron impact reactions are modeled, namely

$$
\begin{aligned}
O + O_2^+ &\rightleftharpoons O_2 + O^+, \\
N_2 + N^+ &\rightleftharpoons N + N_2^+, \\
O + NO^+ &\rightleftharpoons NO + O^+, \\
N_2 + O^+ &\rightleftharpoons O + N_2^+, \\
N + NO^+ &\rightleftharpoons NO + N^+, \\
O_2 + NO^+ &\rightleftharpoons NO + O_2^+, \\
NO^+ + N &\rightleftharpoons N_2^+ + O, \\
O + N &\rightleftharpoons NO^+ + e^-, \\
O + O &\rightleftharpoons O_2^+ + e^-, \\
N + N &\rightleftharpoons N_2^+ + e^-, \\
O + e^- &\rightleftharpoons O^+ + 2e^-, \\
N + e^- &\rightleftharpoons N^+ + 2e^-.
\end{aligned}
\tag{4.8}
$$

Reaction rates and equilibrium constants are given in Park [73]. In the following, this model will be referred to as Air Model 2.

It is noteworthy that different air models and new sets of constants have been proposed recently [74]. However, their implementation is more complex because they involve *effective* temperatures as well as the electron temperature, as will be briefly discussed in §4.3, and it has not been attempted at the present stage.

The third model is the two-reaction hydrogen-air model, presented in Rogers and Chinitz [75]. It utilizes five species, N_2, O_2, H_2, OH, and H_2O, and the two basic reactions

$$
\begin{aligned}
H_2 + O_2 &\rightleftharpoons 2OH, \\
2OH + H_2 &\rightleftharpoons 2H_2O,
\end{aligned}
\tag{4.9}
$$

whereas it neglects the reactions of nitrogen. In the following, this model will be referred to as Hydrogen-Air Model 1.

The last two models, used for a simple plasma, utilize three species, A, A^+, and e^- and one dissociation reaction

$$A + e^- \rightleftharpoons A^+ + 2e^-. \tag{4.10}$$

Argon Model 1 implements the recombination rate of Igra and Barcessat [38], whereas Argon Model 2 follows the result given in Glass and Takano [76]. Both references report the equilibrium constant.

In all of the models presented, the forward reaction rates are given functions of temperature, according to the general formula

$$k_{f,j} = c_{f,j} T^{\eta_{f,j}} e^{-\epsilon_{f,j}/T}, \qquad j = 1, \ldots, J. \tag{4.11}$$

For Argon Model 2, the reaction rate is expressed as the sum of two of such formulas.

The equilibrium constants are given in general as curve fits of experimental data, according to a formula similar to eq.(4.11)

$$K_{e,j} = c_{e,j} T^{\eta_{e,j}} e^{-\epsilon_{e,j}/T}, \qquad j = 1, \ldots, J, \tag{4.12}$$

Air Model 2 has constant given by different curve fits of the form

$$K_{e,j} = e^{a_{1,j} + a_{2,j} z + a_{3,j} z^2 + a_{4,j} z^3 + a_{5,j} z^4}, \qquad z = \frac{10,000}{T}, \qquad j = 1, \ldots, J, \tag{4.13}$$

and Argon Model 1 implements a version of the Saha equation extended to plasmas with two translational temperatures [38].

It is important to point out that the equilibrium constants can be theoretically determined in terms of the species Gibb's free energies from thermodynamic considerations [2]. When a specific thermodynamic model is utilized, as discussed in §2.4, enough information is available to actually write the functional dependence of equilibrium constants on the temperature. In Liu and Vinokur [49], it is advocated

that this is the correct procedure to follow. However, experimental curve fits are supposedly more reliable than theoretically determined formulas, because any approximation and simplification introduced in the thermodynamic model will affect the result. Moreover, when in the presence of thermodynamic non-equilibrium, this theoretical formulation becomes ill-defined. For these reasons, in the present work, theoretical consistency is somewhat sacrificed in favor of accuracy and reliability of the predictions.

The temperature which appears in eqs.(4.11), (4.12) is usually the translational-rotational temperature. However, Argon Model 1 requires the electron translational temperature T_e be used, when this is different from T.

4.3 Thermal Non-Equilibrium

The modeling of thermal non-equilibrium effects is a delicate subject, where no definitive answer has been reached at the present stage. Comparison of numerical simulations with experiments in ballistic ranges and with flight data [40], has shown that these effects play an important role in the physics of hypersonic flows and should be taken into account if accurate predictions are sought.

A fairly common assumption that is made when studying low-density, high Mach number flows is considering the vibrational states of molecules to be out of thermal equilibrium. The rotational contribution is considered to be in equilibrium at the translational temperature, although some authors disagree [31]. Rotational relaxation models have been proposed [77], but their use seems limited to the investigation of the structure of shock waves, where the Navier-Stokes equations are no longer accurate [3], and are usually substituted by the Burnett equations. Electronic excitation is neglected by some authors [6],[27], or considered in equilibrium at a *common* value of vibrational temperature [78], or assumed in equilibrium at the translational temperature of free electrons [31].

Vibrational non-equilibrium is often treated by considering harmonic oscillators and a Landau-Teller model [2]. More refined models were proposed in the 1960's [42–43], and then rediscovered in the 1980's [44],[79], where the different vibrational

levels behave non-uniformly as far as energy exchanges and chemical dissociation are concerned. Preliminary results have been presented [80], where the coupling of rotation with vibration can affect these non-uniformities.

The importance of coupling thermal non-equilibrium effects with chemical kinetics has been investigated [46], and theoretical [43] and *ad hoc* [73] models have been advocated as a means of taking these effects into consideration. In particular, reaction rates for air dissociation have been proposed [74], which are given functions of a *controlling* temperature T_a

$$T_a = T^{\eta_1} T_v^{\eta_2}, \qquad \eta_1 + \eta_2 = 1. \tag{4.14a,b}$$

Here T_v is a common vibrational-electronic temperature, and the coefficients η_1, η_2 can vary from 0.3 to 0.7, and are usually kept equal to 0.5 for ease of calculation.

Further investigation is necessary in order to reach a satisfactory level of confidence on these treatments. More physical insight has to be applied, and new or improved mathematical tools for a thorough analysis of thermal non-equilibrium phenomena are in order. However, satisfactory comparisons with experimental results are already within the reach of present approaches [40], in spite of their many somewhat arbitrary assumptions and approximations.

4.4 Simplified Vibrational Non-Equilibrium

The specific thermal non-equilibrium model that will be applied in the present work has been used in Grossman and Cinnella [6]. Translational and rotational contributions of heavy particles are considered to be in equilibrium at the same temperature T, and vibrational contributions are described by a harmonic oscillator which is not in equilibrium. Electronic excitation is neglected, but free electrons can be present at a translational temperature T_e different from the heavy-particle temperature T.

The source terms in the non-equilibrium energy equation, eq.(3.30), can be modeled by considering only exchanges between the vibrational and the translational-rotational contributions. Interactions with electrons and among the different

species vibrational energies are neglected. Moreover, the inhomogeneity of the *heat bath* in which the vibrating molecule of a particular species is relaxing, due to the presence of other species, is not taken into account. As a result, a Landau-Teller expression can be written for the elastic contributions to the source terms

$$(\dot{Q}_s)_{n,E} = \rho_s \frac{e_{v_s}^*(T) - e_{n_s}}{\tau_s}, \qquad s = 1, \ldots, M, \tag{4.15}$$

where e_v^* is the equilibrium vibrational contribution at the translational temperature T

$$e_{v_s}^* = \frac{R_s \Theta_{v_s}}{e^{\Theta_{v_s}/T} - 1}, \tag{4.16}$$

and τ is a relaxation time, given by Millikan and White [81]

$$\begin{aligned} \tau_s &= \frac{1.013\,10^5}{p} e^{[A_{sr}(T^{-1/3} - 0.015\mu_{sr}^{1/4}) - 18.42]}, \\ A_{rr} &= 1.16\,10^{-3} \mu_{sr}^{1/2} \Theta_{v_r}^{4/3}, \qquad \mu_{sr} = \frac{M_s M_r}{M_s + M_r} = \frac{M_s}{2}. \end{aligned} \tag{4.17a,b,c}$$

In the equations above, Θ_v is a characteristic vibrational temperature, whose values are given in the literature for several species [2],[50],[55],[56],[82].

The previous expressions were derived for diatomic molecules, but can be extended to polyatomic molecules if their vibrational state is modeled by means of a set of characteristic temperatures. This is the case of water [56], whereby the summation of the effects produced by three different vibrational temperatures is enough to reproduce thermodynamic data accurately.

In the electron energy conservation equation, only exchanges between this energy and heavy particle translational-rotational contributions have been included. Interactions with vibrational states have been neglected. The energy source term in eqs.(3.31), (A1.2b) can be written

$$(\dot{Q}_e)_E = 3\hat{R}\rho_e(T - T_e)\sqrt{\frac{8\hat{R}T_e}{\pi M_e}} \sum_{s=1}^{N} \frac{\rho_s N_A}{M_s^2} \sigma_{es}, \tag{4.18}$$

where N_A is Avogadro's number and the collision cross-sections σ_{es} are assumed to be

$$\sigma_{es} = \begin{cases} 10^{-20}\ m^2, & \text{for neutral species,} \\ \frac{8\pi}{27}\frac{N_A\epsilon^2}{\hat{R}T_e} ln\left(1 + \frac{9\hat{R}^3T_e^3}{4\pi M_e N_A^2 \epsilon^6}\right) m^2, & \text{for ions,} \\ 0, & \text{for electrons.} \end{cases} \tag{4.19}$$

and ϵ is the electric charge of an electron. The previous expressions were derived in Lee [1], and have been used by Candler and MacCormack [26–27], who gave an estimate of the value of σ_{es} for neutral species.

The inelastic contribution in eqs.(3.30), (3.31) and (A1.2b) can be modeled by taking into account chemical reactions

$$\begin{aligned} (\dot{Q}_s)_{n,I} &= \dot{\rho}_s e_{n_s} = w_s e_{n_s}, \qquad s = 1, \ldots, M, \\ (\dot{Q}_e)_I &= \dot{\rho}_e e_{0_e} = w_e e_{0_e}, \end{aligned} \tag{4.20a,b}$$

where no attempt has been made of considering coupling effects through equivalent temperatures or by other means.

4.5 Electric Field

The only body force whose contribution cannot be neglected in a weakly ionized gas is the one stemming from a charge-separation induced electric field. External fields can be superimposed to the former, but will be neglected in the present work. Moreover, magnetic fields will not be considered.

An approximate expression for the electric field can be found in Lee [1]. Starting from the electron momentum equation, eq.(3.16) for $s = e$, unsteady, diffusive, viscous and inertial terms are neglected, along with the elastic and inelastic interaction terms. As a result, the body force is balanced by the gradient of the free electron pressure

$$\rho_e g_e \equiv -\epsilon n_e E = \nabla \cdot (p_e \mathbf{I}) = \nabla p_e\,, \tag{4.21}$$

and the electric field is given by

$$E = -\frac{1}{\epsilon n_e}\nabla p_e\,. \tag{4.22}$$

In the above, ϵ is the electron charge and n_e is the electron number density.

For a gas mixture with no external electrical field applied (electrically neutral), the contribution of the electric field to the momentum and energy equations is not zero *because of diffusion*. Had the diffusive properties been neglected, as is the case for the Euler equations, those contributions would have been identically zero, because $\sum_s \epsilon n_s z_s \equiv 0$ in eq.(A1.2b). This result is the effect of the conservation of charge, and is valid *globally* for a mixture whose species are allowed to diffuse, but in a *pointwise* fashion when that is not the case.

5. TREATMENT OF VISCOUS FLUXES

5.1 Introduction

In the governing partial differential equations derived in §3.2, the vectors of viscous fluxes account for transport of mass, momentum and energy, stemming from the fact that the distribution function of the molecular velocity is not in equilibrium at the Maxwellian value [3].

The kinetic theory of flows with these physical properties has been established for conditions of small departures from equilibrium, and a first-order asymptotic analysis yields the Navier-Stokes equations with the shear stress tensor components written as in eq.(3.33) and the heat flux vector written in a form consistent with eq.(3.34c) when thermodynamic equilibrium is assumed [52]. Viscosity and thermal conductivity coefficients are a result of this analysis, as well as multicomponent diffusion terms. Extension to non-equilibrium conditions has been postulated as an almost straightforward extrapolation of those results to more than one temperature, either translational or vibrational [26–27].

Some of the physics is usually simplified when dealing with viscous fluxes. Diffusion induced by temperature, pressure and body forces is neglected, so that mass diffusion can be modeled using Fick's Law [9]. Results have been published where some of those restrictions have been removed for nonreacting mixtures [83]. Temperature-induced, or *thermal*, diffusion is usually very small, and is identically zero if the intermolecular potential is taken to be Maxwellian [2]. However, the other aforementioned effects could be significant in specific instances.

Prediction of transition and modeling of turbulence when in the presence of chemical reactions and thermal non-equilibrium are examples of very important problems with hardly any solution at the present stage [7]. Consequently, the only attempt that has been made to include these effects into the numerical simulation is a straightforward extension of classical models for perfect gases [84–85] to non-equilibrium flows [59].

Specific models for viscosity and thermal conductivity coefficients will be discussed in the next two paragraphs for the case of thermal equilibrium. Then, a description of the mass diffusion treatment will precede an analysis of the extension of the previous models to flows with thermal non-equilibrium.

5.2 Viscosity Coefficient

A theoretical formula for the viscosity coefficient to be used in eq.(3.33) has been given as a result of the asymptotic analysis that led to the Navier-Stokes equations [3]. Such a formula is strictly valid for a single monatomic gas, and relies on an intermolecular potential function being assumed. Results for the Lennard-Jones potential have been tabulated [52] and extensively used for general gases as well. The corresponding formulas for mixtures of monatomic gases have been formulated [86], but they are computationally very expensive, due to the appearance of matrices of coefficients.

Curve fit functional expressions have also been proposed, which are based upon experiments on single components. Their advantage is the simplicity, when compared to theoretical determinations, and the availability of semi-empirical rules for recovering the corresponding mixture values. One of the most widely adopted curve fits is due to Blottner [41], and was originally derived for air components

$$\mu_s = e^{[(A_s lnT + B_s) lnT + C_s]}, \qquad s = 1, \ldots, N^*, \tag{5.1}$$

where A_s, B_s, C_s are coefficients determined by fitting the experimental data. Another very popular approach is the extension of Sutherland's Law for a perfect gas to a generic component

$$\mu_s = T^{1.5} \frac{E_s}{T + F_s}, \qquad s = 1, \ldots, N^*, \tag{5.2}$$

where E_s, F_s are again coefficients empirically derived. Both treatments have been included in the present work.

Values of the viscosity coefficient for the mixture are usually recovered by means of Wilke's semi-empirical rule [87], which is an extension of a Sutherland-type equation to multi-component systems, obtained on the basis of the kinetic theory and several simplifying assumptions. The final result reads

$$\mu = \sum_{s=1}^{N^*} \frac{X_s \mu_s}{\sum_j^{N^*} X_j \phi_{sj}}, \qquad \phi_{sj} = \frac{1}{\sqrt{8}}\left(1 + \frac{M_s}{M_j}\right)^{-1/2}\left[1 + \sqrt{\frac{\mu_s}{\mu_j}}\left(\frac{M_j}{M_s}\right)^{1/4}\right]^2. \quad (5.3a,b)$$

where X_s is the mole fraction of species s.

5.3 Thermal Conductivity Coefficient

Values of the thermal conductivity to be used in eq.(3.34c) are also obtained from an asymptotic analysis for small deviations from equilibrium. In addition, thermal diffusion is universally neglected in the heat flux vector. The single-component theory yields expressions that are functions once again of collision integrals, and the latter are functions of the chosen intermolecular potential. A multi-component theory that takes into account internal degrees of freedom of particles [86] is quite complex and computationally expensive.

Curve fit expressions have also been proposed for thermal conductivity, the most accepted one being Eucken's relation

$$k_s = \mu_s\left(\frac{3}{2}\tilde{c}_{v_{tr,s}} + \tilde{c}_{v_s}\right), \qquad s = 1, \ldots, N^*, \qquad (5.4)$$

where $\tilde{c}_{v_{tr}}$ is the translational contribution to the specific heat at constant volume. It is noteworthy that for a perfect gas with $\tilde{\gamma} = 7/5$, this formula yields a value of the Prandtl number $Pr = 28/38 = 0.737$, which is in very good agreement with experimental values.

A Sutherland type formula can also be used, whereby

$$k_s = T^{1.5}\frac{e_s}{T + f_s}, \qquad s = 1, \ldots, N^*, \qquad (5.5)$$

and e_s, f_s are empirical coefficients. Both treatments have been included in the present work.

Results for the mixture thermal conductivity can be obtained by means of Wilke's rule

$$k = \sum_{s=1}^{N^*} \frac{X_s k_s}{\sum_j^{N^*} X_j \phi_{sj}}, \qquad \phi_{sj} = \frac{1}{\sqrt{8}}\left(1 + \frac{M_s}{M_j}\right)^{-1/2}\left[1 + \sqrt{\frac{\mu_s}{\mu_j}}\left(\frac{M_j}{M_s}\right)^{1/4}\right]^2, \quad (5.6a,b)$$

where the weight coefficients ϕ_{sj} are the same as in the formula for the mixture viscosity.

Another simplified approach for the evaluation of a mixture thermal conductivity is the assumption of a constant Prandtl number, which is a well known empirical result for perfect gases in a wide range of physical conditions [88], so that k can be evaluated from

$$k = \frac{\mu \tilde{c}_p}{Pr}, \qquad Pr = constant, \qquad (5.7a,b)$$

and the determination of species thermal conductivities is avoided. Both options have been implemented in the numerical simulation.

5.4 The Treatment of Diffusion

Mass diffusion is a physical phenomenon that arises mostly because of the presence of gradients of mass or mole concentrations in the mixture. Although pressure and temperature gradients as well as the effect of body forces can influence diffusion, for a simple analysis these variables are often neglected. With these simplifications, it is possible to write the Stefan-Maxwell equation [9]. Solutions to this equation have been attempted in conjunction with numerical simulations of chemically inert flows, as in Baysal, Engelund and Tatum [83], where the pressure gradient is also retained.

Assuming that the mixture behaves like a binary mixture yields a reduced form of the Stefan-Maxwell equation, the so-called Fick's law of diffusion

$$\rho_s V_s = -\rho D_s \nabla\left(\frac{\rho_s}{\rho}\right), \qquad s = 1, \ldots, N^*, \qquad (5.8)$$

where D_s are the diffusion coefficients. Investigations of several transport algorithms have shown that this formula can produce reasonable results at a much lower computational cost [89].

Fick's law is sometimes expressed in terms of the mole fraction gradients, instead of the mass fractions [58]. The two approaches are equivalent in absence of chemical reactions, because the mixture molecular weight is a constant in that instance. However, the diffusion coefficients are *not* the same. Moreover, in both cases those coefficients cannot be prescribed independently of each other, because the diffusive fluxes must satisfy the requirement of eq.(3.4b), $\sum_s \rho_s V_s = 0$.

The simplest modeling of the diffusion coefficients is obtained by assuming a constant Lewis number. The result is

$$D_s = D = \frac{Le}{\rho}\frac{k}{\tilde{c}_p} = \frac{Le}{\rho}\frac{\mu}{Pr}, \qquad s = 1, \ldots, N^*, \tag{5.9}$$

where only one global diffusion coefficient is used. This model satisfies eq.(3.4b) trivially because

$$\sum_{s=1}^{N^*} \rho_s V_s = -\rho D \sum_{s=1}^{N^*} \nabla(\frac{\rho_s}{\rho}), \qquad \sum_{s=1}^{N^*} \nabla(\frac{\rho_s}{\rho}) = \nabla(\sum_{s=1}^{N^*} \frac{\rho_s}{\rho}) = \nabla(1) \equiv 0. \tag{5.10a,b}$$

Multi-component effects can be partially taken into account by more complex choices of diffusion coefficients [52], relating those with binary diffusion coefficients of species s into species j, D_{sj}

$$D_s = \frac{1 - X_s}{\sum_j X_j / D_{sj}}, \qquad s = 1, \ldots, N^*, \tag{5.11}$$

where X_s is the mole fraction of species s.

A complete multi-component solution has been proposed [86], and utilized [41], but it involves inversion of matrices and evaluations of determinants, resulting in a computationally expensive task.

When ions are present in the mixture with an electron pressure gradient, ambipolar diffusion occurs. This effect is usually accounted for by doubling the diffusion coefficient for positive ions [1], and consequently modifying the coefficient for electrons in order to satisfy eq.(3.4b).

In the present numerical simulation, only the simple model with constant D has been implemented, with no corrections for ionic diffusion. This simple approach is believed to capture the bulk of the physical phenomenon. However, more refined models are deemed necessary in order to achieve improved accuracy.

5.5 Thermal Non-Equilibrium

Theoretical solutions of the Boltzmann equations for mixtures of gases out of thermal equilibrium have not been obtained, to the best of the author's knowledge. The numerical treatment of transport properties for these cases consists usually of fairly simple assumptions. Diffusion and viscosity are left unaltered, and thermal conductivity is modified in a straightforward manner, because only the portions of the specific heats that are in thermal equilibrium, $\tilde{c}_v$, $\tilde{c}_p$, are included in eqs.(5.4) and (5.7a).

The treatment of non-equilibrium thermal conductivity and the determination of k_{n_s} are dealt with in a simple way, by using a Eucken-type relation

$$k_{n_s} = \mu_s c_{n_s}, \qquad c_{n_s} = a_s R_s, \qquad s = 1, \ldots, M. \tag{5.12}$$

In eq.(5.12) the non-equilibrium specific heat c_{n_s} is usually approximated by its fully excited value, therefore $a_s = 1$ for diatomic molecules and $a_s = 3$ for H_2O, for cases when only the vibrational non-equilibrium contribution is considered [26].

For the case of free electrons at a different translational temperature, the results of eqs.(5.1–12) are left unaltered, because the electron viscosity is neglected. A non-equilibrium electron thermal conductivity can be assumed using Eucken's relation [27], and the total conductivity associated with the electron temperature made to coincide with the electron energy contribution only : $k_e \equiv k_{e_e}$ in eqs.(3.46–47), (3.50–51).

More sophisticated models and a more complete understanding of the physics of these phenomena are in order, before any numerical prediction can be considered entirely satisfactory.

6. FREE ELECTRONS

6.1 Introduction

Hypersonic flows around aerodynamic bodies or inside combustion chambers are characterized by very high temperatures and low residence times. In this context, processes like chemical reactions or vibrational relaxation to the translational equilibrium temperature cannot proceed to completion because they typically require hundreds of particle collisions and a residence time that can be even orders of magnitude higher than the one available. However, for many purposes, the assumption of a common translational-rotational temperature holds, due to the very efficient energy exchanges among the different particles. Few collisions are typically necessary to equilibrate the thermal velocity and the rotational states. An important exception is found when there is a great difference in molecular masses, as in the interactions between heavy particles and electrons.

An interesting analogy, due to Prof. Christiansen, can be given for this phenomenon, assuming a hard-sphere model for the particle interactions and consequently elastic collisions. The difference in mass between heavy particles and electrons can be compared to the difference between a football and a table-tennis ball. If a motionless football is hit by other footballs a few times, the "particles" will reach a common velocity almost immediately, but now imagine how many table-tennis ball hits are necessary to start moving a football ...

For this reason, free electrons are often modeled as a species with a different translational temperature. Then Maxwellian statistical distributions, with different mean-square values, are assumed to hold for the equilibrium values of thermal velocities of both kinds of particles, only with different mean-square values, and translational non-equilibrium, with the assumption of only small deviations from equilibrium, can be treated as seen in §3.1–2. However, there are many problems that arise when this model is used. The thermodynamic temperature T is usually identified with the temperature that can be defined from the thermal velocity mean-square value, eq.(3.15b). When there are more than one of these temperatures, the

link between macroscopic and microscopic descriptions becomes ill-defined. Usually, the heavy-particle temperature is considered to be the thermodynamic value, and the free-electron temperature is treated as a non-equilibrium contribution. Further assumptions and approximations are necessary in order to overcome or simply avoid some of the problems connected with the multiplicity of translational temperatures.

Simulations of flows with an electron translational temperature [26–27], or an electron-vibrational combined temperature [78] have appeared in the literature. These and other results were obtained introducing some simplifications in the mathematical problem, namely using a method of characteristics where only the equilibrium and the frozen speeds of sound need to be defined [38], and having an approximate flux-splitting technique whereby the electron pressure is neglected in the electron energy equation [27],[31]. No analysis of the mathematical and physical consequences of multiple translational temperatures has been given.

In the following, a discussion of the eigenvalues for the inviscid flux Jacobian will be presented, followed by some considerations on the problems associated with the presence of multiple translational temperatures in a thermodynamic model for a gas mixture. Then, an asymptotic analysis will show how it is feasible to get approximate results that retain much of the mathematics and physics of the problem.

6.2 Eigenvalue Problem for the Inviscid Jacobians

The inviscid flux Jacobians for the general thermal non-equilibrium equations derived in §3.2 have been presented in Appendix 2. An essential step for the derivation of upwind algorithms is the determination of eigenvalues and eigenvectors of those Jacobians. Moreover, the eigenvalues have a physical interpretation, being the speeds of propagation of infinitesimal disturbances, and a mathematical meaning, being the characteristic velocities of the hyperbolic system of governing partial differential equations [90]. The eigenvectors can also be interpreted as the strengths of the infinitesimal disturbances traveling at the characteristic speeds [91].

The results of the search for the eigenvalues are discussed in Appendix 3. Considering the flux in the x_1 direction $\boldsymbol{F}$, when only one translational temperature is

present, the eigenvalues are u_{0_1} repeated N^*+M+2 times, and $u_{0_1} \pm a$, as reported in eq.(A3.2), where a is the frozen speed of sound defined by eq.(2.20). This result is consistent with what one would expect, because it is a straightforward extension of a perfect-gas-type behaviour. However, for the general case a simple solution could not be determined. The repeated eigenvalue u_{0_1}, this time with multiplicity $N+M+2$, is again recovered, but the remaining three are found to be the roots of a third order algebraic equation, with no simple solutions, eq.(A3.3)

$$(\lambda-u_{0_1})^3 + g_1(\lambda-u_{0_1})^2 + g_2(\lambda-u_{0_1}) + g_3 = 0. \tag{6.1}$$

The coefficients g_i are given in Appendix 3, eq.(A3.4a,b,c), and are repeated here for convenience

$$g_1 = - u_{0_1}\left[(\gamma_e-1) + (\tilde{\gamma}-1)\chi_e\right], \tag{6.2}$$

$$g_2 = - \left[\tilde{\gamma}\frac{p}{\rho} - (\tilde{\gamma}-1)\chi_e R_e T_e\right], \tag{6.3}$$

$$g_3 = u_{0_1}\left[(\gamma_e-1)\tilde{\gamma}\frac{p}{\rho} + (\tilde{\gamma}-1)\chi_e R_e T_e\right], \tag{6.4}$$

where χ_e is given in eq.(A2.10)

$$\chi_e = (\gamma_e-1)\frac{\tilde{c}_{v_e}}{R_e} + \frac{\rho_e}{\rho}\left[1 - \frac{\gamma_e - 1}{\tilde{\gamma} - 1}\right], \tag{6.5}$$

and $\gamma_e = 5/3$ is the ratio of specific heats for electrons.

The presence of two translational temperatures alters the eigenvalue structure, and there is no solution of the type $u_{0_1} \pm \tilde{a}$, where $\tilde{a}$ is some relevant speed of sound. It is interesting to investigate where these complications enter the picture. With this in mind, some simplified approaches can be analyzed, including the approximations that have been utilized in the literature [27],[31].

Neglecting electronic excitation of the heavy particles does not help, because it brings only a change in the definition of χ_e, which becomes, when $\tilde{c}_{v_e} \equiv 0$

$$\chi_e = \frac{\rho_e}{\rho}\left[1 - \frac{\gamma_e - 1}{\tilde{\gamma} - 1}\right]. \tag{6.6}$$

Similarly, neglecting all thermal non-equilibrium effects but the presence of an electronic translational temperature does not alter the structure of the eigenvalue problem given by eq.(6.1).

An alternative formulation of the coefficients of eq.(6.1) can be derived when the heavy particle electronic excitation is neglected again, $\tilde{c}_{v_e} \equiv 0$. This formulation turns out to be slightly simpler and will be useful for comparative purposes when other models will be investigated in §6.3. Writing pressure and density in terms of two contributions, from heavy particles with translational temperature T and from electrons, yields respectively

$$p = \sum_{i=1}^{N^*} p_i + p_e = \tilde{p} + p_e, \qquad \rho = \sum_{i=1}^{N^*} \rho_i + \rho_e = \tilde{\rho} + \rho_e \,. \tag{6.7a,b}$$

Furthermore, the coefficients g_i in eq.(6.1) can be expressed as follows

$$\begin{aligned} g_1 &= -\, u_{0_1} \left[(\gamma_e - 1) \frac{\tilde{\rho}}{\rho} + (\tilde{\gamma} - 1) \frac{\rho_e}{\rho} \right], \\ g_2 &= -\, \left[\tilde{\gamma} \frac{\tilde{p}}{\rho} + \gamma_e \frac{p_e}{\rho} \right], \\ g_3 &= u_{0_1} \left[(\gamma_e - 1) \tilde{\gamma} \frac{\tilde{p}}{\rho} + (\tilde{\gamma} - 1) \gamma_e \frac{p_e}{\rho} \right]. \end{aligned} \tag{6.8a,b,c}$$

A closer examination of the mathematical structure of the governing equations shows that the presence of the electron partial pressure p_e is the most striking difference between the electron energy equation and the other non-equilibrium energy equations. Wherever it is possible to neglect p_e in the inviscid fluxes, due to its small value, the eigenvalue problem simplifies dramatically, because the g_i's become

$$\begin{aligned} g_1 &= -\, u_{0_1} (\tilde{\gamma} - 1) \chi_e \,, \\ g_2 &= -\, \tilde{\gamma} \frac{p}{\rho} \,, \\ g_3 &= 0 \,. \end{aligned} \tag{6.9a,b,c}$$

In this instance, the third-order equation has the simple solutions

$$\lambda = \begin{cases} u_{0_1} \,, \\ u_{0_1} - g_1/2 \pm \sqrt{-g_2} \left(1 - g_1^2 / 4 g_2 \right)^{1/2} \,. \end{cases} \tag{6.10}$$

Writing g_2 as the negative of a speed of sound squared

$$g_2 = -\tilde{\gamma}\frac{p}{\rho} = -a^2, \tag{6.11}$$

the last two eigenvalues can be expressed as

$$\lambda_{a,b} = u_{0_1}\left(1 + \chi_e\frac{(\tilde{\gamma}-1)}{2}\right) \pm a\left(1 + \chi_e^2 u_{0_1}^2\frac{(\tilde{\gamma}-1)^2}{4a^2}\right)^{1/2}. \tag{6.12}$$

However, this solution does not fully recover the simple structure $u_{0_1} \pm a$ valid in the absence of a separate electronic temperature.

The conclusion that the presence of a partial electronic pressure in the inviscid fluxes is the main reason for the mathematical complications above is confirmed by the fact that when the kinetic energy contribution $\rho_e u_0^2/2$ is neglected, but p_e is maintained, the resulting expressions for g_2 and g_3 are inaltered, whereas g_1 reduces to

$$g_1 = -(\gamma_e - 1)u_{0_1}\,. \tag{6.13}$$

Overall, no real simplification has occurred for this approximation.

The standard approach undertaken when dealing with electronic energy is to neglect *both* p_e and $\rho_e u_0^2/2$ [31]. This yields the simple solution

$$g_1 = 0, \qquad g_2 = -\tilde{\gamma}\frac{p}{\rho} = -a^2, \qquad g_3 = 0. \tag{6.14a,b,c}$$

The eigenvalues become

$$\lambda = \begin{cases} u_{0_1}\,, \\ u_{0_1} \pm a\,, \end{cases} \tag{6.15}$$

and the value of the speed of sound a is consistent with eq.(2.26) for the generalized frozen speed of sound, once p_e is dropped.

There is a serious objection to this approach. When writing the total internal energy and total entalphy of electrons

$$e_{0_e} = \frac{3}{2}R_e T_e + \frac{u_0^2}{2}, \qquad h_{0_e} = \frac{3}{2}R_e T_e + \frac{p_e}{\rho_e} + \frac{u_0^2}{2} = \frac{3}{2}R_e T_e + R_e T_e + \frac{u_0^2}{2}, \tag{6.16a,b}$$

it is not clear how electron pressure or kinetic energy can be neglected without introducing significant errors. This is the reason why the electronic pressure is usually maintained, but displaced to the vector of source terms [31]. In so doing, the mathematical structure of the problem is altered, and complications arise for the derivation of flux-split algorithms.

In this context, it becomes appealing to obtain an approximate treatment of the general problem of eq.(6.1) which retains all of the contributions to the electron energy equation, but simplifies the mathematics in a consistent way. A very simple asymptotic analysis will be presented in §6.4, leading to some interesting results that constitute a complete and more consistent approach.

6.3 Multiple Translational Temperatures

In the previous section, an introductory analysis was presented to investigate the origin of the complications that arise in the eigenvalue problem for the inviscid flux Jacobian when two translational temperatures are assumed in the thermodynamic model. Neglecting some of the contributions to the electron energy fluxes was shown to simplify the problem, in particular when the electron partial pressure was somehow discarded. The latter result is particularly interesting, because the appearance of pressure is the most important factor which differentiates translational contributions from the other internal energy contributions. Consequently, it seems likely that the presence of two translational temperatures plays a key role in alterating the simple eigenvalue structure that is otherwise preserved, even in presence of other forms of thermal non-equilibrium.

In order to better assess the effect of multiple translational temperatures on the characteristic velocities, a generalized thermodynamic model will be considered in the following, whereby all the species are assumed to have their own translational temperature. The results which stem from this model will be discussed, and some interesting analogies with the more restricted thermal model considered in this work will be found.

The thermodynamic model presented in §2.2 can be generalized by writing the internal energy per unit mass of a gaseous species as follows

$$e_i = \sum_{j=1}^{N} e_{ij}(T_j) + e_{n_i}(\mathbf{x}, t), \tag{6.17}$$

where e_{ij} is the portion of the internal energy of species i that is in equilibrium at the translational temperature T_j of species j. Obviously, the different temperatures T_i need not be equal. The thermodynamic model utilized until now, as in eq.(2.1), is a particular case of this model, when $T_1 = T_2 = \ldots = T_{N^*} \equiv T$ and $T_N \equiv T_e$. Then the diagonal terms $e_{ii}(T_i) \equiv \tilde{e}_i(T)$ for $i = 1, \ldots N^*$, and the contributions $e_{iN} = e_{ie} \equiv e_{e_i}$.

The pressure is given by Dalton's Law and the mixture internal energy by a mass-fraction average

$$p = \sum_{i=1}^{N} p_i = \rho_i R_i T_i, \qquad e = \sum_{i=1}^{N} \frac{\rho_i}{\rho} e_i \,. \tag{6.18a,b}$$

Furthermore, it is possible to define total internal energy and enthalpy for a species

$$e_{0_i} = e_i + \frac{u_0^2}{2}, \qquad h_{0_i} = e_{0_i} + \frac{p_i}{\rho_i} \,. \tag{6.19a,b}$$

The procedure followed in §3.2 for the determination of the governing equations is not altered by the presence of multiple translational temperatures. However, in order to close the system of equations, $N+M$ energy equations must be written. Consequently, the species energy equations, eq.(3.26), and the non-equilibrium energy equations, eq.(3.30), will be utilized, along with species continuity, eq.(3.9), and global momentum, eq.(3.19).

Neglecting the unsteady contribution from the diffusion velocity in the species energy equation, the new vector of conserved variables Q and the flux in the x_1

direction F can be written as follows

$$Q = \begin{pmatrix} \rho_1 \\ \rho_2 \\ \vdots \\ \rho_N \\ \rho u_{0_1} \\ \rho u_{0_2} \\ \rho u_{0_3} \\ \rho_1 e_{n_1} \\ \rho_2 e_{n_2} \\ \vdots \\ \rho_M e_{n_M} \\ \rho_1 e_{0_1} \\ \rho_2 e_{0_2} \\ \vdots \\ \rho N e_{0_N} \end{pmatrix}, \qquad F = \begin{pmatrix} \rho_1 u_{0_1} \\ \rho_2 u_{0_1} \\ \vdots \\ \rho_N u_{0_1} \\ \rho u_{0_1} u_{0_1} + p \\ \rho u_{0_1} u_{0_2} \\ \rho u_{0_1} u_{0_3} \\ \rho_1 e_{n_1} u_{0_1} \\ \rho_2 e_{n_2} u_{0_1} \\ \vdots \\ \rho_M e_{n_M} u_{0_1} \\ \rho_1 h_{0_1} u_{0_1} \\ \rho_2 h_{0_2} u_{0_1} \\ \vdots \\ \rho_N h_{0_N} u_{0_1} \end{pmatrix}. \qquad (6.20a, b)$$

Knowing the state of the system, as described by the vector Q, one can determine all the translational temperatures by solving the system

$$e_i = \sum_{j=1}^{N} \int_{T_{ref}}^{T_j} c_{v_{ij}}(\tau)\, d\tau + h_{f_i} + \sum_{j=1}^{M} e_{n_j}, \qquad i = 1, \ldots, N, \qquad (6.21)$$

where $c_{v_{ij}}$ are given functions of the temperatures. Then, the pressure can be recovered from eq.(6.18a).

Jacobian matrices and their eigenvalues can then be determined using the information already presented. However, in general in order to evaluate pressure and temperature derivatives it will be necessary to invert the matrix of specific heats

$$\mathbf{C}_v = \begin{pmatrix} c_{v_{11}} & c_{v_{12}} & c_{v_{13}} & \cdots & c_{v_{1N}} \\ c_{v_{21}} & c_{v_{22}} & c_{v_{23}} & \cdots & c_{v_{2N}} \\ c_{v_{31}} & c_{v_{32}} & c_{v_{33}} & \cdots & c_{v_{3N}} \\ \vdots & \vdots & \vdots & \ddots & \vdots \\ c_{v_{N1}} & c_{v_{N2}} & c_{v_{N3}} & \cdots & c_{v_{NN}} \end{pmatrix}. \qquad (6.22)$$

The inversion can be performed easily for the specific case of nonzero entries only in the main diagonal and on the last column. This model corresponds more closely

to the thermodynamic model used in §2, because the species internal energy will have only three contributions, one in equilibrium at its translational temperature, one in equilibrium at the electron translational temperature $T_N \equiv T_e$, and the third one in non-equilibrium. However, the heavy particle translational temperatures do not need to be the same.

When the matrix of specific heats is written as follows

$$\mathbf{C}_v = \begin{pmatrix} c_{v_{11}} & 0 & 0 & \cdots & c_{v_{1N}} \\ 0 & c_{v_{22}} & 0 & \cdots & c_{v_{2N}} \\ 0 & 0 & c_{v_{33}} & \cdots & c_{v_{3N}} \\ \vdots & \vdots & \vdots & \ddots & \vdots \\ 0 & 0 & 0 & \cdots & c_{v_{NN}} \end{pmatrix} = \begin{pmatrix} \tilde{c}_{v_1} & 0 & 0 & \cdots & c_{v_{e,1}} \\ 0 & \tilde{c}_{v_2} & 0 & \cdots & c_{v_{e,2}} \\ 0 & 0 & \tilde{c}_{v_3} & \cdots & c_{v_{e,3}} \\ \vdots & \vdots & \vdots & \ddots & \vdots \\ 0 & 0 & 0 & \cdots & c_{v_{e,e}} \end{pmatrix}, \quad (6.23)$$

the Jacobian of the inviscid fluxes can be determined and the eigenvalue problem written without overwhelming algebraic complications. It turns out that the first $N+M+2$ eigenvalues for $\mathbf{A} = \partial \boldsymbol{F}/\partial \boldsymbol{Q}$ are given by $\lambda_i = u_{0_1}$, and an algebraic equation of order $N+1$ must be solved in order to obtain the remaining terms. No simple solution can be found for this equation, which confirms that indeed the eigenvalue structure is complicated by the presence of multiple translational temperatures.

Interesting results can be obtained when considering the case $N = 2$. The third order equation for the eigenvalues is similar to eq.(6.1)

$$(\lambda - u_{0_1})^3 + g_1(\lambda - u_{0_1})^2 + g_2(\lambda - u_{0_1}) + g_3 = 0, \quad (6.24)$$

and has coefficients given by

$$\begin{aligned} g_1 &= -u_{0_1}\left[(\gamma_e - 1)\frac{\rho_1}{\rho} + (\gamma_1 - 1)\frac{\rho_e}{\rho} + \frac{\rho_1 R_1 c_{v_{e,1}}}{\rho \tilde{c}_{v_1} c_{v_{e,e}}}\right], \\ g_2 &= -\left[\gamma_1 \frac{p_1}{\rho} + \gamma_e \frac{p_e}{\rho} + R_e T_e \frac{\rho_1 R_1 c_{v_{e,1}}}{\rho \tilde{c}_{v_1} c_{v_{e,e}}}\right], \\ g_3 &= u_{0_1}\left[(\gamma_e - 1)\gamma_1 \frac{p_1}{\rho} + (\gamma_1 - 1)\gamma_e \frac{p_e}{\rho} + R_e T_e \frac{\rho_1 R_1 c_{v_{e,1}}}{\rho \tilde{c}_{v_1} c_{v_{e,e}}}\right], \end{aligned} \quad (6.25a, b, c)$$

where the specific heat ratios γ_i have been defined to be

$$\gamma_1 = 1 + \frac{R_1}{\tilde{c}_{v_1}}, \qquad \gamma_e = 1 + \frac{R_e}{c_{v_{e,e}}}. \tag{6.26a,b}$$

Neglecting the electronic excitation term $c_{v_{e,1}}$ results in the coefficients

$$\begin{aligned} g_1 &= -u_{0_1}\left[(\gamma_e - 1)\frac{\rho_1}{\rho} + (\gamma_1 - 1)\frac{\rho_e}{\rho}\right], \\ g_2 &= -\left[\gamma_1 \frac{p_1}{\rho} + \gamma_e \frac{p_e}{\rho}\right], \\ g_3 &= u_{0_1}\left[(\gamma_e - 1)\gamma_1 \frac{p_1}{\rho} + (\gamma_1 - 1)\gamma_e \frac{p_e}{\rho}\right], \end{aligned} \tag{6.27a,b,c}$$

where the analogy with the result of eqs.(6.8) is apparent. After some algebraic manipulations, a similar analogy is found between eqs.(6.2–4) and the complete eqs.(6.25). The two mathematical problems are therefore equivalent.

6.4 Asymptotic Analysis

In the previous sections, the complications due to assuming an electron translational temperature different from the heavy particle counterpart have been discussed. In particular, no simple eigenvalues for the inviscid Jacobians were found, nor were the corresponding eigenvectors determined. Approximate treatments for this problem have been reviewed, but they were not entirely satisfactory due to arbitrarily neglecting or displacing pieces of the electron energy fluxes.

In the following, a still approximate but more consistent approach will be proposed, whereby all the contributions of the same importance are treated in the same fashion.

For flows of practical interest, the amount of free electrons is negligible until very high temperatures, of the order of $10,000\ K$, are reached. At higher temperatures, the mass fraction of electrons is still a very small number, due to the great difference in molecular mass between electrons and heavy particles. The specific heat of electrons $c_{v_{e,e}}$ is a large number instead, because the gas constant R_e is equal to the universal gas constant divided by the molecular mass of an electron.

Moreover, the electronic contribution to the internal energy of atoms and molecules is always very small, and is neglected in many thermodynamic models used in the literature [6],[27]. As a result of these considerations, the following assumptions will be made

i) The mass fraction of electrons is a small parameter, of order ϵ, in the analysis : $\rho_e/\rho = O(\epsilon)$;

ii) The ratio of electronic excitation contributions from heavy particles $\tilde{c}_{v_e}$ to the electron specific heat at constant volume $c_{v_{e,e}}$ is a small parameter, of the same order ϵ : $\tilde{c}_{v_e}/c_{v_{e,e}} = O(\epsilon)$. Therefore, $\chi_e = O(\epsilon)$, from eq.(A2.10).

Different asymptotic behaviours for the electron mass fraction and the ratio of specific heats could have been considered, but the analysis would have been greatly complicated, and there seems to be no stringent physical reason for so doing. The previous assumptions were selected for the sake of simplicity. Moreover, the product $R_e T_e$ is a fairly large number, because T_e is of the same order of magnitude than T, but it was assumed to be $O(1)$.

The importance of the terms that will be neglected or treated in a simplified fashion can be studied with an example, considering an air mixture. The equilibrium composition of air at different temperatures, ranging from 4,000 to 20,000 K, was determined. Model 2 in §4.2 was utilized, which includes eleven chemical species. The density was considered to be $\rho = 0.38558\,10^{-1}\,kg/m^3$. Values of the mass fraction ρ_e/ρ and of χ_e are shown in Table 6.1, where electronic excitation was neglected. It can be noticed that the mass fraction is monotonically increasing with temperature, but its value never exceeds $O(10^{-5})$. On the other hand, the value of χ_e reaches a maximum and then decreases slightly, without exceeding $O(10^{-9})$. This is due to the fact that the mixture is almost completely dissociated into its atomic components at high temperatures, with the result that the term in parentheses in the definition of χ_e

$$\chi_e = \frac{\rho_e}{\rho}\left(1 - \frac{\gamma_e - 1}{\tilde{\gamma} - 1}\right) = \frac{\rho_e}{\rho}\left(\frac{\tilde{\gamma} - \gamma_e}{\tilde{\gamma} - 1}\right), \qquad \frac{\tilde{c}_{v_e}}{c_{ve,e}} \equiv 0, \tag{6.28a,b}$$

tends to zero also, for $\tilde{\gamma}$ approaching the monatomic limit 5/3. Had electronic excitation been included, the result would not have been altered substantially.

Once the basic assumptions were stated, a simple asymptotic analysis was performed, where the terms of $O(\epsilon)$ were dropped. This results in the approximate inviscid Jacobian presented in §A2, in its eigenvalues and eigenvectors discussed in §A3, and in the characteric compatibility equations derived in §A4. Those formulas are the basis for the approximate numerical algorithms derived in §7. It is noteworthy that the frozen speed of sound, eq.(2.26), reduces to a form similar to eq.(2.20) for the case with only one translational temperature when this asymptotic analysis is performed. This result is consistent with the value given in Liu and Vinokur [31], where the electronic pressure was included in the source terms for simplicity.

When a mixture of monatomic gases is considered, as is the case for the Argon Models 1 and 2, χ_e reduces to

$$\chi_e = \frac{\tilde{c}_{v_e}}{c_{ve,e}}. \tag{6.29}$$

If electronic excitation is also neglected, which is a good assumption for inert gases, then $\chi_e \equiv 0$. The eigenvalues given in §A3 are then *exact*, and exact eigenvectors could have been derived with a standard procedure. However, this approach has not been pursued, for the sake of generality.

7. NUMERICAL FORMULATION

7.1 Introduction

The governing partial differential equations for hypersonic flows out of chemical and thermal equilibrium have been presented in §3.2, §3.5 and §A1. An integral form has been given in §3.6 by eq.(3.52), which is valid across tangential or normal discontinuities such as slip lines or shock waves. In order for a computer simulation to be possible, these equations must be *discretized*, that is reduced to a set of algebraic equations to be solved.

A very convenient discretization approach is the finite-volume technique [92], whereby the integral form of the governing equations is solved for the unknown volume averages of conserved variables in some small, but finite, control volume. The advantage of this method is its use of the integral form of the equations, which allows a correct treatment of discontinuities and also consistently treats general grid topologies. Other discretizations are also possible, like spectral techniques [93], which have been successfully applied to flow simulations in a chemically active environment [94].

The governing equations previously discussed have been derived in *conservation form*. Mathematically, this means that the coefficients of the derivative terms are constant or, if variable, their derivatives do not appear in the equations [60]. Moreover, the divergence of some physical quantity can usually be identified in the equations. This formulation generally leads to fewer numerical problems in the discretized version for flows with discontinuities.

Related to the conservation form of the governing equations is the *conservative property* of a discrete algorithm. Physically, this means that the conservation principle that was used for the derivation of the equations is enforced exactly over volumes of arbitrary size within the domain of interest. The finite-volume approach has the conservative property.

Discretizing the integral form of the governing equations with a conservative scheme yields the possibility of capturing shocks and other discontinuities.

Shock-fitting techniques have also been attempted for flows out of chemical equilibrium [95], but their implementation is at a relatively initial stage for general thermal non-equilibrium situations.

In the following, the finite-volume technique will be discussed in more detail. Then, flux-split algorithms for the treatment of inviscid fluxes will be presented, and three classes of methods considered, namely flux-vector splittings of the Steger-Warming type [23] and of the Van Leer type [24] and an approximate Riemann solver of the Roe type [25].

These methods have been derived for the one-dimensional governing equations. Extensions to three dimensions are usually accomplished by considering a sequence of three one-dimensional problems. Techniques for the solution of "true" two and three-dimensional problems have been proposed for perfect gases [96],[97], but are still at a very introductory level.

Finally, an analysis of time-integration techniques for steady and unsteady one and three-dimensional problems will be provided. A fully implicit approach will be used throughout this work, whereby chemical and non-equilibrium thermal contributions will be coupled to the fluid dynamic terms. Loosely coupled techniques have been proposed and utilized for their simplicity [94], but in some instances they turn out to be computationally more expensive.

7.2 Finite-Volume Approach

The finite-volume technique takes advantage of the integral form of the governing equations to achieve a discretized algebraic approximation that can be handled by a digital computer. The physical domain of interest is partitioned in a (large) set of subdomains, each one of arbitrary volume Ω and closed by a boundary $\partial\Omega$, where the integral equation of §3.6, eq.(3.52), can be written

$$\iiint_{\Omega} \frac{\partial Q}{\partial t} d\Omega + \oint_{\partial\Omega} (S - S_v) \cdot n d\partial\Omega = \iiint_{\Omega} W d\Omega \,. \tag{7.1}$$

Approximations are then used for the volume and surface integrals to express them in terms of the unknown *volume-averaged* values of each computational cell. This

technique can be applied to arbitrarily shaped volumes, but will be illustrated for *structured* meshes, where a generalized curvilinear frame of reference (ξ, η, ς) can be defined and related through a continuous transformation to a reference set of Cartesian orthogonal coordinates (x_1, x_2, x_3), as discussed in §3.5.

It should be noted that every infinitesimal contribution to the surface integrals is either shared by *two* adjacent cells or belongs to the external boundary. Consequently, every approximation to the surface integrals which is independent of the cell for which the contribution is considered will yield a scheme that has the conservative property, as discussed in the previous section. The reason for this is that when an arbitrary control volume including several cells is considered, the contributions to the discretized equations which correspond to surface integrals that are now *inside* the volume will cancel each other, leaving an equation that is the discretized version of the conservation statement applied to this arbitrary control volume. In the following, only discretizations with the conservative property will be examined.

The first step in the discretization process is to introduce volume-averaged values for the conservative variables Q and the source terms W

$$<Q>= \frac{1}{\Omega} \iiint_{\Omega} Q d\Omega, \qquad <W>= \frac{1}{\Omega} \iiint_{\Omega} W d\Omega, \tag{7.2a,b}$$

where the volume Ω of the generic computational cell is given by

$$\Omega = \iiint_{\Omega} d\Omega = \iiint_{\Omega} dx_1 dx_2 dx_3 = \iiint_{\Omega} J^{-1} d\xi d\eta d\varsigma, \tag{7.3}$$

and the Jacobian J of the coordinate transformation, eq.(3.42), has been introduced. Substituting into eq.(7.1) and noting that the time derivative can be brought outside of the integral yields

$$\frac{\partial <Q>}{\partial t} \Omega + \oint_{\partial\Omega} (S - S_v) \cdot n d\partial\Omega = <W> \Omega . \tag{7.4}$$

For the case of a structured mesh, the computational cell will be defined by two $\xi = constant$, two $\eta = constant$, and two $\varsigma = constant$ surfaces, respectively. Associating indices i, j, k to the ξ, η, ς coordinates, respectively, the arbitrary volume under consideration will be described by the indices ijk and the surface integral will be split into six contributions, one from each delimiting surface. Then area-averaged values of a generic quantity f can be introduced

$$<f>_{i+1/2} = \frac{1}{\partial\Omega_{i+1/2}} \int\int_{\partial\Omega_{i+1/2}} f \, d\partial\Omega_{i+1/2} \,, \tag{7.5}$$

with similar definitions for the other indices, with the area $\partial\Omega_{i+1/2}$ given by

$$\partial\Omega_{i+1/2} = \int\int_{\partial\Omega_{i+1/2}} d\partial\Omega_{i+1/2} = \int\int_{\partial\Omega_{i+1/2}} |\nabla\xi| J^{-1} d\eta d\varsigma \,. \tag{7.6}$$

Specializing the previous results to $f = (S - S_v) \cdot \boldsymbol{n}$, where the flux vectors have Cartesian components $(F - F_v)$, $(G - G_v)$, $(H - H_v)$ and the unit normal to the $i + 1/2$ surface has components $\tilde{\xi}_{x_1}$, $\tilde{\xi}_{x_2}$, $\tilde{\xi}_{x_3}$, with similar relations holding for the other space directions, leads to the following useful formulas

$$\begin{aligned}
<(\tilde{F} - \tilde{F}_v)>_{i+1/2} &= <(F - F_v)\tilde{\xi}_{x_1} + (G - G_v)\tilde{\xi}_{x_2} + (H - H_v)\tilde{\xi}_{x_3}>_{i+1/2} \,, \\
<(\tilde{G} - \tilde{G}_v)>_{j+1/2} &= <(F - F_v)\tilde{\eta}_{x_1} + (G - G_v)\tilde{\eta}_{x_2} + (H - H_v)\tilde{\eta}_{x_3}>_{j+1/2} \,, \\
<(\tilde{H} - \tilde{H}_v)>_{k+1/2} &= <(F - F_v)\tilde{\varsigma}_{x_1} + (G - G_v)\tilde{\varsigma}_{x_2} + (H - H_v)\tilde{\varsigma}_{x_3}>_{k+1/2} \,.
\end{aligned} \tag{7.7a,b,c}$$

Eq.(7.4) can then be written as follows

$$\begin{aligned}
\frac{\partial <Q>}{\partial t}\Omega &+ <(\tilde{F} - \tilde{F}_v)>_{i+1/2}\partial\Omega_{i+1/2} - <(\tilde{F} - \tilde{F}_v)>_{i-1/2}\partial\Omega_{i-1/2} + \\
&+ <(\tilde{G} - \tilde{G}_v)>_{j+1/2}\partial\Omega_{j+1/2} - <(\tilde{G} - \tilde{G}_v)>_{j-1/2}\partial\Omega_{j-1/2} + \\
&+ <(\tilde{H} - \tilde{H}_v)>_{k+1/2}\partial\Omega_{k+1/2} - <(\tilde{H} - \tilde{H}_v)>_{k-1/2}\partial\Omega_{k-1/2} = <W>\,\Omega,
\end{aligned} \tag{7.8}$$

where the orientation of the surfaces has been taken into account

It is important to point out that eq.(7.8) is still *exact*, because volume and area-averaged values have not been approximated. However, at this stage it is

necessary to relate the area-averaged values to the unknown volume-averaged values. The resulting set of *algebraic* equations will be the discretized form of the original problem that is actually solved by means of a digital computer.

An interesting analogy [92] between the finite-volume formulation discussed so far and a more standard finite-difference technique can be obtained when the volume Ω is written in terms of an average Jacobian and average increments in the coordinate directions

$$\Omega = \int\int\int_{\Omega} J^{-1} d\xi d\eta d\zeta = \frac{\Delta\xi\Delta\eta\Delta\zeta}{<J>}. \tag{7.9}$$

Similarly, the areas can be written as follows

$$\partial\Omega_{i+1/2} = \int\int_{\partial\Omega_{i+1/2}} |\nabla\xi| J^{-1} d\eta d\zeta = \Delta\eta\Delta\zeta <\frac{|\nabla\xi|}{J}>_{i+1/2}, \tag{7.10}$$

with corresponding results for the other terms.

Substituting eqs.(7.9), (7.10) into eq.(7.8), dividing by $\Delta\xi\Delta\eta\Delta\zeta$ and dropping the average notation yields

$$\begin{aligned}
&\frac{1}{J}\frac{\partial Q}{\partial t} + \frac{1}{\Delta\xi}\Big[\Big(\frac{|\nabla\xi|}{J}\Big)_{i+1/2}(\tilde{F}-\tilde{F}_v)_{i+1/2} - \Big(\frac{|\nabla\xi|}{J}\Big)_{i-1/2}(\tilde{F}-\tilde{F}_v)_{i-1/2}\Big] + \\
&\quad + \frac{1}{\Delta\eta}\Big[\Big(\frac{|\nabla\eta|}{J}\Big)_{j+1/2}(\tilde{G}-\tilde{G}_v)_{j+1/2} - \Big(\frac{|\nabla\eta|}{J}\Big)_{j-1/2}(\tilde{G}-\tilde{G}_v)_{j-1/2}\Big] + \\
&\quad + \frac{1}{\Delta\zeta}\Big[\Big(\frac{|\nabla\zeta|}{J}\Big)_{k+1/2}(\tilde{H}-\tilde{H}_v)_{k+1/2} - \Big(\frac{|\nabla\zeta|}{J}\Big)_{k-1/2}(\tilde{H}-\tilde{H}_v)_{k-1/2}\Big] = \frac{W}{J}.
\end{aligned} \tag{7.11}$$

Eq.(7.11) is the discretized form of the governing differential equation written in generalized coordinates, eq.(3.39), that would have been obtained using a standard finite-difference approach. Consequently, the two methods are strictly related, the main difference being the interpretation of the unknowns as volume-averages in the case of the finite-volume strategy.

The area-averaged values of the inviscid fluxes are related to the volume-averaged values of the conserved variables through a MUSCL high-order generalized

extrapolation procedure [92],[98], whereby cell-face values for Q are obtained from the cell-center unknowns

$$Q^{\mp}_{i\pm 1/2} = \{I \pm \frac{1}{4}[(1 \mp \kappa)\bar{\nabla} + (1 \pm \kappa)\bar{\Delta}]\}Q, \tag{7.12}$$

with similar results for the other indices, and the fluxes are then constructed from the functional relationships

$$\tilde{F} = \tilde{F}(Q^+, Q^-), \qquad \tilde{G} = \tilde{G}(Q^+, Q^-), \qquad \tilde{H} = \tilde{H}(Q^+, Q^-). \tag{7.13}$$

In the previous formulas, I is the identity operator, ∇, Δ are backward and forward difference operators, respectively, and Q^-, Q^+ are left and right extrapolations of the conservative variables Q, which will be discussed in detail in the next sections. The bars in the difference operators of eq.(7.12) indicate the presence of a limiter [99] for the higher-order corrections, the min-mod limiter being usually employed in the simulations. The parameter κ determines the extrapolation scheme used. A value $\kappa = 1/3$ yields a third-order upwind-biased technique, a value $\kappa = -1$ produces the second-order upwind method, whereas $\kappa = 1$ gives the classic second-order centered scheme, which is unstable without artificial dissipation [60]. The value $\kappa = 1/3$ will be used in the following, unless explicitly stated otherwise.

For most applications the extrapolation of the pressure has been substituted for the extrapolation of the total internal energy per unit volume in the vector Q, for both global and electron energy equations, because numerical experiments have shown that with this procedure more robust codes are obtained for high-speed flows in the case of a perfect gas [92]. Numerical evidence of a similar behaviour for the case of chemically reacting flows has been obtained during this study.

The viscous vectors in the thin-layer approximation are discretized using standard second-order accurate central differences for the second derivatives. Cross-derivative terms in the full Navier-Stokes equations are treated in a diagonal-dominance-preserving fashion [98],[100].

7.3 Flux-Split Algorithms

The discretization of the inviscid fluxes can be accomplished by means of flux-split techniques. Originally developed for a perfect gas [10],[11], they have been extended to flows in chemical equilibrium [12–22], and to mixtures out of chemical and thermal equilibrium [26–35]. They are found to be very accurate and robust when used for transonic, supersonic and hypersonic flows [101], and are fully compatible with conservative finite-volume, shock-capturing approaches.

Probably the two most popular schemes in the flux-vector splitting category are the ones due to Steger and Warming [23] and to Van Leer [24]. The basic idea is to split the inviscid flux vector in one space dimension in two parts, containing the information that propagates downstream and upstream, respectively. Then the two parts are constructed using the extrapolation formulas of eq.(7.12) consistently with the direction of propagation

$$\tilde{F} = \tilde{F}^+ + \tilde{F}^-, \qquad \tilde{F}^+ = \tilde{F}^+(Q^-), \qquad \tilde{F}^- = \tilde{F}^-(Q^+), \tag{7.14}$$

where the downstream propagating flux $\tilde{F}^+$ uses the left extrapolation Q^- and the upstream propagating flux $\tilde{F}^-$ the right extrapolation Q^+. The two techniques differ in the way the flux vectors are split. They will be examined in detail in the following. Extension to more space directions are usually made by superimposing pseudo-one-dimensional problems, where the extrapolation formulas to get left and right states keep track of the relevant direction only [92].

Another very popular scheme, less robust for hypersonic flows [101] but more accurate, is the flux-difference splitting technique due to Roe [25]. It consists of an approximate Riemann solver, where an arbitrary discontinuity is supposed to exist at the cell surface between the left and the right state, and an approximate solution for this situation is written in terms of waves propagating upstream and downstream. In this instance, the inviscid flux vector is not split, but reconstructed from the upstream and downstream contributions, that constitute the left and the right

states in the Riemann problem. Three-dimensional extensions are again formulated by considering three separate one-dimensional problems, and the wave propagation is analyzed in the relevant direction only. The details of these algorithms will be discussed in the following.

7.4 Steger-Warming Splitting

The flux vector splitting technique, originally developed by Steger and Warming [23] for perfect gases, takes advantage of the homogeneity of the Euler equations, property that is carried over to flows in thermochemical non-equilibrium, as noted in §A2.

The Jacobian matrices $\tilde{\mathbf{A}}$, $\tilde{\mathbf{B}}$, $\tilde{\mathbf{C}}$ can be diagonalized by means of the right eigenvectors determined in §A3

$$\tilde{\mathbf{A}} = \tilde{\mathbf{S}}\,\tilde{\mathbf{\Lambda}}\,\tilde{\mathbf{S}}^{-1}\,. \tag{7.15}$$

where $\tilde{\mathbf{S}}^{-1}$ is the inverse of the right eigenvector matrix $\tilde{\mathbf{S}}$. Similar results apply for the other space dimensions. The diagonal matrix $\tilde{\mathbf{\Lambda}}$ contains the characteristic speeds of propagation of information. When $\tilde{\mathbf{\Lambda}}$ is split in a non-negative and a non-positive contributions according to the sign of those characteristic velocities, a splitting of the Jacobian in two parts, propagating downstream and upstream respectively, is recovered

$$\tilde{\mathbf{\Lambda}} = \tilde{\mathbf{\Lambda}}^{+} + \tilde{\mathbf{\Lambda}}^{-}, \qquad \tilde{\mathbf{A}} = \tilde{\mathbf{A}}^{+} + \tilde{\mathbf{A}}^{-}, \qquad \tilde{\mathbf{A}}^{\pm} = \tilde{\mathbf{S}}\,\tilde{\mathbf{\Lambda}}^{\pm}\tilde{\mathbf{S}}^{-1}\,. \tag{7.16a,b,c}$$

Then the splitting of the inviscid flux into a positive and a negative contribution is only a question of using the homogeneity relation eq.(A2.13)

$$\tilde{F} = \tilde{\mathbf{A}}\,Q = \tilde{F}^{+} + \tilde{F}^{-}, \qquad \tilde{F}^{\pm} = \tilde{\mathbf{A}}^{\pm}Q\,. \tag{7.17a,b}$$

For the case of only one translational temperature, the matrix of the right eigenvalues $\tilde{\mathbf{S}}$ is given by collecting reduced forms of the approximate eigenvectors

of eqs.(A3.7–9a), dropping electron continuity and energy contributions. The final result, which is *exact* for this thermodynamic model, reads

$$\rho\tilde{\mathbf{S}} =$$

$$\begin{pmatrix}
\rho_1 & \cdots & 0 & \rho_1 & 0 & 0 & 0 & \cdots & 0 & \rho_1 \\
\vdots & \ddots & \vdots & \vdots & \vdots & \vdots & \vdots & \ddots & \vdots & \vdots \\
0 & \cdots & \rho_{N^*} & \rho_{N^*} & 0 & 0 & 0 & \cdots & 0 & \rho_{N^*} \\
\rho_1 u_{0_1} & \cdots & \rho_{N^*} u_{0_1} & \rho(u_{0_1}+\tilde{\xi}_{x_1} a) & \rho l_1 & \rho m_1 & 0 & \cdots & 0 & \rho(u_{0_1}-\tilde{\xi}_{x_1} a) \\
\rho_1 u_{0_2} & \cdots & \rho_{N^*} u_{0_2} & \rho(u_{0_2}+\tilde{\xi}_{x_2} a) & \rho l_2 & \rho m_2 & 0 & \cdots & 0 & \rho(u_{0_2}-\tilde{\xi}_{x_2} a) \\
\rho_1 u_{0_3} & \cdots & \rho_{N^*} u_{0_3} & \rho(u_{0_3}+\tilde{\xi}_{x_3} a) & \rho l_3 & \rho m_3 & 0 & \cdots & 0 & \rho(u_{0_3}-\tilde{\xi}_{x_3} a) \\
0 & \cdots & 0 & \rho_1 e_{n_1} & 0 & 0 & \rho_1 e_{n_1} & \cdots & 0 & \rho_1 e_{n_1} \\
\vdots & \ddots & \vdots & \vdots & \vdots & \vdots & \vdots & \ddots & \vdots & \vdots \\
0 & \cdots & 0 & \rho_M e_{n_M} & 0 & 0 & 0 & \cdots & \rho_M e_{n_M} & \rho_M e_{n_M} \\
\rho_1(u_0^2-\psi_1) & \cdots & \rho_{N^*}(u_0^2-\psi_{N^*}) & \rho(h_0+\tilde{u}_{0_1} a) & \rho u_{0_2}^* & \rho u_{0_3}^* & \rho_1 e_{n_1} & \cdots & \rho_M e_{n_M} & \rho(h_0-\tilde{u}_{0_1} a)
\end{pmatrix}, \tag{7.18}$$

where the notation of §A3 has been used, and $u_{0_2}^* = (\boldsymbol{u}_0 \cdot \boldsymbol{l})$, $u_{0_3}^* = (\boldsymbol{u}_0 \cdot \boldsymbol{m})$.

The matrix of the eigenvalues $\tilde{\Lambda}$ is

$$\tilde{\Lambda} = \frac{|\nabla\xi|}{J} \begin{pmatrix}
\tilde{u}_{0_1} & \cdots & 0 & 0 & 0 & 0 & 0 & \cdots & 0 & 0 \\
\vdots & \ddots & \vdots & \vdots & \vdots & \vdots & \vdots & \ddots & \vdots & \vdots \\
0 & \cdots & \tilde{u}_{0_1} & 0 & 0 & 0 & 0 & \cdots & 0 & 0 \\
0 & \cdots & 0 & \tilde{u}_{0_1}+a & 0 & 0 & 0 & \cdots & 0 & 0 \\
0 & \cdots & 0 & 0 & \tilde{u}_{0_1} & 0 & 0 & \cdots & 0 & 0 \\
0 & \cdots & 0 & 0 & 0 & \tilde{u}_{0_1} & 0 & \cdots & 0 & 0 \\
0 & \cdots & 0 & 0 & 0 & 0 & \tilde{u}_{0_1} & \cdots & 0 & 0 \\
\vdots & \ddots & \vdots & \vdots & \vdots & \vdots & \vdots & \ddots & \vdots & \vdots \\
0 & \cdots & 0 & 0 & 0 & 0 & 0 & \cdots & \tilde{u}_{0_1} & 0 \\
0 & \cdots & 0 & 0 & 0 & 0 & 0 & \cdots & 0 & \tilde{u}_{0_1}-a
\end{pmatrix}. \tag{7.19}$$

Once the Jacobian matrix has been diagonalized, non-negative and non-positive contributions for the matrix of eigenvalues can be easily defined as follows

$$\tilde{\Lambda}^{\pm} = \frac{\tilde{\Lambda} \pm |\tilde{\Lambda}|}{2}, \qquad \tilde{\Lambda} = \tilde{\Lambda}^{+} + \tilde{\Lambda}^{-}. \tag{7.20a,b}$$

The inverse matrix $\tilde{\mathbf{S}}^{-1}$ can be evaluated in a straightforward fashion, utilizing the relationships summarized in Appendix 1 and the formulas for the pressure

derivatives, eqs.(A2.11). The final result reads

$$2\tilde{\mathbf{S}}^{-1} =$$

$$\begin{pmatrix}
2\rho/\rho_1 - 2\phi\psi_1 & \cdots & -2\phi\psi_{N^\bullet} & 2\phi u_0 & 2\phi & \cdots & 2\phi & -2\phi \\
\vdots & \ddots & \vdots & \vdots & \vdots & \ddots & \vdots & \vdots \\
-2\phi\psi_1 & \cdots & 2\rho/\rho_{N^\bullet} - 2\phi\psi_{N^\bullet} & 2\phi u_0 & 2\phi & \cdots & 2\phi & -2\phi \\
-\tilde{u}_{0_1}/a + \phi\psi_1 & \cdots & -\tilde{u}_{0_1}/a + \phi\psi_{N^\bullet} & \nabla\tilde{\xi}/a - \phi u_0 & -\phi & \cdots & -\phi & \phi \\
-2(u_0 \cdot l) & \cdots & -2(u_0 \cdot l) & 2l & 0 & \cdots & 0 & 0 \\
-2(u_0 \cdot m) & \cdots & -2(u_0 \cdot m) & 2m & 0 & \cdots & 0 & 0 \\
-2\phi\psi_1 & \cdots & -2\phi\psi_{N^\bullet} & 2\phi u_0 & 2\phi + 2\rho/\rho_1 e_{n_1} & \cdots & 2\phi & -2\phi \\
\vdots & \ddots & \vdots & \vdots & \vdots & \ddots & \vdots & \vdots \\
-2\phi\psi_1 & \cdots & -2\phi\psi_{N^\bullet} & 2\phi u_0 & 2\phi & \cdots & 2\phi + 2\rho/\rho_1 e_{n_1} & -2\phi \\
\tilde{u}_{0_1}/a + \phi\psi_1 & \cdots & \tilde{u}_{0_1}/a + \phi\psi_{N^\bullet} & -\nabla\tilde{\xi}/a - \phi u_0 & -\phi & \cdots & -\phi & \phi
\end{pmatrix}, \tag{7.21}$$

where $\phi = (\tilde{\gamma}-1)/a^2$.

Performing the matrix products in eqs.(7.16c) and (7.17b), the final result for the positive and negative contributions to the inviscid fluxes can be written as

$$\tilde{F}^{\pm} = \frac{\tilde{\gamma}-1}{\tilde{\gamma}}\lambda_A^{\pm}\begin{pmatrix} \rho_1 \\ \vdots \\ \rho_{N^\bullet} \\ \rho u_{0_1} \\ \rho u_{0_2} \\ \rho u_{0_3} \\ \rho_1 e_{n_1} \\ \vdots \\ \rho_M e_{n_M} \\ \rho h_0 - \rho a^2/(\tilde{\gamma}-1) \end{pmatrix} + \frac{\lambda_B^{\pm}}{2\tilde{\gamma}}\begin{pmatrix} \rho_1 \\ \vdots \\ \rho_{N^\bullet} \\ \rho(u_{0_1} + \tilde{\xi}_{x_1} a) \\ \rho(u_{0_2} + \tilde{\xi}_{x_2} a) \\ \rho(u_{0_3} + \tilde{\xi}_{x_3} a) \\ \rho_1 e_{n_1} \\ \vdots \\ \rho_M e_{n_M} \\ \rho(h_0 + \tilde{u}_{0_1} a) \end{pmatrix} + \frac{\lambda_C^{\pm}}{2\tilde{\gamma}}\begin{pmatrix} \rho_1 \\ \vdots \\ \rho_{N^\bullet} \\ \rho(u_{0_1} - \tilde{\xi}_{x_1} a) \\ \rho(u_{0_2} - \tilde{\xi}_{x_2} a) \\ \rho(u_{0_3} - \tilde{\xi}_{x_3} a) \\ \rho_1 e_{n_1} \\ \vdots \\ \rho_M e_{n_M} \\ \rho(h_0 - \tilde{u}_{0_1} a) \end{pmatrix}, \tag{7.22}$$

where

$$\lambda_A^{\pm} = \frac{|\nabla\xi|}{J}\frac{\tilde{u}_{0_1} \pm |\tilde{u}_{0_1}|}{2}, \quad \lambda_B^{\pm} = \frac{|\nabla\xi|}{J}\frac{\tilde{u}_{0_1} + a \pm |\tilde{u}_{0_1} + a|}{2}, \quad \lambda_C^{\pm} = \frac{|\nabla\xi|}{J}\frac{\tilde{u}_{0_1} - a \pm |\tilde{u}_{0_1} - a|}{2}. \tag{7.23a,b,c}$$

A similar procedure can be followed for the case with two translational temperatures, when the simple asymptotic analysis of §6.4 is utilized. For those conditions, the eigenvalues are given by the simple formulas of eq.(A3.5), and the matrix $\tilde{\mathbf{\Lambda}}$ can

be easily constructed by a straightforward extension of previous results to general curvilinear coordinates, following the directions given in §A3. The matrix of right eigenvalues can be constructed starting from the results of eq.(A3.7–10). The inverse matrix $\tilde{\mathbf{S}}^{-1}$ can be determined, at least for the general case $a \neq (\gamma_e - 1)\tilde{u}_{0_1}$, and the appropriate matrix multiplications performed again to yield positive and negative contributions to $\tilde{\boldsymbol{F}}$. When $a = (\gamma_e - 1)\tilde{u}_{0_1}$, the matrix $\tilde{\mathbf{S}}$ is *singular*, therefore the inversion cannot be performed. However, no numerical difficulties have been experienced when the algorithm has been applied to flows where the speed of sound was in a range that included the singular value.

The final result for the splitting of the fluxes for two translational temperatures reads

$$\tilde{\boldsymbol{F}}^{\pm} = \frac{\tilde{\gamma}-1}{\tilde{\gamma}}\lambda_A^{\pm}\begin{pmatrix} \rho_1 \\ \vdots \\ \rho_{N^*} \\ \rho_N\tilde{\gamma}/(\tilde{\gamma}-1) \\ \rho u_{0_1} \\ \rho u_{0_2} \\ \rho u_{0_3} \\ \rho_1 e_{n_1} \\ \vdots \\ \rho_M e_{n_M} \\ \tilde{\gamma}\rho_e u_0^2/2(\tilde{\gamma}-1) \\ \rho(h_0 - a^2/(\tilde{\gamma}-1)) \end{pmatrix} + \frac{\lambda_B^{\pm}}{2\tilde{\gamma}}\begin{pmatrix} \rho_1 \\ \vdots \\ \rho_{N^*} \\ 0 \\ \rho(u_{0_1}+\tilde{\xi}_{x_1}a) \\ \rho(u_{0_2}+\tilde{\xi}_{x_2}a) \\ \rho(u_{0_3}+\tilde{\xi}_{x_3}a) \\ \rho_1 e_{n_1} \\ \vdots \\ \rho_M e_{n_M} \\ 0 \\ \rho(h_0+\tilde{u}_{0_1}a) \end{pmatrix} + \tag{7.24}$$

$$+\frac{\lambda_C^{\pm}}{2\tilde{\gamma}}\begin{pmatrix} \rho_1 \\ \vdots \\ \rho_{N^*} \\ 0 \\ \rho(u_{0_1}-\tilde{\xi}_{x_1}a) \\ \rho(u_{0_2}-\tilde{\xi}_{x_2}a) \\ \rho(u_{0_3}-\tilde{\xi}_{x_3}a) \\ \rho_1 e_{n_1} \\ \vdots \\ \rho_M e_{n_M} \\ 0 \\ \rho(h_0-\tilde{u}_{0_1}a) \end{pmatrix} + \lambda_D^{\pm}\begin{pmatrix} 0 \\ \vdots \\ 0 \\ 0 \\ 0 \\ 0 \\ 0 \\ 0 \\ \vdots \\ 0 \\ \rho_e(e_{0_e} - u_0^2/2) \\ 0 \end{pmatrix},$$

where λ_A, λ_B, λ_C have already been defined, and

$$\lambda_D^{\pm} = \frac{|\nabla\xi|}{J}\frac{\tilde{u}_{0_1}+(\gamma_e-1)\tilde{u}_{0_1} \pm |\tilde{u}_{0_1}+(\gamma_e-1)\tilde{u}_{0_1}|}{2}. \tag{7.25}$$

Similar results hold for the fluxes in the other space dimensions. It is interesting to point out that the perfect-gas algorithm can be recovered by simplifying the equations in a fashion consistent with what was discussed in §3.4.

7.5 Van Leer Splitting

An alternative flux-vector splitting has been developed for perfect gases by Van Leer, [24]. His formulation has continuously differentiable flux contributions and has been shown to result in smoother solutions near sonic points [101]. Van Leer-type splittings have been developed by several authors for equilibrium chemistry [13],[14],[18–22], and for thermochemical non-equilibrium [28–33]. Considering only one translational temperature, the procedures of Van Leer [24] may be directly utilized by considering the flux vectors as

$$\begin{aligned}
\tilde{F} &= \tilde{F}\left(\rho,\, a,\, \tilde{M},\, \rho_i/\rho,\, e_{n_i}\right),\\
\tilde{G} &= \tilde{G}\left(\rho,\, a,\, \tilde{M},\, \rho_i/\rho,\, e_{n_i}\right),\\
\tilde{H} &= \tilde{H}\left(\rho,\, a,\, \tilde{M},\, \rho_i/\rho,\, e_{n_i}\right),
\end{aligned} \tag{7.26}$$

where $\tilde{M}$ is the normalized velocity parameter $\tilde{u}_0/a$, often referred to as a Mach number, even if it may be positive or negative. Then the mass flux for the vector $\tilde{F}$, which is $\rho\tilde{u}_{0_1} = \rho a\tilde{M}_1$, may be split as $\rho\tilde{u}_{0_1} = f_m^+ + f_m^-$, where

$$f_m^{\pm} = \pm\rho a\left(\frac{\pm\tilde{M}_1+1}{2}\right)^2. \tag{7.27}$$

The remaining fluxes, when written in the functional form of eq.(7.26), may be split to yield a Van Leer-type flux-vector splitting for the case of a single translational

temperature

$$\tilde{F}^{\pm} = \frac{|\nabla\xi|}{J} f_m^{\pm} \begin{pmatrix} \rho_1/\rho \\ \rho_2/\rho \\ \vdots \\ \vdots \\ \rho_{N^*}/\rho \\ u_{0_1} + \tilde{\xi}_{x_1}(-\tilde{u}_{0_1} \pm 2a)/\tilde{\gamma} \\ u_{0_2} + \tilde{\xi}_{x_2}(-\tilde{u}_{0_1} \pm 2a)/\tilde{\gamma} \\ u_{0_3} + \tilde{\xi}_{x_3}(-\tilde{u}_{0_1} \pm 2a)/\tilde{\gamma} \\ \rho_1 e_{n_1}/\rho \\ \vdots \\ \rho_M e_{n_M}/\rho \\ f_e^{\pm} \end{pmatrix}, \tag{7.28}$$

where

$$f_e^{\pm} = h_0 - \frac{(-\tilde{u}_{0_1} \pm a)^2}{\tilde{\gamma}+1}. \tag{7.29}$$

Also, $\tilde{F}^{\pm} = \tilde{F}$, $\tilde{F}^{\mp} \equiv 0$ in the supersonic range, when $\tilde{M}_1 > 1$ and $\tilde{M}_1 < -1$, respectively. Different authors have developed similar schemes [28–33]. The specific form of eq.(7.29), fits into the class of splittings discussed in Shuen, Liou and Van Leer [30], where $f_e^{\pm} = h_0 - m(-\tilde{u}_{0_1} \pm a)^2$. The value $m = 1/(\tilde{\gamma}+1)$ was used in the present numerical simulations. Other values are used in the literature, but numerical experiments do not show any significant effect on the value of m.

When free electrons are considered, the splitting becomes more complicated because a "velocity" speed of sound a_e can be considered, $a_e = (\gamma_e - 1)|\tilde{u}_{0_1}|$, which is associated with the electron energy equation for the $\tilde{F}$ flux. However, the corresponding Mach number

$$\tilde{M}_{e_1} = \frac{\tilde{u}_{0_1}}{(\gamma_e - 1)|\tilde{u}_{0_1}|}, \qquad |\tilde{M}_{e_1}| = \frac{1}{(\gamma_e - 1)}, \tag{7.30a,b}$$

is always "supersonic" for γ_e ranging from 1 to 2. Consequently, the mass flux for the vector $\tilde{F}$ has an alternative splitting $\rho\tilde{u}_{0_1} = \rho a_e \tilde{M}_{e_1} = f_{m_e}^{+} + f_{m_e}^{-}$, where either portion is identically zero

$$f_{m_e}^{\pm} = \rho a_e \tilde{M}_{e_1}^{\pm}, \qquad \tilde{M}_{e_1}^{\pm} = \frac{\tilde{M}_{e_1} \pm |\tilde{M}_{e_1}|}{2}. \tag{7.31a,b}$$

The previous splitting will be used for the electron continuity and energy equations, yielding the final result

$$\tilde{F}^{\pm} = \frac{|\nabla \xi|}{J} \begin{pmatrix} f_m^{\pm} \rho_1/\rho \\ f_m^{\pm} \rho_2/\rho \\ \vdots \\ f_m^{\pm} \rho_{N^*}/\rho \\ f_{m_e}^{\pm} \rho_e/\rho \\ f_m^{\pm}\left[u_{0_1} + \tilde{\xi}_{x_1}(-\tilde{u}_{0_1} \pm 2a)/\tilde{\gamma}\right] \\ f_m^{\pm}\left[u_{0_2} + \tilde{\xi}_{x_2}(-\tilde{u}_{0_1} \pm 2a)/\tilde{\gamma}\right] \\ f_m^{\pm}\left[u_{0_3} + \tilde{\xi}_{x_3}(-\tilde{u}_{0_1} \pm 2a)/\tilde{\gamma}\right] \\ f_m^{\pm} \rho_1 e_{n_1}/\rho \\ \vdots \\ f_m^{\pm} \rho_M e_{n_M}/\rho \\ f_{m_e}^{\pm} h_{0_e} \\ f_m^{\pm} f_e^{\pm} \end{pmatrix} . \tag{7.32}$$

The method above can be shown to reduce to the perfect-gas form, as discussed for the Steger-Warming-type splitting. The other space dimensions are treated in a similar fashion.

7.6 An Approximate Riemann Solver

The essential features of flux-difference split algorithms involve the solution of local Riemann problems arising from the consideration of discontinuous states at cell interfaces on an initial data line [11]. The scheme developed for perfect gases by Roe [25], falls into this category and has produced excellent results for both inviscid and viscous flow simulations [101]. Extensions of the Roe splitting have been developed by several authors for both equilibrium chemistry [12–17],[19–22], and thermo-chemical non-equilibrium [28–35].

The procedure outlined by Glaister [15],[16] for real gases, which originated from the approach of Roe and Pike [91] for perfect gases, will be followed. In this approach, the first step corresponds to obtaining a solution for the linearized, approximate Riemann problem, valid for small jumps in the interface states. The second step involves the determination of the appropriate averaging procedures,

(often referred to as Roe-averages), in order to render the solution valid for arbitrary jumps in the cell interface values.

To carry out the first step for the case where only one translational temperature is defined, a solution to the approximate Riemann problem is sought, given two states, Q_r, Q_ℓ, which are *close* to an average state Q of the vector of conserved variables. This involves the determination of the relationship between the *jump* in Q, denoted as $[\![Q]\!]$, and the average eigenvectors E_i of the Jacobian matrix, given in §A3. For small $[\![Q]\!]$, one must find the wave strengths α_i, $i = 1, \ldots, N^* + M + 4$, such that

$$[\![Q]\!] = \sum_{i=1}^{N^*+M+4} \alpha_i E_i, \tag{7.33}$$

to within $O([\![Q]\!])^2$. The cell interface jumps, $[\![\cdot]\!] = (\cdot)_r - (\cdot)_\ell$, represent the difference in quantities evaluated at the cell interface using data from the right, $(\cdot)_r$ and the left, $(\cdot)_\ell$. In the following, flow quantities without a superscript, i.e., ρ, correspond to a value between ρ_r and ρ_ℓ. Moreover, the analysis will be performed in Cartesian coordinates, using eigenvalues and eigenvectors given in eqs.(A3.2) and (A3.7–10), respectively. The final results will be presented in the usual generalized coordinates for $\tilde{F}$, and the techniques of Walters and Thomas [92] have been extensively used in order to perform the necessary transformations. The flux vectors in the other space directions can be similarly treated.

The first N^* contributions of eq.(7.33), yield

$$\alpha_i = \frac{\rho}{\rho_i}[\![\rho_i]\!] - (\alpha_{N^*+M+3} + \alpha_{N^*+M+4}), \qquad i = 1, \ldots, N^*, \tag{7.34}$$

and the $N^* + 4$ through $N^* + M + 1$ terms of eq.(7.33) give

$$\alpha_{j+N^*} = \frac{\rho}{\rho_j e_{n_j}}[\![\rho_j e_{n_j}]\!] - (\alpha_{N^*+M+3} + \alpha_{N^*+M+4}), \qquad j = 1, \ldots, M, \tag{7.35}$$

Using the above results along with the first momentum equation gives

$$\alpha_{N^*+M+3} - \alpha_{N^*+M+4} = \frac{\rho}{a}[\![u_{0_1}]\!], \tag{7.36}$$

and the other two momentum equations yield

$$\alpha_{N^*+M+1} = \rho[\![u_{0_2}]\!], \qquad \alpha_{N^*+M+2} = \rho[\![u_{0_3}]\!]. \tag{7.37a,b}$$

The last contribution of eq.(7.33) can be written as follows

$$\alpha_{N^*+M+3} + \alpha_{N^*+M+4} = \frac{\left[[\![\rho e_0]\!] - \rho u_{0_1}[\![u_{0_1}]\!] - \rho u_{0_2}[\![u_{0_2}]\!] - \rho u_{0_3}[\![u_{0_3}]\!] - u_0^2[\![\rho]\!] + \sum_{i=1}^{N^*}\psi_i[\![\rho_i]\!] - \sum_{j=1}^{M}[\![\rho_j e_{n_j}]\!]\right]}{\left[h_0 - u_0^2 + \sum_{i=1}^{N^*}(\rho_i/\rho)\psi_i - \sum_{j=1}^{M}(\rho_j/\rho)e_{n_j}\right]}, \tag{7.38}$$

where ψ_i is defined in eq.(A3.10a). From that definition, it can be shown that

$$\sum_{i=1}^{N^*}\frac{\rho_i}{\rho}\psi_i = \frac{\tilde{R}T}{\tilde{\gamma}-1} - \tilde{e} + \frac{u_0^2}{2}, \tag{7.39}$$

and along with the definition of h_0, the denominator of eq.(7.38) may be written as $a^2/(\tilde{\gamma}-1)$. Then, to $O([\![Q]\!])^2$, the term $[\![\rho e_0]\!]$ may be expanded as

$$[\![\rho e_0]\!] = \sum_{i=1}^{N^*}\left(\rho_i[\![\tilde{e}_i]\!] + \tilde{e}_i[\![\rho]\!]\right) + \sum_{j=1}^{M}[\![\rho_j e_{n_j}]\!] + \rho u_{0_1}[\![u_{0_1}]\!] + \rho u_{0_2}[\![u_{0_2}]\!] + \rho u_{0_3}[\![u_{0_3}]\!] + \frac{u_0^2}{2}[\![\rho]\!]. \tag{7.40}$$

From the results in §2, it follows that $[\![\tilde{e}_i]\!] = \tilde{c}_{v_i}[\![T]\!]$. Using the equation of state for p and the definition of ψ_i, the numerator of eq.(7.38) simply becomes $[\![p]\!]/(\tilde{\gamma}-1)$. Substituting these results into eq.(7.38) yields the following simplification, valid to $O([\![Q]\!])^2$

$$\alpha_{N^*+M+3} + \alpha_{N^*+M+4} = \frac{[\![p]\!]}{a^2}. \tag{7.41}$$

The final result for the α_i is then

$$\alpha_i = \frac{\rho}{\rho_i}[\![\rho_i]\!] - \frac{[\![p]\!]}{a^2}, \qquad i = 1,\ldots,N^*, \tag{7.42a}$$

$$\alpha_{j+N^*} = \frac{\rho}{\rho_j e_{n_j}}[\![\rho_j e_{n_j}]\!] - \frac{[\![p]\!]}{a^2}, \qquad j = 1,\ldots,M, \tag{7.42b}$$

$$\alpha_{N^*+M+1} = \rho[\![u_{0_2}]\!], \tag{7.42c}$$

$$\alpha_{N^*+M+2} = \rho[\![u_{0_3}]\!], \tag{7.42d}$$

$$\alpha_{N^*+M+k} = \frac{1}{2a^2}\left([\![p]\!] \pm \rho a[\![u_{0_1}]\!]\right), \qquad k = 3,4. \tag{7.42e}$$

It may be verified that, with these wave strengths α_i, the flux vector $\boldsymbol{F}$ may be expanded as

$$[\![\boldsymbol{F}]\!] = \sum_{i=1}^{N^*+M+4} \alpha_i \lambda_i \boldsymbol{E}_i , \tag{7.43}$$

where the eigenvalues λ_i are given in eq.(A3.2). As stated in Glaister [15], this decomposition yields the characteristic fields to $O([\![\boldsymbol{Q}]\!])^2$. It should be noted that the wave strengths are consistent with the results presented in Appendix 4 for the characteristic relationships of flows with only one translational temperature.

The next step in the construction of an approximate Riemann solver [15],[91], involves determining appropriate averages, $\hat{\alpha}_i$, $\hat{\lambda}_i$ and $\hat{\boldsymbol{E}}_i$, such that

$$[\![\boldsymbol{Q}]\!] = \sum_{i=1}^{N^*+M+4} \hat{\alpha}_i \hat{\boldsymbol{E}}_i , \tag{7.44}$$

and

$$[\![\boldsymbol{F}]\!] = \sum_{i=1}^{N^*+M+4} \hat{\alpha}_i \hat{\lambda}_i \hat{\boldsymbol{E}}_i , \tag{7.45}$$

for cell interface states which are not necessarily close to each other, so that $[\![\boldsymbol{Q}]\!]$ is not necessarily small. Using the results of §A3, it is possible to define the eigenvalues

$$\hat{\lambda}_i = \begin{cases} \hat{u}_{0_1} , & i = 1,\ldots,N^*+M+2, \\ \hat{u}_{0_1} + \hat{a}, & i = N^*+M+3, \\ \hat{u}_{0_1} - \hat{a}, & i = N^*+M+4, \end{cases} \tag{7.46}$$

and the eigenvectors

$$\hat{\boldsymbol{E}}_i = \begin{pmatrix} 0 \\ \vdots \\ \hat{\rho}_i \\ \vdots \\ 0 \\ \hat{\rho}_i \hat{u}_{0_1} \\ \hat{\rho}_i \hat{u}_{0_2} \\ \hat{\rho}_i \hat{u}_{0_3} \\ 0 \\ \vdots \\ 0 \\ (\hat{u}_0^2 - \hat{\psi}_i)\hat{\rho}_i \end{pmatrix} , \; i = 1,\ldots,N^*, \quad \hat{\boldsymbol{E}}_{j+N^*} = \begin{pmatrix} 0 \\ \vdots \\ 0 \\ \vdots \\ 0 \\ 0 \\ 0 \\ 0 \\ \vdots \\ \hat{e}_{n_j} \\ 0 \\ \hat{e}_{n_j} \end{pmatrix} , \; j = 1,\ldots,M, \tag{7.47a,b,c,d,e}$$

$$\hat{E}_{N^*+M+1} = \begin{pmatrix} 0 \\ \vdots \\ 0 \\ \vdots \\ 0 \\ 0 \\ 1 \\ 0 \\ 0 \\ \vdots \\ 0 \\ \hat{u}_{0_2} \end{pmatrix}, \quad \hat{E}_{N^*+M+2} = \begin{pmatrix} 0 \\ \vdots \\ 0 \\ \vdots \\ 0 \\ 0 \\ 0 \\ 1 \\ 0 \\ \vdots \\ 0 \\ \hat{u}_{0_3} \end{pmatrix}, \quad \hat{E}_{N^*+M+k} = \begin{pmatrix} \hat{\rho}_1 \\ \hat{\rho}_2 \\ \vdots \\ \vdots \\ \hat{\rho}_{N^*} \\ \hat{u}_{0_1} \pm \hat{a} \\ \hat{u}_{0_2} \\ \hat{u}_{0_3} \\ \hat{e}_{n_1} \\ \vdots \\ \hat{e}_{n_M} \\ \hat{h}_0 \pm \hat{u}_{0_1}\hat{a} \end{pmatrix} \quad k = 3, 4,$$

along with the corresponding wave strengths

$$\hat{\alpha}_i = \frac{[\![\rho_i]\!]}{\hat{\rho}_i} - \frac{[\![p]\!]}{\hat{a}^2}, \qquad i = 1, \ldots, N^*, \tag{7.48a}$$

$$\hat{\alpha}_{j+N^*} = \frac{[\![\rho_j e_{n_j}]\!]}{\hat{e}_{n_j}} - \frac{[\![p]\!]}{\hat{a}^2}, \qquad j = 1, \ldots, M, \tag{7.48b}$$

$$\hat{\alpha}_{N^*+M+1} = \hat{\rho}[\![u_{0_2}]\!], \tag{7.48c}$$

$$\hat{\alpha}_{N^*+M+2} = \hat{\rho}[\![u_{0_3}]\!], \tag{7.48d}$$

$$\hat{\alpha}_{N^*+M+k} = \frac{1}{2\hat{a}^2}\left([\![p]\!] \pm \hat{\rho}\hat{a}[\![u_{0_1}]\!]\right), \qquad k = 3, 4. \tag{7.48e}$$

The solution of the approximate Riemann problem involves determining algebraic averages $\hat{\rho}$, $\hat{u}_0$, $\hat{a}$, $\hat{p}$, $\hat{h}_0$, $\hat{\rho}_i$, $\hat{e}_{n_i}$, $\hat{\psi}_i$, such that eqs.(7.44), (7.45) are satisfied. In the above, the definitions

$$\hat{\rho}_i \equiv \left(\widehat{\frac{\rho_i}{\rho}}\right), \qquad \hat{e}_{n_i} \equiv \left(\widehat{\frac{\rho_i e_{n_i}}{\rho}}\right), \tag{7.49a, b}$$

have been used.

The first N^* contributions of eq.(7.44) yield

$$[\![\rho_i]\!] = \hat{\rho}_i(\hat{\alpha}_i + \hat{\alpha}_{N^*+M+3} + \hat{\alpha}_{N^*+M+4}), \qquad i = 1, \ldots, N^*, \tag{7.50}$$

and the N^*+4 through N^*+M+3 contributions of eq.(7.44) give

$$[\![\rho_j e_{n_j}]\!] = \hat{e}_{n_j}(\hat{\alpha}_{j+N^*} + \hat{\alpha}_{N^*+M+3} + \hat{\alpha}_{N^*+M+4}), \qquad j = 1, \ldots, M, \tag{7.51}$$

which are identically satisfied when using eqs.(7.48). The N^*+1 contribution of eq.(7.44) yields

$$\begin{aligned}[\![\rho u_{0_1}]\!] &= \sum_{i=1}^{N^*} \hat{\rho}_i \hat{u}_{0_1} \hat{\alpha}_i + (\hat{u}_{0_1} + \hat{a})\hat{\alpha}_{N^*+M+3} + (\hat{u}_{0_1} - \hat{a})\hat{\alpha}_{N^*+M+4} \\ &= \hat{u}_{0_1}[\![\rho]\!] + \hat{\rho}[\![u_{0_1}]\!], \end{aligned} \tag{7.52}$$

where use has been made of $[\![\rho]\!] = \sum^N [\![\rho_i]\!]$ and of $\sum^{N^*} \hat{\rho}_i = 1$. On the other hand, the N^*+1 contribution of eq.(7.45) gives

$$[\![p + \rho u_{0_1}^2]\!] = \sum_{i=1}^{N^*} \hat{\rho}_i \hat{u}_{0_1}^2 \hat{\alpha}_i + (\hat{u}_{0_1} + \hat{a})^2 \hat{\alpha}_{N^*+M+3} + (\hat{u}_{0_1} - \hat{a})^2 \hat{\alpha}_{N^*+M+4}, \tag{7.53}$$

which, upon substitution of eqs.(7.48), reduces to

$$[\![\rho u_{0_1}^2]\!] = \hat{u}_{0_1}^2 [\![\rho]\!] + 2\hat{\rho}\hat{u}_{0_1}[\![u_{0_1}]\!]. \tag{7.54}$$

Solving for $\hat{\rho}$ and $\hat{u}_{0_1}$ from eqs.(7.52), (7.54) yields

$$\hat{\rho} = <\sqrt{\rho}>^2 - \frac{1}{4}[\![\sqrt{\rho}]\!]^2 = \sqrt{\rho_r \rho_\ell}, \tag{7.55a}$$

and

$$\hat{u}_{0_1} = \frac{<u_{0_1}\sqrt{\rho}>}{<\sqrt{\rho}>} = \frac{(u_{0_1})_r\sqrt{\rho_r} + (u_{0_1})_\ell\sqrt{\rho_\ell}}{\sqrt{\rho_r} + \sqrt{\rho_\ell}}, \tag{7.55b}$$

where the notation for the arithmetic average $<\cdot>= [(\cdot)_r + (\cdot)_\ell]/2$ has been used. The results in eqs.(7.55) are the usual Roe-averages for ρ and u_{0_1} as developed for a perfect gas [25].

The other two momentum equations of eq.(7.44) yield

$$\begin{aligned}[\![\rho u_{0_2}]\!] &= \hat{u}_{0_2}[\![\rho]\!] + \hat{\rho}[\![u_{0_2}]\!], \\ [\![\rho u_{0_3}]\!] &= \hat{u}_{0_3}[\![\rho]\!] + \hat{\rho}[\![u_{0_3}]\!]. \end{aligned} \tag{7.56a,b}$$

The first N^* contributions of eq.(7.45) give

$$[\![\rho_i u_{0_1}]\!] = \hat{u}_{0_1}[\![\rho_i]\!] + \hat{\rho}\hat{\rho}_i[\![u_{0_1}]\!], \qquad i = 1, \ldots, N^*. \tag{7.57}$$

It is possible to solve for $\hat{\rho}_i$ by expanding terms such as

$$[\![\rho_i u_{0_1}]\!] = [\![(\frac{\rho_i}{\rho}\sqrt{\rho})(u_{0_1}\sqrt{\rho})]\!] = <\frac{\rho_i}{\rho}\sqrt{\rho}>\,[\![u_{0_1}\sqrt{\rho}]\!] + <u_{0_1}\sqrt{\rho}>\,[\![\frac{\rho_i}{\rho}\sqrt{\rho}]\!] \tag{7.58}$$

(Expansions of this type will be used throughout the development of the average quantities in this section). The result is

$$\hat{\rho}_i = \frac{<(\rho_i/\rho)\sqrt{\rho}>}{<\sqrt{\rho}>}, \qquad i = 1, \ldots, N^*. \tag{7.59}$$

Similarly, the N^*+4 through N^*+M+3 contributions of (7.45) are solved for $\hat{e}_{n_j}$ as

$$\hat{e}_{n_j} = \frac{<(\rho_j e_{n_j}/\rho)\sqrt{\rho}>}{<\sqrt{\rho}>}, \qquad j = 1, \ldots, M. \tag{7.60}$$

The similarity of the results of eqs.(7.52) and (7.56) suggests the following forms for the averages $\hat{u}_{0_2}$, $\hat{u}_{0_3}$

$$\begin{aligned} \hat{u}_{0_2} &= \frac{<u_{0_2}\sqrt{\rho}>}{<\sqrt{\rho}>} = \frac{(u_{0_2})_r\sqrt{\rho_r} + (u_{0_2})_\ell\sqrt{\rho_\ell}}{\sqrt{\rho_r} + \sqrt{\rho_\ell}}, \\ \hat{u}_{0_3} &= \frac{<u_{0_3}\sqrt{\rho}>}{<\sqrt{\rho}>} = \frac{(u_{0_3})_r\sqrt{\rho_r} + (u_{0_3})_\ell\sqrt{\rho_\ell}}{\sqrt{\rho_r} + \sqrt{\rho_\ell}}. \end{aligned} \tag{7.61a,b}$$

The two remaining momentum equations of eq.(7.45) yield

$$\begin{aligned} [\![\rho u_{0_1} u_{0_2}]\!] &= \hat{u}_{0_1}\hat{u}_{0_2}[\![\rho]\!] + \hat{\rho}\hat{u}_{0_2}[\![u_{0_1}]\!] + \hat{\rho}\hat{u}_{0_1}[\![u_{0_2}]\!], \\ [\![\rho u_{0_1} u_{0_3}]\!] &= \hat{u}_{0_1}\hat{u}_{0_3}[\![\rho]\!] + \hat{\rho}\hat{u}_{0_3}[\![u_{0_1}]\!] + \hat{\rho}\hat{u}_{0_1}[\![u_{0_3}]\!], \end{aligned} \tag{7.62a,b}$$

and are identically satisfied by the assumed average forms. Using the previous results, the following important relations can be derived

$$\begin{aligned} [\![\rho u_{0_2}^2]\!] &= \hat{u}_{0_2}^2[\![\rho]\!] + 2\hat{\rho}\hat{u}_{0_2}[\![u_{0_2}]\!], \\ [\![\rho u_{0_3}^2]\!] &= \hat{u}_{0_3}^2[\![\rho]\!] + 2\hat{\rho}\hat{u}_{0_3}[\![u_{0_3}]\!]. \end{aligned} \tag{7.63a,b}$$

The two remaining equations to be considered are the energy equations in both eq.(7.44) and eq.(7.45). The former may be written as

$$[\![\rho e_0]\!] = \hat{u}_0^2 [\![\rho]\!] - \sum_{i=1}^{N^*} \hat{\psi}_i [\![\rho_i]\!] + \sum_{j=1}^{M} [\![\rho_j e_{n_j}]\!] + \hat{\rho}\hat{u}_{0_1} [\![u_{0_1}]\!] + \hat{\rho}\hat{u}_{0_2} [\![u_{0_2}]\!] + \hat{\rho}\hat{u}_{0_3} [\![u_{0_3}]\!] + \\ + \frac{[\![p]\!]}{\hat{a}^2} \left[\hat{h}_0 - \hat{u}_0^2 + \sum_{i=1}^{N^*} \hat{\rho}_i \hat{\psi}_i - \sum_{j=1}^{M} \hat{e}_{n_j} \right]. \tag{7.64}$$

The latter is evaluated more simply by subtracting $\hat{u}_{0_1} [\![\rho e_0]\!]$ from eq.(7.64) and using the definition $\rho e_0 = \rho h_0 - p$, to give

$$[\![\rho u_{0_1} h_0]\!] = \hat{u}_{0_1} [\![\rho h_0]\!] + \hat{\rho} \hat{h}_0 [\![u_{0_1}]\!]. \tag{7.65}$$

This may be solved for $\hat{h}_0$ as

$$\hat{h}_0 = \frac{\langle h_0 \sqrt{\rho} \rangle}{\langle \sqrt{\rho} \rangle}. \tag{7.66}$$

The only remaining formula to be satisfied is eq.(7.64) and the averages to be determined are $\hat{a}$ and $\hat{\psi}_i$.

Considering the definition of ψ_i, eq.(A3.10a), and the result of eq.(7.39), it seems natural to assume that $\hat{\psi}_i$ satisfies the equation

$$\sum_{i=1}^{N^*} \hat{\rho}_i \hat{\psi}_i = \frac{\hat{a}^2}{\hat{\gamma} - 1} + \hat{u}_0^2 - \hat{h}_0 + \sum_{j=1}^{M} \hat{e}_{n_j}, \tag{7.67}$$

where $\hat{a}$ and $\hat{\gamma}$ are not yet defined. It is also convenient to introduce a new quantity, $\hat{\sigma}_i$, defined as

$$\hat{\sigma}_i = \hat{\psi}_i - \frac{\hat{u}_0^2}{2}. \tag{7.68}$$

Going back to eq.(7.64), it is convenient to expand ρe_0 as $\rho \tilde{e} + \sum \rho_j e_{n_j} + \rho u_0^2/2$. Substituting eqs.(7.67) and (7.68) and using eqs.(7.63) gives

$$[\![\rho \tilde{e}]\!] = - \sum_{i=1}^{N^*} \hat{\sigma}_i [\![\rho_i]\!] + \frac{1}{\hat{\gamma} - 1} [\![p]\!]. \tag{7.69}$$

The equation of state yields

$$[\![p]\!] = \hat{\rho}\hat{R}[\![T]\!] + \hat{T}\sum_{i=1}^{N^*} R_i[\![\rho_i]\!], \tag{7.70}$$

where

$$\hat{R} = \sum_{i=1}^{N^*} \hat{\rho}_i R_i = \frac{<\tilde{R}\sqrt{\rho}>}{<\sqrt{\rho}>}, \tag{7.71}$$

and

$$\hat{T} = \frac{<T\sqrt{\rho}>}{<\sqrt{\rho}>}. \tag{7.72}$$

The definition of $\tilde{e}_i$, eq.(2.4), produces

$$[\![\tilde{e}_i]\!] = c^*_{v_i}[\![T]\!], \tag{7.73}$$

where

$$c^*_{v_i} \equiv \frac{1}{[\![T]\!]}\int_{T_\ell}^{T_r} \tilde{c}_{v_i}\, dT\,. \tag{7.74}$$

Using the previous result, it is possible to write

$$[\![\rho\tilde{e}]\!] = \hat{\rho}\hat{c}^*_v[\![T]\!] + \sum_{i=1}^{N^*} \hat{e}_i[\![\rho_i]\!], \tag{7.75}$$

where

$$\hat{c}^*_v = \sum_{i=1}^{N^*} \hat{\rho}_i c^*_{v_i}\,, \tag{7.76}$$

and

$$\hat{e}_i \equiv \widehat{(\tilde{e}_i)} = \frac{<\tilde{e}_i\sqrt{\rho}>}{<\sqrt{\rho}>}. \tag{7.77}$$

Substituting these results into eq.(7.69) yields

$$\sum_{i=1}^{N^*}\left(\hat{\sigma}_i + \hat{e}_i - \frac{R_i\hat{T}}{\hat{\gamma}-1}\right)[\![\rho_i]\!] + \hat{\rho}\left(\hat{c}^*_v - \frac{\hat{R}}{\hat{\gamma}-1}\right)[\![T]\!] = 0\,. \tag{7.78}$$

The only two undefined quantities at $\hat{\sigma}_i$ and $\hat{\gamma}$. They may be defined to satisfy eq.(7.78) as

$$\hat{\gamma} - 1 = \frac{\hat{R}}{\hat{c}^*_v}. \tag{7.79}$$

and

$$\hat{\sigma}_i = \frac{R_i \hat{T}}{\hat{\gamma} - 1} - \hat{e}_i \,, \tag{7.80}$$

Finally, $\hat{a}$ is determined from eqs.(7.67), (7.68), (7.76), (7.79), (7.80) as

$$\hat{a}^2 = (\hat{\gamma} - 1)\Big[\hat{h}_0 - \frac{\hat{u}_0^2}{2} + \hat{c}_v^* \hat{T} - \sum_{i=1}^{N^*} \hat{\rho}_i \hat{e}_i - \sum_{j=1}^{M} \hat{e}_{n_j}\Big] \,. \tag{7.81}$$

At this stage, all the averages that render eq.(7.45) an approximate Riemann solver have been defined. It is noteworthy that these averages are *not unique*. As pointed out by Abgrall [34], the algebraic problem posed in eqs.(7.44), (7.45) has more solutions, and different values have been published in the literature for some of the Roe-type averages [28–35]. The major differences between the present approach and others is in the evaluation of averages of the pressure derivatives, or equivalently of $\hat{\psi}_i$, whereas the same results are obtained for mass fractions and non-equilibrium contributions, if present. No numerical evidence has been presented of the superiority of one scheme over the others.

Rewriting eq.(7.44) by grouping the repeated eigenvalues, simplifying the result and transforming it back to generalized coordinates [92] yields

$$[\![\tilde{F}]\!] = [\![\tilde{F}]\!]_A + [\![\tilde{F}]\!]_B + [\![\tilde{F}]\!]_C \,. \tag{7.82}$$

The $[\![\tilde{F}]\!]_A$ term arises from the first $N^* + M + 2$ terms of the sum in eq.(7.45), corresponding to the repeated eigenvalue $\lambda_i = \hat{\tilde{u}}_{0_1}$, and may be written as

$$[\![\tilde{F}]\!]_A = \frac{|\nabla\xi|}{J}\left([\![\rho]\!] - \frac{[\![p]\!]}{\hat{a}^2}\right)\hat{\tilde{u}}_{0_1}\begin{pmatrix} \hat{\rho}_1 \\ \hat{\rho}_2 \\ \vdots \\ \vdots \\ \hat{\rho}_{N^*} \\ \hat{u}_{0_1} \\ \hat{u}_{0_2} \\ \hat{u}_{0_3} \\ \hat{e}_{n_1} \\ \vdots \\ \hat{e}_{n_M} \\ \hat{h}_0 - \hat{a}^2/(\hat{\gamma}-1) \end{pmatrix} + \frac{|\nabla\xi|}{J}\hat{\rho}\hat{\tilde{u}}_{0_1}\begin{pmatrix} [\![\rho_1/\rho]\!] \\ [\![\rho_2/\rho]\!] \\ \vdots \\ \vdots \\ [\![\rho_{N^*}/\rho]\!] \\ [\![u_{0_1}]\!] - \tilde{\xi}_{x_1}[\![\tilde{u}_{0_1}]\!] \\ [\![u_{0_2}]\!] - \tilde{\xi}_{x_2}[\![\tilde{u}_{0_1}]\!] \\ [\![u_{0_3}]\!] - \tilde{\xi}_{x_3}[\![\tilde{u}_{0_1}]\!] \\ [\![\rho_1 e_{n_1}/\rho]\!] \\ \vdots \\ [\![\rho_M e_{n_M}/\rho]\!] \\ \Theta \end{pmatrix} , \tag{7.83}$$

where

$$\Theta = \sum_{j=1}^{M} [\![\frac{\rho_j e_{n_j}}{\rho}]\!] - \sum_{i=1}^{N^*} \hat{\psi}_i [\![\frac{\rho_i}{\rho}]\!] + \left(\hat{u}_{0_1} [\![u_{0_1}]\!] + \hat{u}_{0_2} [\![u_{0_2}]\!] + \hat{u}_{0_3} [\![u_{0_3}]\!] \right) - \hat{\tilde{u}}_{0_1} [\![\tilde{u}_{0_1}]\!], \quad (7.84)$$

and $\hat{\tilde{u}}_{0_1}$ is trivially defined starting from the averages of the Cartesian components $\hat{u}_{0_1}, \hat{u}_{0_2}, \hat{u}_{0_3}$

$$\hat{\tilde{u}}_{0_1} = \tilde{\xi}_{x_1} \hat{u}_{0_1} + \tilde{\xi}_{x_2} \hat{u}_{0_2} + \tilde{\xi}_{x_3} \hat{u}_{0_3} \,. \quad (7.85)$$

The $[\![\tilde{F}]\!]_B$ and $[\![\tilde{F}]\!]_C$ contributions arise from the last two terms in the summation of eq.(7.45), corresponding to the eigenvalues $\hat{\tilde{u}}_{0_1} + \hat{a}$ and $\hat{\tilde{u}}_{0_1} - \hat{a}$, and are found to be

$$[\![\tilde{F}]\!]_{B,C} = \frac{|\nabla \xi|}{J} \frac{1}{2\hat{a}^2} \left([\![p]\!] \pm \hat{\rho} \hat{a} [\![\tilde{u}_{0_1}]\!] \right) (\hat{\tilde{u}}_{0_1} \pm \hat{a}) \begin{pmatrix} \hat{\rho}_1 \\ \hat{\rho}_2 \\ \vdots \\ \vdots \\ \hat{\rho}_{N^*} \\ \hat{u}_{0_1} \pm \tilde{\xi}_{x_1} \hat{a} \\ \hat{u}_{0_2} \pm \tilde{\xi}_{x_2} \hat{a} \\ \hat{u}_{0_3} \pm \tilde{\xi}_{x_3} \hat{a} \\ \hat{e}_{n_1} \\ \vdots \\ \hat{e}_{n_M} \\ \hat{h}_0 \pm \hat{\tilde{u}}_{0_1} \hat{a} \end{pmatrix} . \quad (7.86)$$

The approximate Riemann solver is implemented by computing the cell face fluxes as a summation over wave speeds [11]

$$\tilde{F}_{i+1/2} = \frac{1}{2} \left(\tilde{F}_r + \tilde{F}_\ell \right) - \frac{1}{2} \sum_{i=1}^{N^*+M+4} \hat{\alpha}_i \, |\hat{\lambda}_i| \, \hat{E}_i, \quad (7.87)$$

which can be written as follows, using eqs.(7.83–86)

$$\tilde{F}_{i+1/2} = <\tilde{F}> - \frac{1}{2} ([\![\tilde{F}]\!]_A + [\![\tilde{F}]\!]_B + [\![\tilde{F}]\!]_C), \quad (7.88)$$

with the absolute value of the wave speeds substituted in the equations.

7.7 Time Integration

In the previous sections, three different algorithms for evaluating the inviscid fluxes have been discussed, and the standard technique for discretizing the viscous fluxes has been mentioned. The remaining relevant problem is how to advance the numerical solution in time, given a known initial state. Some algorithms that were very popular even in recent years [60] use a coupled approach, whereby time integration and space discretization are interconnected. However, the finite-volume technique lends itself to a fully uncoupled procedure, the time integration being segregated from the space discretization procedures. In the following, several time integration techniques will be discussed which are consistent with the uncoupled approach. On the other hand, a fully coupled procedure is advocated for the combined treatment of chemical, thermal and fluid dynamic phenomena, due to its robustness and efficiency.

The equation to be advanced in time is eq.(7.8), which can be written in terms of a *residual*, grouping fluxes and source terms, as follows

$$\frac{\partial Q}{\partial t}\Omega + \boldsymbol{R}(Q) = 0\,. \tag{7.89}$$

In eq.(7.89) the average notation has been dropped and the residual $\boldsymbol{R}$ is given by

$$\begin{aligned}\boldsymbol{R}(Q) =&(\tilde{F} - \tilde{F}_v)_{i+1/2}\partial\Omega_{i+1/2} - (\tilde{F} - \tilde{F}_v)_{i-1/2}\partial\Omega_{i-1/2}+\\ &+(\tilde{G} - \tilde{G}_v)_{j+1/2}\partial\Omega_{j+1/2} - (\tilde{G} - \tilde{G}_v)_{j-1/2}\partial\Omega_{j-1/2}+\\ &+(\tilde{H} - \tilde{H}_v)_{k+1/2}\partial\Omega_{k+1/2} - (\tilde{H} - \tilde{H}_v)_{k-1/2}\partial\Omega_{k-1/2} - W\Omega\,.\end{aligned} \tag{7.90}$$

Two classes of problems usually arise when dealing with time integration. The first class contains the *unsteady* problems, where an accurate time integration is essential for the overall validity of the simulation. A popular and computationally nonexpensive scheme that is second-order accurate in time is the m-stage Jameson-style explicit Runge-Kutta method, which advances the solution in time according

to the following

$$
\begin{aligned}
Q^0 &= Q^n, \\
Q^1 &= Q^0 - \alpha_1 \frac{\Delta t}{\Omega} R(Q^0), \\
Q^2 &= Q^0 - \alpha_2 \frac{\Delta t}{\Omega} R(Q^1), \\
&\vdots \qquad\qquad \vdots \\
Q^m &= Q^0 - \alpha_m \frac{\Delta t}{\Omega} R(Q^{m-1}), \\
Q^{n+1} &= Q^m,
\end{aligned}
\tag{7.91}
$$

where the weighting coefficients α_i guarantee second-order time-accuracy when

$$
\alpha_i = \frac{1}{m - i + 1}. \tag{7.92}
$$

In the above, the superscript, n, denotes the conditions at time level n and Δt the time step. This explicit scheme has the major drawback of becoming extremely inefficient for *stiff* problems, that is when some of the characteristic times associated with chemical reactions or thermal relaxation become much faster than the fluid dynamics characteristic time [103],[104]. In these conditions, the time step necessary for stability can become even orders of magnitude smaller than the value which would be necessary for an efficient resolution of the overall gas dynamic transient [105]. For this reason, time-implicit schemes are advocated [106], and they show an increase in efficiency that can be dramatic, as discussed in §8.

For cases where time accuracy is important, as in unsteady problems, an implicit two-step Runge-Kutta scheme [107] will be used

$$
\left[\mathbf{I} \frac{\Omega}{\Delta t} + \alpha_1 \frac{\partial}{\partial Q} R(Q^n) \right] \Delta Q_1 = -R(Q^n), \tag{7.93a}
$$

$$
\left[\mathbf{I} \frac{\Omega}{\Delta t} + \alpha_2 \frac{\partial}{\partial Q} R(Q^n) \right] \Delta Q_2 = -R(Q^n + \beta_{21} \Delta Q_1), \tag{7.93b}
$$

$$
\Delta Q = Y_1 \Delta Q_1 + Y_2 \Delta Q_2 , \tag{7.93c}
$$

where $\Delta Q = Q^{n+1} - Q^n$, corresponds to the change in Q over one time step Δt, and $\partial R/\partial Q$ denotes the Jacobian contributions from fluxes and source terms. The constants α_1, α_2, Y_1, Y_2 and β_{21} were determined by Iannelli and Baker [107] as $\alpha_1 = \alpha_2 = (2-\sqrt{2})/2$, $Y_1 = (6-\sqrt{2})/8$, $Y_2 = (2+\sqrt{2})/8$ and $\beta_{21} = 2(3\sqrt{2}-4)$, such that the algorithm is second-order accurate in time. An important feature of the method is the fact that the left-hand-side of the equations needs to be evaluated only once, at time level n. This contributes noticeably to the global efficiency of the algorithm.

The second class of problems to be dealt with is the one which includes steady calculations. A pseudo-transient problem is usually solved in this case, where the solution is advanced in a pseudo-time until convergence to a steady-state is reached. Time accuracy is of no concern here, but an implicit treatment is even more necessary for efficiency. The usual scheme employed, and the one considered in the following, is the Euler-Implicit method, which is first-order accurate in time

$$\left[\mathrm{I}\frac{\Omega}{\Delta t} + \frac{\partial}{\partial Q}\boldsymbol{R}(Q^n)\right]\Delta Q = -\boldsymbol{R}(Q^n), \tag{7.94}$$

and which could be considered to be a special case of the two-step Runge-Kutta when $\alpha_1 = 1$, $\alpha_2 = 0$, $Y_1 = 1$ and $Y_2 = 0$.

The residual Jacobian contribution $(\partial \boldsymbol{R}/\partial Q)\Delta Q$ is a symbolic operator, that should interpreted as follows

$$\begin{aligned}\frac{\partial \boldsymbol{R}}{\partial Q}\Delta Q = &\left(\frac{\partial(\tilde{\boldsymbol{F}} - \tilde{\boldsymbol{F}}_v)}{\partial Q}\Delta Q\right)_{i+1/2}\partial\Omega_{i+1/2} - \left(\frac{\partial(\tilde{\boldsymbol{F}} - \tilde{\boldsymbol{F}}_v)}{\partial Q}\Delta Q\right)_{i-1/2}\partial\Omega_{i-1/2} + \\ &+\left(\frac{\partial(\tilde{\boldsymbol{G}} - \tilde{\boldsymbol{G}}_v)}{\partial Q}\Delta Q\right)_{j+1/2}\partial\Omega_{j+1/2} - \left(\frac{\partial(\tilde{\boldsymbol{G}} - \tilde{\boldsymbol{G}}_v)}{\partial Q}\Delta Q\right)_{j-1/2}\partial\Omega_{j-1/2} + \\ &+\left(\frac{\partial(\tilde{\boldsymbol{H}} - \tilde{\boldsymbol{H}}_v)}{\partial Q}\Delta Q\right)_{k+1/2}\partial\Omega_{k+1/2} - \left(\frac{\partial(\tilde{\boldsymbol{H}} - \tilde{\boldsymbol{H}}_v)}{\partial Q}\Delta Q\right)_{k-1/2}\partial\Omega_{k-1/2} - \\ &-\frac{\partial \boldsymbol{W}}{\partial Q}\Delta Q\Omega,\end{aligned} \tag{7.95}$$

where the inviscid space contributions are evaluated with a first-order approach for simplicity

$$\left(\frac{\partial \tilde{F}}{\partial Q}\Delta Q\right)_{i+1/2} = (\tilde{\mathbf{A}}\,\Delta Q)_{i+1/2} = (\tilde{\mathbf{A}}^{+}\Delta Q^{-})_{i+1/2} + (\tilde{\mathbf{A}}^{-}\Delta Q^{+})_{i+1/2} = \\ = (\tilde{\mathbf{A}}^{+}\Delta Q)_{i} + (\tilde{\mathbf{A}}^{-}\Delta Q)_{i+1}\,. \tag{7.96}$$

The viscous terms are treated in an approximate fashion, using only the Thin-Layer contributions and neglecting the cross-derivative terms in the Jacobians. As a result, it is possible to write

$$\left(\frac{\partial \tilde{F}_v}{\partial Q}\Delta Q\right)_{i+1/2} = (\tilde{\mathbf{A}}_v\,\Delta Q)_{i+1/2} = \frac{\partial}{\partial Q}\left[\alpha_{i+1/2}\left(\frac{\partial \beta}{\partial \xi}\right)_{i+i/2}\right]\Delta Q_{i+1/2}\,, \tag{7.97}$$

where α represents contributions that multiply the gradient of β, and the derivatives with respect to the conservative variables can be evaluated to yield the result [108],[109]

$$\left(\frac{\partial \tilde{F}_v}{\partial Q}\Delta Q\right)_{i+1/2} = (\tilde{\mathbf{A}}_v^{+}\Delta Q)_{i} + (\tilde{\mathbf{A}}_v^{-}\Delta Q)_{i+1}\,, \\ \tilde{\mathbf{A}}^{\pm}_{v,i} = \mp\left[\alpha_{i\pm1/2}\left(\frac{\partial \beta}{\partial Q}\right)_{i} \mp \frac{1}{2}\left(\frac{\partial \alpha}{\partial Q}\right)_{i}\left(\frac{\partial \beta}{\partial \xi}\right)_{i\pm1/2}\right]. \tag{7.98a,b}$$

Similar results hold for the other space directions.

The resulting *linear* algebraic problem is solved for the time increments ΔQ using different techniques. For one-dimensional problems, eq.(7.94) is a block-tridiagonal system of equations, and is solved *exactly* using a direct substitution algorithm [60]. Two and three-dimensional problems, however, yield sparse matrices with more non-zero diagonals even if a first-order approach is used. Two techniques have been implemented for two-dimensional problems, a global LU decomposition, which is still an exact solution, and an Approximate Factorization, which reduces the problem to a sequence of two block-tridiagonal systems of equations. For three-dimensional problems, the storage requirements for an exact solution are too restrictive. The technique applied has been to implement the LU or AF algorithms

in a plane and to relax in the third direction, symbolically chosen as ξ, through a non-linear update of the residual.

For the LU algorithm, eq.(7.94) can be written as

$$\hat{\mathsf{M}}\Delta Q = -R(Q^n, Q^{n+1}), \tag{7.99}$$

where

$$\begin{aligned}\hat{\mathsf{M}} = &\frac{\Omega}{\Delta t}\mathsf{I} + (\tilde{\mathsf{A}}_i^+ - \tilde{\mathsf{A}}_{v,i}^+)\partial\Omega_{i+1/2} - (\tilde{\mathsf{A}}_i^- - \tilde{\mathsf{A}}_{v,i}^-)\partial\Omega_{i-1/2} + \\ &+\Big(\frac{\partial(\tilde{G}-\tilde{G}_v)}{\partial Q}\Big)_{j+1/2}\partial\Omega_{j+1/2} - \Big(\frac{\partial(\tilde{G}-\tilde{G}_v)}{\partial Q}\Big)_{j-1/2}\partial\Omega_{j-1/2} + \\ &+\Big(\frac{\partial(\tilde{H}-\tilde{H}_v)}{\partial Q}\Big)_{k+1/2}\partial\Omega_{k+1/2} - \Big(\frac{\partial(\tilde{H}-\tilde{H}_v)}{\partial Q}\Big)_{k-1/2}\partial\Omega_{k-1/2} - \frac{\partial W}{\partial Q}\Omega,\end{aligned} \tag{7.100}$$

and only the diagonal contributions in the ξ direction have been retained. The off-diagonal contributions are either relaxed or accounted for in the non-linear residual update, and alternating-direction sweeps are performed.

The AF algorithm considers a problem in the η direction and another in the ς directions, both of which are block-tridiagonal in nature. Eq.(7.94) becomes in this case

$$\begin{aligned}&\Big[\hat{\mathsf{M}} + \Big(\frac{\partial(\tilde{G}-\tilde{G}_v)}{\partial Q}\Big)_{j+1/2}\partial\Omega_{j+1/2} - \Big(\frac{\partial(\tilde{G}-\tilde{G}_v)}{\partial Q}\Big)_{j-1/2}\partial\Omega_{j-1/2}\Big]\hat{\mathsf{M}}^{-1}\cdot \\ &\cdot\Big[\hat{\mathsf{M}} + \Big(\frac{\partial(\tilde{H}-\tilde{H}_v)}{\partial Q}\Big)_{k+1/2}\partial\Omega_{k+1/2} - \Big(\frac{\partial(\tilde{H}-\tilde{H}_v)}{\partial Q}\Big)_{k-1/2}\partial\Omega_{k-1/2}\Big]\Delta Q = \\ &= -R(Q^n, Q^{n+1}),\end{aligned} \tag{7.101}$$

where

$$\hat{\mathsf{M}} = \frac{\Omega}{\Delta t}\mathsf{I} + (\tilde{\mathsf{A}}_i^+ - \tilde{\mathsf{A}}_{v,i}^+)\partial\Omega_{i+1/2} - (\tilde{\mathsf{A}}_i^- - \tilde{\mathsf{A}}_{v,i}^-)\partial\Omega_{i-1/2} - \frac{\partial W}{\partial Q}\Omega, \tag{7.102}$$

and the time increment ΔQ is obtained by solving the two steps

$$\begin{aligned}\Delta Q^* &= -\Big[\hat{\mathsf{M}} + \Big(\frac{\partial(\tilde{G}-\tilde{G}_v)}{\partial Q}\Big)_{j+1/2}\partial\Omega_{j+1/2} - \Big(\frac{\partial(\tilde{G}-\tilde{G}_v)}{\partial Q}\Big)_{j-1/2}\partial\Omega_{j-1/2}\Big]^{-1} R(Q^n, Q^{n+1}), \\ \Delta Q &= \Big[\hat{\mathsf{M}} + \Big(\frac{\partial(\tilde{H}-\tilde{H}_v)}{\partial Q}\Big)_{k+1/2}\partial\Omega_{k+1/2} - \Big(\frac{\partial(\tilde{H}-\tilde{H}_v)}{\partial Q}\Big)_{k-1/2}\partial\Omega_{k-1/2}\Big]^{-1} \hat{\mathsf{M}}\Delta Q^*.\end{aligned} \tag{7.103}$$

The relaxation in the ξ direction is the same as in the previous case.

Both algorithms vectorize and can be coded very efficiently [59]. However, unsteady problems have been considered only in one space dimension, where the two-step Runge-Kutta implicit method was used.

The Jacobian contributions for the source terms can be obtained by analytical evaluation of derivatives. The Jacobians for the Steger-Warming algorithm are obtained as a part of the derivation of the algorithm in §7.4. Those for the Van Leer splitting are straightforward. The Jacobians associated with the approximate Riemann solver of the Roe type are complex to obtain. For perfect gas flows, approximate Jacobians have been developed [110]. An alternative approach is to utilize the Jacobians produced by the flux-vector algorithms [111], and this is the procedure followed in the present numerical simulations.

8. RESULTS

8.1 Introduction

The governing differential equations derived in §3 and written in integral form have been discretized in space and time according to the procedure of §7. Numerical results have been obtained for some test-cases in one and two space dimensions, using two different codes. The first one was written by the author for one-dimensional and quasi-one-dimensional inviscid simulations, following the formulation of §3.7. The second one was written by Prof. R. Walters of VPI, the author and D. Slack [59] for general three-dimensional viscous flows out of thermal and chemical equilibrium (Generalized Aerodynamic Simulation Program, or GASP). A presentation of some interesting computations made using both codes will be provided.

A fully-coupled approach for the combined treatment of gas-dynamics and thermochemical phenomena has been employed, as discussed in §7. Analytical Jacobians for the source terms have been derived and implemented, and the resulting algorithms have proven to be very efficient [32],[59]. For supersonic steady-state calculations with the quasi-one-dimensional code, residual reductions of seven orders of magnitude have been obtained in a matter of 80 to 120 iterations for 161 mesh points, working with a CFL number from 10 to 15, and a CPU time per iteration varying largely with the complexity of the thermal and chemical model, but ranging from a few seconds to four minutes on a Sun 3/50 minicomputer. Calculations where embedded shock waves are present show a deterioration of the convergence rate, but the same residual reduction was typically experienced in 800 to 1200 iterations for the same grid, working with a CFL number of 3 to 6 without any attempt of optimization. Unsteady calculations for a shock tube were performed with a CFL number of 0.5, and showed the same accuracy as explicit calculations which used a CFL number of 0.02 and about ten times more CPU time per run, in spite of having a CPU time requirement per iteration of about one third.

Two-dimensional steady calculations were performed very efficiently, with CFL numbers as high as 100 from the beginning, or after a very short transient. Both

LU and AF algorithms vectorize, and a few strategies for freezing the Jacobians were successfully implemented [59]. The CPU time requirement per iteration per mesh point is of the order of a few hundred microseconds. Specifically, it can be as low as 60 μsec for an AF iteration with a perfect gas or as high as 950 μsec for an LU iteration with Air Model 1 and the Vibrational Equilibrium Model on a 41×41 grid. A corresponding iteration when the Left Hand Side is kept frozen will be performed in approximately one eighth of the above time. More complex thermodynamic models, or flow conditions where significantly more chemical reactions are considered, will require larger CPU times.

The generality of the approach chosen for handling chemical reactions allows comparisons of several models without any difficulty. A few results will be shown, where the effects of choosing different models for reacting air, changing reaction rates, or including more species, will be examined. Similar studies have been conducted for the other chemical models. Moreover, calculations with the chemistry kept frozen will be compared to finite-rate and chemical-equilibrium simulations, and the dramatic changes that occur in the flow features underlined.

In addition, different thermodynamic models can be easily compared, and cases will be presented where the choice of a model can make a significant difference in the predictions. More physical insight is necessary in order to assess the accuracy and superiority of one treatment over another.

In the following, a discussion of several results for flows in a nozzle will be presented, using both the quasi-one-dimensional approach and axisymmetric calculations. Supersonic flows and cases where an embedded shock stands approximately in the middle of the rapidly-expanding diffuser studied by Drummond, Hussaini and Zang [93] will be detailed. Then, calculations for hypersonic simple geometries will be examined, including blunt bodies and a 10° wedge.

8.2 Quasi-One-Dimensional Steady Results

The geometry chosen for the quasi-one-dimensional inviscid steady simulations is represented in Fig. 1. The rapidly expanding supersonic diffuser has an area ratio of 4:1 over a length of 2 meters [93], according to the formula

$$A = \frac{\pi}{16}[1 + sin(\frac{\pi x_1}{2L})]^2, \qquad 0 \leq x_1 \leq L, \tag{8.1a,b}$$

where $L = 2\ m$. Unless indicated otherwise, all calculations were performed on 161 evenly spaced grid points with a third-order upwind-biased spatial discretization, as discussed in §7.2, and are believed to be grid-converged. A qualitative representation of the axisymmetric mesh used for the simulations discussed in the next section is also visible in the figure. For supersonic calculations, Steger-Warming and Van Leer flux-vector splitting methods coincide within round-off errors, and Roe flux-difference splitting technique yields very similar results, indistinguishable within plotting accuracy. When a shock wave is embedded in the diffuser, the approximate Riemann solver captures it in a slightly better way, as is the case for perfect gas [101]. Consequently, the results presented are the ones obtained using Roe's method.

A comparison of different chemistry models for dissociating air is shown in Fig. 2. Air Models 1, and 2, along with a reduced version of the latter are used. The reduced version is obtained by considering only the 5 neutral species and dropping the ionization reactions. As a result, the model considers the same species and chemical reactions as Air Model 1. The Vibrational Equilibrium Model was used. Plots of the fluid dynamic quantities in Fig. 2a do not show any major discrepancy between the models, even if Air Model 1 gives a temperature profile that is slightly lower than those obtained using Air Model 2 and its reduced version. However, the mass fractions plots, although qualitatively similar, show some discrepancy. The reason is due to the fact that the flow was considered to be in chemical equilibrium at the inlet conditions. Consequently, for the *same* values of temperature and density,

Air Models 1 and 2 yield *different* equilibrium compositions. It is impossible to read it from the plots, but the inlet pressure is also different for the different models. It can be noticed from Fig. 2b that the relevant reaction for the range of temperatures considered is the recombination of oxygen, and that including ionized species does not change the results within plotting accuracy.

A comparison of different thermodynamic models for the same problem is shown in Fig. 3. Air Model 1 was utilized for this case. The Vibrational Equilibrium and the Curve Fit Models, discussed in §2.5, agree very well in this temperature range, whereas the Simplified Vibrational Non-Equilibrium Model, presented in §4.4, predicts a lower temperature. This can be explained by the fact that a non-negligible freezing of the vibrational states occurs, because of a relatively slow relaxation time. The mass fraction plots with the non-equilibrium model show only a very mild tendency towards a higher level of oxygen recombination for the non-equilibrium model, due to the lower temperature predicted.

The effect of assuming a frozen chemistry or a local chemical equilibrium for the same problem is investigated in Fig. 4, where the Vibrational Equilibrium Model was used in conjunction with Air Model 2. The temperature predictions are in vast disagreement, with the finite-rate calculations correctly in the middle of the two limiting cases. It can be noticed that some *mechanical* quantities, such as pressure and velocity, are hardly affected by the differences in the chemical behaviour. The mass fractions, however, which are constant for frozen calculations, are greatly affected by the assumption of local chemical equilibrium, as seen in Figs. 4b,4c. It is noteworthy that the finite-rate results do not always fall within the bounds set by the two limiting cases, in particular for the NO and the N_2^+ plots. The reason is found in the large nonlinearities of the model, which specifically show a maximum for the production of NO in a mass fraction versus temperature diagram. The equilibrium predictions were obtained by multiplying the rate constants by a factor of 10^6 and running the finite-rate code. A calculation with a factor of 10^{12} did not change the results. There are more efficient ways of performing calculations

using a local chemical equilibrium assumption, but the information on the species distributions is usually lost to global curve fits [12–22]. Techniques based upon free energy minimization [69], and/or equilibrium constant calculations [49] will be implemented in the near future.

Simulations similar to those given in Figs. 2–4, but with a higher inlet temperature, are shown in Figs. 5–7. The different temperature range brings about some interesting results. The comparison between the different chemistry models, Fig. 5, shows that Air Models 1 and 2 differ noticeably for both temperature and composition predictions, although the qualitative picture is unchanged. The question of which model should be preferred for these extreme conditions is a difficult one. However, Air Model 2 is more recent and based upon relatively new experimental results. Newer models have been proposed recently [74], and should also be taken into consideration.

On the other hand, the thermodynamic model comparison in Fig. 6 shows that vibrational equilibrium is fully established, because of the very fast relaxation times, whereas the curve-fit model yields predictions in disagreement with the other two models. The reason for this is likely due to extrapolating to high temperatures a model that is valid only up to $5,000\ K$.

The comparison between frozen, chemical-equilibrium, and finite-rate results, Fig. 7, shows again that the assumption of a limiting case is not often justified if accurate predictions are sought for mechanical and particularly thermal loads. However, the problem of obtaining a reliable and possibly simple finite-rate reaction model is unsolved for most cases of practical interest.

The same diffuser geometry was used for an investigation of hydrogen-air chemistry [28]. A comparison of the present results with those obtained by Drummond, Hussaini and Zang [93] is presented in Fig. 8. The Curve Fit Model was used, and all calculations are in agreement. The (pseudo-)spectral method only used 17 grid points, unevenly spaced, and the finite-difference code 101 evenly spaced points,

the number of cycles for convergence being of the order of a few thousands for both methods.

The comparison between different thermodynamic models, Fig. 9, shows that there is a noticeable freezing of vibrational energy in the non-equilibrium predictions. Both equilibrium models are in excellent agreement, due to the moderate temperatures. The discrepancy in the temperature prediction affects the intermediate step of the combustion, the production of OH, but does not alter the final level of water mass fraction.

Results obtained with Argon Models 1 and 2 for the simple Argon plasma are shown in Fig. 10. Argon Model 1 yields predictions virtually coinciding with chemical equilibrium when only one translational temperature is considered. The mass fraction of A^+ coincide with the degree of ionization ϕ defined in Vincenti and Kruger [2], apart from a factor very close to 1 due to the difference between molecular mass of neutral and ionized Argon.

Argon Model 1 is used again in Fig. 11 for a simulation with two translational temperatures. The results are compared with a similar calculation, using only one translational temperature in the thermo-chemical model. The discrepancy is moderate, but visible. Similar comparisons at higher inlet temperatures, not shown here, result in a closer agreement between the two models, because the energy exchange between heavy particles and electrons is more efficient.

The same diffuser was utilized for calculations where the outlet pressure was raised in order to obtain a shock wave standing approximately in the middle of domain. Fig. 12 shows the result for air, with different thermodynamic models, same inlet conditions as Figs. 2–4, and Air Model 1. Immediately behind the shock there is a very small relaxation zone, as shown in the temperature plot. This relaxation is amplified by the non-equilibrium model, where the after-shock values should be consistent with the Rankine-Hougoniot jump conditions for a flow with frozen vibrational states and consequently higher $\tilde{\gamma}$. The undershoot in the temperature profile before the shock is probably due to numerical difficulties, but

the highly nonlinear behaviour of the *NO* mass fraction is due to the chemistry model. Shuen, Liou and Van Leer [30] present arguments for disregarding this result as non-physical.

A comparison of frozen, chemical-equilibrium and finite-rate models is shown in Fig. 13. The shock location is different for the three simulations. The finite-rate predictions show a small relaxation zone, particularly visible in the temperature plots. It can be also noticed that the shock is essentially frozen, but this feature disappears if local chemical equilibrium is assumed. Plots of mass fractions show that, after the shock, the flow quickly reaches chemical equilibrium.

The same inlet conditions of Figs. 8–9 are used in Fig. 14 for Hydrogen-Air Model 1 and several thermodynamic models. A small relaxation zone, this time due almost exclusively to the vibrational energy, is observed. Again, the production of the intermediate species *OH* is affected by the chosen thermodynamical model in a noticeable amount.

Argon Models 1 and 2 are used in Fig. 15 for the same inlet conditions as in Fig. 10. Again, Argon Model 1 almost coincides with the chemical equilibrium simulation, when only one temperature is used.

8.3 Two-Dimensional Steady Results

The usual supersonic diffuser geometry was employed for axisymmetric calculations in order to test the new GASP code. A qualitative drawing of the relatively coarse 41×6 grid used is shown in Fig. 1. The same chemistry and thermodynamics models and a similar set of inlet and back-pressure conditions have been implemented, and the results compared with the corresponding quasi-one-dimensional predictions. Only a few of the results will be shown here, representative of a larger set of similar simulations.

A comparison of several thermodynamic models for Air Model 1 is shown in Fig. 16. The inlet conditions are the same as the results of Figs. 2–4, and quasi-one-dimensional predictions are reproduced again for illustrative purposes. For

this plot, only area-averaged results for the axisymmetric calculations are shown, because those are the values that should be checked versus quasi-one-dimensional results, as discussed in §3.7. The plots show an excellent agreement between the axisymmetric and the corresponding quasi-one-dimensional curves, and confirm the general trend reproduced in Fig. 3 for the differences among the thermodynamic models.

An interesting result is found in Fig. 17, where the inlet conditions of Figs. 5–7 were used, along with the Vibrational Equilibrium Model and Air Model 2. Quasi-one-dimensional results are compared with the corresponding axisymmetric calculations, and the area-averaged values are plotted along with surface and centerline distributions. It can be noticed that the gradients in the cross-sectional direction are not negligible in general, and particularly in the first portion of the diffuser. The centerline values show a physically correct lagging in the expansion process when compared with surface values. However, the averaged results are in a remarkably good agreement with the quasi-one-dimensional predictions.

The inlet conditions of Figs. 8–9 and the Hydrogen-Air Model 1 were used to compare different thermal models in the axisymmetric case. Again, the two equilibrium models are in agreement, as shown in Fig. 18 for the area-averaged values, and the same is true for the axisymmetric and quasi-one-dimensional Simplified Vibrational Non-Equilibrium Models. The grid is probably too coarse to resolve properly the inlet region, however the fully satisfactory comparison with quasi-one-dimensional results makes a grid refinement study unnecessary.

The effect of assuming frozen flow or local chemical equilibrium was investigated again in the axisymmetric case, and the results show the same qualitative and quantitative trends as those in Fig. 7. Air Model 2 was used in this case, along with the Vibrational Equilibrium Model and the usual inlet conditions of Figs. 2–4. The results are shown in Fig. 19.

One of the cases of Fig. 12 was rerun with the axisymmetric code, as shown in Fig. 20. Air Model 1, Vibrational Equilibrium Model and the same inlet conditions and outlet back-pressure were utilized. The axisymmetric grid is definitely

too coarse for this case, and some of the features of the shock are not resolved, namely the relaxation zone behind it. The shock appears to be almost normal, but a grid refinement is necessary before attempting any conclusions. The mass fraction plots appear to be in qualitative agreement with their quasi-one-dimensional counterparts, and the agreement is noticeably better in the second half of the diffuser, behind the shock.

A plot of the normalized residual versus CPU time for the Air Model 1 and different time integration algorithms is presented in Fig. 21. All computations have been performed on a Cray-YMP machine, with a residual reduction of 10^{-10} as a convergence criterion. The explicit second-order Runge-Kutta algorithm turned out to be completely inadequate, due to the severe restrictions on its stability brought about by the chemical *stiffness*. The curve shown has been obtained with a CFL number of 0.1. A CFL number of 100 has been used for the LU Decomposition algorithm and the Approximate Factorization. A further reduction of CPU time has been obtained by means of a reuse of the LU decomposition and of the Approximate Factors, after a residual reduction of two orders of magnitude. It is useful to point out that *no further* Left Hand Side evaluations were performed after the switch.

A similar behaviour has been observed for the Hydrogen-Air Model 1, as shown in Fig. 22. Here, the Runge-Kutta algorithm had to work with a CFL number of 10^{-4}, due to the *extreme* stiffness of the two-reaction model. The LU and AF algorithms, as well as the reuse strategies discussed, used a CFL of 100. Due to convergence problems, the reuse is started after a residual reduction of four orders of magnitude, with LHS recalculated every five iterations.

It can be noticed that the plots of residual versus iteration number in Figs. 21 and 22 hardly show any difference between AF and LU. This is likely due to the predominance of the diagonal terms, associated with the source terms Jacobians, in the algebraic problem.

Once some confidence on the three-dimensional generalized code was gained, a simple blunt body in a Mach 25 hypersonic flow was considered as a non-trivial test

case. The geometry is shown in Fig. 23, where the body is made of a semi-ellipse followed by a short linear afterbody, not represented in the picture, and corresponds to the formula

$$\left(\frac{x_1}{0.6}\right)^2 + \left(\frac{x_3}{0.15}\right)^2 = 1, \qquad x_1 \leq 0. \tag{8.2a,b}$$

The 41×41 mesh is visible, and the angle of attack for the calculation was $\alpha = 30°$. Air Model 1 and the Vibrational Equilibrium Model were used. Van Leer's flux-vector splitting method was employed in the transverse direction, and Roe's technique in the circumferential direction. The low freestream temperature and density represent conditions at an altitude of 75 *km*.

Plots of some relevant quantities on the body are shown in Fig. 24. The pressure coefficient is defined, as usual, as $(p-p_\infty)/\frac{1}{2}\rho_\infty u_{0_\infty}^2$, and the Mach number is referred to the frozen speed of sound. The stagnation point occurs on the windward side, as expected, and the flow is fully supersonic right after the ellipse tip, with the result that the subsonic bubble is very contained. The atomic oxygen mass fraction plot shows a noticeable freezing on the leeward side, where a rapid temperature drop is present.

Another simple hypersonic calculation was attempted for testing the Thin-Layer approach. A Mach 10 flow over a 10° wedge was considered, and several transport models tested for frozen chemistry conditions. The flow is assumed one-dimensional in nature, and a $2 \times 49 \times 2$ grid was used for the simulations. Profiles of velocity and pressure along the transverse direction are shown in Fig. 25, obtained using Roe's method. The Nitrogen-Oxygen result was obtained using Blottner's curve fit and Eucken's relation, as discussed in §5.2 and §5.3, whereas the perfect gas result was obtained using Sutherland's formula, and a molecular mass corresponding to air. The results are in agreement, as expected. Also shown on the plot is the corresponding result obtained by Prof. R. Walters for a perfect gas, which, again, is in agreement.

9. SUMMARY AND CONCLUSIONS

The objective of the present work has been a development of state-of-the-art algorithms for the numerical simulation of fluid flows with thermo-chemical non-equilibrium, such as those occurring at very high temperature and moderate density. The final goal of this effort is the enhancement of the knowledge of high speed, high temperature phenomena, so that accurate predictions of very complex flows can be achieved. Although some interesting advances have been registered in the last few years, there is still a lack of information in some key areas, such as thermal non-equilibrium effects, turbulence, transport properties, etc., so that more in-depth physical investigations are needed.

High-speed related phenomena are discussed, with special attention to the on-set of thermodynamic non-equilibrium. A generalized model for the species internal energy has been proposed, whereby Maxwellian distributions are considered, requiring one or more temperatures for different contributions. Physical arguments yield the corresponding values for the mixture, as well as the relevant equations of state, which, in general, will be nonlinear relationships between the pressure and the particle translational temperatures. General results for macroscopic quantities such as the frozen speed of sound can then be obtained. A few practical thermodynamic models have been selected and implemented in a computer simulation, with the perfect gas model as a special case, and more refined models can be easily implemented within the present framework.

Non-equilibrium kinetic theory, along with some assumptions regarding the nature of intermolecular forces and the behaviour of the species distribution functions, serves as the basis for the derivation of the governing partial differential equations for a flow out of chemical and thermal equilibrium. A general equation of transfer for a species is obtained, and utilized to establish the conservation equations of species mass, momentum, energy and non-equilibrium energy. Global equations for the

mixture are obtained by direct summation over the species contributions, and noticeable simplifications occur. The mathematical problem for the simulation of non-equilibrium flow with two different translational temperatures and non-equilibrium energy contribution is fully established, and several simplified approaches have been discussed. The usual Navier-Stokes and Euler equations are recovered as special cases of this general model in the absence of non-equilibrium phenomena and with simplifying assumptions on the particle thermodynamic behaviour. Transformations to generalized, non-orthogonal, structured coordinate systems are discussed, and the integral form of the governing equations is introduced, suitable for use in a finite-volume spatial discretization. The important quasi-one-dimensional inviscid approach is found to yield remarkably good predictions even in presence of severe gradients in the transversal plane.

The problems associated with modeling chemical kinetics are presented, and the limiting cases of frozen flow and local chemical equilibrium discussed. However, only homogeneous, non-catalytical reactions are considered, so that the problem of a realistic treatment of wall catalysis still needs to be addressed. Specific chemical models found in the recent literature are implemented in the numerical simulation, namely : two models for air chemistry, one involving dissociation and 5 species and the other including ionization and 11 species, one model for hydrogen–oxygen combustion in presence of inert nitrogen, and two models for a simple Argon based plasma. A review of the most recent work in the field of modeling thermal non-equilibrium and its influence on chemical reactions follows. A simple vibrational relaxation model that retains as much of the relevant physics as possible, with a minimum mathematical complexity, is presented. The most common assumptions for the modeling of the charge-separation induced electrical field are given, specifically for cases where magnetic phenomena and external electric fields are not important.

Some considerations on the basic modeling of viscous fluxes precede a detailed analysis of the current assumptions and approximations about transport properties, needed to keep the computational load at a level compatible with the present

capabilities. Models for the species viscosity coefficient based upon curve fit values are given, and a semi-empirical rule for obtaining mixture properties introduced. Similar experimentally-based relationships are utilized for the thermal conductivity coefficient, along with global models at constant Prandtl number. Very simple equations are written for mass diffusion, and several second-order effects neglected in order to arrive at a gradient-based law of diffusion. Simple binary diffusion coefficients are then considered for practical computations. The lack of a general theory of mass, momentum or energy transport in the presence of thermal non-equilibrium forces the use of simple, straightforward extensions of results obtained in less extreme cases in order to capture at least the essential physics of the problems of concern.

In very high-speed régimes, when ionization effects become noticeable, the difference in mass between electrons and heavy particles acts as an obstacle to effective and prompt energy exchanges. In these conditions, it is customary to assume that free and bound electrons reach a common equilibrium temperature, different from the heavy particle translational temperature. The presence of translational contributions to the electron temperature, however, introduces physical and mathematical complications to the problem. The inviscid flux Jacobians lose their simple eigenvalue structure when more than one translational temperature is assumed into the model. Consequently, the problem of propagation of information along the characteristic directions becomes more difficult to analyze. More refined models for the species internal energy show the same drawbacks, as long as more than one translational temperature enters the picture. There is a considerable lack of work done on this subject, and current investigations do not seem to be fully satisfactory nor consistent. A simple asymptotic analysis is proposed in order to recover approximate analytical solutions to the mathematical problem, whose positive aspect is the internal consistency in the treatment of fluxes, Jacobians, etc.

The governing equations are discretized in time and space in order to be transformed into algebraic equations to be solved via a digital computer. The finite-volume approach is utilized, whereby the equations written in integral form are

approximated in terms of unknown volume-averaged values for each (small) computational cell. The method is valid in presence of discontinuities in the solutions, such as shock waves or slip lines, and has the conservative property for arbitrary volumes within the computational domain. Flux-split algorithms are used to discretize the inviscid fluxes, and high-order accuracy is obtained using flux limiters in the extrapolation procedure. The propagation of information along characteristic directions is accounted for by these algorithms, so that the explicit introduction of artificial viscosity for stability purposes is avoided. A Steger-Warming-type algorithm is developed for flows with one translational temperature by diagonalizing the inviscid Jacobian and exploiting the homogeneity property of the Euler equations. A corresponding result can be developed for flows with free electrons by means of the asymptotic analysis already introduced. A Van-Leer-type splitting can be similarly obtained, and results in smoother predictions near sonic points. Also, an approximate Riemann solver has been derived, and the corresponding Roe-type averages determined. These averages are not unique, and different values have been reported in the literature. Several time integration algorithms are discussed and implemented, including an implicit two-step Runge-Kutta unsteady solver and a very efficient fully implicit Euler steady solver. For three-dimensional problems, approximate techniques, based upon LU decomposition or Approximate Factorization in a plane plus relaxation in the third direction, are employed.

Some results have been presented for one and two space dimensions, for simple flows out of chemical and thermal equilibrium. Inviscid internal flows in a supersonic nozzle, with and without an embedded shock wave, have been calculated using several chemical and thermodynamic models. Quasi-one-dimensional predictions have been compared to axisymmetric simulations, and found to be in good agreement. External flows over a simple ellipse at a high angle of attack and Mach 25 have been successfully calculated, as well as Mach 10 viscous flows over a 10° wedge.

Some tentative conclusions have been reached as a result of the present effort. The new algorithms developed have demonstrated their accuracy and robustness

for challenging flow problems. Virtually arbitrary chemical models can be studied and efficiently tested, and refined thermodynamic models can be included in the numerical simulations using the present framework. Comparisons of results obtained with competing thermal and chemical hypotheses are made possible with relative ease. The influence of several assumptions on the chemical and thermal behaviour of the flows has been investigated, and the inadequacy of simplified models for representing the physics of hypersonic flows has been confirmed. Large differences in the results obtained with different models are documented. It will take a careful comparison with experimental data to assess the preferability of a model over the others for various ranges of flow conditions.

Comparisons with other inviscid calculations yielded favorable results. Comparison of numerical simulations with experiments has not been possible at the present stage, because the modeling of the viscous phenomena is still at an introductory level. However, elementary viscous calculations can be made within the framework presented.

A theoretical study of the main features of flows with free electrons, for conditions that require the use of two translational temperatures in the thermal model, has been developed. Interesting and unexpected results have been obtained, because the acoustic wave speeds no longer have the symmetric form $u \pm a$. A simple but powerful asymptotic analysis has been developed which has allowed the establishment of the fundamental gasdynamic properties of flows with multiple translational temperatures.

In conclusion, much more must be understood before a satisfactory level of knowledge in the field of high-speed, high-temperature fluid flows can be reached. However, substantial, even impressive progress has been made in recent years, and both economical and scientific interests are creating the opportunity for a better mastery of this challenging chapter of physics and engineering.

BIBLIOGRAPHY

1. Lee, J.-H., "Basic Governing Equations for the Flight Regimes of Aeroassisted Orbital Transfer Vehicles", *Progress in Astronautics and Aeronautics*, Vol. 96, 1985.
2. Vincenti, W. G. and Kruger, C. H. Jr., *Introduction to Physical Gas Dynamics*, ISBN 0-88275-309-6, Robert E. Krieger, 1965.
3. Hirschfelder, J. O.,Curtiss, C. F. and Bird, R. B., *Molecular Theory of Gases and Liquids*, Library of Congress CCN 54-7621, John Wiley & Sons, 1954.
4. Saaty, T. L. and Bram, J., *Nonlinear mathematics*, ISBN 0-486-64233-X, Dover Publications Inc., 1981.
5. Lam, S. H. and Goussis, D. A., "Time-Resolved Simplified Chemical Kinetics Modelling Using Computational Singular Perturbation", AIAA Paper No. 89-0575, 1989.
6. Grossman, B. and Cinnella, P., "Flux-Split Algorithms for Flows with Non-equilibrium Chemistry and Vibrational Relaxation", ICAM Report 88-08-03, VPI & SU, 1988 (to appear *Journal of Computational Physics*).
7. Bushnell, D. M. and Reshotko, E., "Proceedings of NASP High-Speed Roughness/Waviness-Transition Interaction Workshop", NASP WP 1005, 1989.
8. Anderson, J. D. Jr., "A Survey of Modern Research in Hypersonic Aerodynamics", AIAA Paper No. 84-1578, 1984.
9. Bruno, C., "Real Gas Effects", *Hypersonics*, Vol. 1, eds. J. J. Bertin, R. Glowinski, J. Periaux, ISBN 0-8176-3420-7, Birkhäuser Boston, 1989.
10. Harten, A., Lax, P. D. and Van Leer, B., "On Upstream Differencing and Godunov-Type Schemes for Hyperbolic Conservation Laws", *SIAM Review*, Vol. 25, No. 1, 1983.
11. Roe, P. L., "Characteristic-Based Schemes for the Euler Equations", *Annual Review of Fluid Mechanics*, Vol. 18, 1986.
12. Colella, P. and Glaz, H. M., "Efficient Solution Algorithms for the Riemann Problem for Real Gases", *Journal of Computational Physics*, Vol. 59, 1985.

13. Vinokur, M. and Liu, Y., "Equilibrium Gas Flow Computations II: An Analysis of Numerical Formulations of Conservation Laws", AIAA Paper No. 88-0127, 1988.

14. Liou, M.-S., Van Leer, B. and Shuen, J.-S., "Splitting of Inviscid Fluxes for Real Gases", NASA TM 100856, 1988.

15. Glaister, P., An Approximate Linearised Riemann Solver for the Euler Equations for Real Gases", *Journal of Computational Physics*, Vol. 74, 1988.

16. Glaister, P., "An Approximate Linearised Riemann Solver for the Three-Dimensional Euler Equations for Real Gases Using Operator Splitting", *Journal of Computational Physics*, Vol. 77, 1988.

17. Vinokur, M., "Flux Jacobian Matrices and Generalized Roe Average for an Equilibrium Real Gas", NASA CR 117512, 1988.

18. Vinokur, M. and Montagné, J.-L., "Generalized Flux-Vector Splitting for an Equilibrium Real Gas", NASA CR 117513, 1988.

19. Grossman, B. and Walters, R. W., "Flux-Split Algorithms for the Multi-Dimensional Euler Equations with Real Gases", *Computers and Fluids*, Vol. 17, No. 1, 1989.

20. Grossman, B. and Walters, R. W., "Analysis of Flux-Split Algorithms for Euler's Equations with Real Gases", *AIAA Journal*, Vol. 27, No. 5, 1989.

21. Montagné, J.-L., Yee, H. C. and Vinokur, M., "Comparative Study of High-Resolution Shock-Capturing Schemes for a Real Gas", *AIAA Journal*, Vol. 27, No. 10, 1989.

22. Larrouturou, B. and Fezoui, L., "On the Equations of Multi-Component Perfect or Real Gas Inviscid Flow", (to appear in *Non linear hyperbolic problems*, eds. Carasso, Charrier, Hanouzet and Joly, *Lecture Notes in Mathematics*, Springer-Verlag, 1989).

23. Steger, J. L. and Warming, R. F., "Flux Vector Splitting of the Inviscid Gasdynamic Equations with Applications to Finite-Difference Methods", *Journal of Computational Physics*, Vol. 40, 1981.

24. Van Leer, B., "Flux-vector Splitting for the Euler equations", in *Lecture Notes in Physics*, Vol. 170, ISBN 0-387-11948-5, Springer-Verlag, 1982.

25. Roe, P. L., "Approximate Riemann Solvers, Parameter Vectors, and Difference Schemes", *Journal of Computational Physics*, Vol. 43, 1981.

26. Candler, G. V. and MacCormack, R. W., "The Computation of Hypersonic Flows in Chemical and Thermal Nonequilibrium", *Third National Aero-Space Plane Technology Symposium*, NASA Ames, 1987.

27. Candler, G. V. and MacCormack, R. W., "The Computation of Hypersonic Ionized Flows in Chemical and Thermal Nonequilibrium", AIAA Paper No. 88-0511, 1988.

28. Grossman, B. and Cinnella, P., "The Development of Flux-Split Algorithms for Flows with Non-Equilibrium Thermodynamics and Chemical Reactions", AIAA Paper No. 88-3595-CP, 1988.

29. Grossman, B. and Cinnella, P., "The Computation of Non-Equilibrium, Chemically-Reacting Flows", *Computers and Structures*, Vol. 30, No. 1/2, 1988.

30. Shuen, J.-S., Liou, M.-S. and Van Leer, B., "Inviscid Flux Splitting Algorithms for Real Gases with Nonequilibrium Chemistry", submitted to *Journal of Computational Physics*, 1988.

31. Liu, Y. and Vinokur, M., "Nonequilibrium Flow Computations: I. An Analysis of Numerical Formulations of Conservation Laws", NASA CR 177489, 1988.

32. Grossman, B. and Cinnella, P., "Upwind Methods for Flows with Non-Equilibrium Chemistry and Thermodynamics", *Third International Conference on Numerical Combustion*, Antibes, 1989.

33. Grossman, B., Cinnella, P. and Garrett, J., "A Survey of Upwind Methods for Flows with Equilibrium and Non-Equilibrium Chemistry and Thermodynamics", AIAA Paper No. 89-1653, 1989.

34. Abgrall, R., "Preliminary results on an extension of Roe's approximate Riemann solver to equilibrium and nonequilibrium flows", *Third International*

Conference on Numerical Combustion, Antibes, 1989 (submitted to *Computers and Fluids*).

35. Wada, Y., Kubota, H., Ogawa, S. and Ishiguro, T., "A Generalized Roe's Approximate Riemann Solver for Chemically Reacting Flows", AIAA Paper No. 89-0202, 1989.
36. Appleton, J. P. and Bray, K. N. C., "The conservation equations for a non-equilibrium plasma", *Journal of Fluid Mechanics*, Vol. 20, No. 4, 1964.
37. Igra, O., "Supersonic Expansion on Non-Equilibrium Plasmas", *Progress in Aerospace Sciences*, Vol. 16, 1975.
38. Igra, O. and Barcessat, M., "Supersonic, nonequilibrium corner expansion flow of ionized argon", *The Physics of Fluids*, Vol. 20, No. 9, 1977.
39. Candler, G. and Park, C., "The Computation of Radiation from Nonequilibrium Hypersonic Flows", AIAA Paper No. 88-2678, 1988.
40. Candler, G., "On the Computation of Shock Shapes in Nonequilibrium Hypersonic Flows", AIAA Paper No. 89-0312, 1989.
41. Blottner, F. G., Johnson, M. and Ellis, M., "Chemically Reacting Viscous Flow Program for Multi-Component Gas Mixtures", Sandia Laboratories, SC-RR-70-754, 1971.
42. Treanor, C. E. and Marrone, P. V., "Effect of Dissociation on the Rate of Vibrational Relaxation", *The Physics of Fluids*, Vol. 5, No. 9, 1962.
43. Marrone, P. V. and Treanor, C. E., "Chemical Relaxation with Preferential Dissociation from Excited Vibrational Levels", *The Physics of Fluids*, Vol. 6, No. 9, 1963.
44. Candler, G., "Translation-Vibration-Dissociation Coupling in Nonequilibrium Hypersonic Flows", AIAA Paper No. 89-1739, 1989.
45. Park, C. and Yoon, S., "A Fully-Coupled Implicit Method for Thermo-Chemical Nonequilibrium Air at Sub-Orbital Flight Speeds", AIAA Paper No. 89-1974, 1989.

46. Brun, R., Colas, P., Gubernatis, P. and Zeitoun, D., "Practical Phisico-Chemical Models for High Speed Air Flow-Field Computations", (to appear *Journal of Thermophysics*).

47. Carlson L. A. and Gally, T. A., "The effect of Electron Temperature and Impact Ionization on Martian Return AOTV Flowfields", AIAA Paper No. 89-1729, 1989.

48. Jaffe, R. L., "The Calculations of High Temperature Equilibrium and Nonequilibrium Specific Heat Data for N_2, O_2 and NO", AIAA Paper No. 87-1633, 1987.

49. Liu, Y. and Vinokur, M., "Equilibrium Gas Flow Computations. I. Accurate and Efficient Calculations of Equilibrium Gas Properties", AIAA Paper No. 89-1736, 1989.

50. Herzberg, G., *Molecular Spectra and Molecular Structure. I. Spectra of Diatomic Molecules*, ISBN 0-442-03385-0, D. van Nostrand Inc., 1950.

51. Srinivasan, S., Tannehill, J. C. and Weilmuenster, K. J., "Simplified Curve Fits for the Thermodynamic Properties of Equilibrium Air", NASA RP 1181, 1987.

52. Anderson, J. D. Jr., *Hypersonic and High Temperature Gas Dynamics*, ISBN 0-07-001671-2, McGraw-Hill, 1989.

53. Kauzmann, W., "Kinetic Theory of Gases", Library of Congress CCN 66-19995, W. A. Benjamin Inc., 1966.

54. Clarke, J. F. and McChesney, M., *The Dynamics of Real Gases*, Butterworth & Co. Ltd., 1964 (second edition under the title *The Dynamics of Relaxing Gases*, 1975).

55. Hill, T. L., *An Introduction to Statistical Thermodynamics*, Library of Congress CCN 60-9745, Addison-Wesley Publishing Company Inc., 1960.

56. Strehlow, R. A., *Combustion Fundamentals*, ISBN 0-07-06221-3, McGraw-Hill Inc., 1984.

57. McBride, B. J., Heimel, S., Ehlers, J. G. and Gordon, S., "Thermodynamic Properties to 6000 K for 210 Substances Involving the First 18 Elements", NASA SP-3001, 1963.

58. Bird, R. B., Stewart, W. E. and Lightfoot, E. N., *Transport Phenomena*, Library of Congress CCN 60-11717, John Wiley & Sons, 1960.

59. Walters, R. W., Cinnella, P., Slack, D. C. and Halt, D., "Characteristic Based Algorithms for Flows in Thermo-Chemical Nonequilibrium", AIAA Paper No. 90-0393, 1990.

60. Anderson, D. A., Tannehill, J. C. and Pletcher, R. H., *Computational Fluid Mechanics and Heat Transfer*, ISBN 0-89116-471-5, Hemisphere Publishing Corporation, 1984.

61. Pulliam, T. H. and Steger, J. L., "On Implicit Finite-Difference Simulations of Three Dimensional Flow", AIAA Paper No. 78-10, 1978.

62. Lapidus, A., "A Detached Shock Calculation by Second-Order Finite Differences", *Journal of Computational Physics*, Vol. 2, 1967.

63. Vinokur, M., "Conservation Equations of Gasdynamics in Curvilinear Coordinate Systems", *Journal of Computational Physics*, Vol. 14, 1974.

64. Viviand, H., "Formes Conservatives des Équations de la Dynamique des Gaz", *La Recherche Aérospatiale*, No. 1974-1, 1974.

65. Anderson, J. L., Preiser, S. and Rubin, E. L., "Conservation Form of the Equations of Hydrodynamics in Curvilinear Coordinate Systems", *Journal of Computational Physics*, Vol. 2, 1968.

66. Anderson, J. D. Jr., *Modern Compressible Flow With Hystorical Perspective*, ISBN 0-07-001654-2, McGraw-Hill, 1982.

67. Lax, P. D., "Weak Solutions of Nonlinear Hyperbolic Equations and their Numerical Computation", *Communications in Pure and Applied Mathematics*, Vol. 7, 1954.

68. Bauer, S. H., "Chemical Kinetics: A General Introduction", *Progress in Astronautics and Rocketry*, Vol. 7, 1962.

69. Davy, W. C., Lombard, C. K. and Green, M. J., "Forebody and Base Region Real-Gas Flow in Severe Planetary Entry by a Factored Implicit Numerical Method - Part II: Equilibrium Reactive Gas", AIAA Paper No. 81-0282, 1981.

70. Rogers, R. C. and Schexnayder, C. R. Jr., "Chemical Kinetic Analysis of Hydrogen-Air Ignition and Reaction Times", NASA TP 1856, 1981.

71. Carpenter, M., "A Generalized Chemistry Version of SPARK", NASA CR 4196, 1988.

72. Kang, S.-W. and Dunn, M. G., "Theoretical and Measured Electron-Density Distributions for the RAM Vehicle at High Altitudes", AIAA Paper No. 72-689, 1972.

73. Park, C., "On Convergence of Computation of Chemically Reacting Flows", AIAA Paper No. 85-0247, 1985.

74. Park, C., "A Review of Reaction Rates in High Temperature Air", AIAA Paper No. 89-1740, 1989.

75. Rogers, R. C. and Chinitz, W., "Using a Global Hydrogen-Air Combustion Model in Turbulent Reacting Flow Calculations", *AIAA Journal*, Vol. 21, No. 4, 1983.

76. Glass, I. I. and Takano, A., "Nonequilibrium Expansion Flows of Dissociated Oxygen and Ionized Argon Around a Corner", *Progress in Aerospace Sciences*, Vol. 6, 1965.

77. Lumpkin, F. E. III, Chapman, D. R. and Park, C., "A New Rotational Relaxation Model For Use In Hypersonic Computational Fluid Mechanics", AIAA Paper No. 89-1737, 1989.

78. Gnoffo, P. A., "A Code Calibration Program in Support of the Aeroassist Flight Experiment", AIAA Paper No. 89-1673, 1989.

79. Sagnier, P. and Marraffa, L., "Parametric Study of Thermal and Chemical Nonequilibrium Nozzle Flow", AIAA Paper No. 89-1856, 1989.

80. Sharma, S. P. and Schwenke, D. W., "The Rate Parameters for Coupled Rotation-Vibration-Dissociation Phenomenon in H_2", AIAA Paper No. 89-1738, 1989.

81. Millikan, R. C. and White, D. R., "Systematics of Vibrational Relaxation", *The Journal of Chemical Physics*, Vol. 39, No. 12, 1963.

82. Herzberg, G., *The Spectra and Structures of Simple Free Radicals*, ISBN 0-8014-0584-x, Cornell University Press, 1971.

83. Baysal, O., Engelund, W. C. and Tatum, K. E., "Navier-Stokes Calculations of Scramjet-Afterbody Flowfields", *Symposium on Advances and Applications in Computational Fluid Dynamics*, Chicago, 1988.

84. Baldwin, B. S. and Lomax, H., "Thin Layer Approximation and Algebraic Model for Separated Turbulent Flows", AIAA Paper No. 78-257, 1978.

85. Degani, D. and Schiff, L. B., "Computation of Supersonic Viscous Flows Around Pointed Bodies at Large Incidence", AIAA Paper No. 83-0034, 1983.

86. Curtiss, C. F. and Hirschfelder, J. O., "Transport Properties of Multicomponent Gas Mixtures", *The Journal of Chemical Physics*, Vol. 17, No. 6, 1949.

87. Wilke, C. R., "A Viscosity Equation for Gas Mixtures", *The Journal of Chemical Physics*, Vol. 18, No. 4, 1950.

88. Schetz, J. A., *Foundations of Boundary Layer Theory for Momentum, Heat and Mass Transfer*, ISBN 0-13-329334-3, Prentice-Hall Inc., 1984.

89. Heimerl, J. M. and Coffee, T. P., "Results of a Study of Several Transport Algorithms for Premixed, Laminar Flame Propagation", in *Numerical Methods in Laminar Flame Propagation*, eds. N. Peters and J. Warnatz, ISBN 3-528-08080-9, Friedr. Vieweg & Sohn, 1982.

90. Wood, W. W. and Kirkwood, J. G., "Hydrodynamics of a Reacting and Relaxing Fluid", *Journal of Applied Physics*, Vol. 28, No. 4, 1957.

91. Roe, P. L. and Pike, J., "Efficient Construction and Utilisation of Approximate Riemann Solutions", in *Computing Methods in Applied Sciences and Engineering VI*, eds. R. Glowinski and J.-L. Lions, ISBN 0-444-87597-2, Elsevier Science Publishing Co., 1984.

92. Walters, R. W. and Thomas, J. L., "Advances in Upwind Relaxation Methods", in *State-of-the-Art Surveys on Computational Mechanics*, ed. A. K. Noor, ISBN 0-7918-0303-1, ASME Publication, 1988.

93. Drummond, J. P., Hussaini, M. J. and Zang, T. A., "Spectral Methods for Modeling Supersonic Chemically Reacting Flowfields", *AIAA Journal*, Vol. 24, No. 9, 1986.

94. Eklund, D. R., Drummond, J. P. and Hassan, H. A., "The Efficient Calculation of Chemically Reacting Flow", AIAA Paper No. 86-0563, 1986.

95. Aftosmis, M. J. and Baron, J. R., "Adaptive Grid Embedding in Nonequilibrium Hypersonic Flow", AIAA Paper No. 89-1652, 1989.

96. Roe, P. L., "Discrete Models for the Numerical Analysis of Time Dependent Multidimensional Gas Dynamics", *Journal of Computational Physics*, Vol. 63, 1986.

97. Hirsch, C. and Lacor, C., "Upwind Algorithms Based on a Diagonalization of the Multidimensional Euler Equations", AIAA Paper No. 89-1958, 1989.

98. Chakravarthy, S. R., Szema, K.-Y., Goldberg, U. C., Gorski, J. J. and Osher, S., "Application of a New Class of High Accuracy TVD Schemes to the Navier-Stokes Equations", AIAA Paper No. 85-0165, 1985.

99. Sweby, P. K., "High Resolution Schemes Using Flux Limiters for Hyperbolic Conservation Laws", *SIAM Journal of Numerical Analysis*, Vol. 21, No. 5, 1984.

100. Greenspan, D. and Jain, P. C., "On Non-Negative Difference Analogues of Elliptic Differential Equations", *Journal of The Franklin Institute*, Vol. 279, No. 5, 1965.

101. Van Leer, B., Thomas, J. L., Roe, P. L. and Newsome, R. W., "A Comparison of Numerical Flux Formulas for the Euler and Navier-Stokes Equations", AIAA Paper No. 87-1104-CP, 1987.

102. Anderson, W. K., Thomas, J. L. and Van Leer, B., "Comparison of Finite Volume Flux Vector Splittings for the Euler Equations", *AIAA Journal*, Vol. 24, No. 9, 1986.

103. Oran, E. S. and Boris, J. P., *Numerical Simulation of Reactive Flow*, ISBN 0-444-01251-6, Elsevier Science Publishing Co., 1987.

104. Kee, R. J. and Dwyer, H. A., "Review of Stiffness and Implicit Finite-Difference Methods in Combustion Modeling", *Progress in Astronautics and Aeronautics*, Vol. 76, 1979.

105. Bussing, T. R. A. and Murman, E. M., "A Finite-Volume Method for the Calculation of Compressible Chemically Reacting Flows", AIAA Paper No. 85-0331, 1985.

106. Yee, H. C. and Shinn, J. L., "Semi-Implicit and Fully Implicit Shock Capturing Methods for Hyperbolic Conservation Laws with Stiff Source Terms", NASA TM 89415, 1986.

107. Iannelli, G. S. and Baker, A. J., "A Stiffly-Stable Implicit Runge-Kutta Algorithm for CFD Applications", AIAA Paper No. 88-0416, 1988.

108. Thomas, J. L. and Walters, R. W., "Upwind Relaxation Algorithms for the Navier-Stokes Equations", *AIAA Journal*, Vol. 25, No. 4, 1987.

109. Newsome, R. W., Walters, R. W. and Thomas, J. L., "An Efficient Iteration Strategy for Upwind/Relaxation Solutions to the Thin-Layer Navier-Stokes Equations", AIAA Paper No. 87-1113-CP, 1987.

110. Barth, T. J., "Analysis of Implicit Local Linearization Techniques for Upwind and TVD Algorithms", AIAA Paper No. 87-0595, 1987.

111. Liou, M.-S. and Van Leer, B., "Choice of Implicit and Explicit Operators for the Upwind Difference Method", NASA TM 100857, 1988.

FIGURES

Table 6.1

Equilibrium Air

$\rho = 0.038558\ kg/m^3, \qquad \tilde{c}_{v_e} \equiv 0$

Temperature	Mass fraction e^-	χ_e
4000 K	$1.88\ \ 10^{-11}$	$-1.82\ \ 10^{-11}$
9000 K	$1.26\ \ 10^{-7}$	$-4.81\ \ 10^{-9}$
15000 K	$5.13\ \ 10^{-6}$	$-3.20\ \ 10^{-9}$
20000 K	$1.76\ \ 10^{-5}$	$-2.10\ \ 10^{-9}$

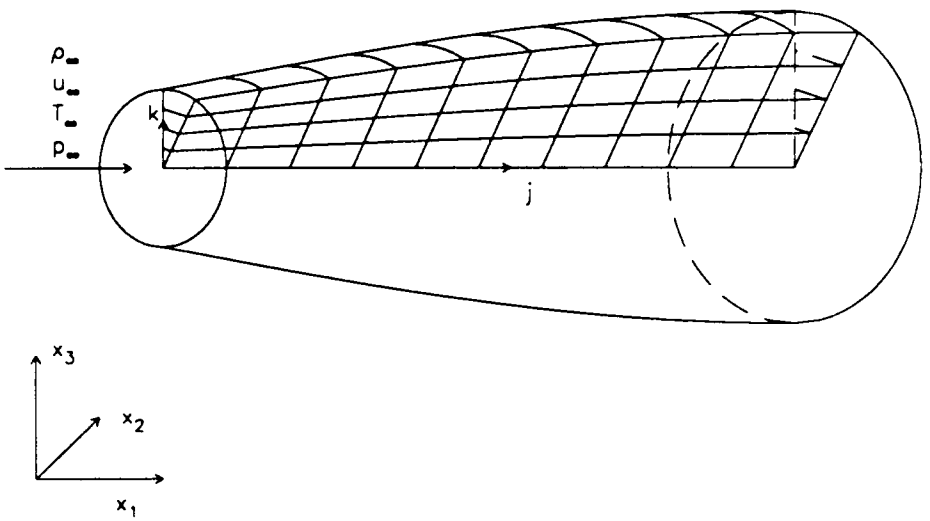

Fig. 1 Geometry of the axisymmetric, rapid-expansion diffuser used in the present calculations. A qualitative representation of the mesh is also visible.

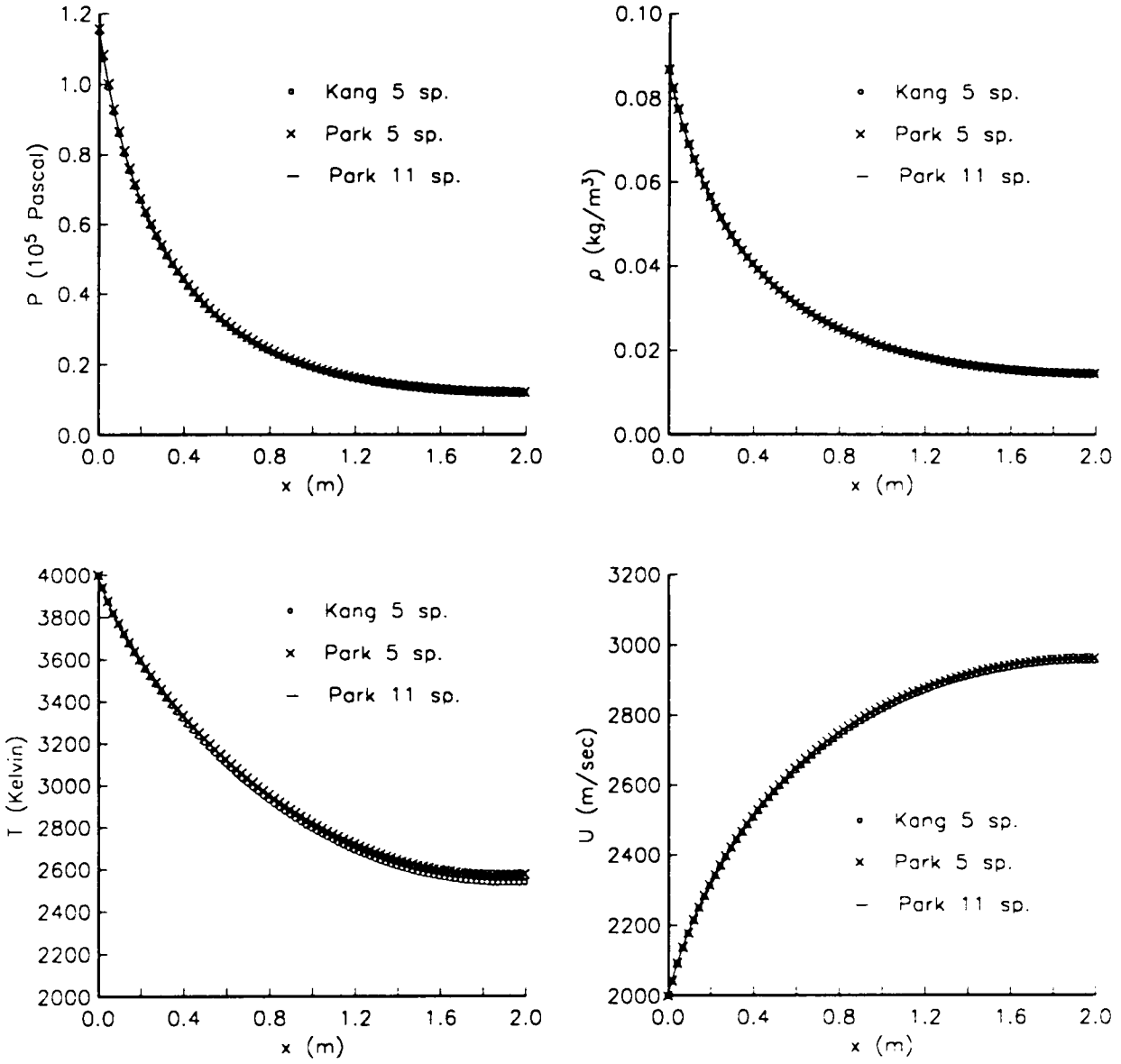

Fig. 2a Comparison of different air chemistry models using the Vibrational Equilibrium Model. Pressure, density, temperature, and velocity plots.

Inlet $T = 4000\ K, \quad \rho = 8.6756\ 10^{-2}\ kg/m^3, \quad U = 2000\ m/sec$

Kang 5 sp. Air Model 1

Park 5 sp. Air Model 2 reduced to five neutral species

Park 11 sp. Air Model 2

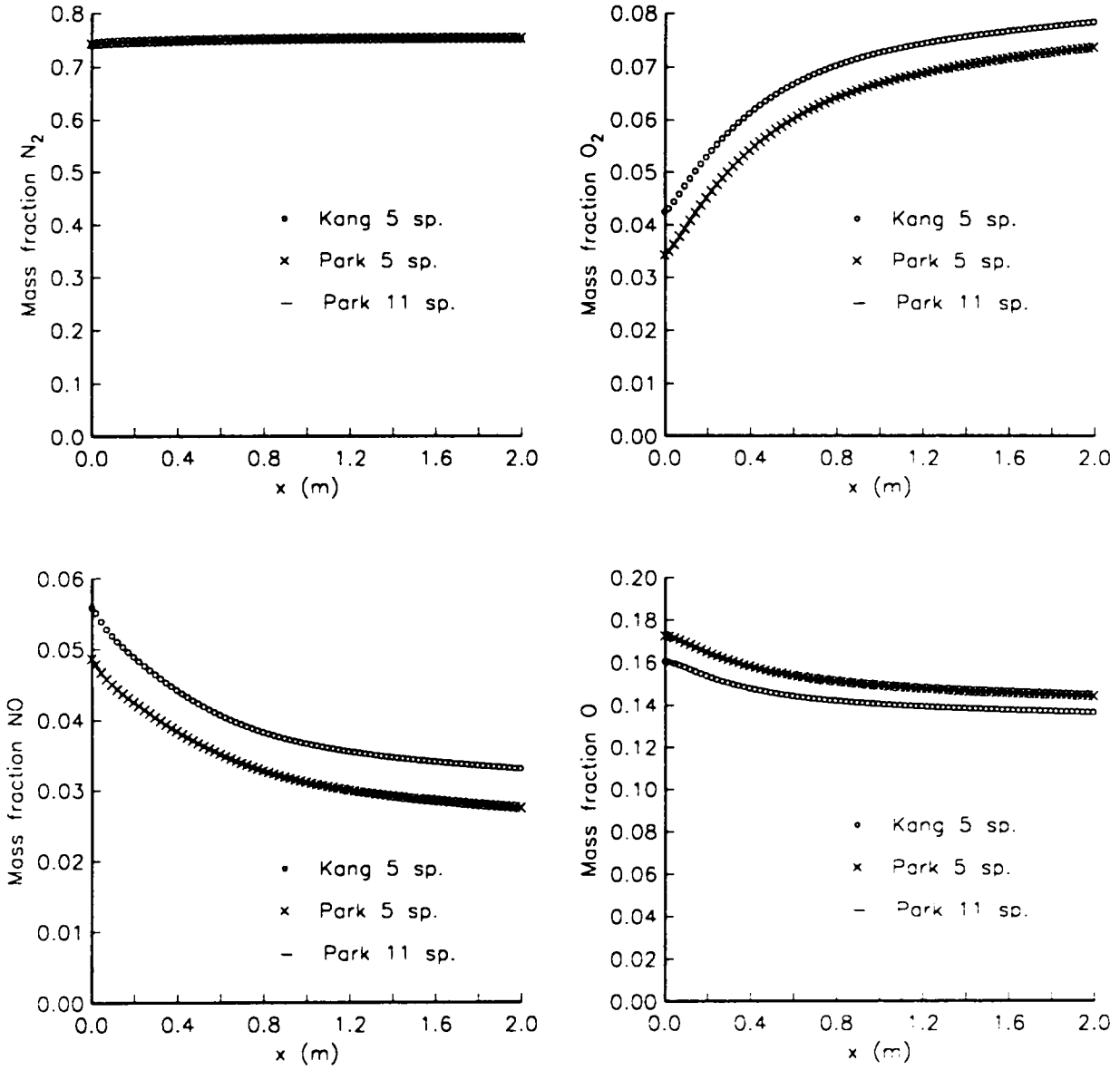

Fig. 2b Comparison of different air chemistry models using the Vibrational Equilibrium Model. Mass fraction plots of N_2, O_2, NO, O.

Inlet $T = 4000\ K$, $\rho = 8.6756\ 10^{-2}\ kg/m^3$, $U = 2000\ m/sec$

Kang 5 sp. Air Model 1

Park 5 sp. Air Model 2 reduced to five neutral species

Park 11 sp. Air Model 2

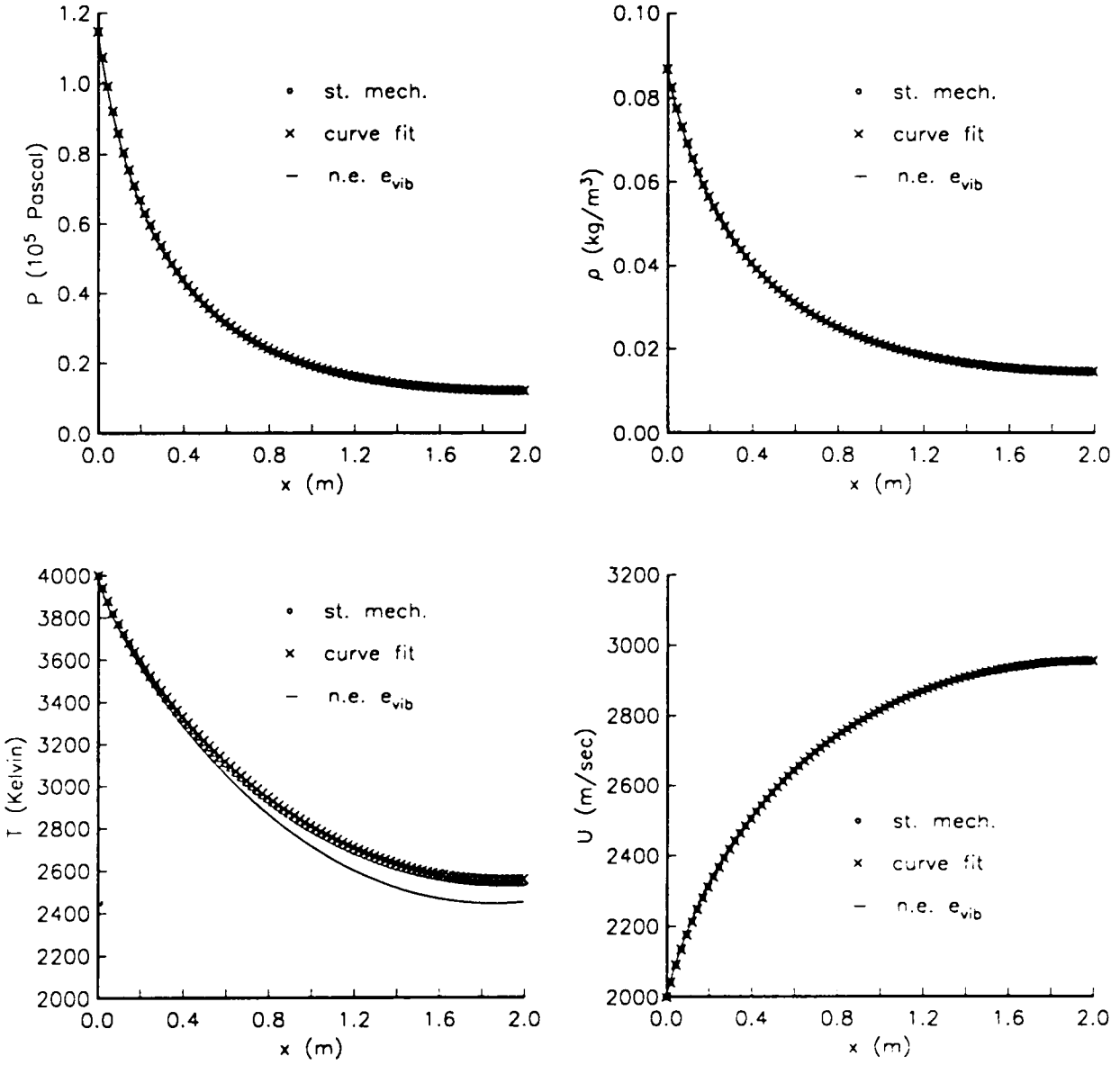

Fig. 3a Comparison of different thermodynamic models using Air Model 1. Pressure, density, temperature, and velocity plots.

Inlet $T = 4000\ K, \quad \rho = 8.6756\ 10^{-2}\ kg/m^3, \quad U = 2000\ m/sec$

st. mech. Vibrational Equilibrium Model

curve fit Curve Fit Model

n.e. e_{vib} Simplified Vibrational Non-Equilibrium Model

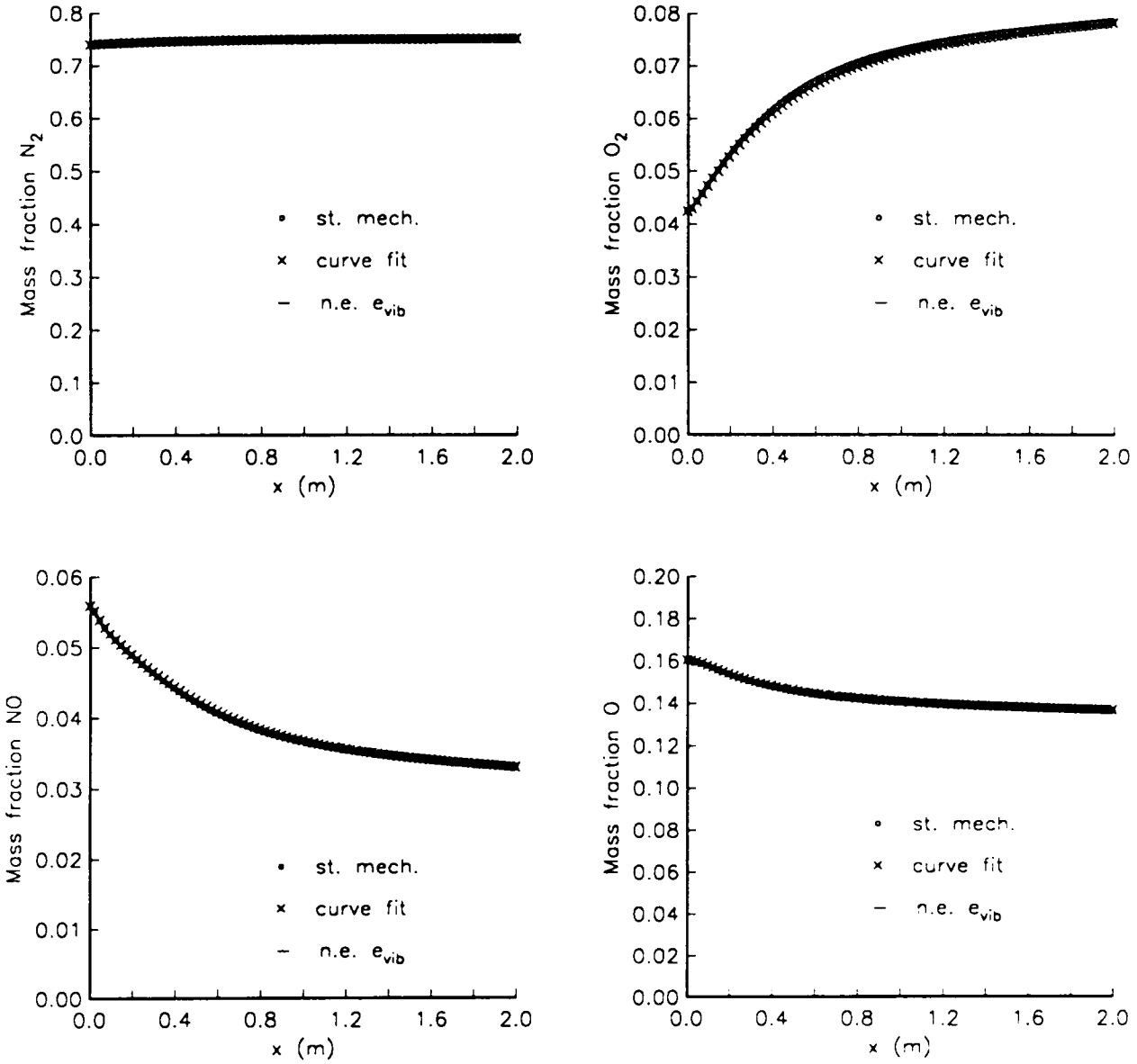

Fig. 3b Comparison of different thermodynamic models using Air Model 1. Mass fraction plots of N_2, O_2, NO, O.

Inlet $T = 4000\ K, \quad \rho = 8.6756\ 10^{-2}\ kg/m^3, \quad U = 2000\ m/sec$

st. mech. Vibrational Equilibrium Model

curve fit Curve Fit Model

n.e. e_{vib} Simplified Vibrational Non-Equilibrium Model

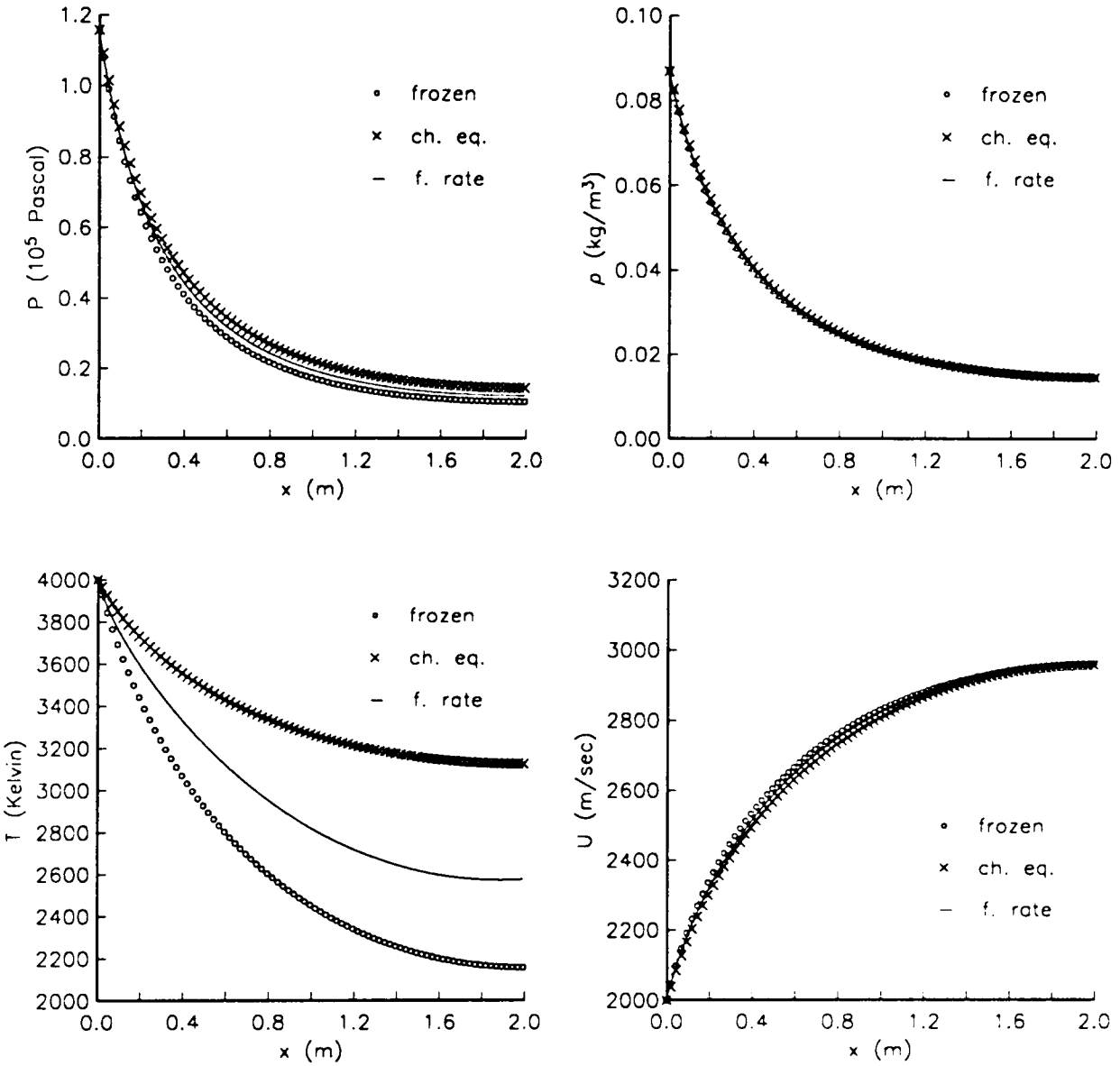

Fig. 4a Comparison of different air chemistry models using the Vibrational Equilibrium Model. Pressure, density, temperature, and velocity plots.

Inlet $T = 4000\ K, \quad \rho = 8.6756\ 10^{-2}\ kg/m^3, \quad U = 2000\ m/sec$

frozen Frozen chemistry

ch. eq. Chemical equilibrium

f. rate Air Model 2

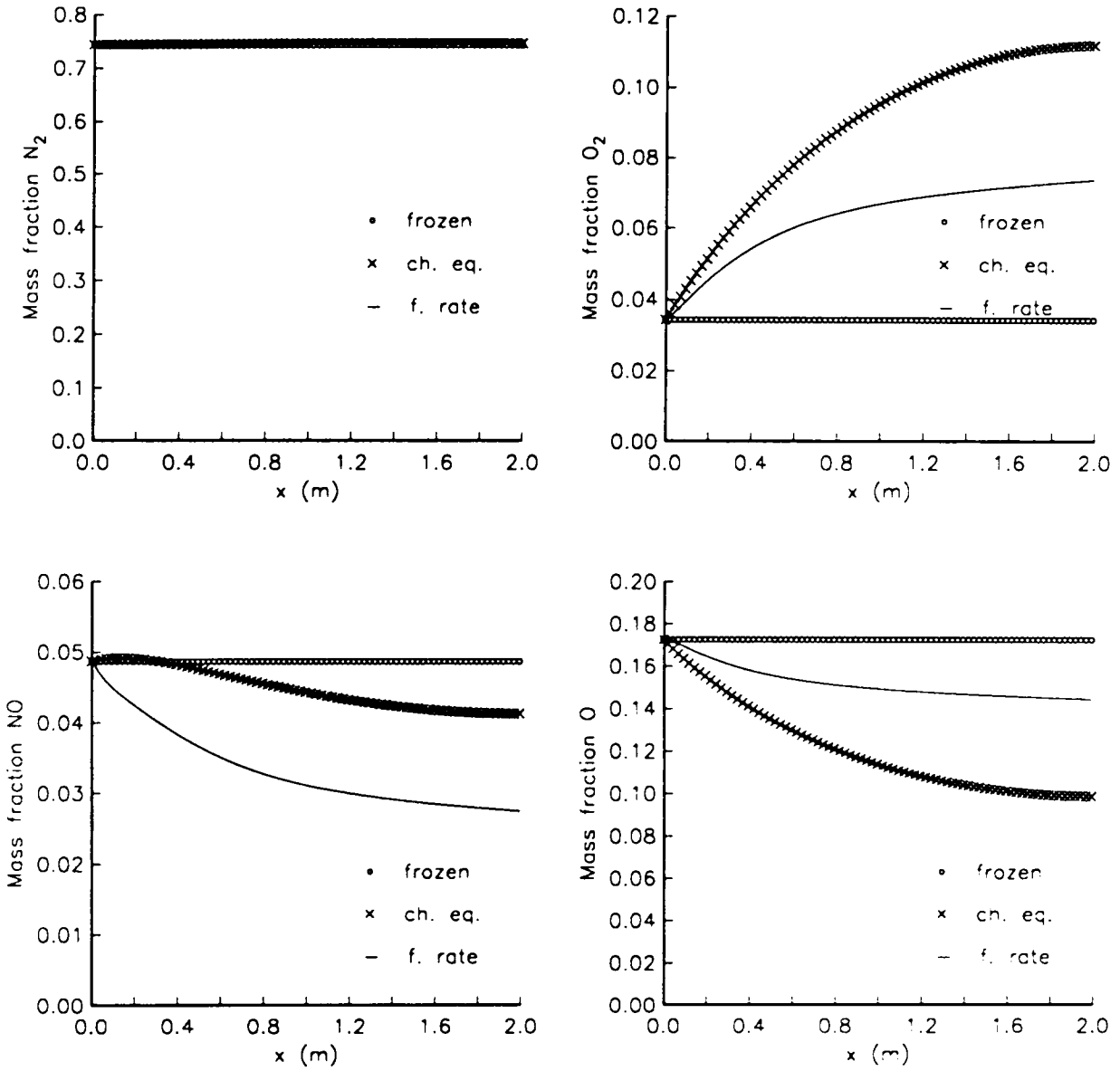

Fig. 4b Comparison of different air chemistry models using the Vibrational Equilibrium Model. Mass fraction plots of N_2, O_2, NO, O.

Inlet $T = 4000\ K$, $\rho = 8.6756\ 10^{-2}\ kg/m^3$, $U = 2000\ m/sec$

frozen Frozen chemistry

ch. eq. Chemical equilibrium

f. rate Air Model 2

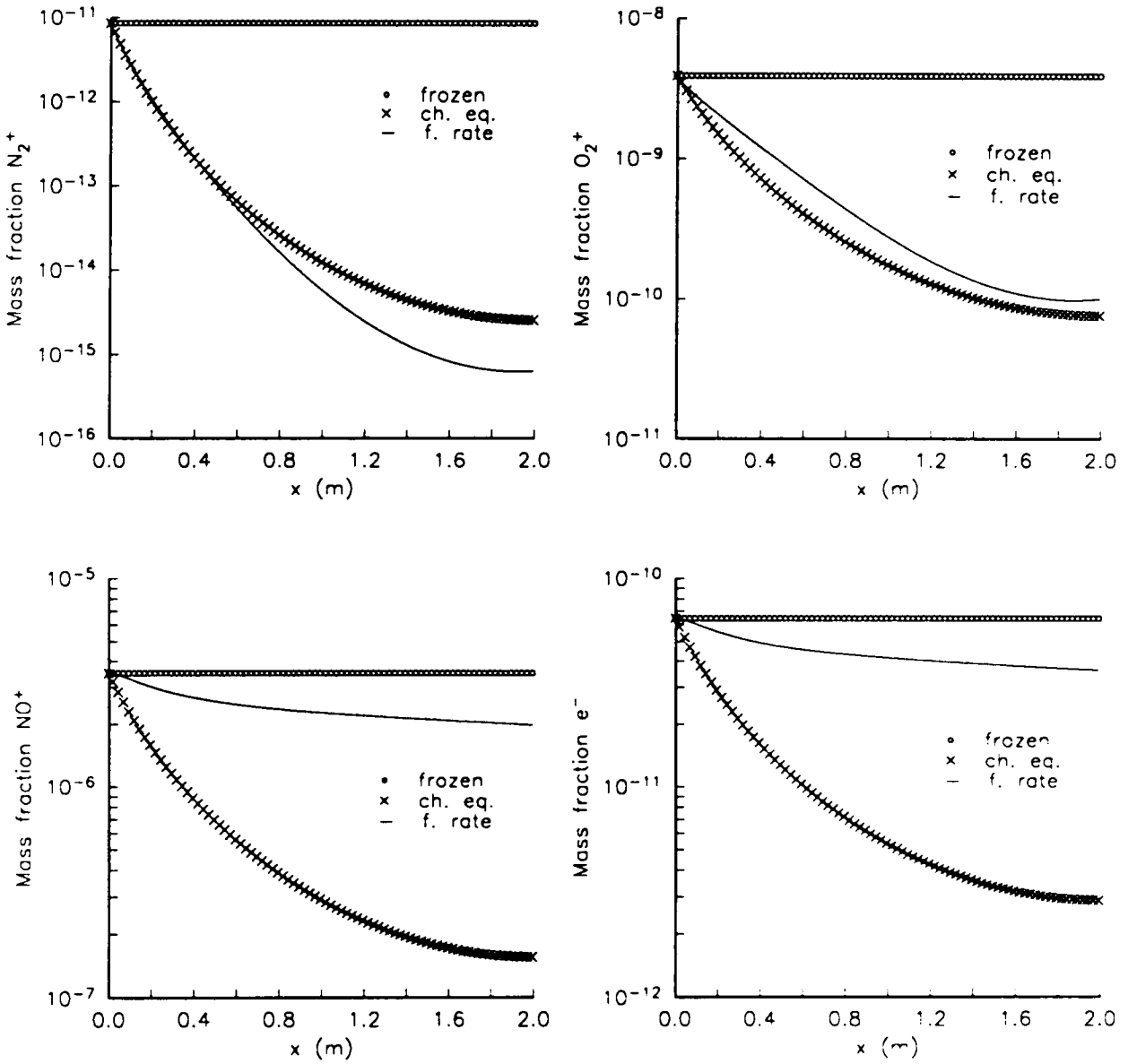

Fig. 4c Comparison of different air chemistry models using the Vibrational Equilibrium Model. Mass fraction plots of N_2^+, O_2^+, NO^+, e^- in logarithmic scales.

Inlet $T = 4000\ K$, $\rho = 8.6756\ 10^{-2}\ kg/m^3$, $U = 2000\ m/sec$

frozen Frozen chemistry

ch. eq. Chemical equilibrium

f. rate Air Model 2

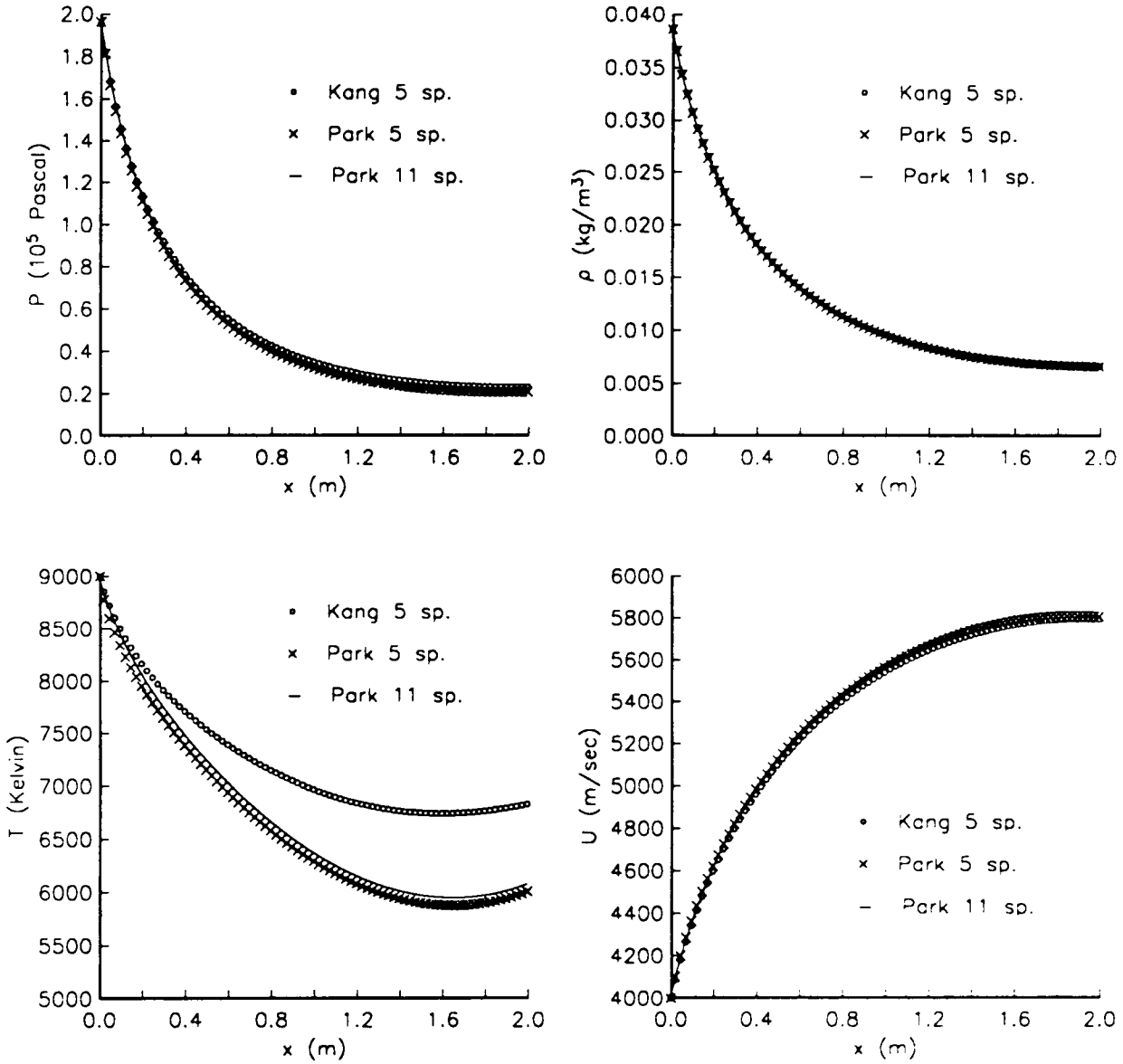

Fig. 5a Comparison of different air chemistry models using the Vibrational Equilibrium Model. Pressure, density, temperature, and velocity plots.

Inlet $T = 9000\ K, \quad \rho = 3.8558\ 10^{-2}\ kg/m^3, \quad U = 4000\ m/sec$

Kang 5 sp. Air Model 1

Park 5 sp. Air Model 2 reduced to five neutral species

Park 11 sp. Air Model 2

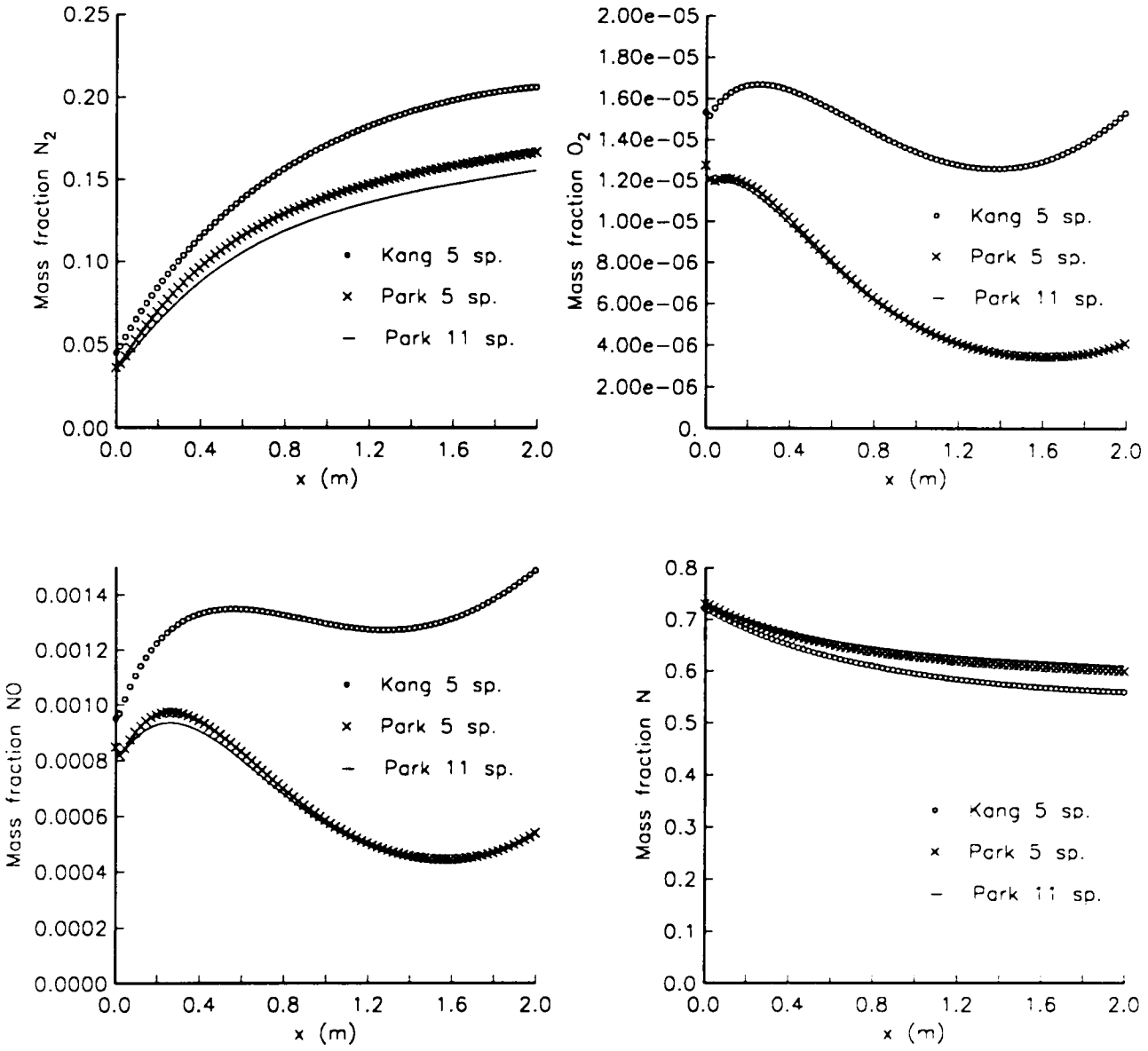

Fig. 5b Comparison of different air chemistry models using the Vibrational Equilibrium Model. Mass fraction plots of N_2, O_2, NO, N.

Inlet $T = 9000\ K$, $\rho = 3.8558\ 10^{-2}\ kg/m^3$, $U = 4000\ m/sec$

Kang 5 sp. Air Model 1

Park 5 sp. Air Model 2 reduced to five neutral species

Park 11 sp. Air Model 2

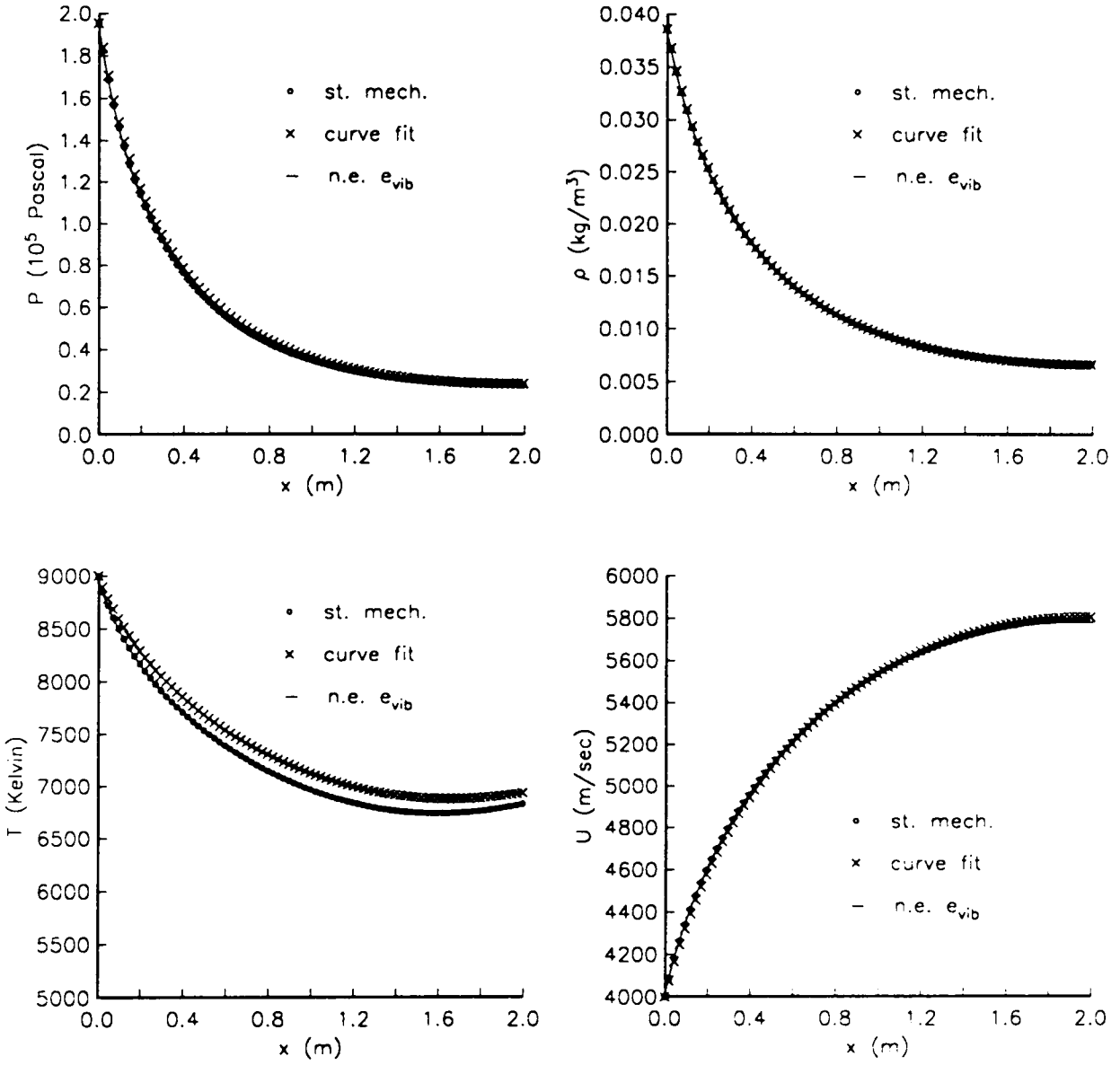

Fig. 6a Comparison of different thermodynamic models using Air Model 1. Pressure, density, temperature, and velocity plots.

Inlet $T = 9000\ K, \quad \rho = 3.8558\ 10^{-2}\ kg/m^3, \quad U = 4000\ m/sec$

st. mech. Vibrational Equilibrium Model

curve fit Curve Fit Model

n.e. e_{vib} Simplified Vibrational Non-Equilibrium Model

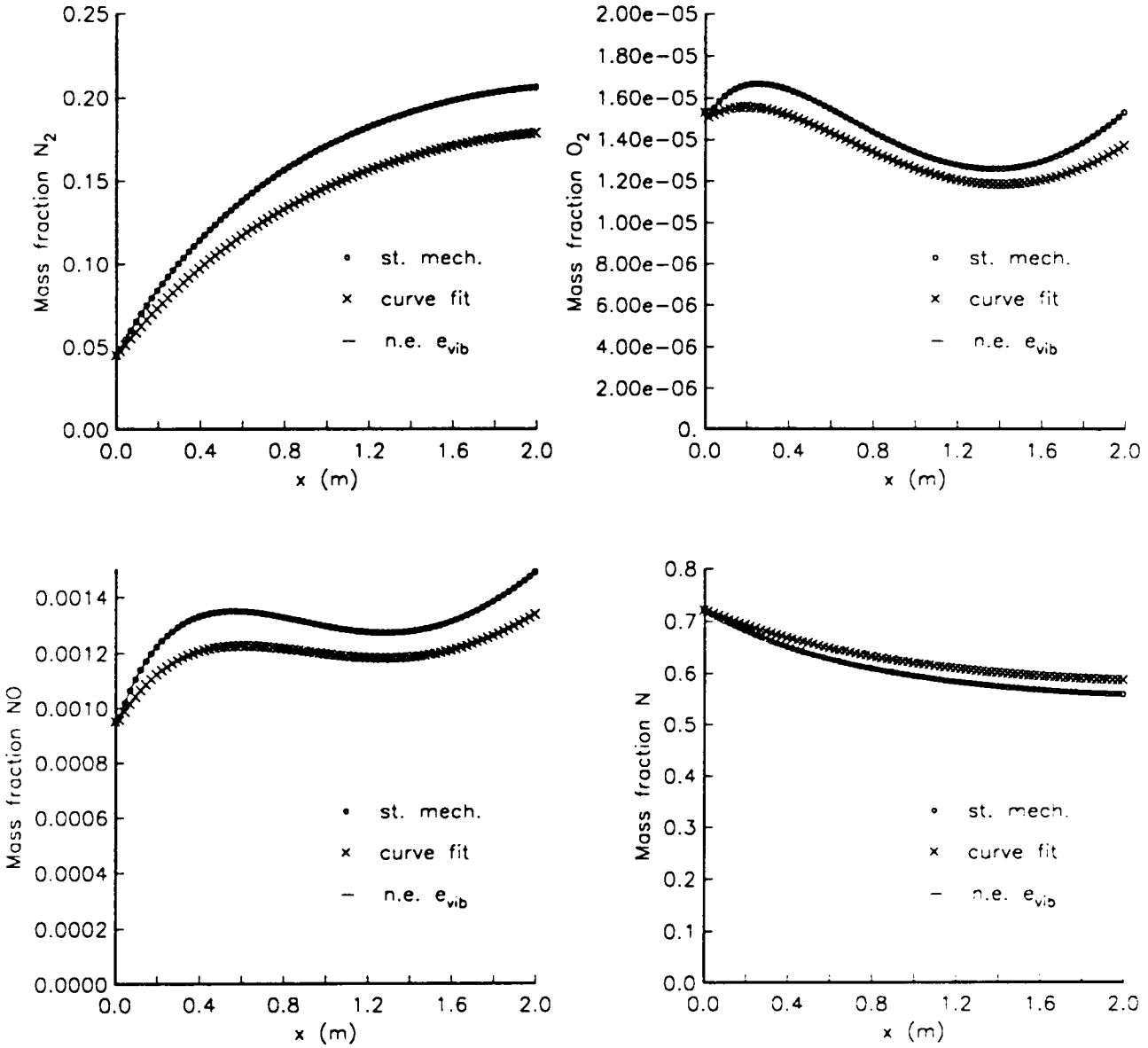

Fig. 6b Comparison of different thermodynamic models using Air Model 1. Mass fraction plots of N_2, O_2, NO, N.

Inlet $T = 9000\ K, \quad \rho = 3.8558\ 10^{-2}\ kg/m^3, \quad U = 4000\ m/sec$

st. mech. Vibrational Equilibrium Model

curve fit Curve Fit Model

n.e. e_{vib} Simplified Vibrational Non-Equilibrium Model

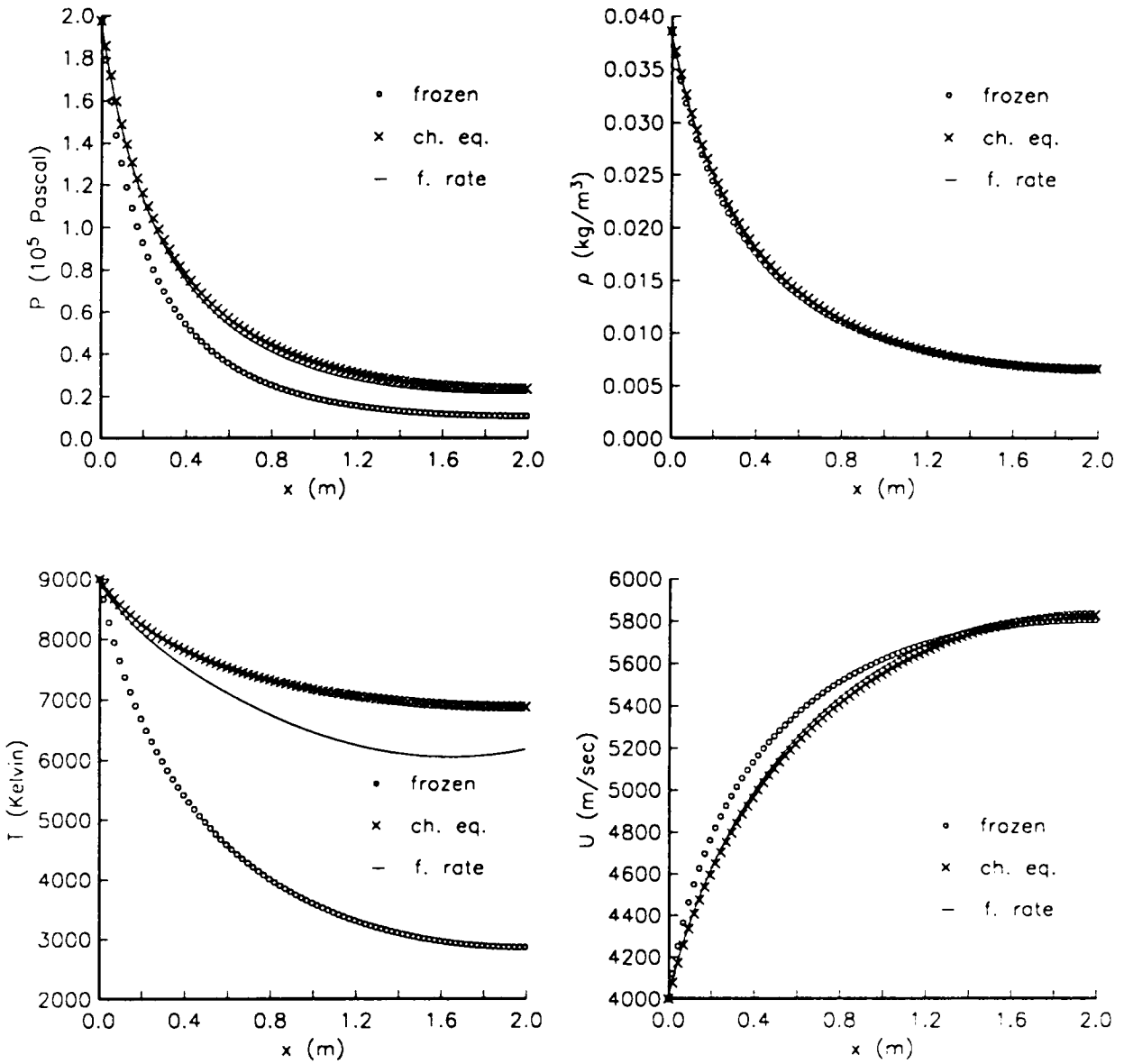

Fig. 7a Comparison of different air chemistry models using the Vibrational Equilibrium Model. Pressure, density, temperature, and velocity plots.

Inlet $T = 9000\ K, \quad \rho = 3.8558\ 10^{-2}\ kg/m^3, \quad U = 4000\ m/sec$

frozen Frozen chemistry

ch. eq. Chemical equilibrium

f. rate Air Model 2

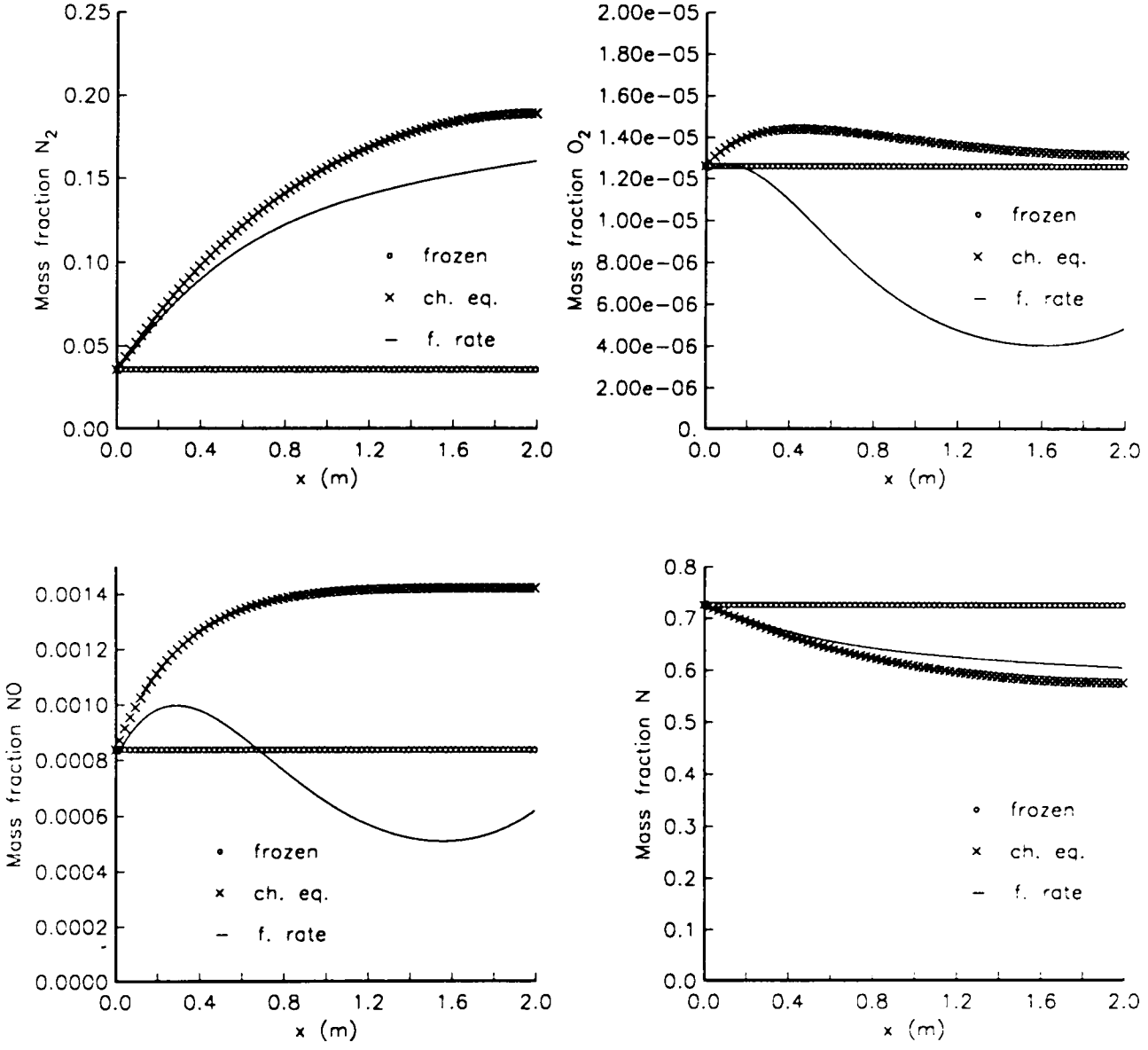

Fig. 7b Comparison of different air chemistry models using the Vibrational Equilibrium Model. Mass fraction plots of N_2, O_2, NO, N.

Inlet $T = 9000\ K$, $\rho = 3.8558\ 10^{-2}\ kg/m^3$, $U = 4000\ m/sec$

frozen Frozen chemistry

ch. eq. Chemical equilibrium

f. rate Air Model 2

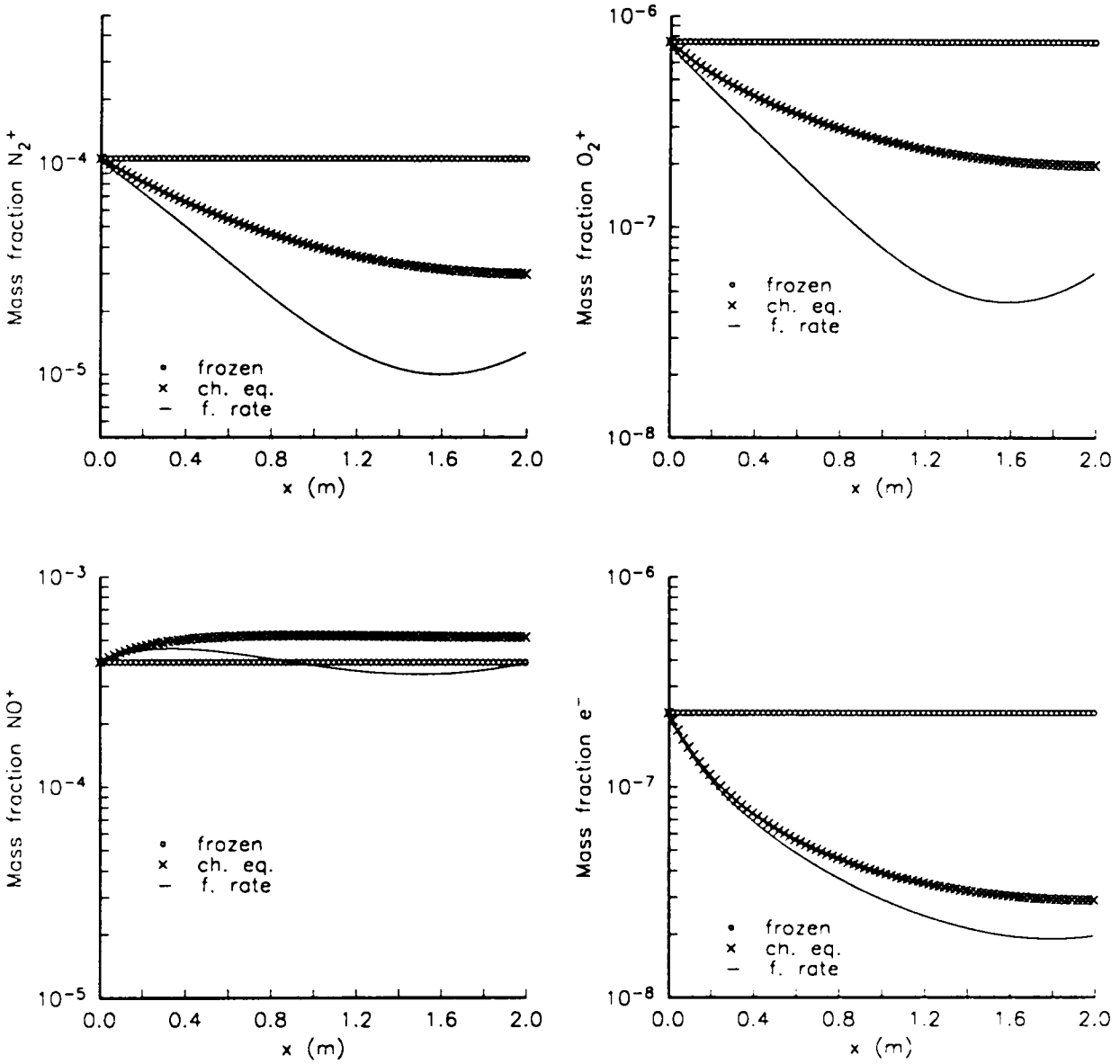

Fig. 7c Comparison of different air chemistry models using the Vibrational Equilibrium Model. Mass fraction plots of N_2^+, O_2^+, NO^+, e^- in logarithmic scales.

Inlet $T = 9000\ K$, $\rho = 3.8558\ 10^{-2}\ kg/m^3$, $U = 4000\ m/sec$

frozen Frozen chemistry

ch. eq. Chemical equilibrium

f. rate Air Model 2

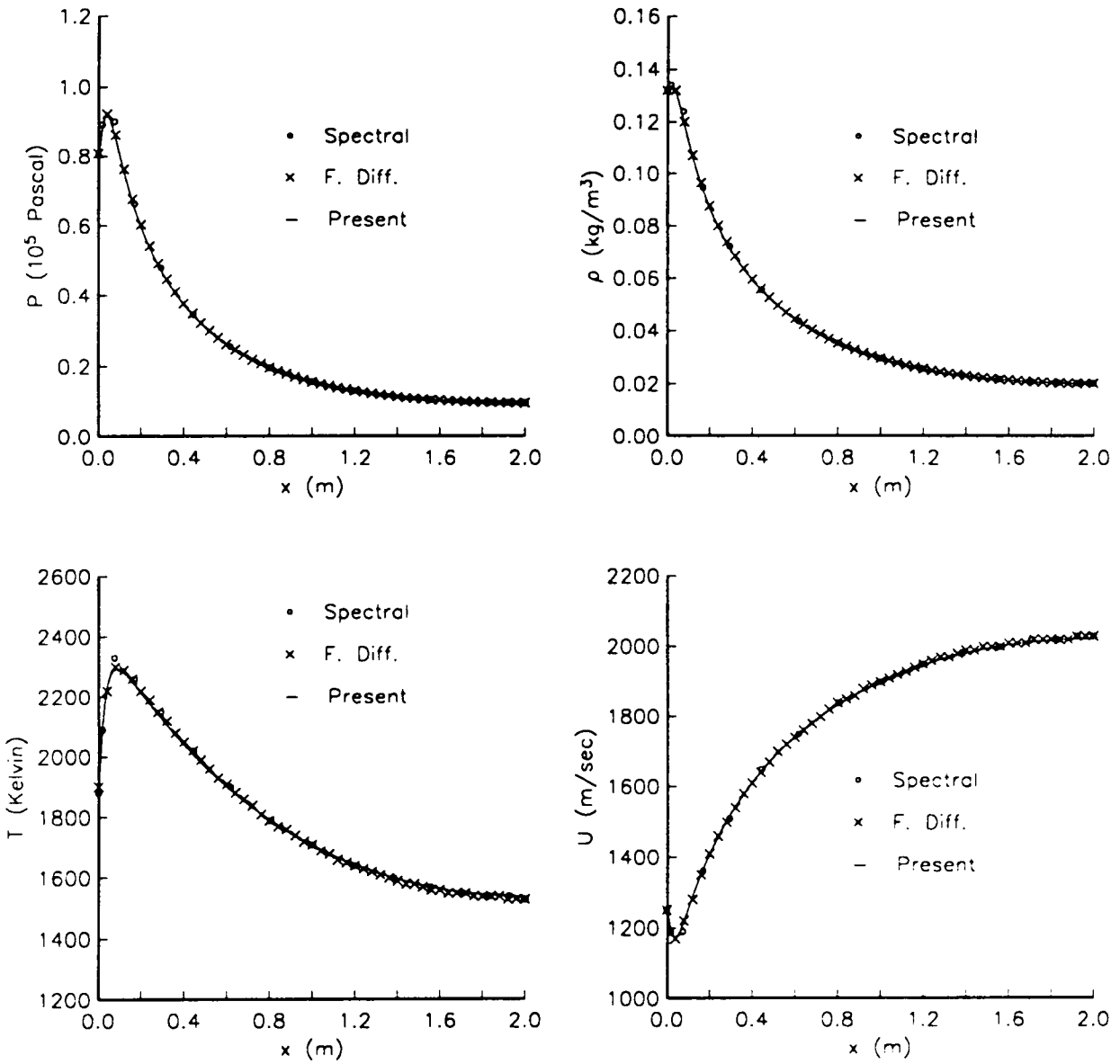

Fig. 8 Comparison of different H_2-air chemistry calculations using the Curve Fit Model. Pressure, density, temperature, and velocity plots.

Inlet $T = 1884.3\ K, \quad p = 8.0263\ 10^4\ N/m^2, \quad U = 1245\ m/sec$

Spectral Results from [93] with a spectral solver

F. Diff. Results from [93] with a finite difference solver

Present Present results with a finite volume solver

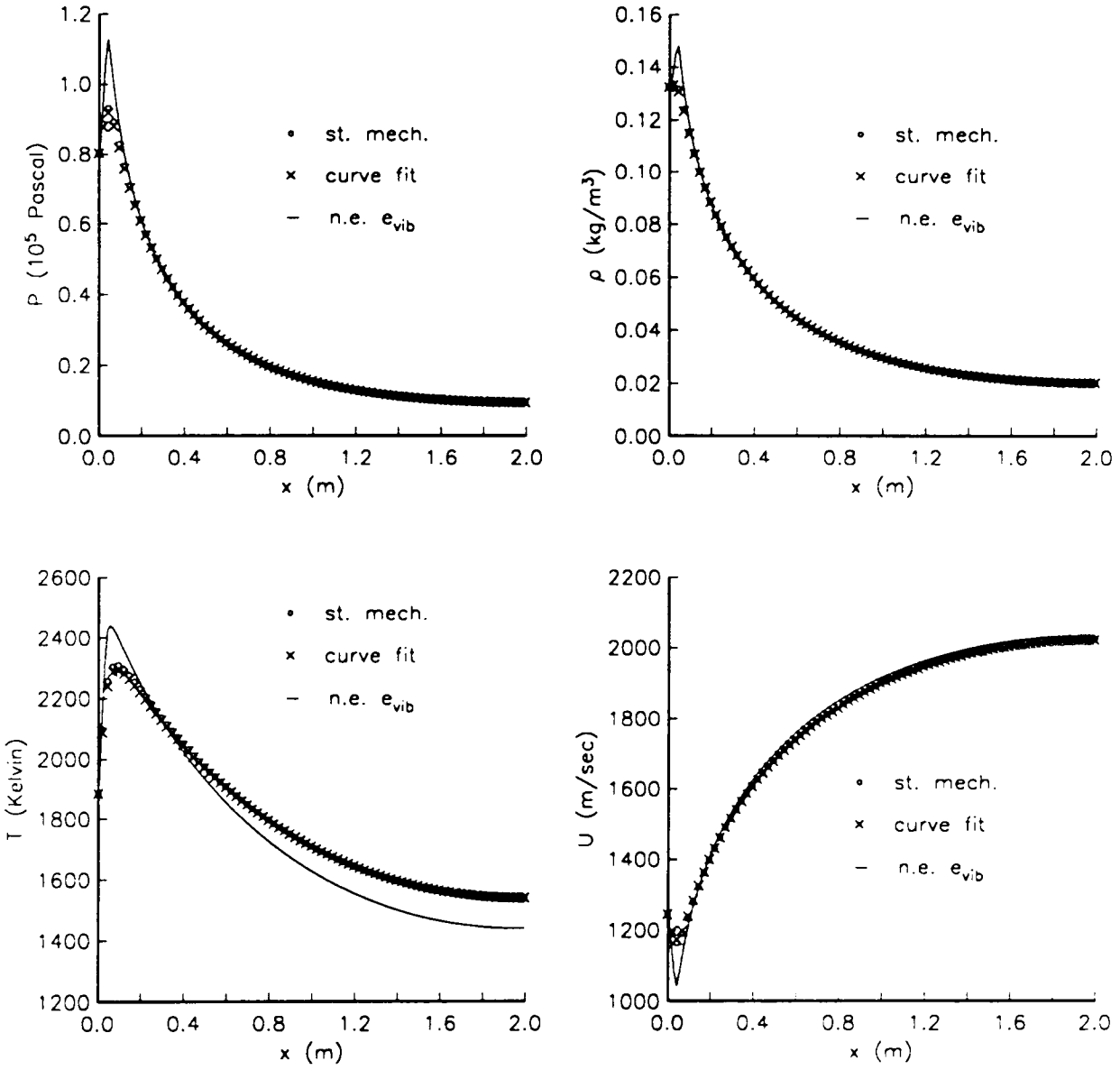

Fig. 9a Comparison of different thermodynamic models using Hydrogen-Air Model 1. Pressure, density, temperature, and velocity plots.

Inlet $T = 1884.3\ K, \quad p = 8.0263\ 10^4\ N/m^2, \quad U = 1245\ m/sec$

st. mech. Vibrational Equilibrium Model

curve fit Curve Fit Model

n.e. e_{vib} Simplified Vibrational Non-Equilibrium Model

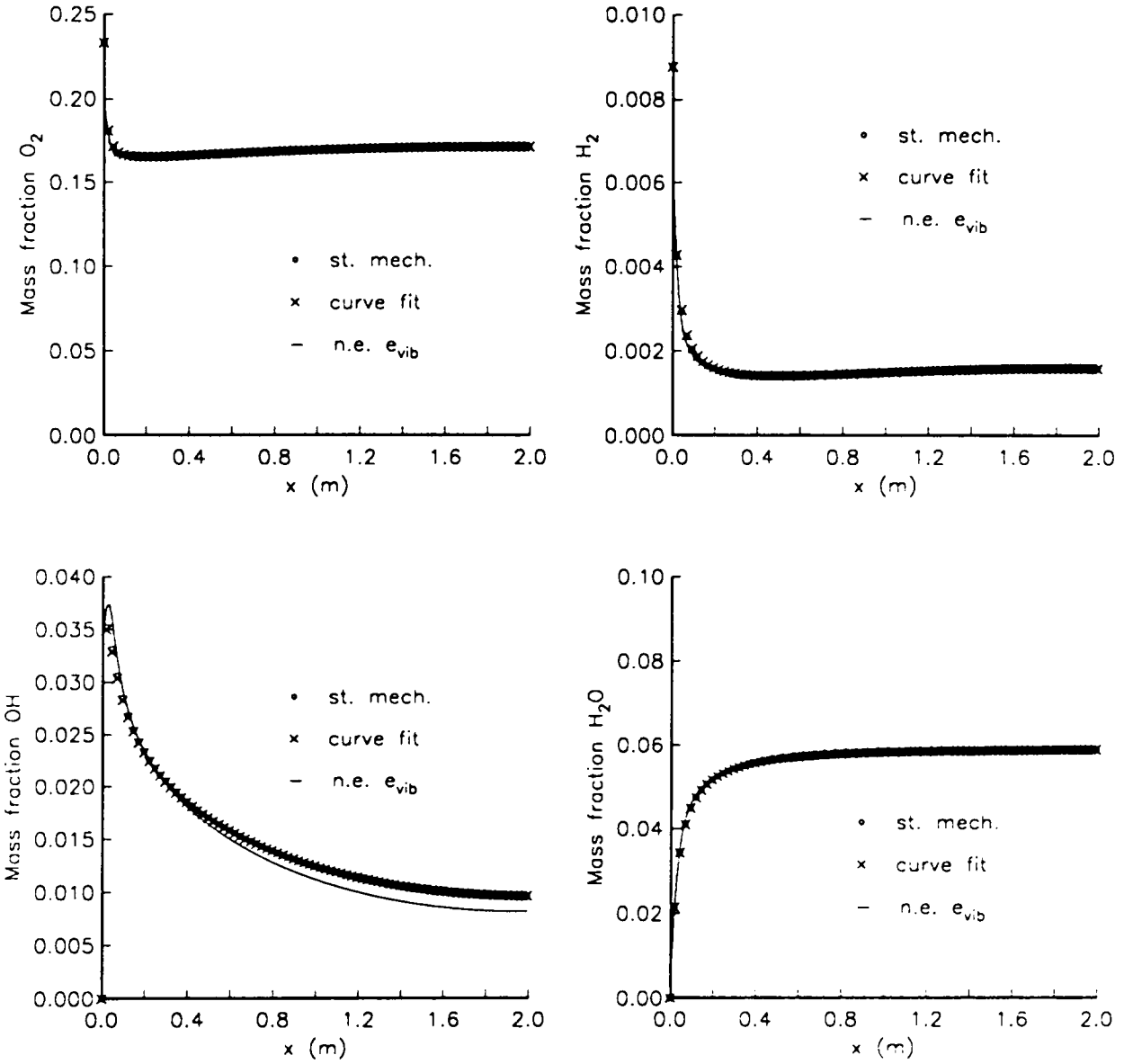

Fig. 9b Comparison of different thermodynamic models using Hydrogen-Air Model 1. Mass fraction plots of O_2, H_2, OH, H_2O.

Inlet $T = 1884.3\ K$, $p = 8.0263\ 10^4\ N/m^2$, $U = 1245\ m/sec$

st. mech. Vibrational Equilibrium Model

curve fit Curve Fit Model

n.e. e_{vib} Simplified Vibrational Non-Equilibrium Model

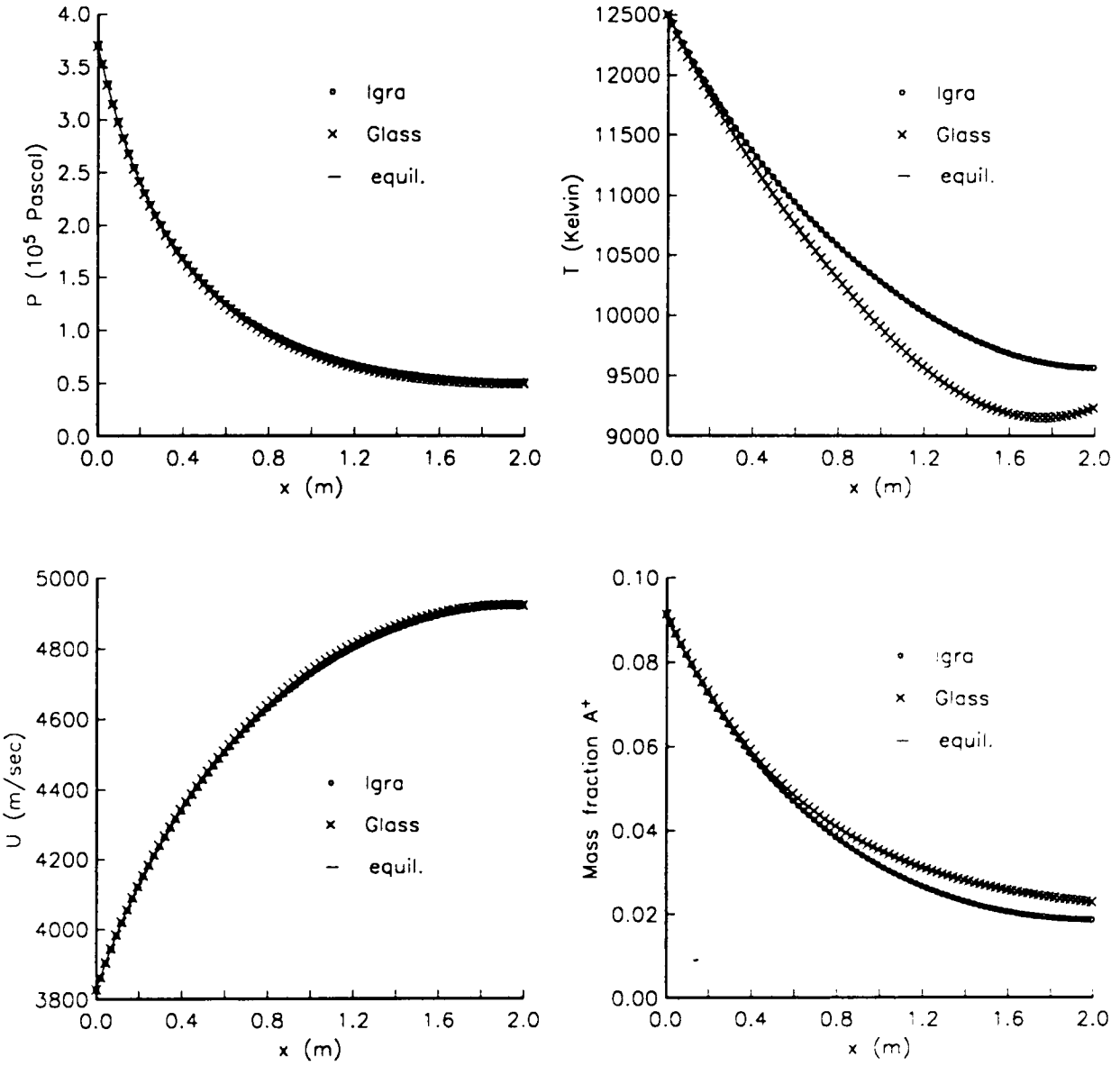

Fig. 10 Comparison of different chemistry models for an Argon plasma. Pressure, temperature, velocity, and mass fraction of A^+.

Inlet $T = 12500\ K, \quad \rho = 0.1303\ kg/m^3, \quad U = 3828\ m/sec$

Igra Argon Model 1, one translational temperature

Glass Argon Model 2

ch. eq. Chemical equilibrium calculation

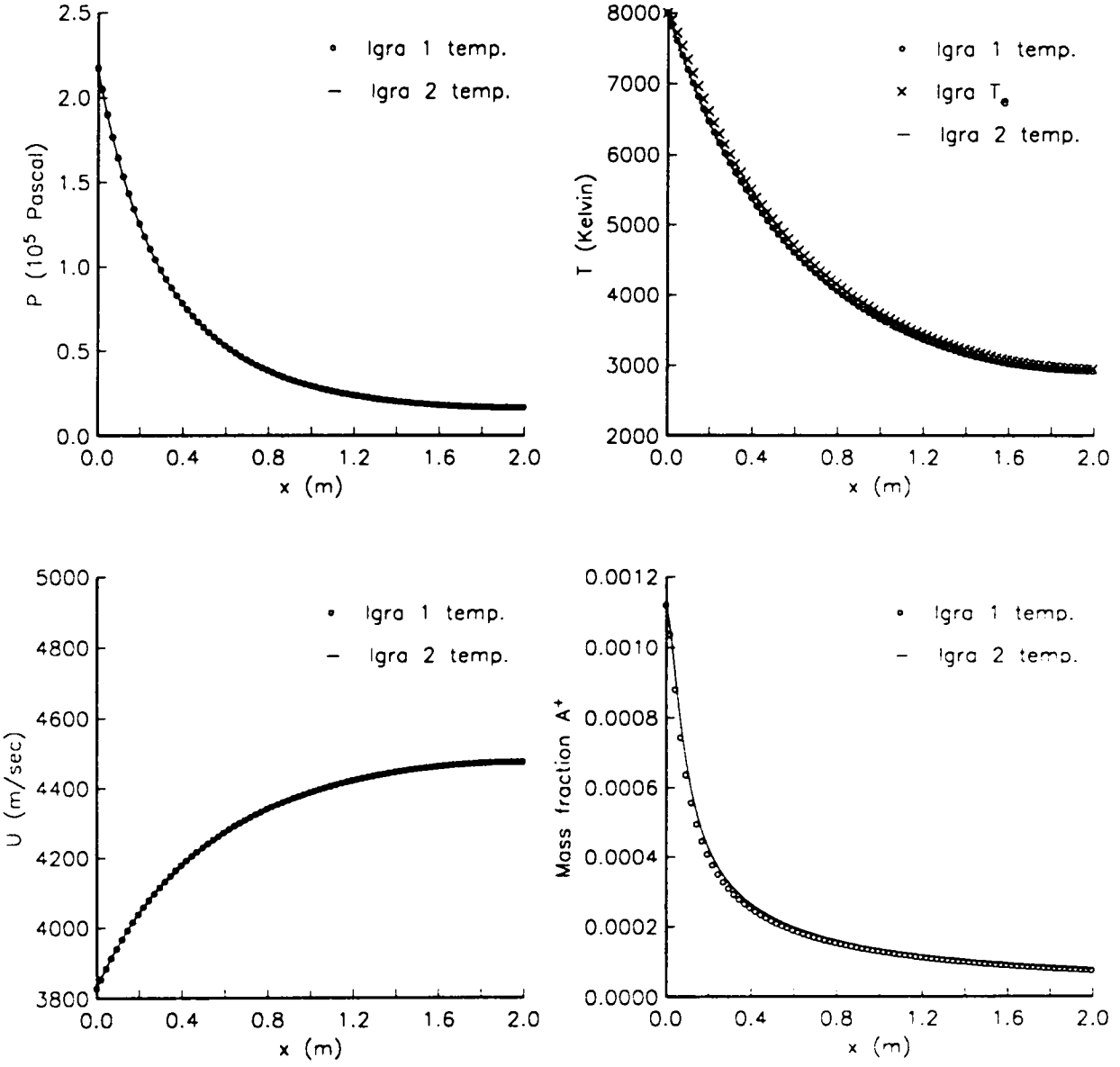

Fig. 11 Comparison of different chemistry models for an Argon plasma. Pressure, temperature, velocity, and mass fraction of A^+.

Inlet $T = 8000\ K, \quad \rho = 0.1303\ kg/m^3, \quad U = 3828\ m/sec$

Igra 1 temp. Argon Model 1, one translational temperature

Igra 2 temp. Argon Model 1, two translational temperatutes

Igra T_e Argon Model 1, electronic translational temperature

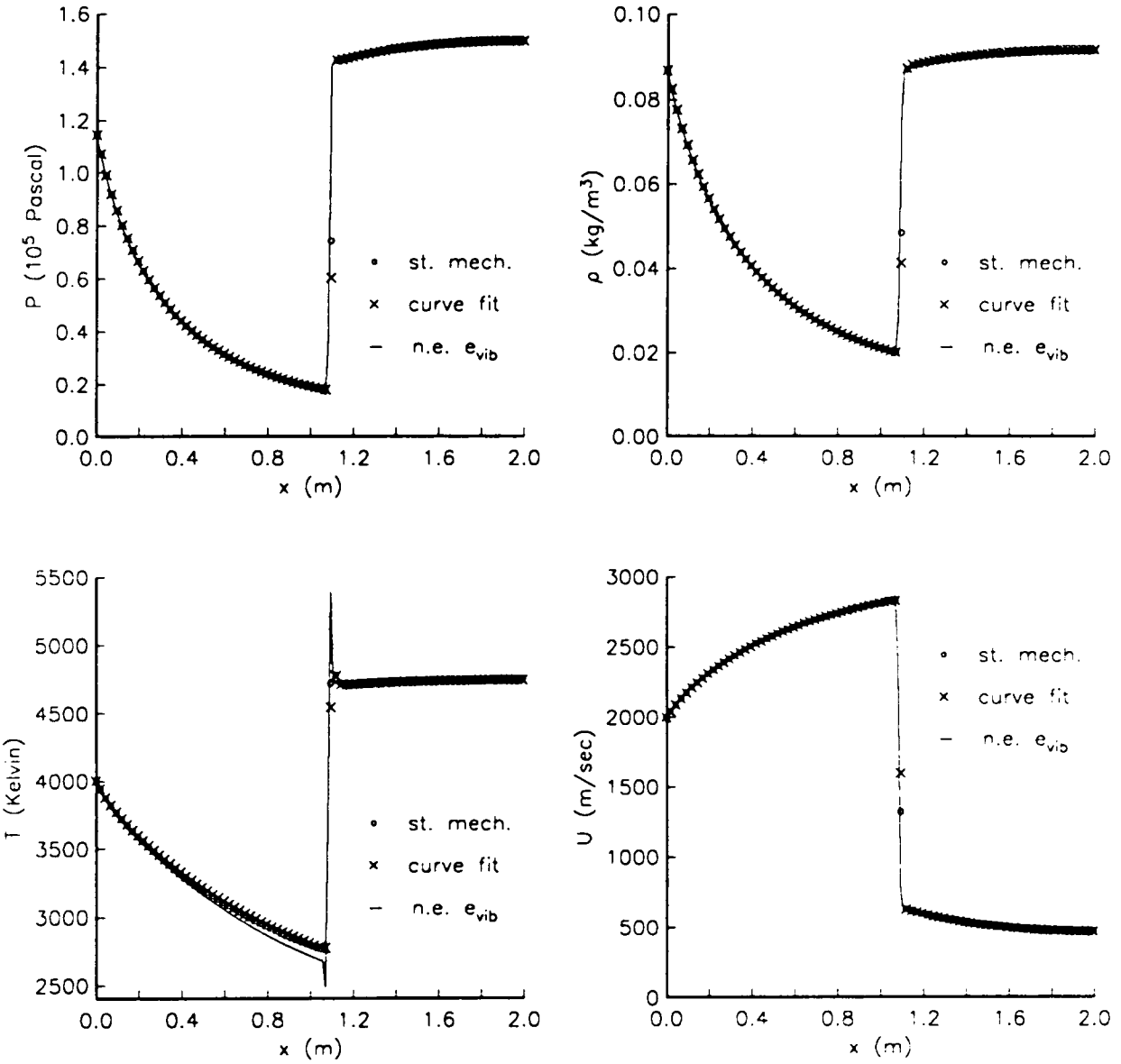

Fig. 12a Comparison of different thermodynamic models using Air Model 1. Pressure, density, temperature, and velocity plots.

Inlet $T = 4000\ K, \quad \rho = 8.6756\ 10^{-2}\ kg/m^3, \quad U = 2000\ m/sec$

Outlet $p_{exit} = 1.5\ 10^5\ N/m^2$

st. mech. Vibrational Equilibrium Model

curve fit Curve Fit Model

n.e. e_{vib} Simplified Vibrational Non-Equilibrium Model

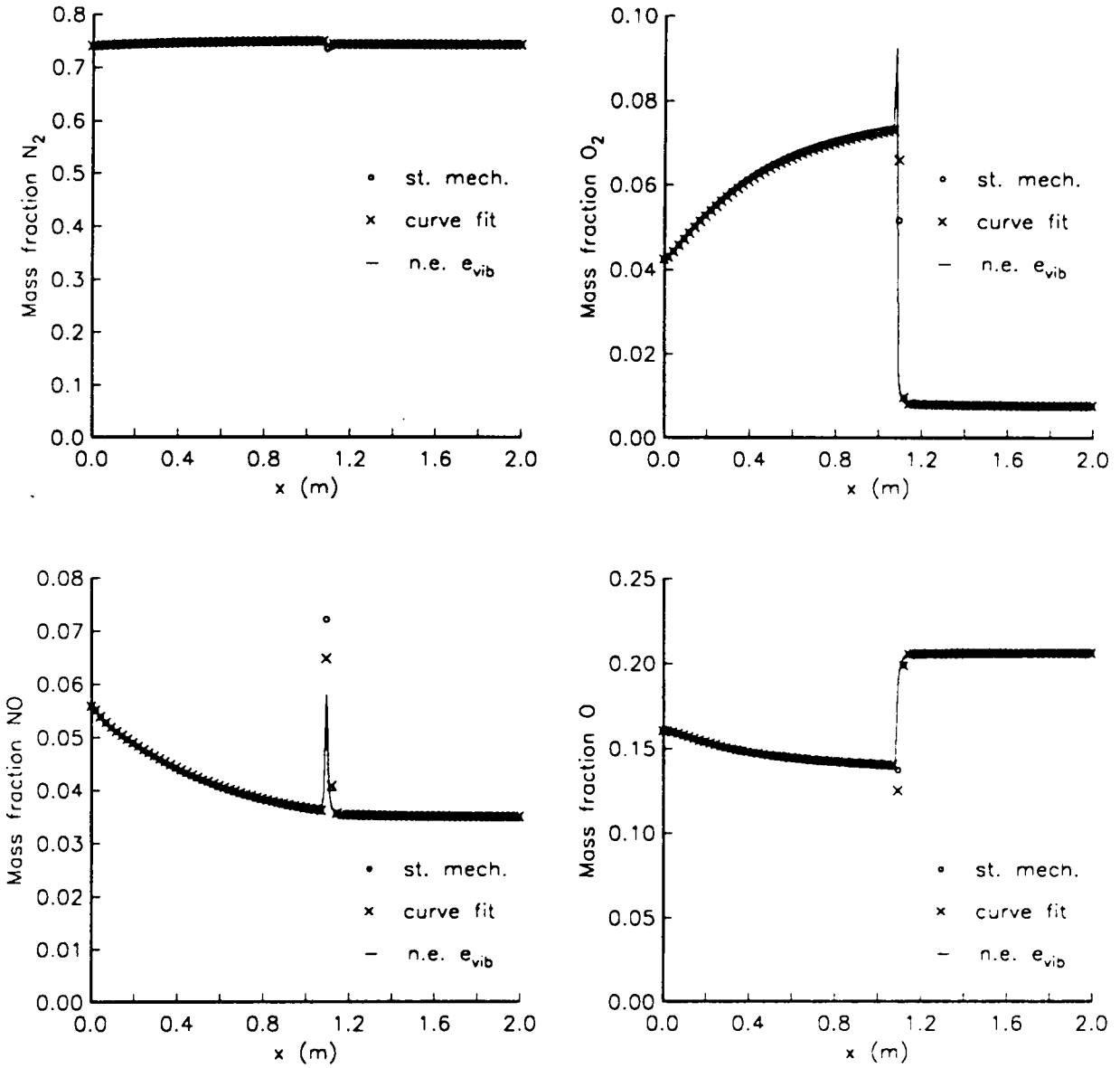

Fig. 12b Comparison of different thermodynamic models using Air Model 1. Mass fraction plots of N_2, O_2, NO, O.

Inlet $T = 4000\ K, \quad \rho = 8.6756\ 10^{-2}\ kg/m^3, \quad U = 2000\ m/sec$

Outlet $p_{exit} = 1.5\ 10^5\ N/m^2$

st. mech. Vibrational Equilibrium Model

curve fit Curve Fit Model

n.e. e_{vib} Simplified Vibrational Non-Equilibrium Model

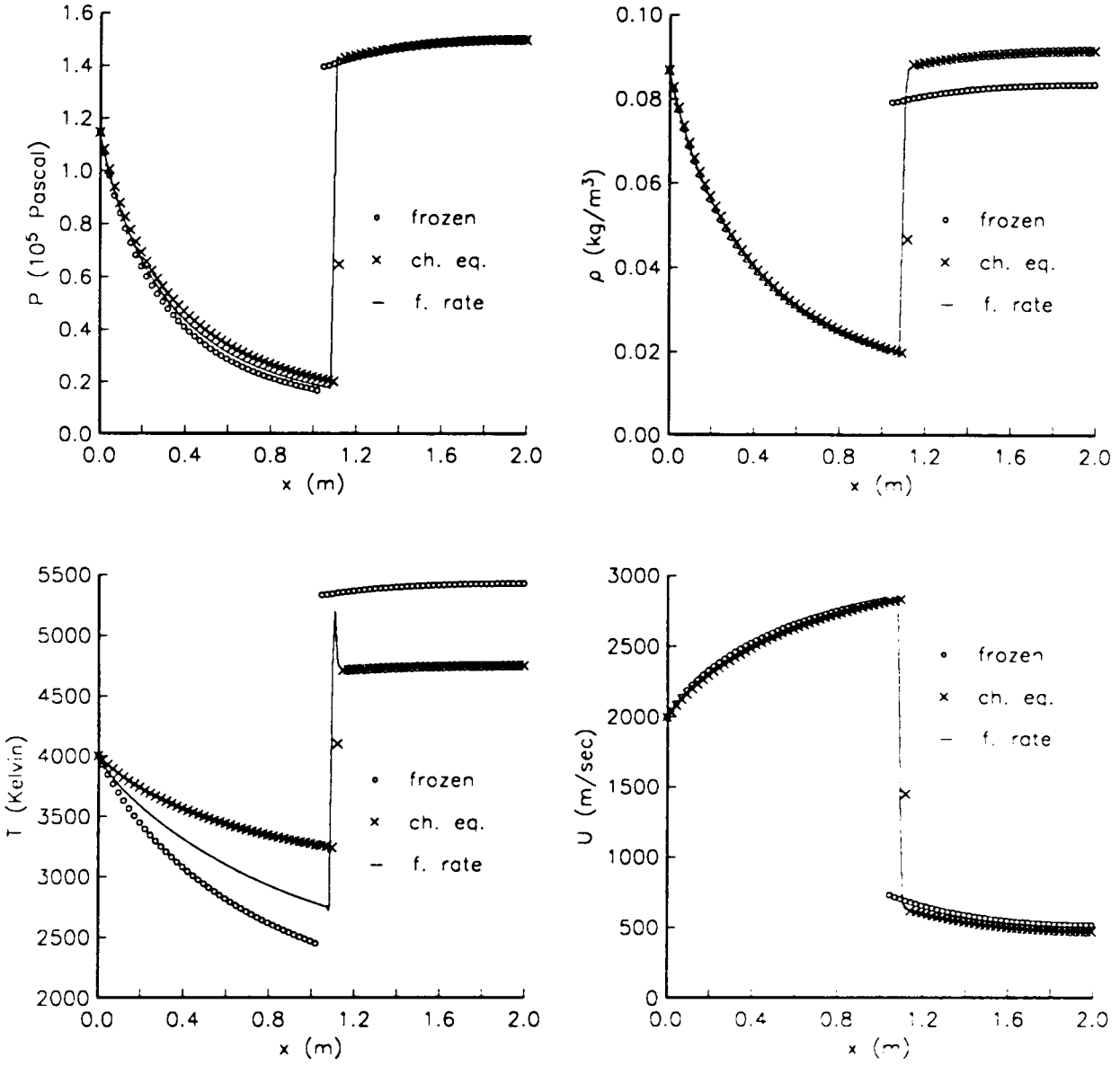

Fig. 13a Comparison of different air chemistry models using the Vibrational Equilibrium Model. Pressure, density, temperature, and velocity plots for the same inlet and outlet conditions of fig. 12a,b.

frozen Frozen chemistry
ch. eq. Chemical equilibrium
f. rate Air Model 1

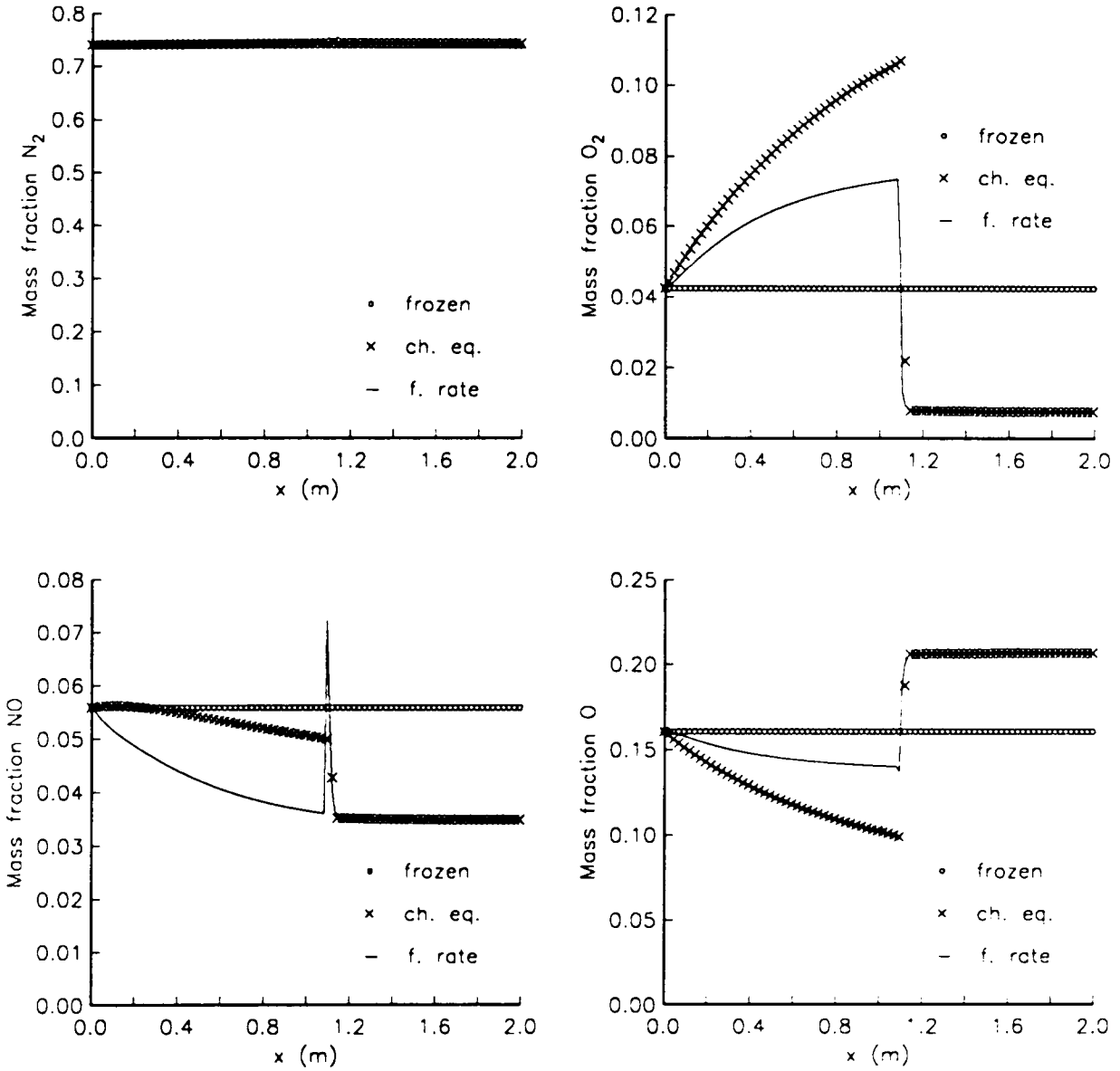

Fig. 13b Comparison of different air chemistry models using the Vibrational Equilibrium Model. Mass fraction plots of N_2, O_2, NO, O for the same inlet and outlet conditions of fig. 12a,b.

frozen Frozen chemistry
ch. eq. Chemical equilibrium
f. rate Air Model 1

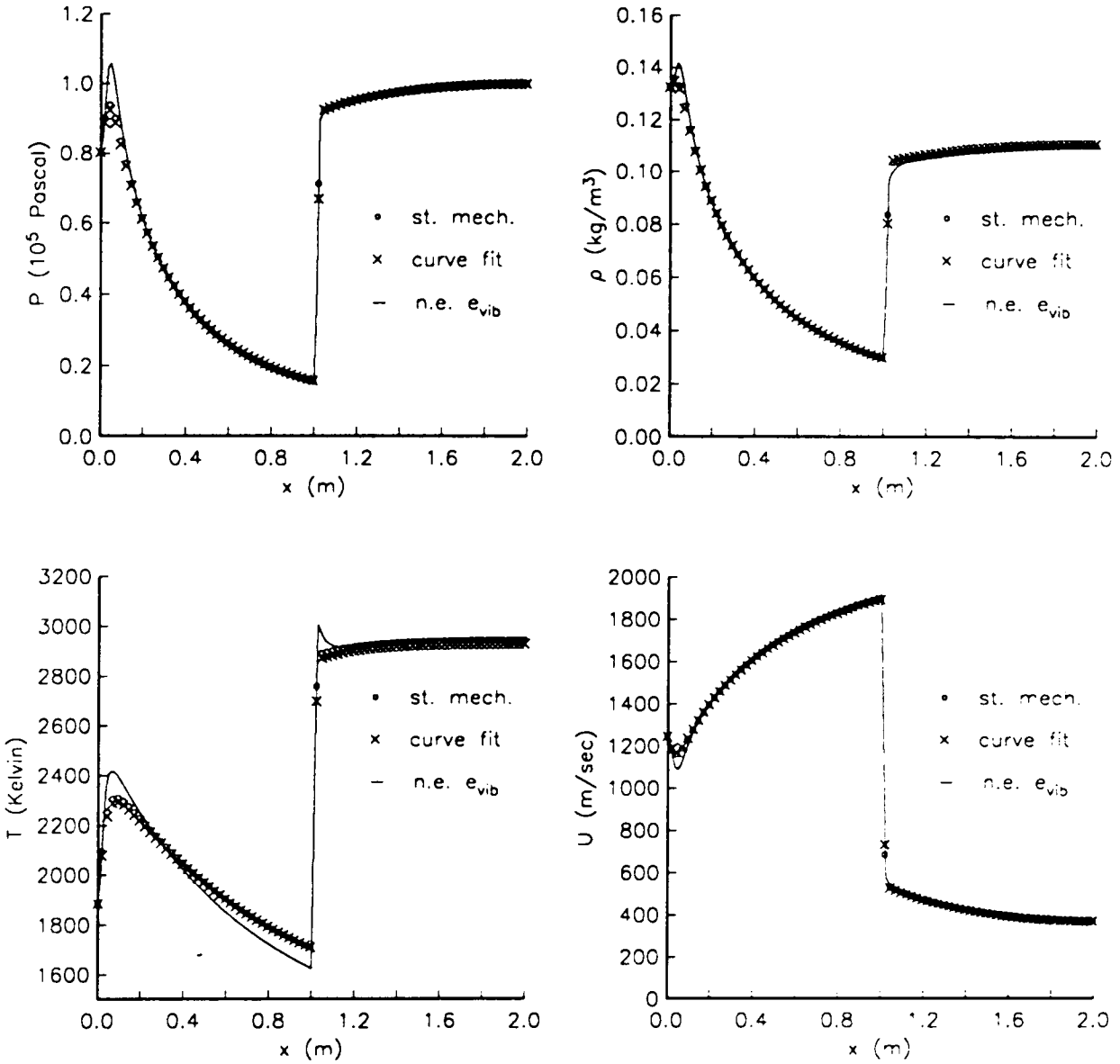

Fig. 14a Comparison of different thermodynamic models using Hydrogen-Air Model 1. Pressure, density, temperature, and velocity plots.

Inlet $T = 1884.3\ K, \quad p = 8.0263\ 10^4\ N/m^2, \quad U = 1245\ m/sec$

Outlet $p_{exit} = 10^5\ N/m^2$

st. mech. Vibrational Equilibrium Model

curve fit Curve Fit Model

n.e. e_{vib} Simplified Vibrational Non-Equilibrium Model

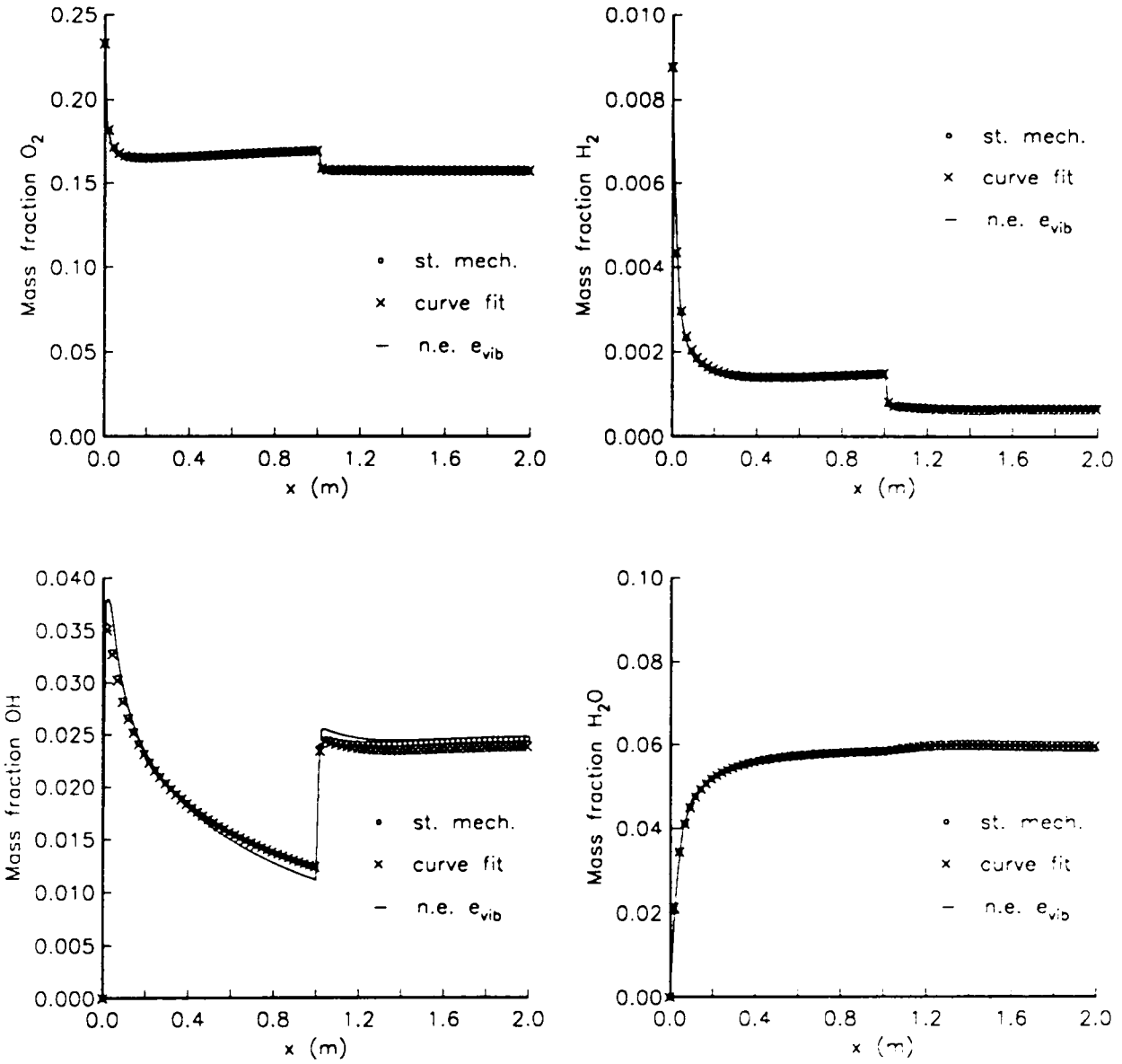

Fig. 14b Comparison of different thermodynamic models using Hydrogen-Air Model 1. Mass fraction plots of O_2, H_2, OH, H_2O.

Inlet $T = 1884.3\ K, \quad p = 8.0263\ 10^4\ N/m^2, \quad U = 1245\ m/sec$

Outlet $p_{exit} = 10^5\ N/m^2$

st. mech. Vibrational Equilibrium Model

curve fit Curve Fit Model

n.e. e_{vib} Simplified Vibrational Non-Equilibrium Model

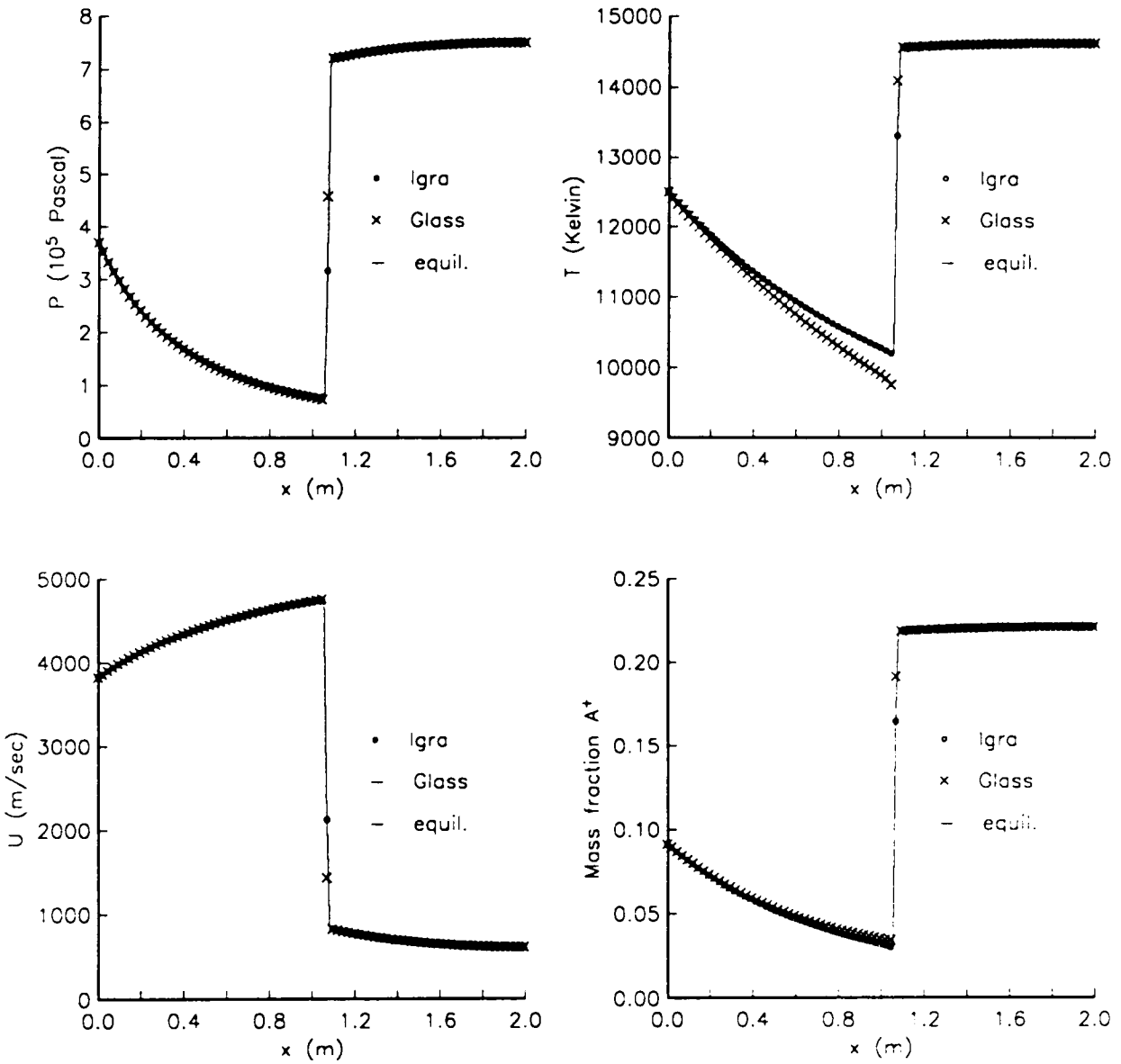

Fig. 15 Comparison of different chemistry models for an Argon plasma. Pressure, temperature, velocity, and mass fraction of A^+.

Inlet	$T = 12500\ K, \quad \rho = 0.1303\ kg/m^3, \quad U = 3828\ m/sec$
Outlet	$p_{exit} = 7.5\ 10^5\ N/m^2$
Igra	Argon Model 1
Glass	Argon Model 2
ch. eq.	Chemical equilibrium calculation

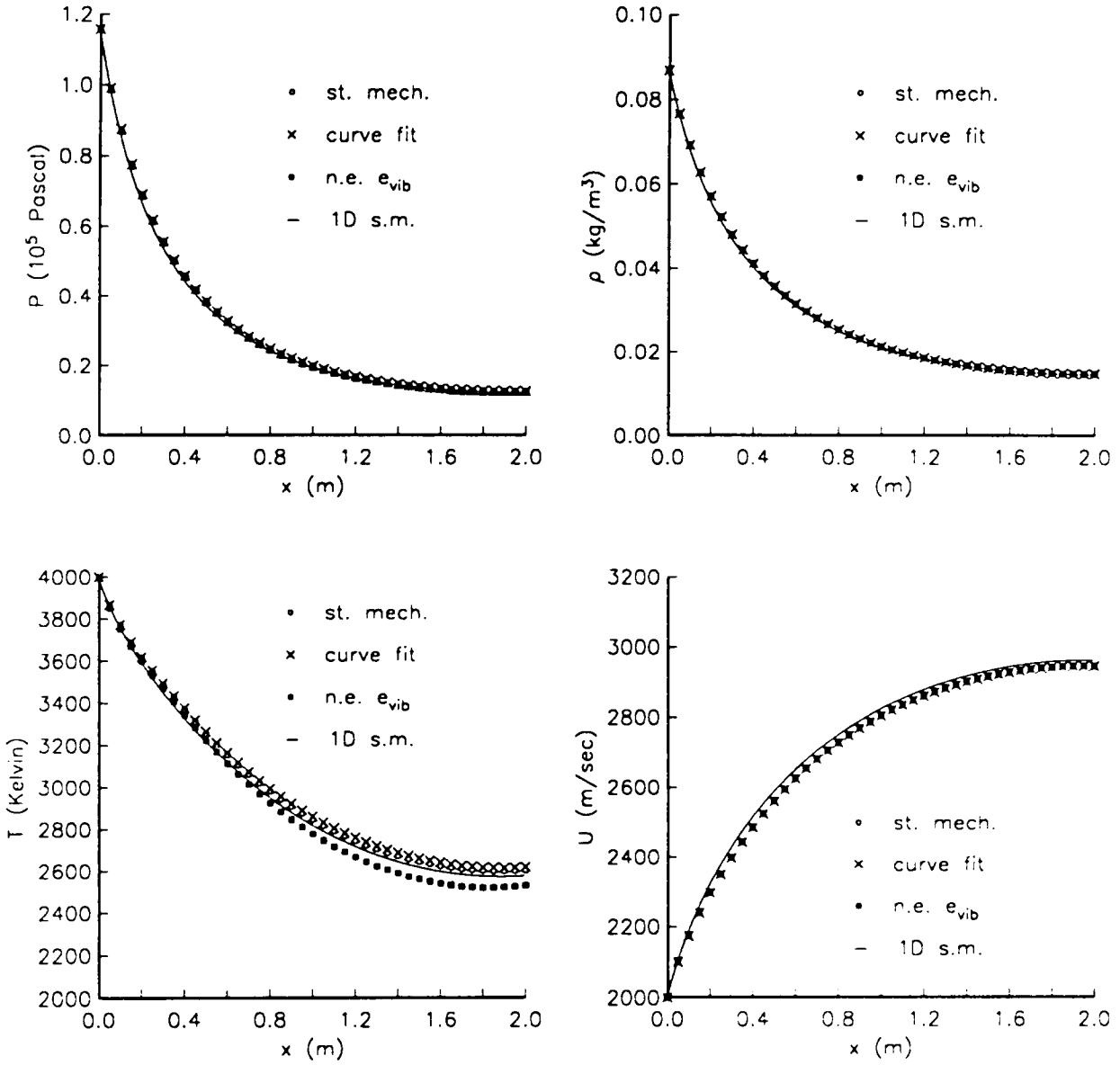

Fig. 16a Comparison of different thermodynamic models using Air Model 1. Pressure, density, temperature, and velocity plots.

Inlet	$T = 4000\ K, \quad \rho = 8.6756\ 10^{-2}\ kg/m^3, \quad U = 2000\ m/sec$
st. mech.	Vibrational Equilibrium Model, area-averaged
curve fit	Curve Fit Model, area-averaged
n.e. e_{vib}	Simplified Vibrational Non-Equilibrium Model, area-averaged
1D s.m.	Quasi-1D results, Vibrational Equilibrium Model

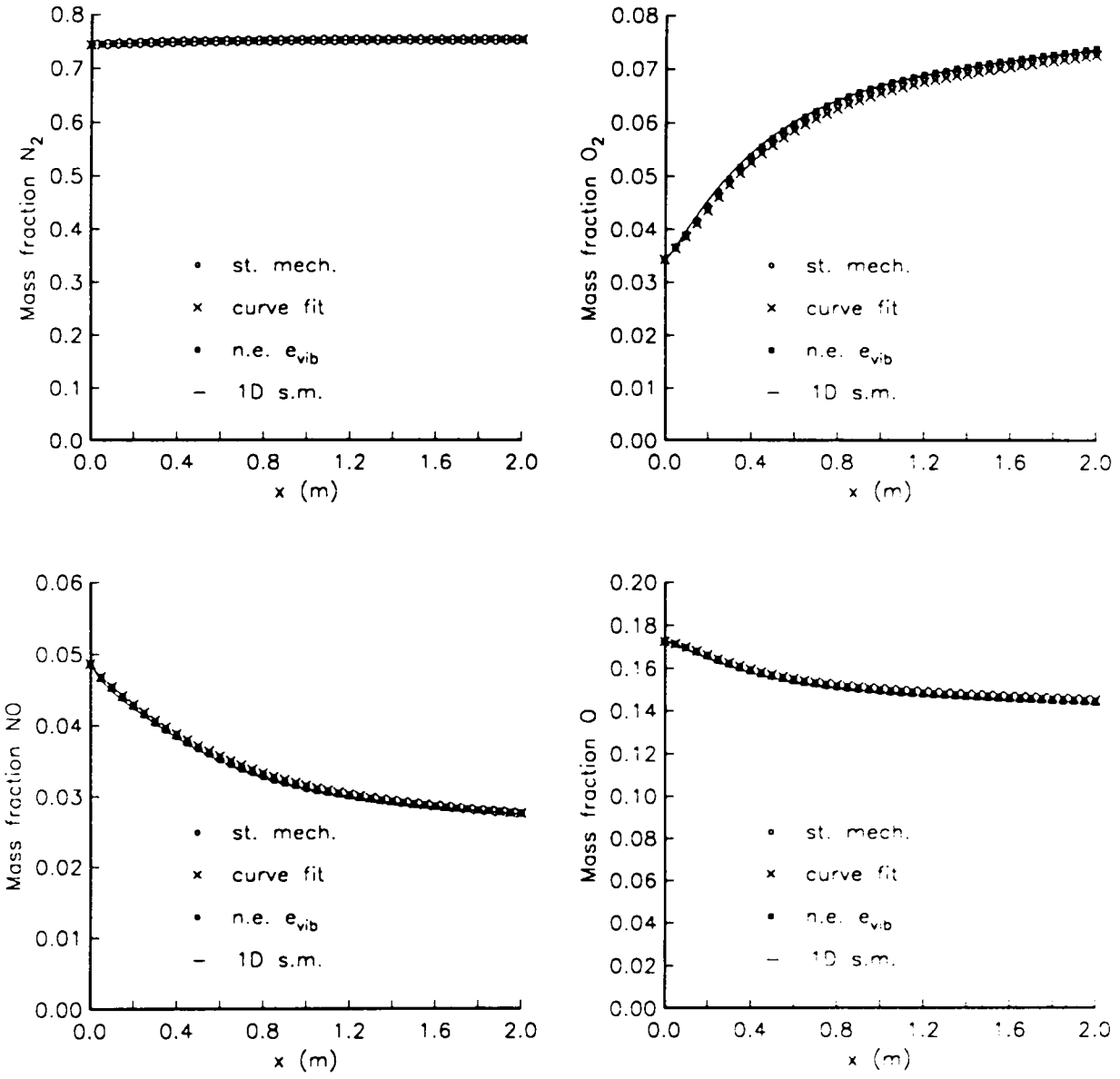

Fig. 16b Comparison of different thermodynamic models using Air Model 1. Mass fraction plots of N_2, O_2, NO, O.

Inlet $T = 4000\ K$, $\rho = 8.6756\ 10^{-2}\ kg/m^3$, $U = 2000\ m/sec$

st. mech. Vibrational Equilibrium Model, area-averaged

curve fit Curve Fit Model, area-averaged

n.e. e_{vib} Simplified Vibrational Non-Equilibrium Model, area-averaged

1D s.m. Quasi-1D results, Vibrational Equilibrium Model

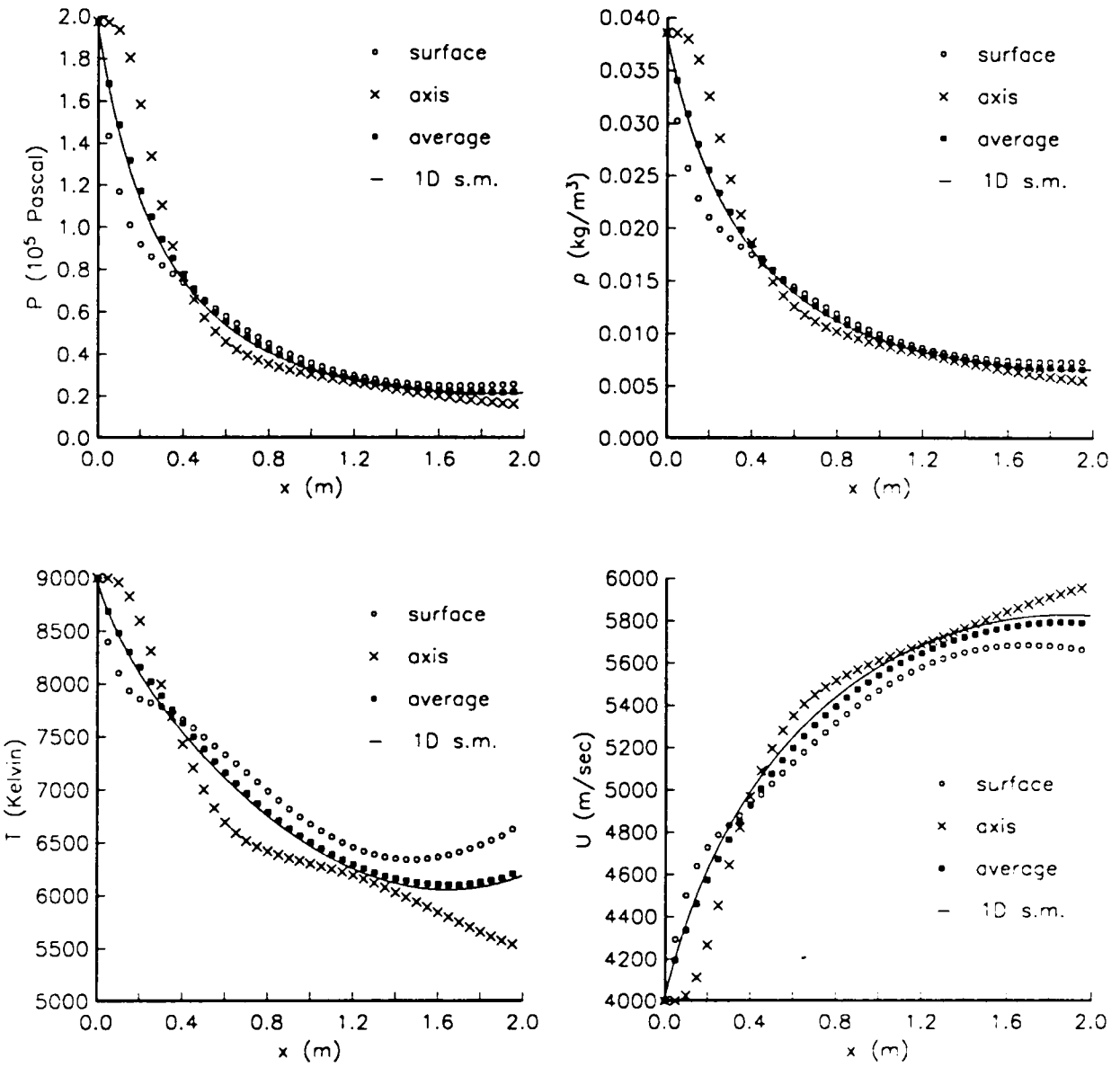

Fig. 17a 2-D results with Air Model 2 and the Vibrational Equilibrium Model. Pressure, density, temperature, and velocity plots.

Inlet $T = 9000\ K, \quad \rho = 3.8558\ 10^{-2}\ kg/m^3, \quad U = 4000\ m/sec$

surface Nozzle surface

axis Nozzle centerline

average Area-averaged values

1D s.m. Quasi-1D results for the same conditions

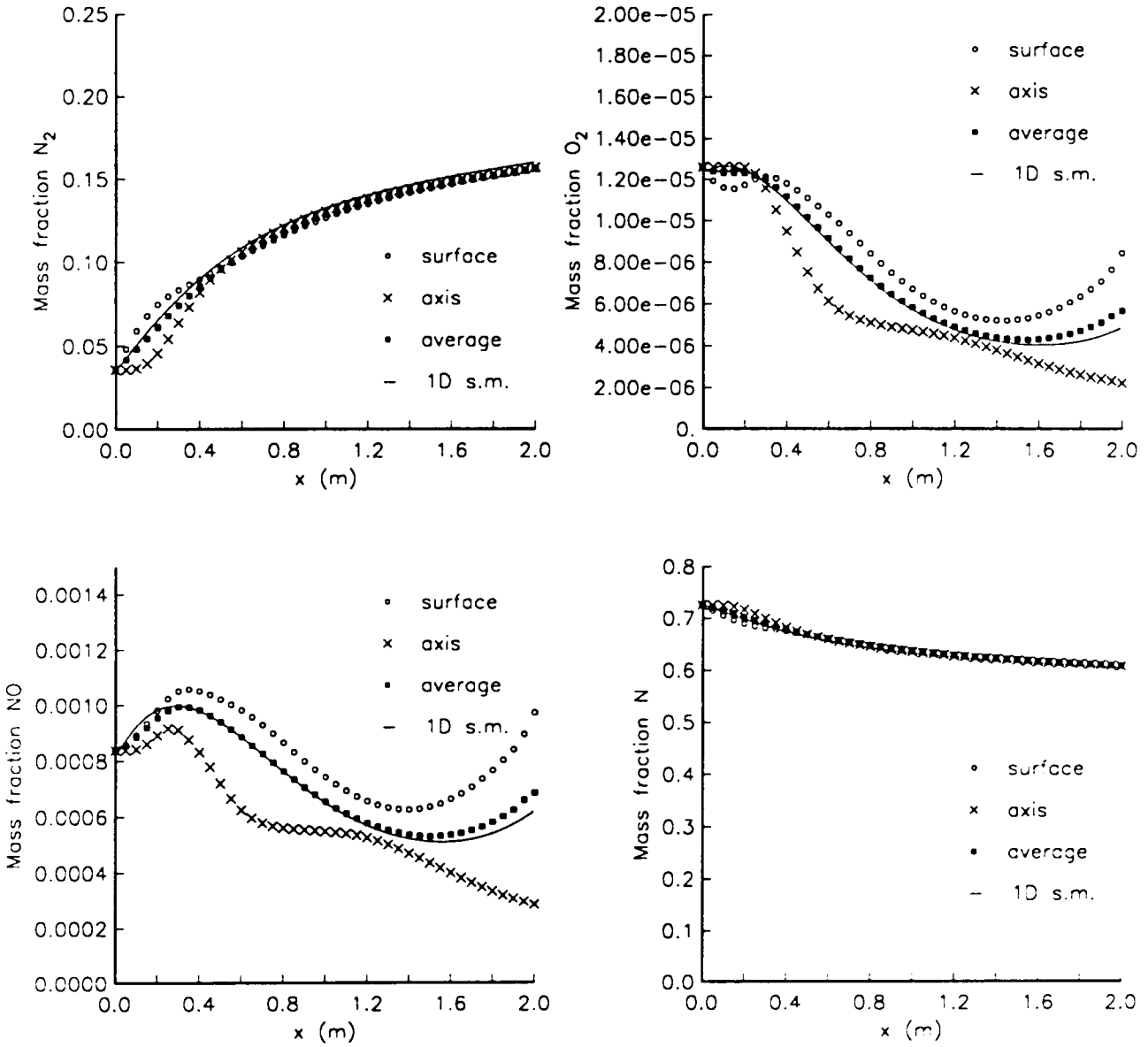

Fig. 17b 2-D results with Air Model 2 and the Vibrational Equilibrium Model. Mass fraction plots of N_2, O_2, NO, N.

Inlet $T = 9000\ K$, $\rho = 3.8558\ 10^{-2}\ kg/m^3$, $U = 4000\ m/sec$

surface Nozzle surface

axis Nozzle centerline

average Area-averaged values

1D s.m. Quasi-1D results for the same conditions

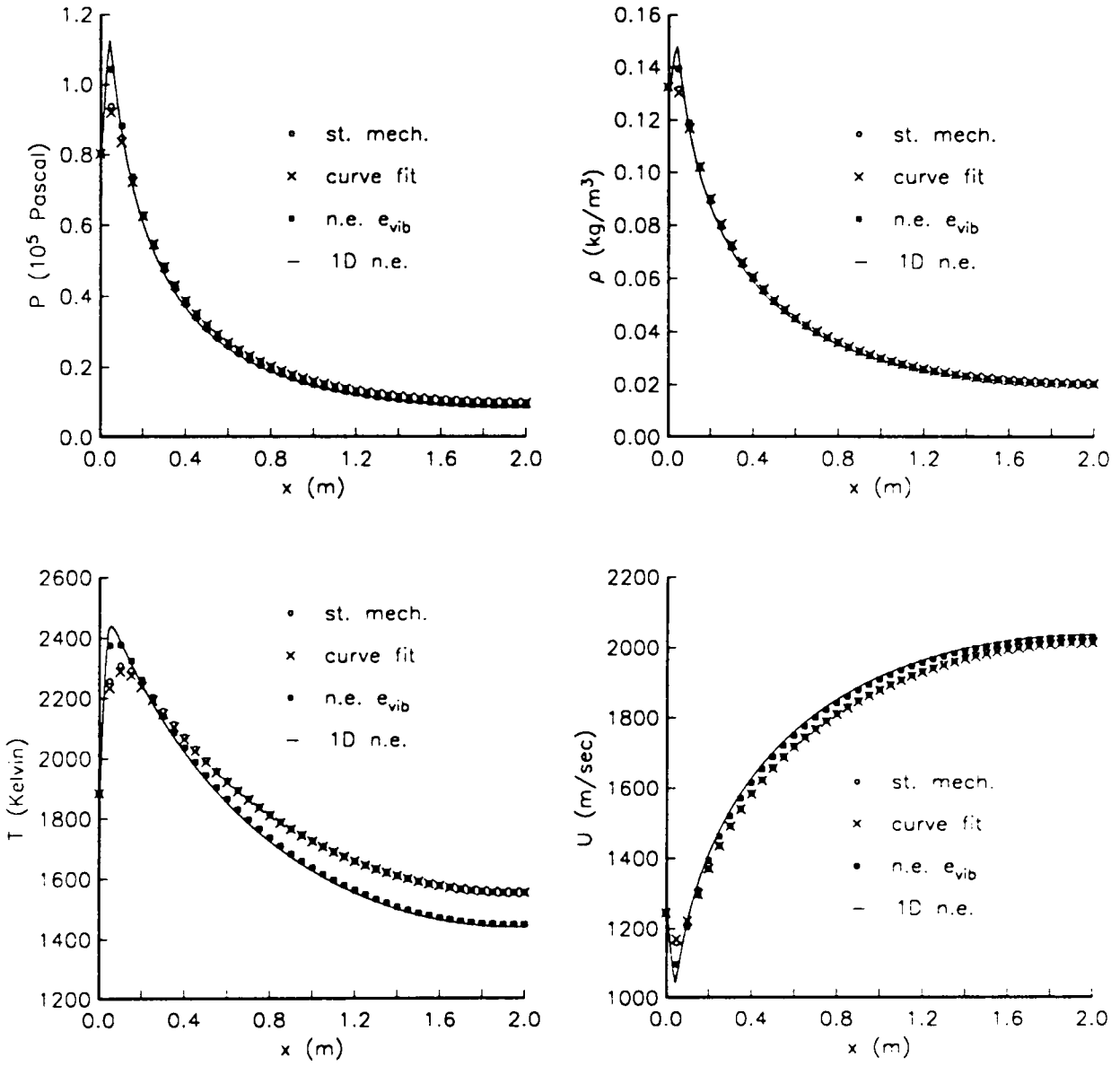

Fig. 18a Comparison of different thermodynamic models using Hydrogen-Air Model 1. Pressure, density, temperature, and velocity plots.

Inlet $T = 1884.3\ K, \quad p = 8.0263\ 10^4\ N/m^2, \quad U = 1245\ m/sec$

st. mech. Vibrational Equilibrium Model, area-averaged

curve fit Curve Fit Model, area-averaged

n.e. e_{vib} Simplified Vibrational Non-Equilibrium Model, area-averaged

1D s.m. Quasi-1D results, Vibrational Equilibrium Model

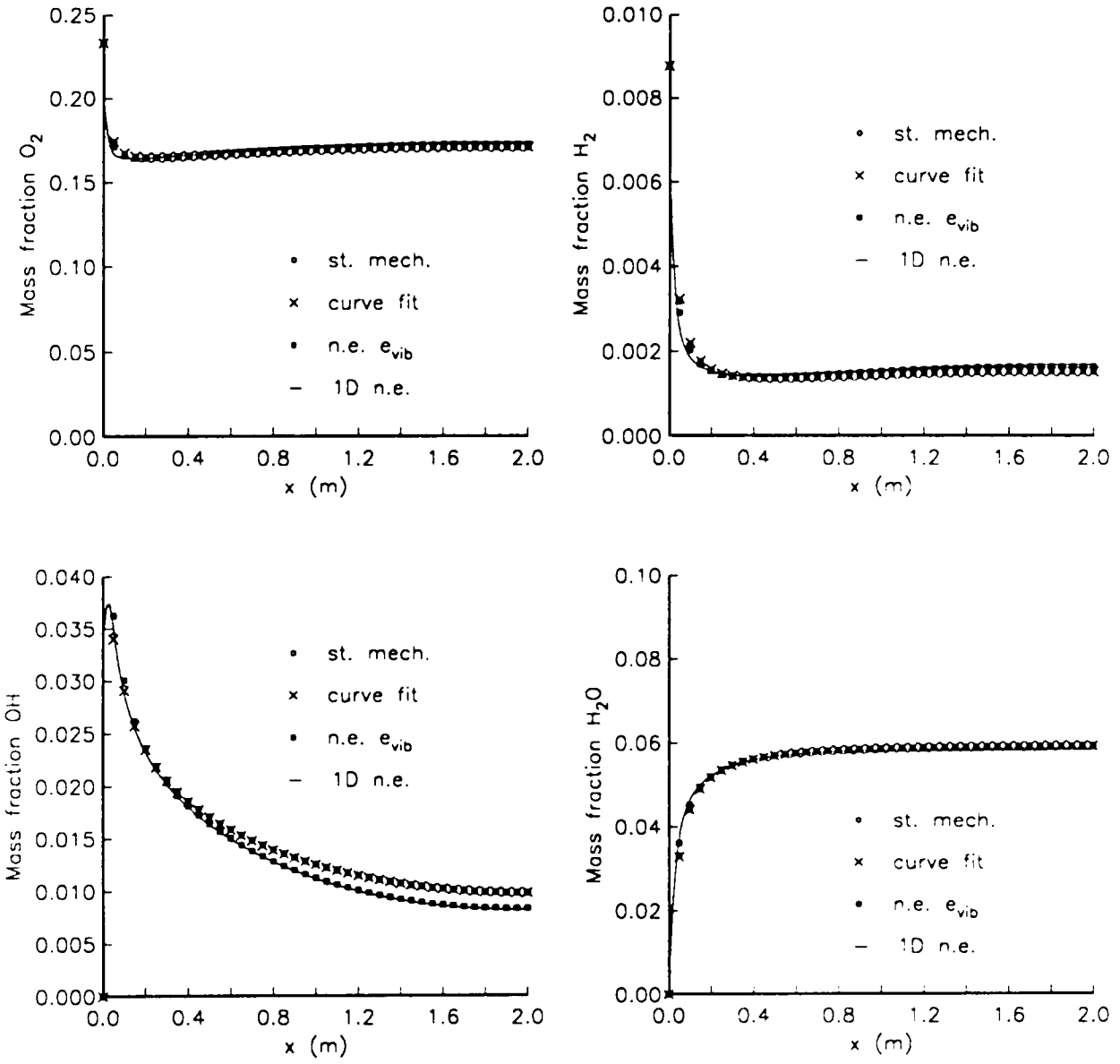

Fig. 18b Comparison of different thermodynamic models using Hydrogen-Air Model 1. Mass fraction plots of O_2, H_2, OH, H_2O.

Inlet $T = 1884.3\ K$, $p = 8.0263\ 10^4\ N/m^2$, $U = 1245\ m/sec$

st. mech. Vibrational Equilibrium Model, area-averaged

curve fit Curve Fit Model, area-averaged

n.e. e_{vib} Simplified Vibrational Non-Equilibrium Model, area-averaged

1D s.m. Quasi-1D results, Vibrational Equilibrium Model

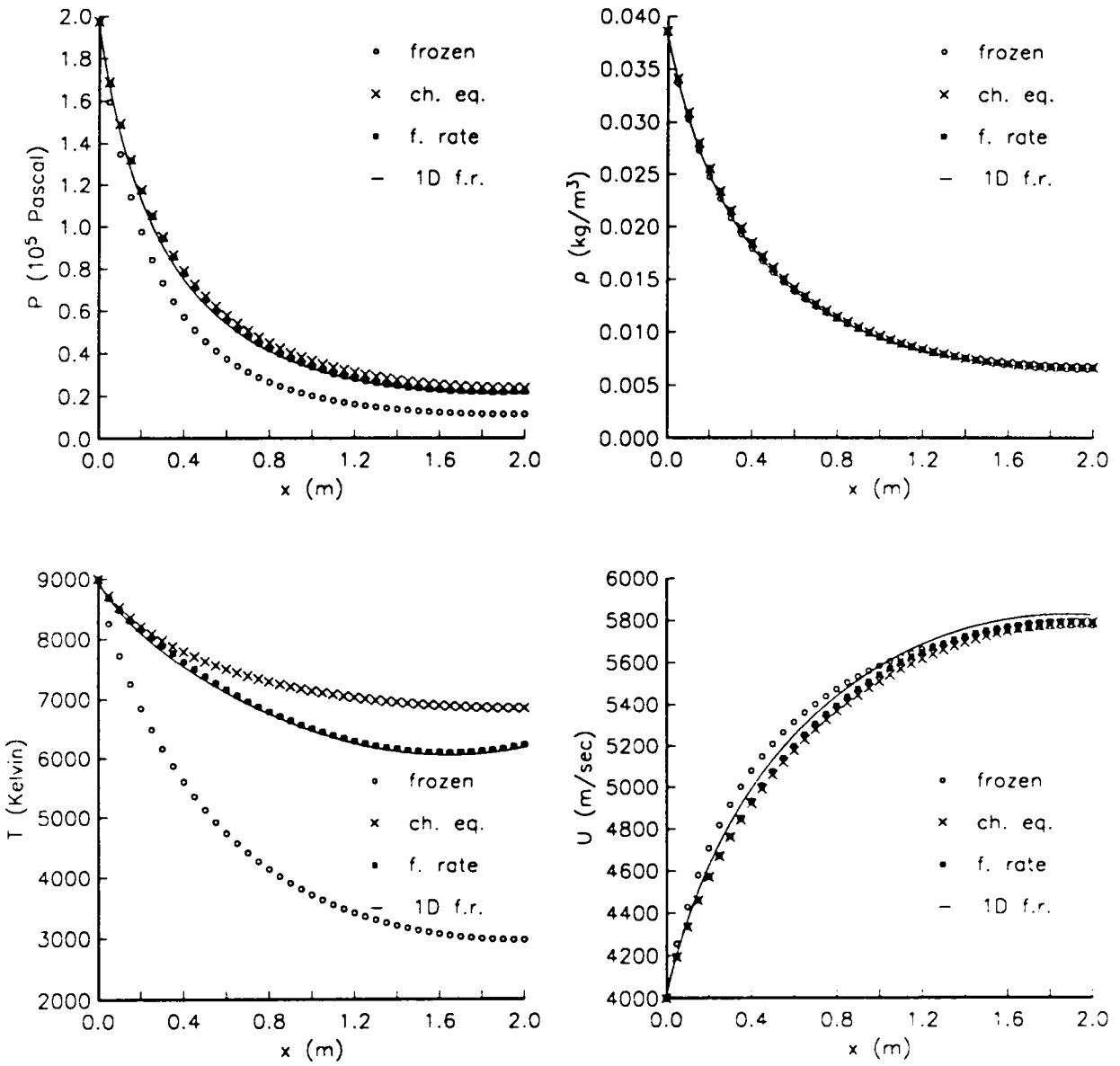

Fig. 19a Comparison of different air chemistry models using the Vibrational Equilibrium Model. Pressure, density, temperature, and velocity plots.

Inlet $T = 9000\ K, \quad \rho = 3.8558\ 10^{-2}\ kg/m^3, \quad U = 4000\ m/sec$

frozen Frozen chemistry, area-averaged

ch. eq. Chemical equilibrium, area-averaged

f. rate Air Model 2, area-averaged

1D f.r. Quasi-1D results, finite rate

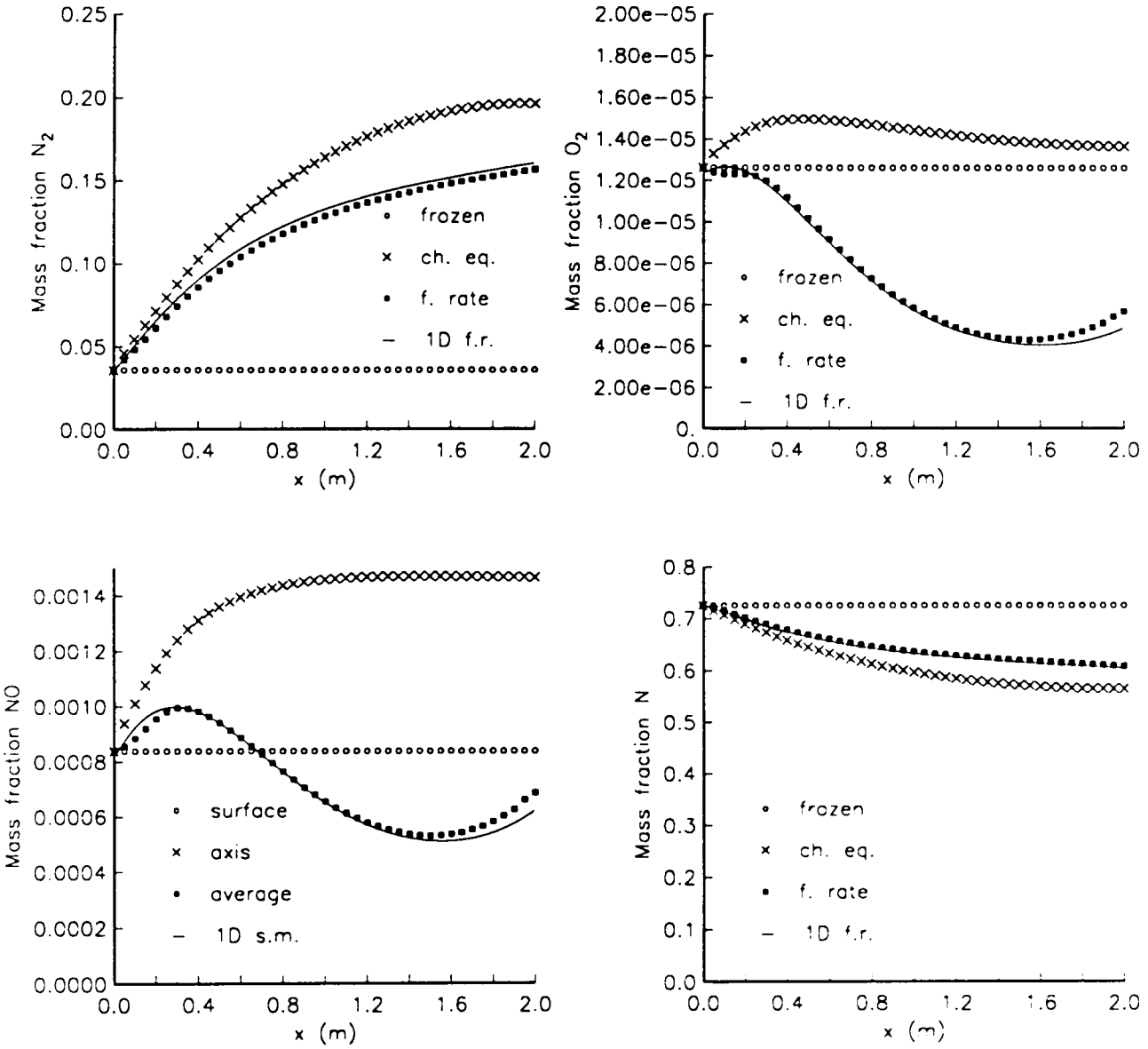

Fig. 19b Comparison of different air chemistry models using the Vibrational Equilibrium Model. Mass fraction plots of N_2, O_2, NO, N.

Inlet $T = 9000\ K$, $\rho = 3.8558\ 10^{-2}\ kg/m^3$, $U = 4000\ m/sec$

frozen Frozen chemistry, area-averaged

ch. eq. Chemical equilibrium, area-averaged

f. rate Air Model 2, area-averaged

1D f.r. Quasi-1D results, finite rate

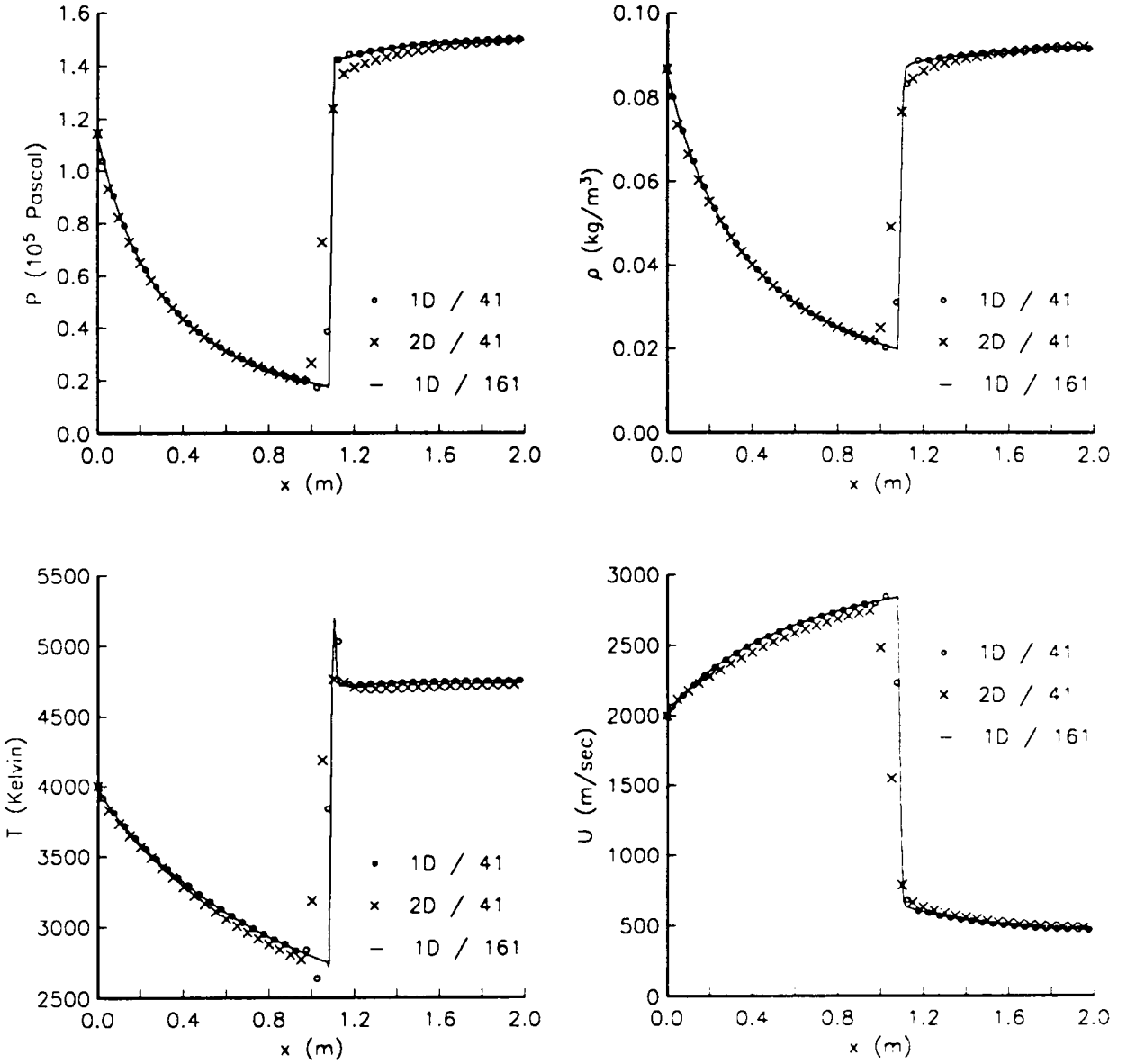

Fig. 20a 2-D results with Air Model 1 and the Vibrational Equilibrium Model. Pressure, density, temperature, and velocity plots.

Inlet $T = 4000\ K, \quad \rho = 8.6756\ 10^{-2}\ kg/m^3, \quad U = 2000\ m/sec$

Outlet $p_{exit} = 1.5\ 10^5\ N/m^2$

1D / 41 Quasi-1D results for 41 mesh points

2D / 41 Axisymmetric results for a 41 × 6 grid

1D / 161 Quasi-1D results for 161 mesh points

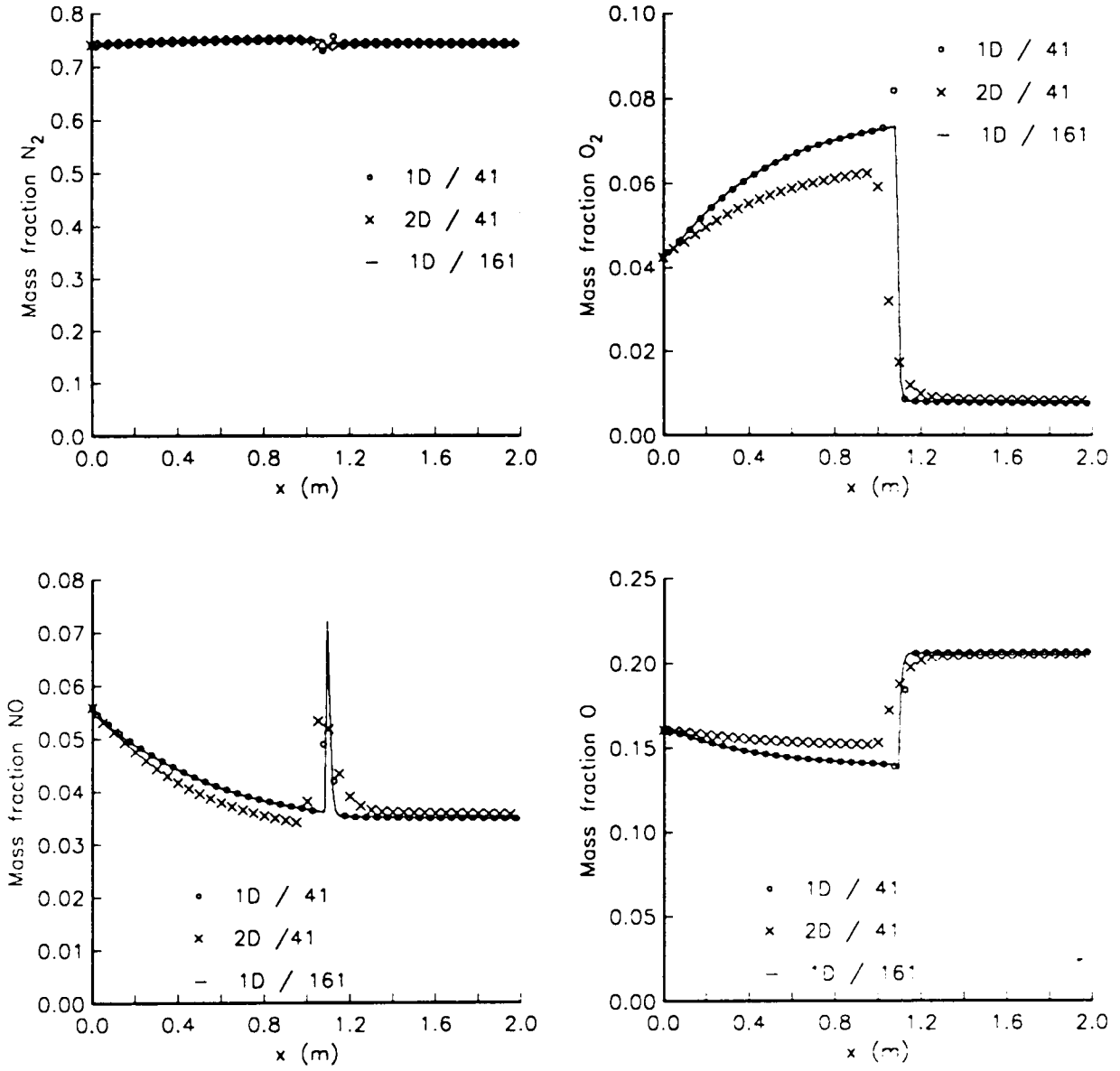

Fig. 20b 2-D results with Air Model 1 and the Vibrational Equilibrium Model. Plots of N_2, O_2, NO, O mass fractions.

Inlet	$T = 4000\ K, \quad \rho = 8.6756\ 10^{-2}\ kg/m^3, \quad U = 2000\ m/sec$
Outlet	$p_{exit} = 1.5\ 10^5\ N/m^2$
1D / 41	Quasi-1D results for 41 mesh points
2D / 41	Axisymmetric results for a 41 × 6 grid
1D / 161	Quasi-1D results for 161 mesh points

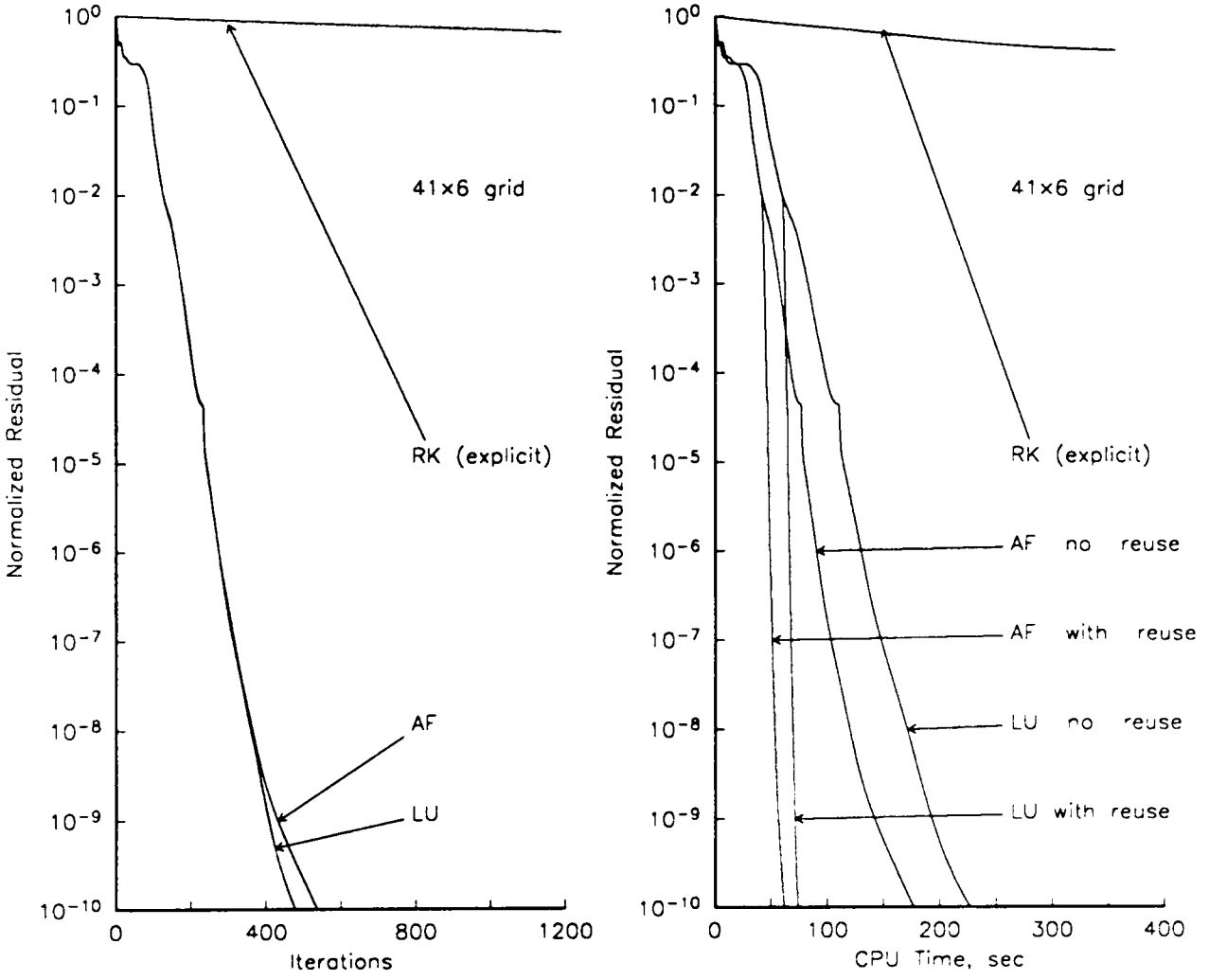

Fig. 21 Convergence history for Air Model 1 on a Cray-YMP machine. Vibrational Equilibrium Model.

RK	Runge-Kutta 4 steps, $CFL = 0.1$
LU no reuse	LU decomposition, Jacobians recalculated every iteration
LU with reuse	LU decomposition, Jacobians frozen after a residual reduction of 10^{-2}
AF no reuse	Approximate Factorization, Jacobians recalculated every iteration
AF with reuse	Approximate Factorization, Jacobians frozen after a residual reduction of 10^{-2}

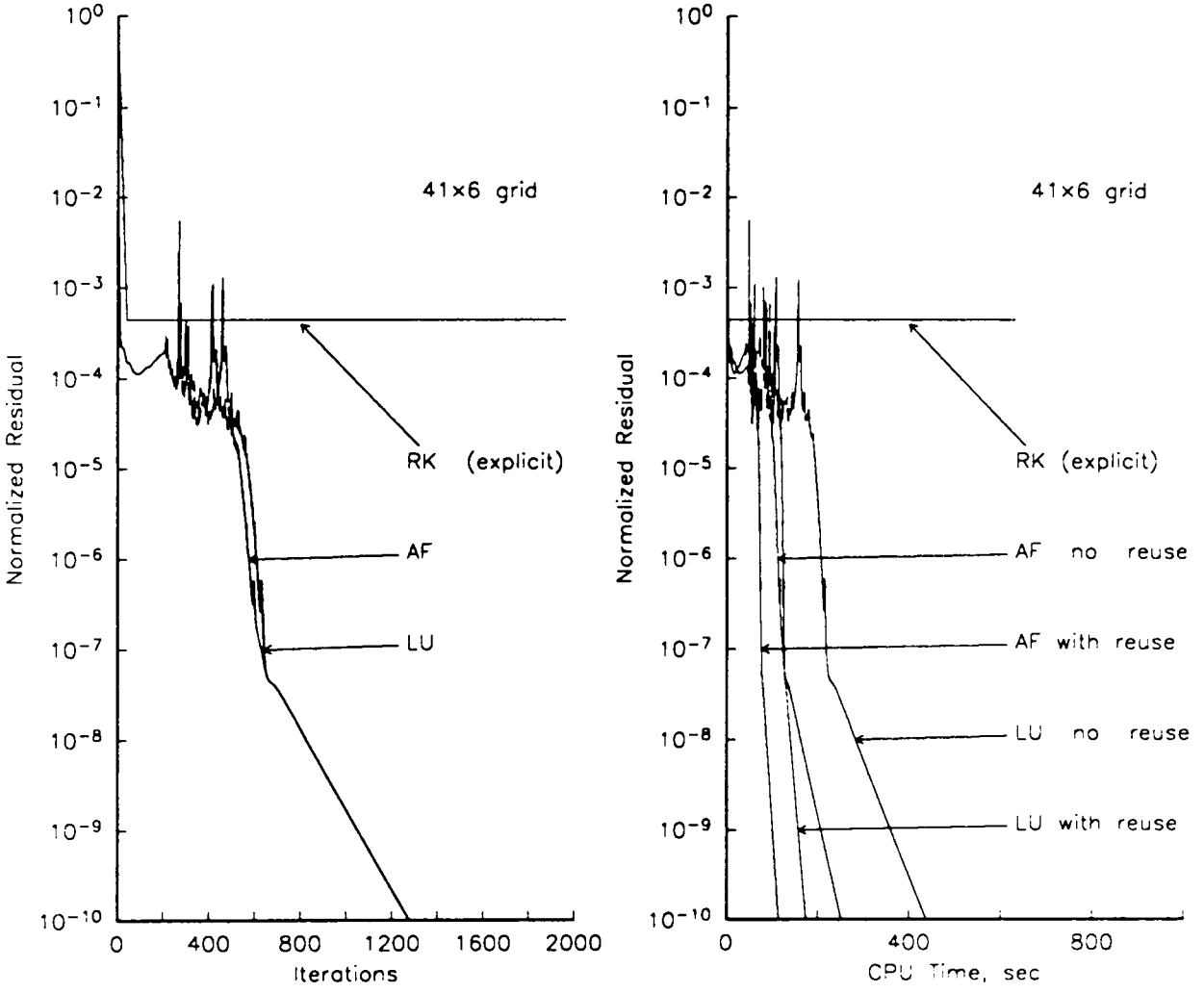

Fig. 22 Convergence history for Hydrogen-Air Model 1 on a Cray-YMP machine. Vibrational Equilibrium Model.

RK	Runge-Kutta 4 steps, $CFL = 10^{-4}$
LU no reuse	LU decomposition, Jacobians recalculated every iteration
LU with reuse	LU decomposition, Jacobians recalculated every 5 iterations after a residual reduction of 10^{-4}
AF no reuse	Approximate Factorization, Jacobians recalculated every iteration
AF with reuse	Approximate Factorization, Jacobians recalculated every 5 iterations after a residual reduction of 10^{-4}

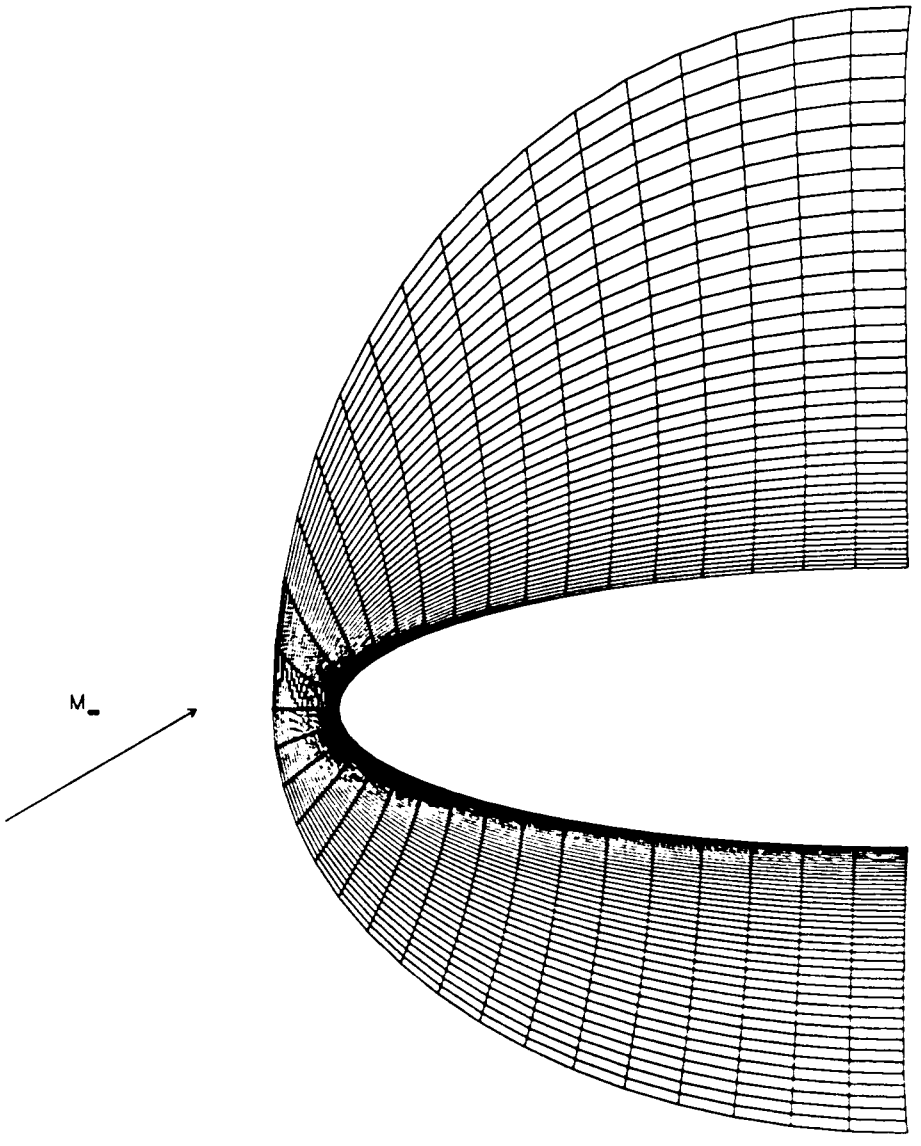

Fig. 23 Geometry of the single ellipse at $\alpha = 30°$ and $M = 25$. The 41×41 mesh is also visible.

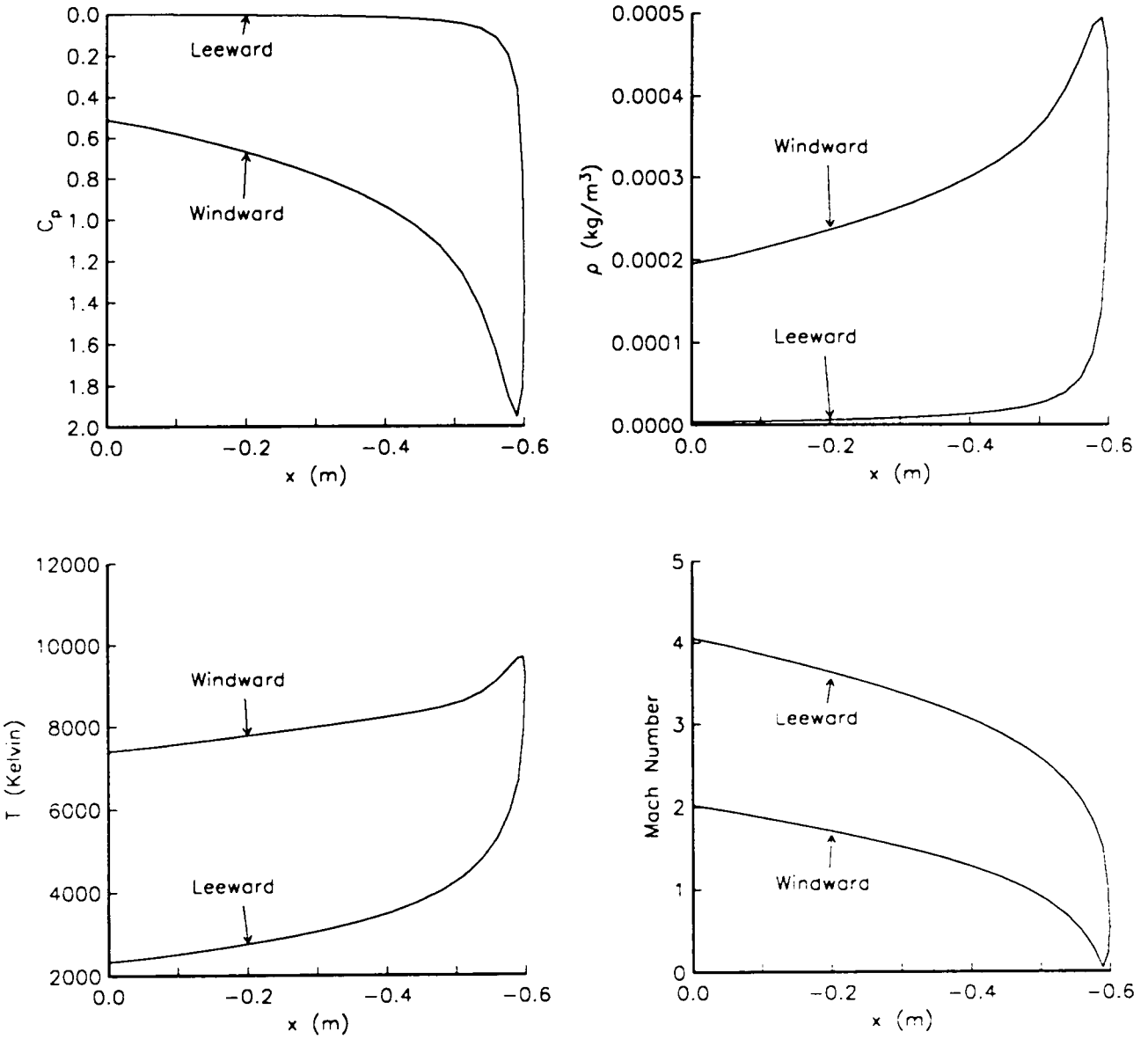

Fig. 24a Single ellipse at $\alpha = 30°$ and $M = 25$. Air Model 1 and Vibrational Equilibrium Model. Pressure coefficient, density, temperature, and Mach number on the body.

Freestream $T = 205.3\ K, \quad \rho = 4.2597\ 10^{-5}\ kg/m^3, \quad U = 7195\ m/sec$

Windward Windward Side

Leeward Leeward Side

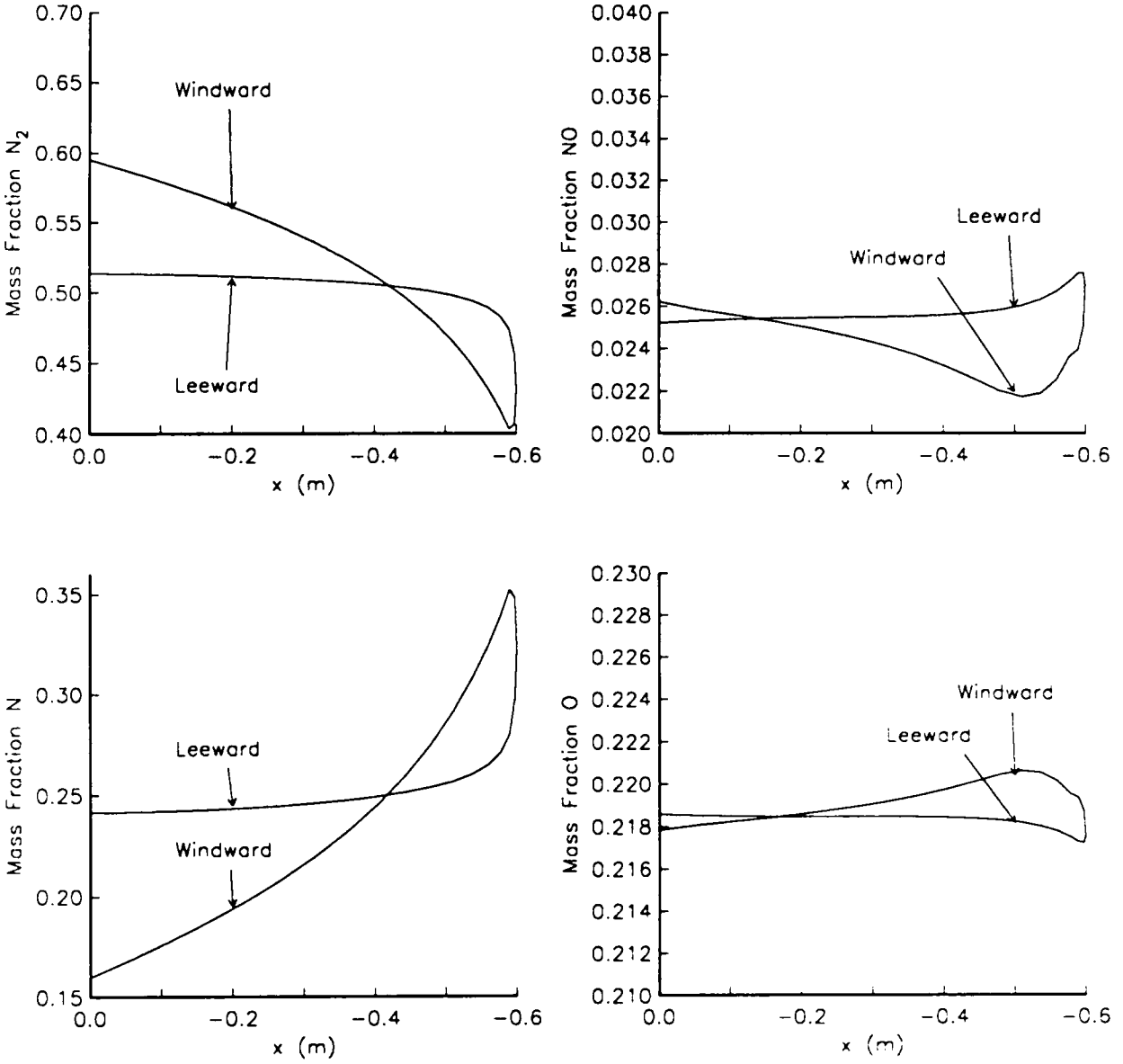

Fig. 24b Single ellipse at $\alpha = 30°$ and $M = 25$. Air Model 1 and Vibrational Equilibrium Model. Mass fraction plots of N_2, NO, N, O on the body.
Freestream $T = 205.3\ K$, $\rho = 4.2597\ 10^{-5}\ kg/m^3$, $U = 7195\ m/sec$
Windward Windward Side
Leeward Leeward Side

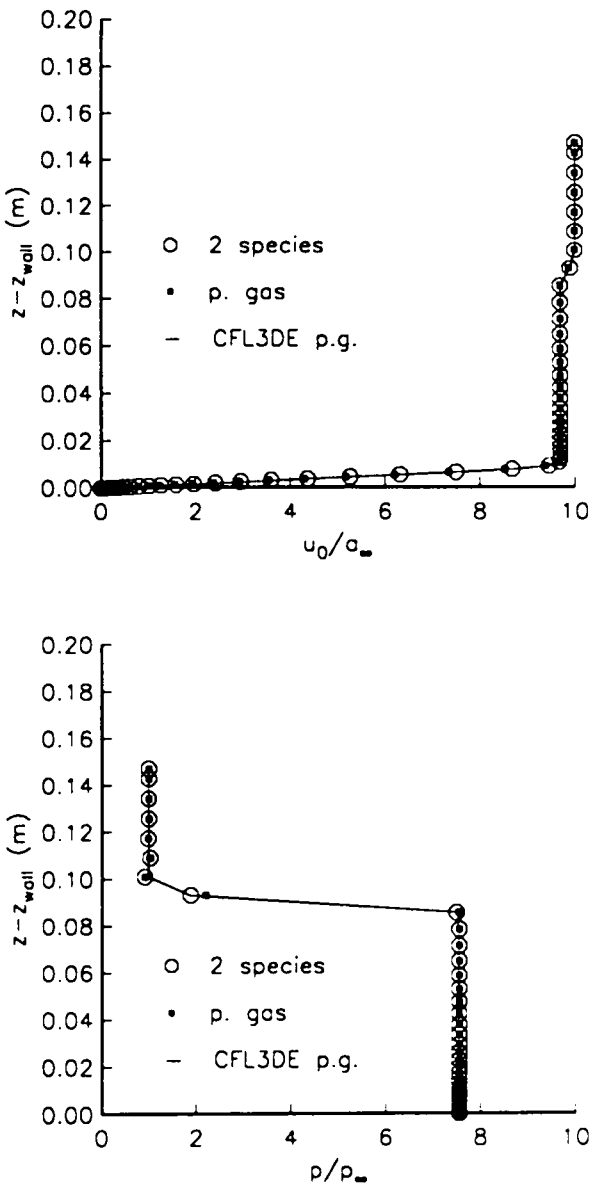

Fig. 25 Viscous flow past a wedge at $\vartheta = 10°$ and $M = 10$. Frozen chemistry. Plots of u_0/a_∞ and p/p_∞.

Freestream $T = 105\ K$, $\rho = 3.5463\ 10^{-3}\ kg/m^3$, $Pr = 0.72$

2 species Nitrogen-Oxygen mixture, Vibrational Equilibrium Model

p. gas Perfect gas, $\mathcal{M} = 29\ kg/kmole$

CFL3DE p.g. Perfect gas, courtesy of Prof. R. Walters

APPENDICES

A1. NAVIER-STOKES EQUATIONS

The extended Navier-Stokes equations for a general flow out of chemical and thermal equilibrium were presented in §3.2

$$\frac{\partial Q}{\partial t}+\frac{\partial(F-F_v)}{\partial x_1}+\frac{\partial(G-G_v)}{\partial x_2}+\frac{\partial(H-H_v)}{\partial x_3}=W, \qquad (A1.1)$$

where Q is the vector of conserved variables, F, G, H are the inviscid flux vectors, F_v, G_v, H_v are the viscous flux vectors, and W is the vector of source terms. Q and W are given by

$$Q=\begin{pmatrix}\rho_1\\ \rho_2\\ \vdots\\ \vdots\\ \rho_N\\ \rho u_{0_1}\\ \rho u_{0_2}\\ \rho u_{0_3}\\ \rho_1 e_{n_1}\\ \rho_2 e_{n_2}\\ \vdots\\ \rho_M e_{n_M}\\ \rho_e e_{0_e}\\ \rho e_0\end{pmatrix}, \qquad W=\begin{pmatrix}w_1\\ w_2\\ \vdots\\ \vdots\\ w_N\\ \sum_s \epsilon n_s z_s E_1\\ \sum_s \epsilon n_s z_s E_2\\ \sum_s \epsilon n_s z_s E_3\\ (\dot{Q}_1)_{n,E}+(\dot{Q}_1)_{n,I}\\ (\dot{Q}_2)_{n,E}+(\dot{Q}_2)_{n,I}\\ \vdots\\ (\dot{Q}_M)_{n,E}+(\dot{Q}_M)_{n,I}\\ -\epsilon n_e(E\cdot u_e)+(\dot{Q}_e)_E+(\dot{Q}_e)_I\\ \sum_s \epsilon n_s z_s(E\cdot u_s)\end{pmatrix}, \qquad (A1.2a,b)$$

where only the electrical field E has been considered in the body forces. In the above, ρ_s, $s=1,\dots N$ is the species density, ρ is the mixture density, u_0 is the mass-averaged velocity vector, e_{0_e} is the electron total internal energy, e_0 is the mixture total internal energy, n_s is the species number density , z_s is the species charge number ($z_e=-1$), and ϵ is the electron charge. The different source terms are defined or modeled in §4 and §5.

The inviscid flux vectors are

$$F = \begin{pmatrix} \rho_1 u_{0_1} \\ \rho_2 u_{0_1} \\ \vdots \\ \vdots \\ \rho_N u_{0_1} \\ \rho u_{0_1} u_{0_1} + p \\ \rho u_{0_1} u_{0_2} \\ \rho u_{0_1} u_{0_3} \\ \rho_1 e_{n_1} u_{0_1} \\ \rho_2 e_{n_2} u_{0_1} \\ \vdots \\ \rho_M e_{n_M} u_{0_1} \\ \rho_e h_{0_e} u_{0_1} \\ \rho h_0 u_{0_1} \end{pmatrix}, \quad G = \begin{pmatrix} \rho_1 u_{0_2} \\ \rho_2 u_{0_2} \\ \vdots \\ \vdots \\ \rho_N u_{0_2} \\ \rho u_{0_2} u_{0_1} \\ \rho u_{0_2} u_{0_2} + p \\ \rho u_{0_2} u_{0_3} \\ \rho_1 e_{n_1} u_{0_2} \\ \rho_2 e_{n_2} u_{0_2} \\ \vdots \\ \rho_M e_{n_M} u_{0_2} \\ \rho_e h_{0_e} u_{0_2} \\ \rho h_0 u_{0_2} \end{pmatrix}, \quad H = \begin{pmatrix} \rho_1 u_{0_3} \\ \rho_2 u_{0_3} \\ \vdots \\ \vdots \\ \rho_N u_{0_3} \\ \rho u_{0_3} u_{0_1} \\ \rho u_{0_3} u_{0_2} \\ \rho u_{0_3} u_{0_3} + p \\ \rho_1 e_{n_1} u_{0_3} \\ \rho_2 e_{n_2} u_{0_3} \\ \vdots \\ \rho_M e_{n_M} u_{0_3} \\ \rho_e h_{0_e} u_{0_3} \\ \rho h_0 u_{0_3} \end{pmatrix}. \tag{A1.3a, b, c}$$

In order to close the inviscid (Euler) problem, the following relationships must be used

$$\rho = \sum_{s=1}^{N} \rho_s, \qquad p = \sum_{s=1}^{N} p_s = \sum_{s=1}^{N^*} \rho_s R_s T + \rho_e R_e T_e, \tag{A1.4a, b}$$

$$\rho h_0 = \rho e_0 + p = \rho(e + \frac{u_0^2}{2}) + p, \qquad \rho_e h_{0_e} = \rho_e e_{0_e} + p_e = \rho_e(e_{e_e} + \frac{u_0^2}{2}) + p_e, \tag{A1.5a, b}$$

and the thermal equations of state

$$\rho e = \sum_{i=1}^{N^*} \rho_i \Big(\int_{T_{ref}}^{T} \tilde{c}_{v_i}(\tau)\, d\tau + h_{f_i} \Big) + \sum_{i=1}^{M} \rho_i e_{n_i} + \rho_e e_{e_e} + \sum_{i=1}^{N^*} \rho_i \int_0^{T_e} c_{v_{e,i}}(\tau)\, d\tau, \tag{A1.6}$$

$$\rho_e e_{e_e} = \frac{3}{2} \rho_e R_e T_e = \frac{\rho_e R_e T_e}{\gamma_e - 1}. \tag{A1.7}$$

In the above, p_s is the partial pressure of species s, p is the pressure of the mixture, h_{0_e} is the electron total enthalpy, h_0 is the mixture total enthalpy, T is the heavy-particle translational-rotational temperature, and T_e is the electron temperature. Also, the ratio of specific heats for electrons, γ_e, has been introduced.

For a known vector Q, iterations are necessary, in general, to recover the value of T from eq.(A1.6). Then the pressure is evaluated from eq.(A1.4b).

The viscous flux vectors are given by

$$F_v = \begin{pmatrix} -\rho_1 V_{1_1} \\ -\rho_2 V_{2_1} \\ \vdots \\ \vdots \\ -\rho_N V_{N_1} \\ \tau_{11} \\ \tau_{21} \\ \tau_{31} \\ -q_{n_{1,1}} \\ -q_{n_{2,1}} \\ \vdots \\ -q_{n_{M,1}} \\ \Theta_{e_1} \\ -q_1 + (u_0 \cdot \mathbf{T})_1 \end{pmatrix}, \quad G_v = \begin{pmatrix} -\rho_1 V_{1_2} \\ -\rho_2 V_{2_2} \\ \vdots \\ \vdots \\ -\rho_N V_{N_2} \\ \tau_{12} \\ \tau_{22} \\ \tau_{32} \\ -q_{n_{1,2}} \\ -q_{n_{2,2}} \\ \vdots \\ -q_{n_{M,2}} \\ \Theta_{e_2} \\ -q_2 + (u_0 \cdot \mathbf{T})_2 \end{pmatrix}, \quad H_v = \begin{pmatrix} -\rho_1 V_{1_3} \\ -\rho_2 V_{2_3} \\ \vdots \\ \vdots \\ -\rho_N V_{N_3} \\ \tau_{13} \\ \tau_{23} \\ \tau_{33} \\ -q_{n_{1,3}} \\ -q_{n_{2,3}} \\ \vdots \\ -q_{n_{M,3}} \\ \Theta_{e_3} \\ -q_3 + (u_0 \cdot \mathbf{T})_3 \end{pmatrix}, \tag{A1.8a,b,c}$$

where

$$\Theta_{e_i} = -q_{e_i} - \rho_e \frac{u_0^2}{2} V_{e_i} - \rho_e (u_0 \cdot V_e) u_{0_i}, \qquad i = 1,2,3, \tag{A1.9}$$

and the other terms were defined in §3.3 and §5. The viscous problem is closed when diffusion velocities and transport coefficients are given in terms of conserved variables, directly or through intermediate unknowns such as temperatures or primitive variables.

A2. JACOBIANS OF THE INVISCID FLUX VECTORS

The inviscid flux vectors F, G, H are functions of the vector of conserved variables Q. A major role in flux-vector split algorithms and in any implicit formulation is played by the Jacobian matrices $\mathbf{A} \equiv \partial F/\partial Q$, $\mathbf{B} \equiv \partial G/\partial Q$, $\mathbf{C} \equiv \partial H/\partial Q$. $\mathbf{A}$ can be evaluated from F, written as a function of Q, using eqs.(A1.2) through (A1.7). The following result is obtained

$$
-\rho\mathbf{A} = \begin{pmatrix}
(\rho_1-\rho)u_{0_1} & \cdots & \rho_1 u_{0_1} & -\rho_1 i & 0 & \cdots & 0 & 0 & 0 \\
\rho_2 u_{0_1} & \cdots & \rho_2 u_{0_1} & -\rho_2 i & 0 & \cdots & 0 & 0 & 0 \\
\vdots & \vdots & \vdots & \vdots & \vdots & \vdots & \vdots & \vdots & \vdots \\
\vdots & \vdots & \vdots & \vdots & \vdots & \vdots & \vdots & \vdots & \vdots \\
\rho_N u_{0_1} & \cdots & (\rho_N-\rho)u_{0_1} & -\rho_N i & 0 & \cdots & 0 & 0 & 0 \\
a_1^T & \cdots & a_N^T & \mathbf{a} & \rho\ell i^T & \cdots & \rho\ell i^T & a_{N+M+4}^T & -\rho\ell i^T \\
\rho_1 e_{n_1} u_{0_1} & \cdots & \rho_1 e_{n_1} u_{0_1} & -\rho_1 e_{n_1} i & -\rho u_{0_1} & \cdots & 0 & 0 & 0 \\
\vdots & \ddots & \vdots & \vdots & \vdots & \ddots & \vdots & \vdots & \vdots \\
\rho_M e_{n_M} u_{0_1} & \cdots & \rho_M e_{n_M} u_{0_1} & -\rho_M e_{n_M} i & 0 & \cdots & -\rho u_{0_1} & 0 & 0 \\
d_1 & \cdots & d_N & \mathbf{d} & 0 & \cdots & 0 & -\gamma_e \rho u_{0_1} & 0 \\
f_1 & \cdots & f_N & \mathbf{f} & \rho\ell u_{0_1} & \cdots & \rho\ell u_{0_1} & f_{N+M+4} & -\tilde{\gamma}\rho u_{0_1}
\end{pmatrix}, \tag{A2.1}
$$

where $\ell \equiv (\tilde{\gamma}-1)$, i is the unit vector in the x_1 direction, $i = (1,0,0)$, i^T is its transpose, and

$$a_i^T = \rho(u_0 \cdot i^T)u_0^T - \rho i^T \frac{\partial p}{\partial \rho_i}, \qquad i = 1,\ldots,N, \tag{A2.2}$$

$$d_i = \rho(u_0 \cdot i^T)(h_{0_e} - \frac{\partial p_e}{\partial \rho_i}), \qquad i = 1,\ldots,N, \tag{A2.3}$$

$$f_i = \rho(u_0 \cdot i^T)(h_0 - \frac{\partial p}{\partial \rho_i}), \qquad i = 1,\ldots,N, \tag{A2.4}$$

$$\mathbf{a} = \rho(\tilde{\gamma}-1)(1-\chi_e)[u_0^T i]^T - \rho u_0^T i - \rho(u_0 \cdot i^T)\mathbf{I}, \tag{A2.5}$$

$$\mathbf{d} = \rho_e(u_0 \cdot i)(\gamma_e-1)u_0 - \rho_e h_{0_e} i, \tag{A2.6}$$

$$\mathbf{f} = \rho(u_0 \cdot i)(\tilde{\gamma}-1)(1-\chi_e)u_0 - \rho h_0 i, \tag{A2.7}$$

$$a_{N+M+4} = \frac{\rho^2}{\rho_e}(\tilde{\gamma}-1)\chi_e i, \tag{A2.8}$$

$$f_{N+M+4} = \frac{\rho^2}{\rho_e}(\tilde{\gamma}-1)\chi_e u_{0_1}, \tag{A2.9}$$

where χ_e can be defined to be

$$\chi_e = \frac{\tilde{c}_{v_e}}{c_{v_{e,e}}} + \frac{\rho_e}{\rho}\left(1 - \frac{\gamma_e - 1}{\tilde{\gamma} - 1}\right). \tag{A2.10}$$

The other matrices can be written in a similar way, once $u_{0_1} = (\boldsymbol{u}_0 \cdot \boldsymbol{i})$ is substituted by $u_{0_2} = (\boldsymbol{u}_0 \cdot \boldsymbol{j})$ or $u_{0_3} = (\boldsymbol{u}_0 \cdot \boldsymbol{k})$, and $\boldsymbol{j}, \boldsymbol{k}$ replace $\boldsymbol{i}$, where $\boldsymbol{j} = (0,1,0)$, $\boldsymbol{k} = (0,0,1)$.

When generalized coordinates are used, (§3.5), the corresponding Jacobians $\tilde{\mathbf{A}} \equiv \partial\tilde{\boldsymbol{F}}/\partial\boldsymbol{Q}$, $\tilde{\mathbf{B}} \equiv \partial\tilde{\boldsymbol{G}}/\partial\boldsymbol{Q}$, $\tilde{\mathbf{C}} \equiv \partial\tilde{\boldsymbol{H}}/\partial\boldsymbol{Q}$ can be written in the same way, when the vectors normal to the x_1, x_2, x_3 surfaces, namely $\boldsymbol{i}$, $\boldsymbol{j}$, $\boldsymbol{k}$, are replaced by the vectors normal to the $\tilde{\xi}$, $\tilde{\eta}$, $\tilde{\zeta}$ surfaces, namely $\nabla\tilde{\xi}$, $\nabla\tilde{\zeta}$, $\nabla\tilde{\eta}$.

The pressure derivatives to be used in the previous equations can be readily evaluated using the formulas in Appendix 1. The result is valid for flows with two translational temperatures, and reads

$$\begin{aligned}
\frac{\partial p}{\partial \rho_i} &= R_i T - (\tilde{\gamma}-1)\left(\tilde{e}_i + e_{e_i} - \frac{u_0^2}{2} + \chi_e u_0^2\right), && i = 1,\ldots,N^*,\\
\frac{\partial p}{\partial \rho_e} &= R_e T_e - (\tilde{\gamma}-1)\left(e_{e_e} - \frac{u_0^2}{2} + \chi_e u_0^2 - \frac{\rho}{\rho_e}\chi_e e_{0_e}\right),\\
\frac{\partial p}{\partial \rho u_{0_j}} &= -(\tilde{\gamma}-1)(1-\chi_e)u_{0_j}, && j = 1,2,3,\\
\frac{\partial p}{\partial \rho_i e_{n_i}} &= -(\tilde{\gamma}-1), && i = 1,\ldots,M,\\
\frac{\partial p}{\partial \rho_e e_{0_e}} &= -\frac{\rho}{\rho_e}\chi_e(\tilde{\gamma}-1),\\
\frac{\partial p}{\partial \rho e_0} &= (\tilde{\gamma}-1).
\end{aligned} \tag{A2.11a,b,c,d,e,f}$$

The electron pressure derivatives can be similarly determined for flows with

two translational temperatures. The final result reads

$$
\begin{aligned}
\frac{\partial p_e}{\partial \rho_i} &= \frac{\rho_e}{\rho}(\gamma_e - 1)u_0^2, \qquad i = 1, \ldots, N^*, \\
\frac{\partial p_e}{\partial \rho_e} &= R_e T_e + (\gamma_e - 1)\left(\frac{\rho_e}{\rho}u_0^2 - e_{0_e}\right), \\
\frac{\partial p_e}{\partial \rho u_{0_j}} &= -\frac{\rho_e}{\rho}(\gamma_e - 1)u_{0_j}, \qquad j = 1, 2, 3, \\
\frac{\partial p_e}{\partial \rho_i e_{n_i}} &= 0, \qquad i = 1, \ldots, M, \\
\frac{\partial p_e}{\partial \rho_e e_{0_e}} &= (\gamma_e - 1), \\
\frac{\partial p_e}{\partial \rho e_0} &= 0.
\end{aligned}
\qquad (A2.12a, b, c, d, e, f)
$$

It can be shown that for this set of equations, the Jacobian matrices have the homogeneity property

$$F = \mathbf{A}Q \qquad G = \mathbf{B}Q \qquad H = \mathbf{C}Q. \qquad (A2.13)$$

When free electrons are neglected and a single translational temperature model is used (§2.5), the resulting Jacobians are obtained from eq.(A2.1) by simply dropping rows and columns corresponding to electron continuity and energy and $\chi_e \equiv 0$.

When a simple asymptotic analysis is performed for cases where $\chi_e \approx \rho_e/\rho \to 0$, as discussed in §6, the corresponding Jacobian reads

$$
-\rho\mathbf{A} = \begin{pmatrix}
(\rho_1 - \rho)u_{0_1} & \cdots & \rho_1 u_{0_1} & -\rho_1 \mathbf{i} & 0 & \cdots & 0 & 0 & 0 \\
\rho_2 u_{0_1} & \cdots & \rho_2 u_{0_1} & -\rho_2 \mathbf{i} & 0 & \cdots & 0 & 0 & 0 \\
\vdots & \vdots & \vdots & \vdots & \vdots & \vdots & \vdots & \vdots & \vdots \\
\vdots & \vdots & \vdots & \vdots & \vdots & \vdots & \vdots & \vdots & \vdots \\
0 & \cdots & -\rho u_{0_1} & \mathbf{o} & 0 & \cdots & 0 & 0 & 0 \\
a_1^T & \cdots & a_N^T & \mathbf{a} & \rho \mathbf{l} \mathbf{i}^T & \cdots & \rho \mathbf{l} \mathbf{i}^T & a_{N+M+4}^T & -\rho \mathbf{l} \mathbf{i}^T \\
\rho_1 e_{n_1} u_{0_1} & \cdots & \rho_1 e_{n_1} u_{0_1} & -\rho_1 e_{n_1} \mathbf{i} & -\rho u_{0_1} & \cdots & 0 & 0 & 0 \\
\vdots & \ddots & \vdots & \vdots & \vdots & \ddots & \vdots & \vdots & \vdots \\
\rho_M e_{n_M} u_{0_1} & \cdots & \rho_M e_{n_M} u_{0_1} & -\rho_M e_{n_M} \mathbf{i} & 0 & \cdots & -\rho u_{0_1} & 0 & 0 \\
d_1 & \cdots & d_N & \mathbf{o} & 0 & \cdots & 0 & -\gamma_e \rho u_{0_1} & 0 \\
f_1 & \cdots & f_N & \mathbf{f} & \rho \mathbf{l} u_{0_1} & \cdots & \rho \mathbf{l} u_{0_1} & f_{N+M+4} & -\tilde{\gamma} \rho u_{0_1}
\end{pmatrix}, \qquad (A2.14)
$$

where a_i, $f_{i,}$, for $i = 1 \ldots N$ and $\mathbf{a}$, f are given by eqs.(A2.2), (A2.4) and (A2.7) with the pressure derivatives given by

$$
\begin{aligned}
\frac{\partial p}{\partial \rho_i} &= R_i T - (\tilde{\gamma}-1)\left(\tilde{e}_i + e_{e_i} - \frac{u_0^2}{2}\right), && i = 1, \ldots, N^*, \\
\frac{\partial p}{\partial \rho_e} &= R_e T_e - (\tilde{\gamma}-1)\left(e_{e_e} - \frac{u_0^2}{2} - \frac{\rho}{\rho_e}\chi_e e_{0_e}\right), && \\
\frac{\partial p}{\partial \rho u_{0_j}} &= -(\tilde{\gamma}-1)u_{0_j}, && j = 1,2,3, \\
\frac{\partial p}{\partial \rho_i e_{n_i}} &= -(\tilde{\gamma}-1), && i = 1, \ldots, M, \\
\frac{\partial p}{\partial \rho_e e_{0_e}} &= -\frac{\rho}{\rho_e}\chi_e(\tilde{\gamma}-1), && \\
\frac{\partial p}{\partial \rho e_0} &= (\tilde{\gamma}-1), &&
\end{aligned}
\qquad (A2.15a,b,c,d,e,f)
$$

and the electron pressure derivatives given by

$$
\begin{aligned}
\frac{\partial p_e}{\partial \rho_i} &= 0, && i = 1, \ldots, N^*, \\
\frac{\partial p_e}{\partial \rho_e} &= R_e T_e - (\gamma_e-1)e_{0_e}, && \\
\frac{\partial p_e}{\partial \rho u_{0_j}} &= 0, && j = 1,2,3, \\
\frac{\partial p_e}{\partial \rho_i e_{n_i}} &= 0, && i = 1, \ldots, M, \\
\frac{\partial p_e}{\partial \rho_e e_{0_e}} &= (\gamma_e-1), && \\
\frac{\partial p_e}{\partial \rho e_0} &= 0. &&
\end{aligned}
\qquad (A2.16a,b,c,d,e,f)
$$

The matrix $\mathbf{a}$ is given by eq.(A2.5) with $\chi_e \equiv 0$, and $d_i = 0$, for $i = 1 \ldots N-1$, whereas $d_N = (\gamma_e-1)\rho u_0^2(\boldsymbol{u}_0 \cdot \boldsymbol{i})/2$. Also, a_{N+M+4} and f_{N+M+4} are unchanged.

It is important to point out that the homogeneity property is preserved for this reduced Jacobian.

A3. EIGENVALUES AND EIGENVECTORS

In §A2, the Jacobian matrices **A**, **B**, **C** were determined for the general case of two translational temperatures. When solving the eigenvalue problem associated with any of them, that is the evaluation of scalars λ and *nontrivial* vectors $\boldsymbol{x}$ such that the following relationship holds

$$\mathbf{A}\boldsymbol{x} = \lambda \boldsymbol{x}, \tag{A3.1}$$

unexpected phenomena occur. For the case of one translational temperature, published values of eigenvalues [6] show the relevance of the frozen speed of sound, defined in §2.4, for this problem. The result is

$$\text{eigenvalues of } \mathbf{A}: \lambda_i = \begin{cases} u_{0_1}, & i = 1, \ldots, N^*+M+2, \\ u_{0_1} + a, & i = N^*+M+3, \\ u_{0_1} - a, & i = N^*+M+4. \end{cases} \tag{A3.2}$$

For the general case considered in this work, the repeated eigenvalue u_{0_1} is again recovered with multiplicity $N+M+2$, but the remaining *three* (one more than the previous case, due to the presence of the electron energy equation), give rise to a third-order equation with no simple algebraic solutions

$$(\lambda - u_{0_1})^3 + g_1(\lambda - u_{0_1})^2 + g_2(\lambda - u_{0_1}) + g_3 = 0, \tag{A3.3}$$

where the coefficients g_i are given by

$$\begin{aligned} g_1 &= -u_{0_1}\left[(\gamma_e - 1) + (\tilde{\gamma} - 1)\chi_e\right], \\ g_2 &= -\left[\tilde{\gamma}\frac{p}{\rho} - (\tilde{\gamma} - 1)\chi_e R_e T_e\right], \\ g_3 &= u_{0_1}\left[(\gamma_e - 1)\tilde{\gamma}\frac{p}{\rho} + (\tilde{\gamma} - 1)\chi_e R_e T_e\right], \end{aligned} \tag{A3.4a, b, c}$$

and χ_e was defined in eq.(A2.10).

It is important to point out that the speed of sound defined in eq.(2.26) does not yield solutions to eq.(A3.3) of the kind $u_{0_1} \pm a$, as could be expected. In §6, it is shown that the assumption of more than one translational temperature is the reason for these complications in the eigenvalue problem. However, when a simple asymptotic analysis is performed for $\chi_e \approx \rho_e/\rho \to 0$, an approximate solution is recovered

$$\lambda_i = \begin{cases} u_{0_1}, & i = 1,\ldots,N+M+2, \\ u_{0_1} + a, & i = N+M+3, \\ u_{0_1} - a, & i = N+M+4, \\ u_{0_1} + (\gamma_e - 1)u_{0_1} = \gamma_e u_{0_1}, & i = N+M+5, \end{cases} \tag{A3.5}$$

where a is a consistently reduced expression for the frozen speed of sound

$$a^2 = \tilde{\gamma}\frac{p}{\rho}. \tag{A3.6}$$

The eigenvectors corresponding to these approximate eigenvalues are given as follows

$$E_i = \begin{pmatrix} 0 \\ \vdots \\ \rho_i/\rho \\ \vdots \\ 0 \\ \rho_i u_0^T/\rho \\ 0 \\ \vdots \\ 0 \\ 0 \\ (u_0^2 - \psi_i)\rho_i/\rho \end{pmatrix}, \qquad E_N = \begin{pmatrix} 0 \\ \vdots \\ \vdots \\ \vdots \\ \rho_e/\rho \\ \rho_e u_0^T/\rho \\ 0 \\ \vdots \\ 0 \\ \rho_e u_0^2/2\rho \\ [u_0^2 - \psi_e + \vartheta u_0^2/2(\tilde{\gamma}-1)]\rho_e/\rho \end{pmatrix}, \tag{A3.7a,b}$$

$i = 1,\ldots,N-1$

$$E_{N+j} = \begin{pmatrix} 0 \\ \vdots \\ 0 \\ \vdots \\ 0 \\ \mathbf{o} \\ \vdots \\ \rho_j e_{n_j}/\rho \\ 0 \\ 0 \\ \rho_j e_{n_j}/\rho \end{pmatrix}, \quad E_{N+M+1} = \begin{pmatrix} 0 \\ \vdots \\ 0 \\ \vdots \\ 0 \\ \boldsymbol{l}^T \\ 0 \\ \vdots \\ 0 \\ 0 \\ (\boldsymbol{u}_0 \cdot \boldsymbol{l}) \end{pmatrix}, \quad E_{N+M+2} = \begin{pmatrix} 0 \\ \vdots \\ 0 \\ \vdots \\ 0 \\ \boldsymbol{m}^T \\ 0 \\ \vdots \\ 0 \\ 0 \\ (\boldsymbol{u}_0 \cdot \boldsymbol{m}) \end{pmatrix},$$

$j = 1, \ldots, M$

(A3.8a, b, c)

$$E_{N+M+k} = \begin{pmatrix} \rho_1/\rho \\ \rho_2/\rho \\ \vdots \\ \vdots \\ 0 \\ \boldsymbol{u}_0^T \pm a\boldsymbol{i}^T \\ \rho_1 e_{n_1}/\rho \\ \vdots \\ \rho_M e_{n_M}/\rho \\ 0 \\ h_0 \pm u_{0_1} a \end{pmatrix}, \quad E_{N+M+5} = \begin{pmatrix} \vartheta\rho_1/\rho \\ \vartheta\rho_2/\rho \\ \vdots \\ \vdots \\ 0 \\ \vartheta[\boldsymbol{u}_0^T + (\gamma_e - 1)u_{0_1}\boldsymbol{i}^T] \\ \vartheta\rho_1 e_{n_1}/\rho \\ \vdots \\ \vartheta\rho_M e_{n_M}/\rho \\ a^2 - (\gamma_e - 1)^2 u_{0_1}^2 \\ \vartheta(h_0 + (\gamma_e - 1)u_{0_1}^2) \end{pmatrix}, \qquad (A3.9a, b)$$

$k = 3, 4$

where

$$\psi_i \equiv \frac{1}{\tilde{\gamma} - 1}\frac{\partial p}{\partial \rho_i}, \quad i = 1, \ldots, N, \qquad \vartheta \equiv \frac{\rho}{\rho_e}\chi_e(\tilde{\gamma} - 1), \qquad (A3.10a, b)$$

with $\partial p/\partial \rho_i$ defined in eq.(A2.11), and $\boldsymbol{l}$, $\boldsymbol{m}$ being a set of arbitrarily defined tangent vectors in the plane perpendicular to $\boldsymbol{i}$.

Again, the same results apply to **B** and **C** once u_{0_1} is replaced by u_{0_2} or u_{0_3} and $\boldsymbol{i}$ is replaced by $\boldsymbol{j}$ or $\boldsymbol{k}$, respectively. The extension to generalized coordinates requires substitution of $\boldsymbol{i}$, $\boldsymbol{j}$, $\boldsymbol{k}$ with $\nabla\tilde{\xi}$, $\nabla\tilde{\eta}$, $\nabla\tilde{\zeta}$ and of u_{0_1}, u_{0_2}, u_{0_3} with $\tilde{u}_{0_1}$, $\tilde{u}_{0_2}$, $\tilde{u}_{0_3}$, defined in eq.(3.44).

The eigenvectors for the one temperature case are recovered by simply dropping the rows corresponding to electron continuity and energy, along with the N^{th} and $(N+M+5)^{th}$ contributions, eqs.(A3.7b) and (A3.9b), and by simplifying the pressure derivative expressions of eqs.(A2.11) in a consistent way.

It is noteworthy that these eigenvectors are *not* linearly independent for the special case $a = (\gamma_e - 1)u_{0_i} = 2u_{0_i}/3$, because the $(N+M+3)^{th}$ and $(N+M+5)^{th}$ contributions coincide (apart from the constant factor ϑ) in that instance. However, this local mathematical singularity does not seem to affect the numerical simulation.

A4. CHARACTERISTIC RELATIONSHIPS

The asymptotic analysis developed in §6 allows for the determination of approximate eigenvalues and eigenvectors for the inviscid Jacobians, as discussed in §A3. Using the previous information, the compatibility equations that hold along characteristic directions can be derived for the case of flows with two translational temperatures. Neglecting the effect of source terms, the final result for the direction x_1 reads

$$
\begin{aligned}
&\frac{dx_1}{dt} = u_{0_1}, \qquad i = 1,\ldots,N^*, && \frac{\rho}{\rho_i} d\rho_i - \frac{dp}{a^2} - \frac{\rho}{\rho_e}\chi_e \frac{\gamma_e - 1}{\tilde{\gamma} - 1}\frac{dp_e}{a^2} = 0,\\
&\frac{dx_1}{dt} = u_{0_1}, && \frac{\rho}{\rho_e} d\rho_e = 0,\\
&\frac{dx_1}{dt} = u_{0_1}, \qquad j = 1,\ldots,M, && \frac{\rho}{\rho_j e_{n_j}} d\rho_j e_{n_j} - \frac{dp}{a^2} - \frac{\rho}{\rho_e}\chi_e \frac{\gamma_e - 1}{\tilde{\gamma} - 1}\frac{dp_e}{a^2} = 0,\\
&\frac{dx_1}{dt} = u_{0_1}, && du_{0_2} = 0,\\
&\frac{dx_1}{dt} = u_{0_1}, && du_{0_3} = 0,\\
&\frac{dx_1}{dt} = u_{0_1} + (\gamma_e - 1)u_{0_1} = \gamma_e u_{0_1}, && dp_e + \rho_e(\gamma_e - 1) d\frac{u_0^2}{2} = 0,\\
&\frac{dx_1}{dt} = u_{0_1} \pm a, && dp \pm \rho a du_{0_1} \mp (\tilde{\gamma} - 1)\frac{\rho}{\rho_e}\chi_e \frac{u_{0_1} dp_e \pm \rho_e a du_0^2/2}{a \mp (\gamma_e - 1)u_{0_1}} = 0.
\end{aligned}
$$

The compatibility equations for the case of only one translational temperature can be recovered from the above result neglecting terms like dp_e and $\rho_e a du_0^2/2$, and dropping electron continuity and energy equations. The result reads

$$
\begin{aligned}
&\frac{dx_1}{dt} = u_{0_1}, \qquad i = 1,\ldots,N^*, && \frac{\rho}{\rho_i} d\rho_i - \frac{dp}{a^2} = 0,\\
&\frac{dx_1}{dt} = u_{0_1}, \qquad j = 1,\ldots,M, && \frac{\rho}{\rho_j e_{n_j}} d\rho_j e_{n_j} - \frac{dp}{a^2} = 0,\\
&\frac{dx_1}{dt} = u_{0_1}, && du_{0_2} = 0,\\
&\frac{dx_1}{dt} = u_{0_1}, && du_{0_3} = 0,\\
&\frac{dx_1}{dt} = u_{0_1} \pm a, && dp \pm \rho a du_{0_1} = 0.
\end{aligned}
$$

It should be noted that Wood and Kirkwood [90] present a similar analysis taking the source term effects into account, but only for the case of one translational temperature.

The vita has been removed from the scanned document